IN-1403

UC-80

SIMULATED DESIGN BASIS ACCIDENT TESTS OF THE CAROLINAS VIRGINIA TUBE REACTOR CONTAINMENT -- FINAL REPORT

R. C. Schmitt, G. E. Bingham, J. A. Norberg

IDAHO NUCLEAR CORPORATION
NATIONAL REACTOR TESTING STATION
IDAHO FALLS, IDAHO 83401

Date Published - December 1970

PREPARED FOR

U. S. ATOMIC ENERGY COMMISSION
IDAHO OPERATIONS OFFICE
UNDER CONTRACT NO. AT(10-1)-1230

Printed in the United States of America
Available from
National Technical Information Service
U. S. Department of Commerce
Springfield, Virginia 22151
Price: Printed Copy $3.00; Microfiche $0.65

IN-1403

Reactor Technology
TID-4500

SIMULATED DESIGN BASIS ACCIDENT TESTS OF THE CAROLINAS VIRGINIA TUBE REACTOR CONTAINMENT -- FINAL REPORT

BY

R. C. Schmitt, G. E. Bingham, J. A. Norberg

IDAHO NUCLEAR CORPORATION

A Jointly Owned Subsidiary of

AEROJET GENERAL CORPORATION
ALLIED CHEMICAL CORPORATION
PHILLIPS PETROLEUM COMPANY

Bethesda Technical Library
U. S. Atomic Energy Commission
Washington, D. C. 20545
STOP 4

Date Published - December 1970

PREPARED FOR THE U. S. ATOMIC ENERGY COMMISSION
IDAHO OPERATIONS OFFICE
UNDER CONTRACT NO. AT(10-1)-1230

ACKNOWLEDGMENTS

The authors wish to acknowledge Mr. D. A. Waddoups, Idaho Nuclear Corporation, who contributed to this report, particularly in the areas of temperature and pressure data reduction, condensation interpretation, and error analysis. Acknowledgment is also extended to Mr. R.N. Millhollin who developed many of the Carolinas Virginia Tube Reactor (CVTR) data reduction computer codes.

ABSTRACT

Several simulated design basis accident (DBA) tests were performed early in 1969 on the Carolinas Virginia Tube Reactor (CVTR) containment system. The final results of these DBA tests are presented in this report, and include results of calculations of the containment heat transfer properties and comparisons of the measured and calculated containment responses to simulated DBA conditions. Steam injection conditions and flow rates, containment pressure and temperature response histories, pressure suppression spray system flow rates and effects, and a description of data acquisition instrumentation and equipment and data acquisition methods are also included.

SUMMARY

Final results of the simulated design basis accident (DBA) tests of the Carolinas Virginia Tube Reactor (CVTR) containment system are presented. These tests were accomplished by injecting slightly superheated steam into the closed containment system, and were representative of an intermediate size pipe break.

Condensing steam heat transfer coefficients for the transfer of heat from the air-steam atmosphere to the structural heat sinks of this representative containment are derived from measured data. The heat transfer data are compared with common heat transfer assumptions in the industry and also are used as input data to the CONTEMPT containment response analytical model. The CONTEMPT code is evaluated by comparing analytically predicted pressure-temperature response to the measured response. Both pretest and posttest calculations are presented.

The heat transfer coefficients for CVTR were found to be a factor of three to five larger than predicted pretest coefficients. No nonconservatism was detected for the important peak pressure prediction from CONTEMPT. However, CONTEMPT being a single node analytical model, failed to indicate temperature stratification as measured at CVTR and underestimated the maximum containment temperature. These findings could be significant, and more nearly accurate containment response predictions may require an analytical model with additional nodes. Calculated results from a developmental two-node analytical model are included as a part of the analysis.

Other test results discussed in this report are related to containment response with the addition of pressure reduction spray in two tests, the effect of DBA conditions on containment integrity, and other behavior during a DBA as observed from several experiments such as those in which paint samples were exposed to the DBA environment.

The report also includes descriptions of data acquisition instrumentation and equipment and data acquisition methods.

CONTENTS

FIGURES

TABLES

SIMULATED DESIGN BASIS ACCIDENT TESTS OF THE CAROLINAS VIRGINIA TUBE REACTOR CONTAINMENT -- FINAL REPORT

I. INTRODUCTION

This report presents the results of the computer analysis of test data from the simulated design basis accident (DBA) tests performed in the Carolinas Virginia Tube Reactor (CVTR) containment system. The DBA tests were included in the CVTR In-Plant Testing Project[1] which was performed as part of the U. S. Atomic Energy Commission's Water Reactor Safety Program by the Atomic Energy Division of Phillips Petroleum Company[a] and the Carolinas Virginia Nuclear Power Associates, Incorporated, owners of the CVTR facility. The purpose of the project was to utilize the CVTR containment system for experiments that would provide information directly applicable to the safety evaluation of power reactors.

In addition to the simulated DBA tests, the CVTR In-Plant Testing Project consisted of two other major test series:

(1) Vibration tests using two independent techniques to determine the vibrational characteristics of the containment

(2) Leakage rate tests to evaluate containment leakage as a function of containment pressure and temperature.

The results of the containment vibration tests were reported by Earth Sciences[2], the University of California, Los Angeles[3], and Idaho Nuclear Corporation[4]. Reports covering the results of the containment leakage rate tests[5,6,7], and a preliminary report of the simulated DBA tests[6,8] have also been published.

1. SIMULATED DBA TEST OBJECTIVES

Safety evaluations of power reactors require estimates of expected containment atmosphere pressure-temperature histories for postulated loss-of-coolant accidents in order to establish containment loading design criteria and to evaluate the potential for release of radioactive materials. At present, determination of the containment response to postulated accident conditions is based primarily on analytical computations. Only limited experimental data exist for evaluating the accuracy and applicability of these analyses. The CVTR simulated DBA tests provide the only large-scale containment response data currently available for evaluating computational techniques used in the safety analysis of power reactors.

---

[a] Now part of Idaho Nuclear Corporation.

Simulated DBA tests were performed in the CVTR containment to provide experimental information for use in developing and evaluating analytical methods for safety analyses of nuclear power plants. The specific objectives of the simulated DBA tests were to:

(1) Obtain experimental data on containment pressure and temperature response to assess the capability of typical computer codes to predict the response of a containment atmosphere subjected to DBA conditions

(2) Obtain time-dependent heat transfer data at various locations throughout the containment structure to assess currently accepted heat transfer correlations used in containment response computations and to provide a basis for recommendations to improve heat transfer models

(3) Determine the capability of a pressure-reduction containment spray system and the gross effectiveness of the spray

(4) Determine the gross effects of DBA conditions, exclusive of radiation, on the CVTR containment integrity.

2. REPORT ORGANIZATION

The general organization of this report is as follows: Section II contains a description of the experimental method, including brief descriptions of the CVTR facility, the testing methods, the process (steam and spray water) systems, and the measurement systems; Section III presents the results obtained from each measurement system; Section IV contains the results of heat transfer calculations obtained from several separate measuring methods, presents a best estimate for the CVTR containment heat transfer coefficient, and compares this estimate with the heat transfer assumptions commonly employed for power reactor containment calculations; Section V presents pretest and posttest CONTEMPT and CONDRU II calculations, compares the results of these calculations, and discusses possible needed improvements in analytical models; Section VI contains a discussion of miscellaneous test information including containment convective current measurements and results, test photography, containment vessel expansion measurements, paint samples, and fixed leak data.

The appendices of the report contain detailed supporting information including: (a) descriptions of the test instrumentation, data acquisition systems, and data reduction methods; (b) a data summary including temperature, pressure, condensation rate, spray rate and distribution, and liner strain; and (c) descriptions of the computer programs used to analyze the test data. The appendices provide information that is believed to be of sufficient detail to permit independent analysis and computer code comparisons by other interested parties.

This report and the preliminary DBA report[8] comprise the major dissemination mechanism for the information obtained from the DBA tests performed in the CVTR containment system.

II. EXPERIMENTAL METHOD

The CVTR facility is owned by the Carolinas Virginia Nuclear Power Associates (CVNPA), Incorporated, a corporation formed by four Carolina area private utilities. The CVTR was a D_2O-moderated and -cooled pressure tube power-prototype reactor, built and operated under the Commission's third-round power demonstration program. The reactor was decommissioned in late 1967 after about four years of successful operation. The In-Plant Testing Project was performed as a joint effort of CVNPA and the Atomic Energy Division of Phillips Petroleum Company[a].

1. FACILITY DESCRIPTION[9]

The simulated DBA test effort involved only the reactor containment system; therefore, the reactor is not described in this report.

The CVTR vapor container, shown in Figure 1, is a reinforced concrete, right vertical cylindrical structure with a flat base and hemispherical dome, having an internal diameter of 57 ft 11-1/2 in. and an inside height of about 114 ft. The vessel has a 2-ft-thick reinforced concrete cylindrical wall that supports a 1/2-in.-thick steel dome covered by 20-1/2 in. of concrete for shielding. A 5-ft 9-in.-thick reinforced concrete foundation mat supports the containment structure. The top of the foundation mat and the vertical cylinder walls are lined with 1/4-in.-thick steel plates to make the containment vessel vapor tight. The basement floor consists of 4 ft 6 in. of concrete over the steel plates.

The containment structure was provided as a safeguard against the possibility of release of fission products to the surrounding area in the event of an accident, and was designed to withstand the CVTR postulated DBA for which a containment pressure of 35 psia and a temperature of 215°F were calculated. The structure housed the reactor and primary system, the steam generator, and various auxiliary systems and components. The structure has a free volume of about 227,000 ft^3 and is physically divided by floors and equipment into three rather distinct regions, which, for the purpose of this report, are designated as the operating, intermediate, and basement regions.

---

[a] Now part of Idaho Nuclear Corporation.

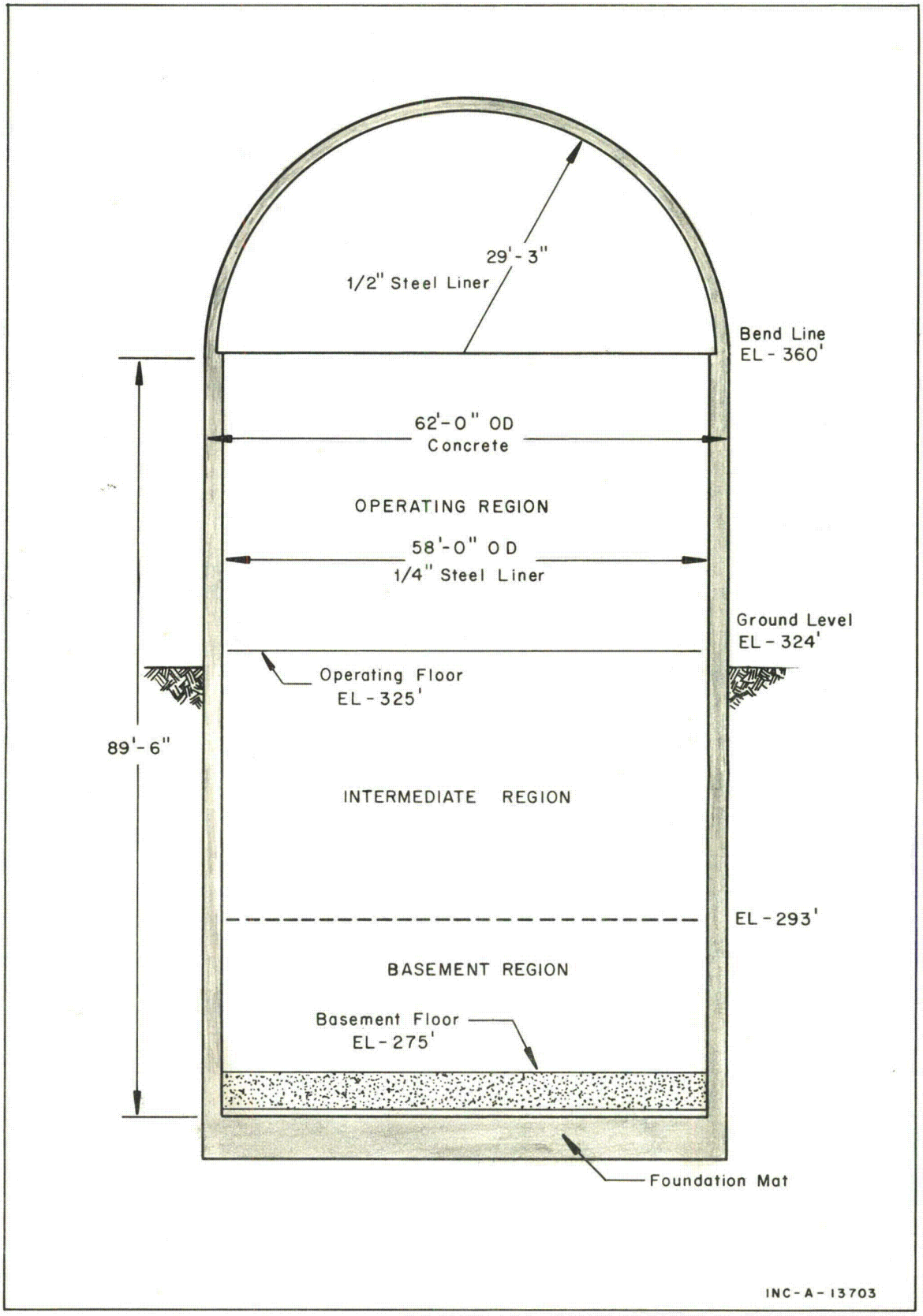

FIG. 1 CVTR CONTAINMENT STRUCTURE.

2. PROCESS SYSTEMS

Performance of the simulated DBA tests required the fabrication of two process systems, a containment steam injection system, and a containment pressure reduction spray system.

2.1 Steam Injection System

Steam for the simulated DBA tests was obtained from the Parr Station Steam Plant, a South Carolina Electric and Gas Company coal-fired electric generating station located about 500 ft from the CVTR. An existing 10-in. steam line that originally supplied steam from the nuclear plant through an oil-fired superheater to the Parr Station header was modified to permit reverse flow. The system modifications included bypassing the oil-fired superheater; installing a desuperheater to adjust the injection steam conditions to near saturation conditions; installing two cylinder operated valves to control steam flow to the containment; modifying the line inside the containment to allow steam injection directly to the containment atmosphere; and installing flow orifices, pressure taps, and thermocouple wells at several locations in the steam line to provide knowledge of steam injection conditions. The steam was released vertically above the operating floor. A diffuser was installed on the discharge nozzle of the steam line to eliminate the possibility of containment damage from localized steam impingement during injection. The diffuser consisted of a 10-ft pipe that was capped and welded to the end of the steam line, and into which approximately 126, 1-in. diameter holes had been drilled. The steam injection system is shown schematically in Figure 2 and the diffuser is shown in Figure 3.

2.2 Pressure Reduction Spray System

A containment pressure reduction water spray system, shown in Figure 4, was installed in CVTR for the simulated DBA tests. The spray header was installed about 6 in. above the containment bend line. The geometrical arrangement of the spray header and nozzles was patterned after the Connecticut Yankee containment spray system. Spray nozzles were selected to produce a droplet size range of 400 to 1400 microns, based on calculated pressure differentials and recommendations of the manufacturer.

The nozzles were arranged to provide maximum spray coverage of the containment. Two nozzles were installed at each nozzle location, a 3/4-in. Type 7G3 nozzle, and alternately either a 1-in. Type 11-1/2 F18 or a 1-1/2-in. Type F35 nozzle. The 3/4-in. nozzles, which yielded the smallest sized droplets, were installed such that they pointed downward at an angle of 45° from the horizontal; the 1-in. nozzles were directed toward the center of the containment on the horizontal; and the 1-1/2-in. nozzles, which provided the largest drops and the greatest trajectory, were directed upward at an angle of 45° from the horizontal. The nozzle locations were equally spaced around the containment circumference.

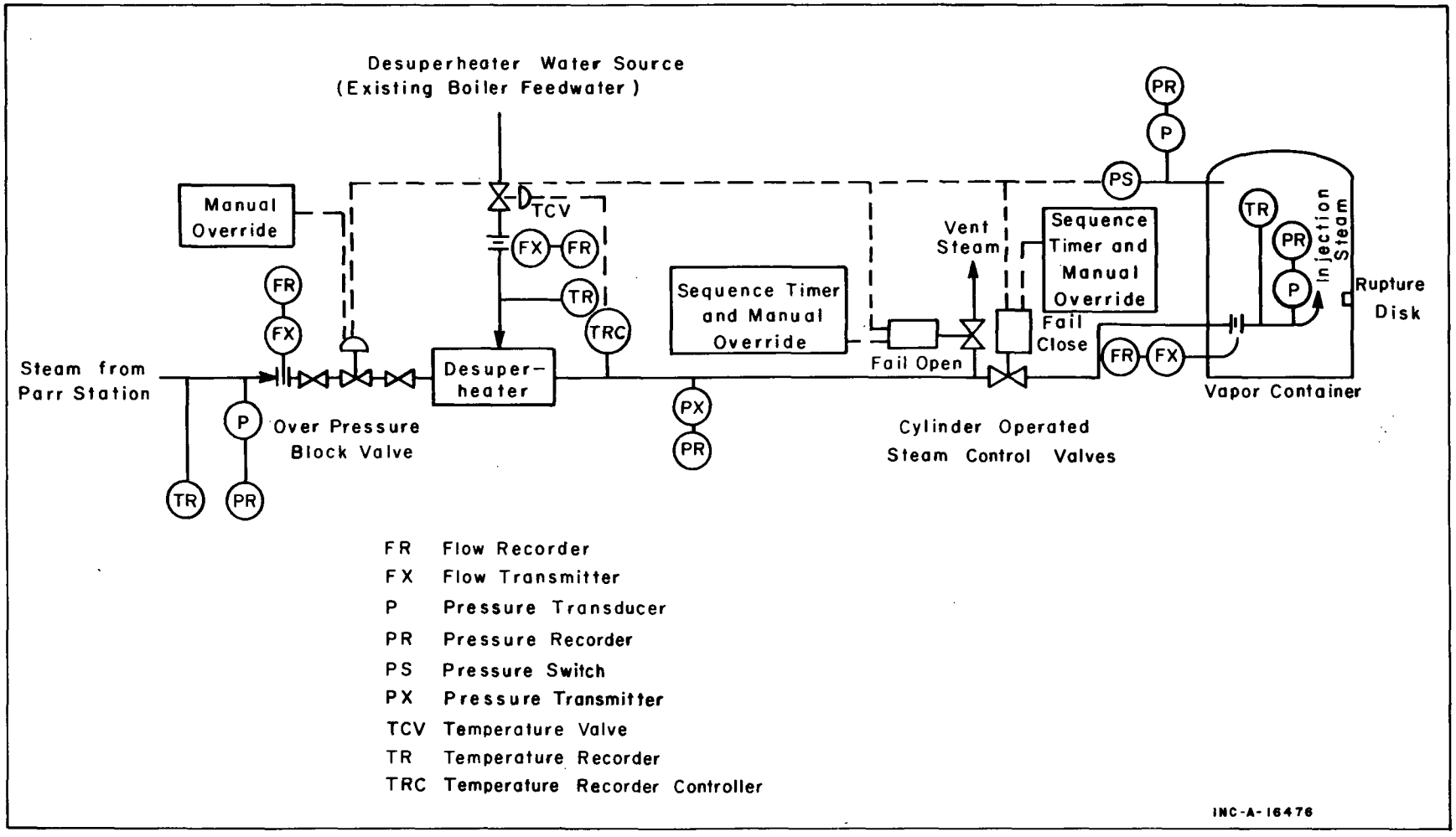

FIG. 2 CVTR STEAM ADDITION SYSTEM.

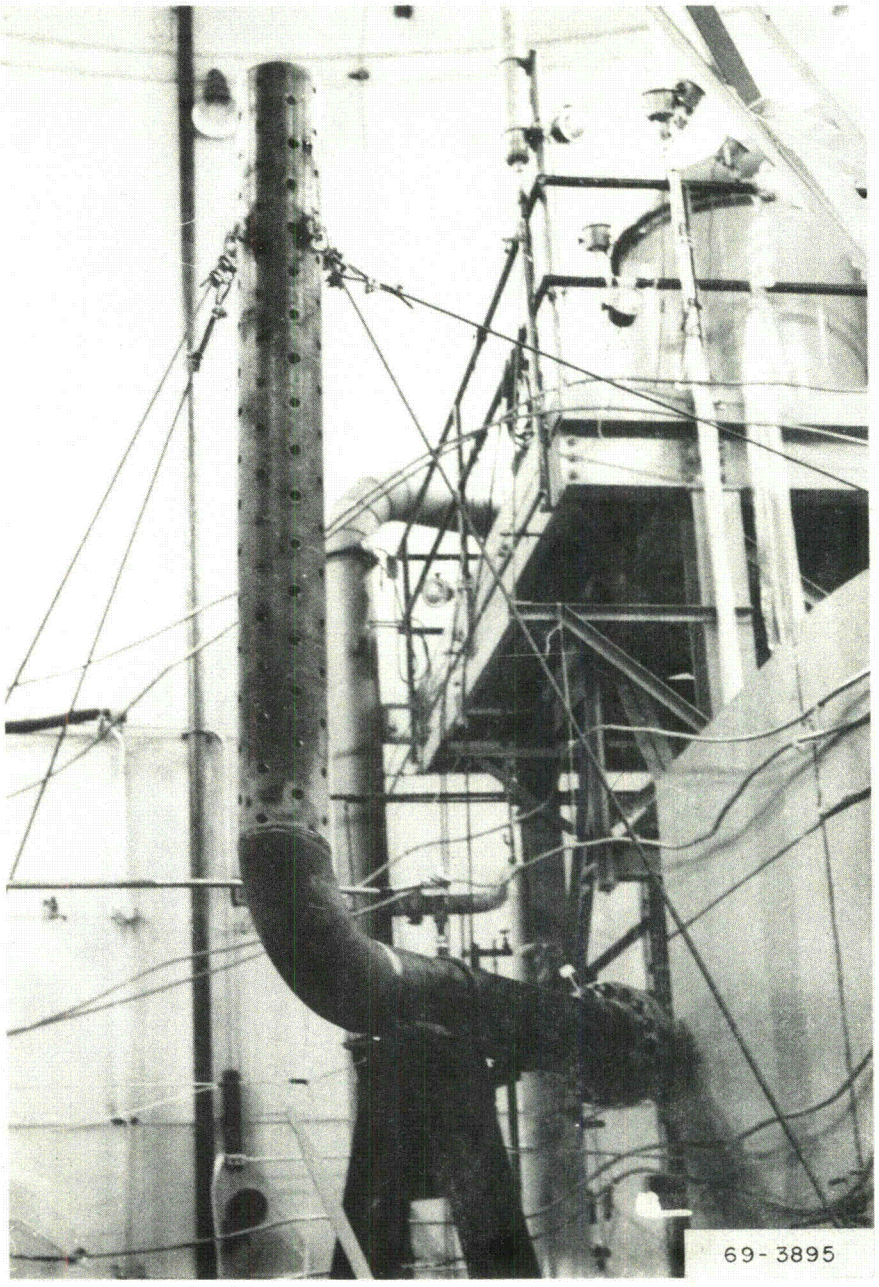

FIG. 3 CVTR STEAM LINE DIFFUSER.

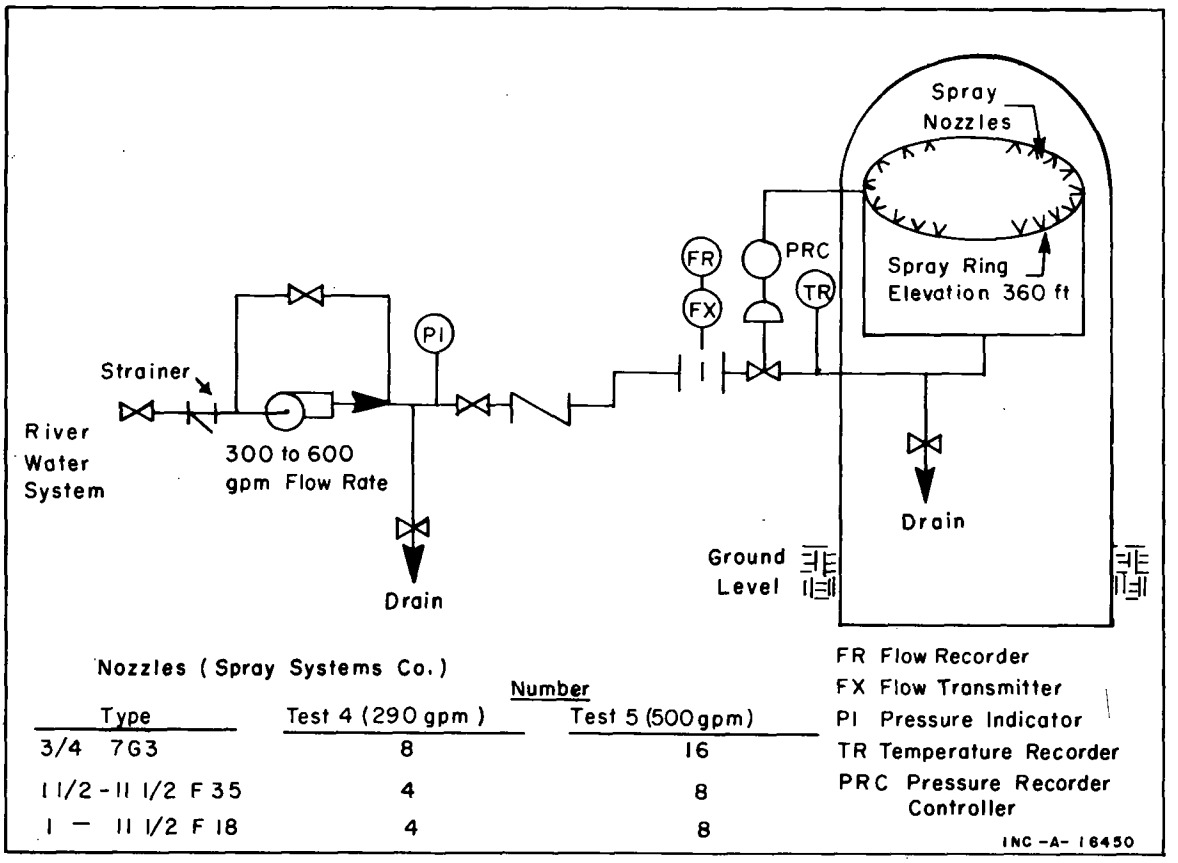

Nozzles (Spray Systems Co.)

Type	Number Test 4 (290 gpm)	Test 5 (500 gpm)
3/4 7G3	8	16
1 1/2 - 11 1/2 F 35	4	8
1 — 11 1/2 F 18	4	8

FIG. 4 CVTR PRESSURE REDUCTION SPRAY SYSTEM.

3. TEST DESCRIPTION

Five steam tests were performed during the CVTR project; two system checkout tests and three simulated DBA tests:

(1) A steam line checkout test for which a temporary elbow and a vent nozzle were installed in the steam line outside the containment. This arrangement allowed checkout of the steam plant and steam line (including valves and desuperheater) at operating conditions without injecting steam into the containment.

(2) A semi-DBA test for which steam injection was terminated at a containment pressure of about 8 psig and following which the pressure reduction spray system was operated for about three minutes. This test served as a basis from which the DBA steam injection time and spray operation time were calculated.

(3) A natural decay test that (following steam injection) allowed the containment atmosphere to return to ambient conditions by natural decay. The primary objectives of this test were to provide accurate pressure-temperature histories of the

containment atmosphere for comparison with predictions calculated by CONTEMPT, and to provide base conditions for evaluating the effectiveness of the containment pressure reduction spray.

(4) A steam-spray test during which (following steam injection) the pressure reduction spray system was activated at a flow rate of 290 gpm. The purposes of this test were to demonstrate the capability of the spray system and the effectiveness of the spray and to compare the experimental containment response with that predicted by computer codes.

(5) A second steam-spray test identical to the previous test, except that the spray flow rate was increased to 500 gpm.

4. TEST PROCEDURE

To perform a DBA test, two of the Parr Station boilers were brought to full capacity by venting steam to the atmosphere through the cylinder-operated vent valve adjacent to the CVTR containment. When the boilers reached full capacity, the desuperheater was brought on-line by increasing desuperheating water flow until the temperature of the venting steam had been reduced to about 10°F above the saturation temperature. Once desuperheating water flow for desuperheating the superheated steam had been established, and the steam flow to the atmosphere had been stabilized, the cylinder-operated charge valve was opened and the vent valve was closed to direct the total steam flow into the containment. Figure 5 shows the charge and vent valves and Figure 6 shows steam being vented to the atmosphere prior to injection into the containment. Steam injection was terminated by reversing the valve operation when the containment pressure reached above 17.5 psig. This procedure allowed close control of the steam conditions and the pressure rise in the containment, and permitted controlled startup and shutdown of the steam plant boilers.

To insure proper operation of the steam control valves during a steam test, the action of each valve was checked prior to each test before any steam flow was allowed through the steam line. Valve limit switch signals that indicated valve positions and from which the time of total valve movement could be obtained, were recorded on an oscillograph. The oscillograph record, of which Figure 7 is typical, was then checked for valve movement times. The valve check was repeated three times to provide assurance that the steam valves were operating correctly and would function properly for the steam test.

Pressure reduction spray system flow rates of 290 and 500 gpm were used during Steam Tests 4 and 5, respectively. These flow rates were achieved by changing the total number of nozzles in the spray header (Figure 4). Spray flow was initiated about 30 seconds after termination of steam injection and was stopped after about 12 minutes of operation. No provisions were made for recirculation of the spray water.

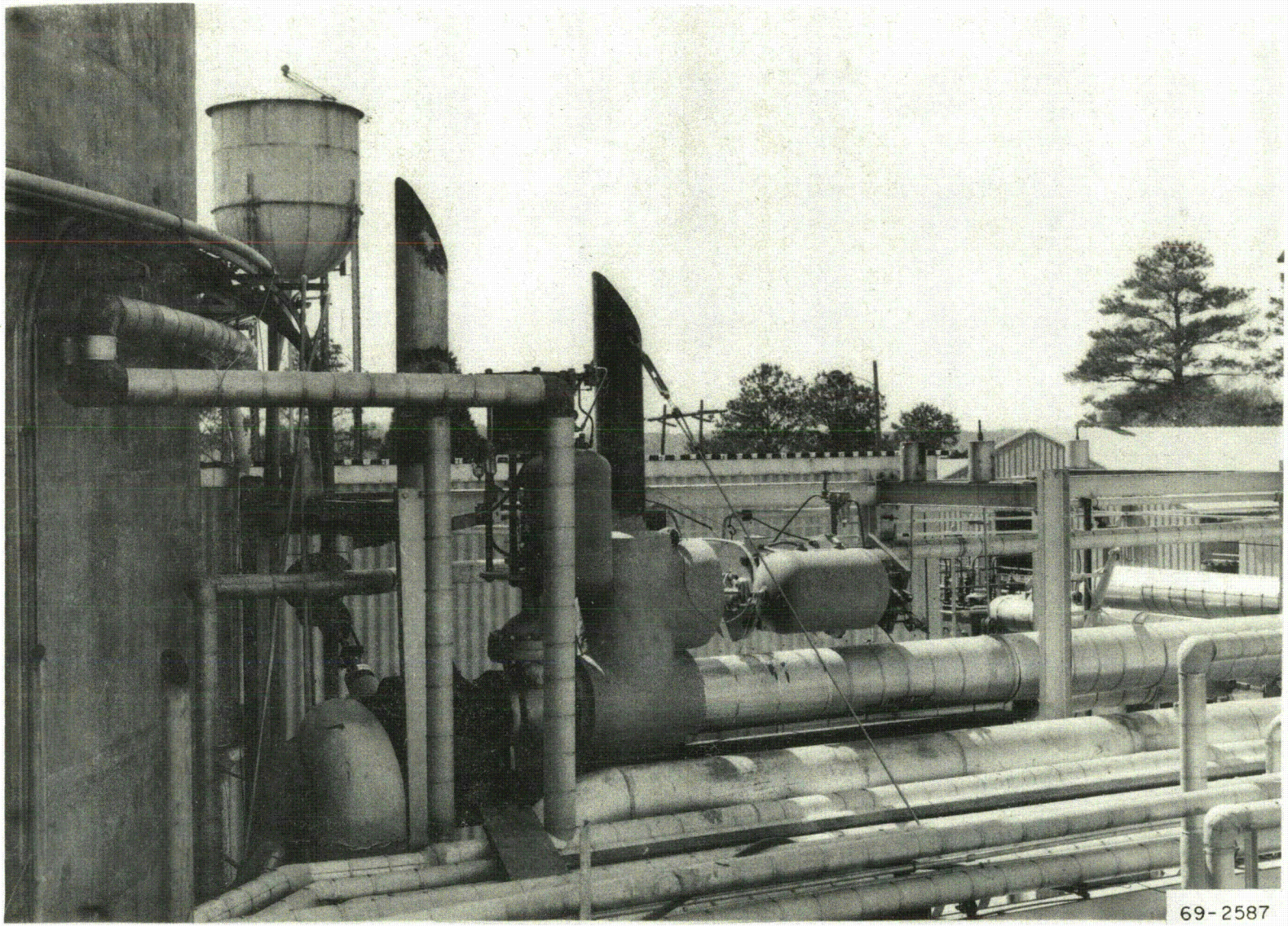

FIG. 5 CVTR STEAM VALVES.

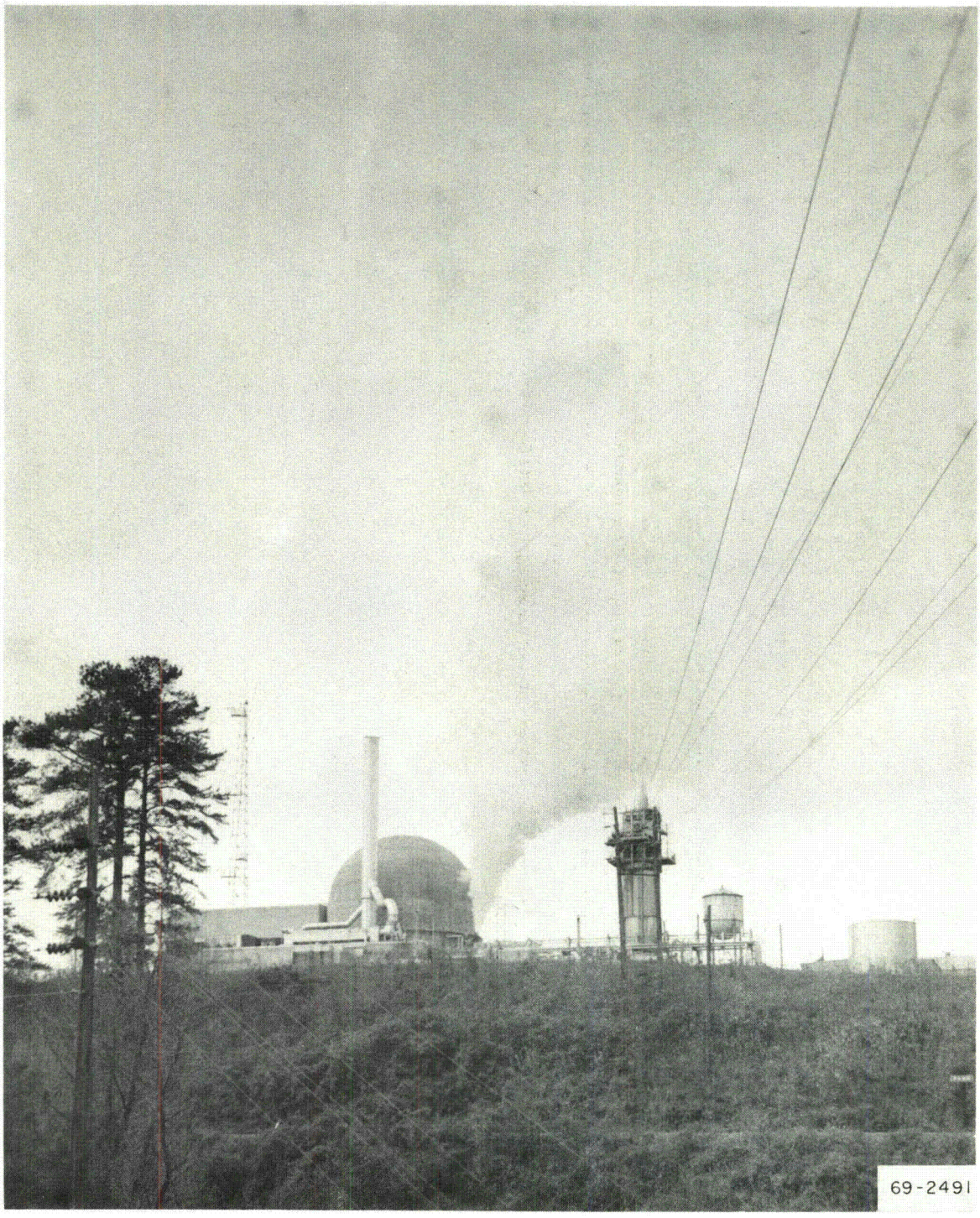

FIG. 6 STEAM BEING VENTED TO ATMOSPHERE PRIOR TO STEAM TEST.

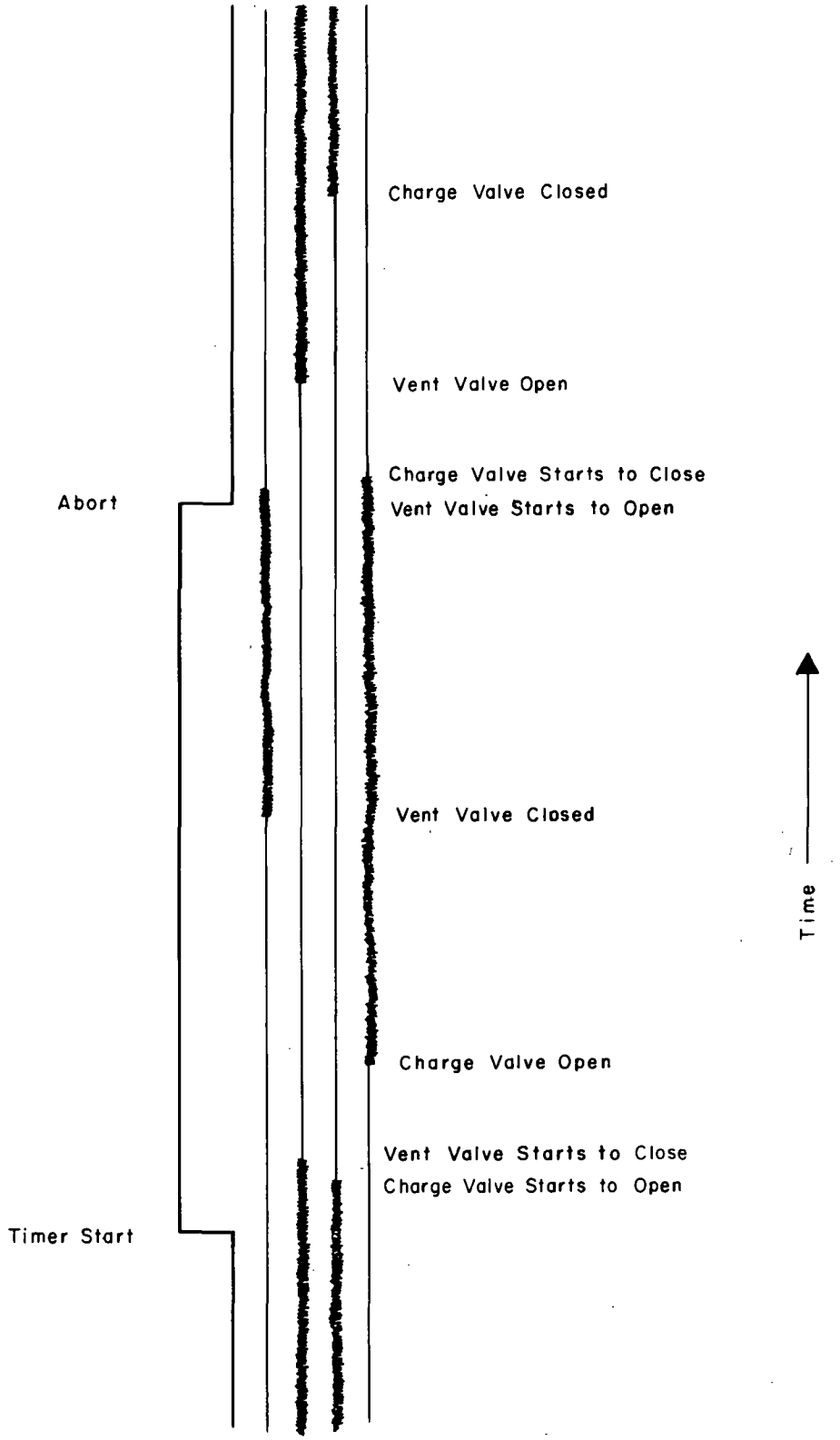

INC-B-16451

FIG. 7 TYPICAL STEAM VALVE MOVEMENT FROM OSCILLOGRAPH TRACE.

5. DATA MEASUREMENT AND ACQUISITION SYSTEMS[a]

In addition to the process data measurements associated with the steam injection system and the pressure reduction spray system, a number of measurements were made to determine the containment response to rapid steam injection and to relate the experimental response to that calculated by current analytical techniques. The following instrument systems and methods were used to obtain the containment response measurements.

5.1 Containment Atmospheric Pressure

The containment atmospheric pressure was measured by use of seven 0- to 25-psig fast-response pressure transducers and a 0- to 30-psig Heise gauge. Six of the pressure transducers were located inside the containment and one was positioned outside the containment on a pipe that was open to the containment atmosphere. The Heise gauge readout was located in the control room and was visually monitored to aid in controlling steam injection for the DBA tests. When the containment pressure reached a predetermined value, as indicated on the Heise gauge, steam injection was terminated.

5.2 Containment Atmospheric Temperature

The containment atmospheric temperature was measured by 34 Chromel-Alumel thermocouples and 15 platinum resistance thermometers located throughout the containment volume. Two additional atmospheric thermocouples were located in special containment compartments, one in the reactor header cavity and one in the refueling canal. The purpose of these thermocouples was to measure the temperature of these partially isolated regions and determine whether thermal lags occurred between these regions and the main containment.

5.3 Containment Surface Temperature

Twenty-three Chromel-Alumel thermocouples were positioned at selected locations on the containment liner surface and on the surface of interior concrete structural sections to determine the temperature response of these structures.

5.4 Temperature Profile Through the Containment Liner and Wall

Two heat transfer assemblies were installed in the wall of the operating region of the containment. Each assembly consisted of a 10-in.-diameter, 1/4-in.-thick, steel plate with special thermocouples embedded across the thickness of the plate. To install each assembly, a 10-in.-diameter section of the containment liner was removed and a 1-in.-diameter hole was drilled through the containment wall. The 10-in. plate containing the thermocouples was then welded into the liner and a concrete rod with thermocouples embedded along its length was inserted in the hole through the containment wall. Further discussion of these devices and the results obtained are presented in Section IV.

---

[a] A detailed description of the CVTR instrumentation systems is contained in Appendix A and Reference 8.

III. TEST RESULTS

One semi-DBA test and three simulated DBA steam injection tests were performed in the CVTR containment system. These tests included:

(1) A semi-DBA test in which the containment was pressurized to about 8 psig and the pressure reduction spray system operated for about three minutes

(2) An initial DBA test in which the containment was pressurized to about 18 psig and the resulting pressure was allowed to decay by natural processes

(3) A second test in which the containment was again pressurized to about 18 psig, followed immediately by operation of the pressure reduction spray system at 290 gpm for about 12 minutes

(4) A third test, identical to the second test, except that the pressure reduction spray system flow rate was increased to 500 gpm.

1. STEAM FLOW RATES AND INJECTION CONDITIONS

Steam injection to simulate DBA conditions was performed by injecting the full steam capacity of two of the Parr Station boilers into the containment. No attempt was made to limit, restrict, or control steam flow into the containment other than to terminate flow when the maximum allowable containment pressure was reached. The flow rates for the three DBA tests were almost identical. The slight differences which did occur resulted from different desuperheating water flow rates and from a slightly different boiler output for each steam test.

The total mass flow rates for the three DBA tests ranged from 360,000 to 380,000 lb/hr. The mass flow was obtained by mixing desuperheating water with the superheated steam from the boilers to adjust the injection steam conditions to as near saturation conditions as possible. The average enthalpy of the injection steam was almost identical in all three tests, about 1196 Btu/lb. Curves of mass flow versus time for the superheated steam, desuperheating water, and saturated steam for the three tests are shown in Figures 8, 9, and 10. Also shown are the enthalpy of the injection steam and the total energy added to the containment by the steam. A summary of the steam data from the three tests is presented in Table I.

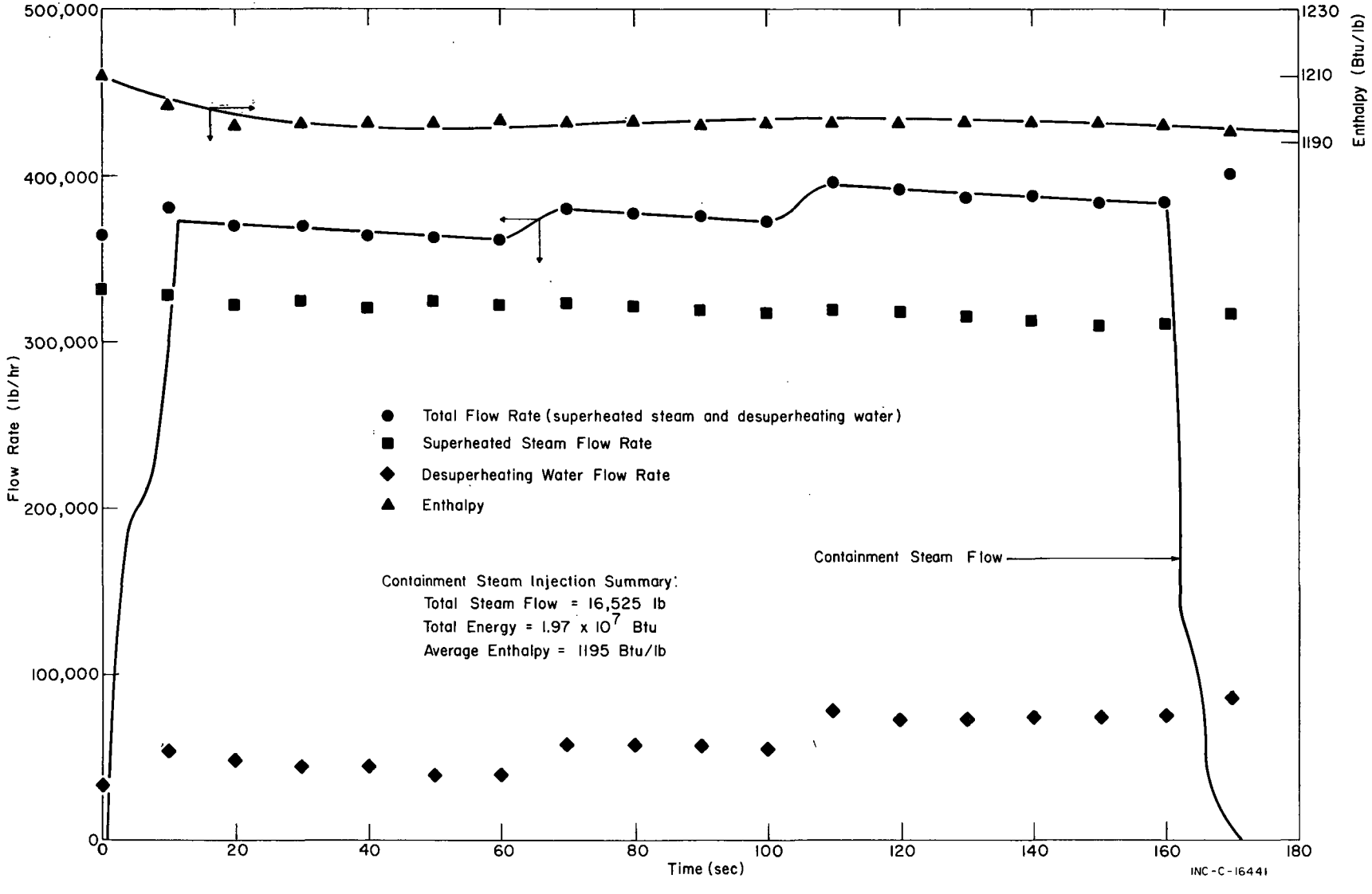

FIG. 8 STEAM INJECTION HISTORY, TEST 3.

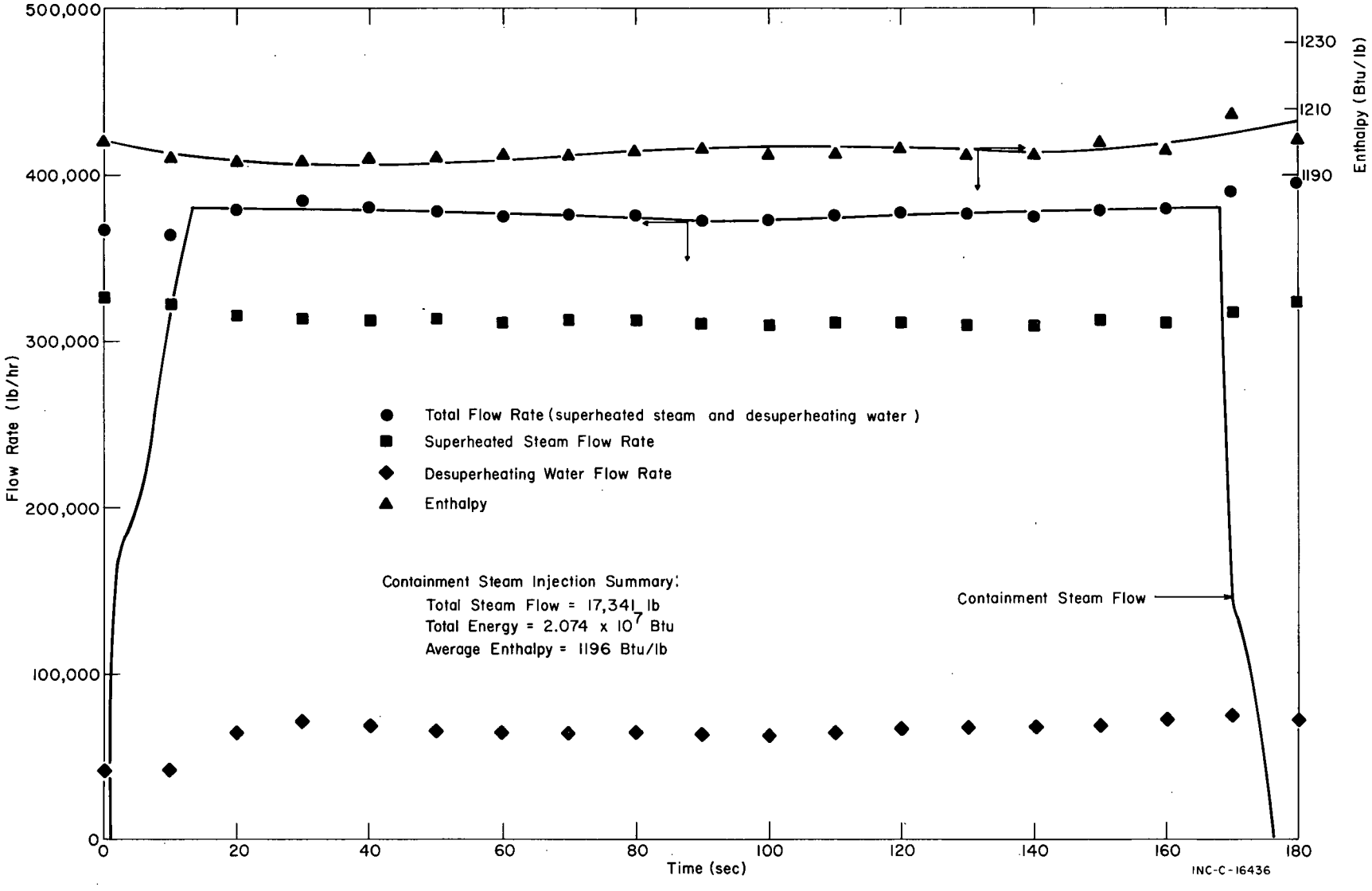

FIG. 9 STEAM INJECTION HISTORY, TEST 4.

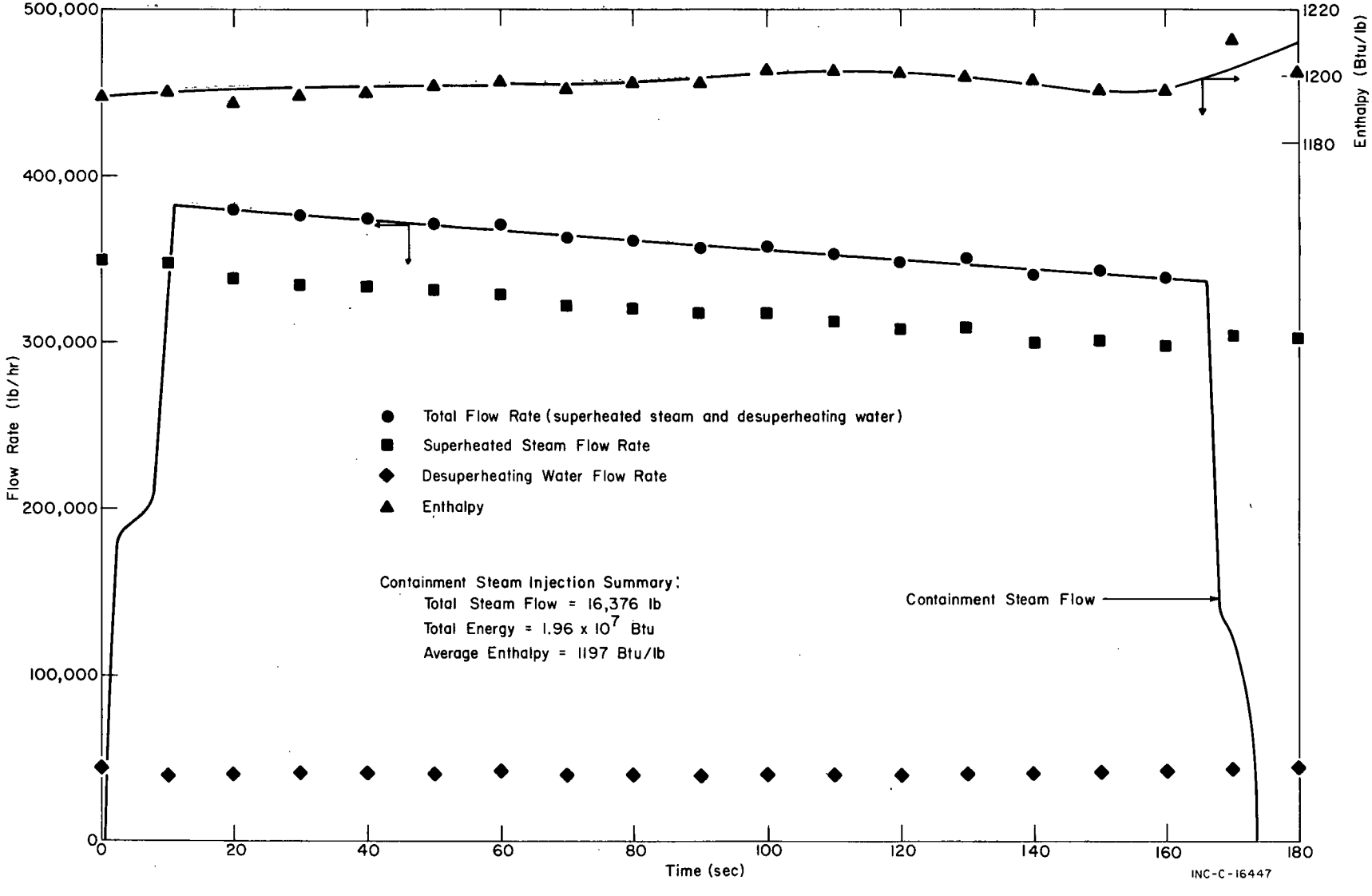

FIG. 10 STEAM INJECTION HISTORY, TEST 5.

TABLE I

STEAM DATA SUMMARY

Test[a]	Steam Injection Time (sec)[b]	Superheated Steam Flow Rate (lb/hr)	Average Flow Rate of Desuperheating Water (lb/hr)	Saturated Steam Flow Rate (lb/hr)	Total Flow (lb)	Average Enthalpy (Btu/lb)	Total Energy (Btu)
3	166.4	320,000	60,000	380,000	16,525	1195	1.97×10^7
4	174.8	310,000	65,000	375,000	17,341	1196	2.07×10^7
5	173.1	320,000	40,000	360,000	16,376	1197	1.96×10^7

[a] Test 1 was a system checkout test and Test 2 was a semi-DBA test for establishing the steam injection time and spray operation time for succeeding tests.

[b] Injection time was measured from the time the charge valve started to open until it was closed again.

2. PRESSURE HISTORY

The containment pressure was used as the basis for controlling the steam injection time during the DBA tests. The containment pressure was visually monitored on a Heise gauge. In addition to the Heise gauge, seven pressure transducers, five of which measured pressure in the main containment volume, one of which measured the reactor header cavity pressure, and one of which measured the refueling canal pressure, were used to measure the containment pressure.

A plot of containment pressure versus time for the three DBA tests as obtained from the Heise gauge is shown in Figure 11. Figures 12, 13, and 14 present the pressure of the main containment volume as a function of time for each test as obtained from four of the five pressure transducers and the Heise gauge. Temperature corrections[a] have been applied to these data, and as can be seen, excellent agreement among the results from various pressure measuring devices was obtained. Also, as expected, no pressure gradients or other special pressure dependence were observed for this relatively slow containment pressurization of the DBA tests.

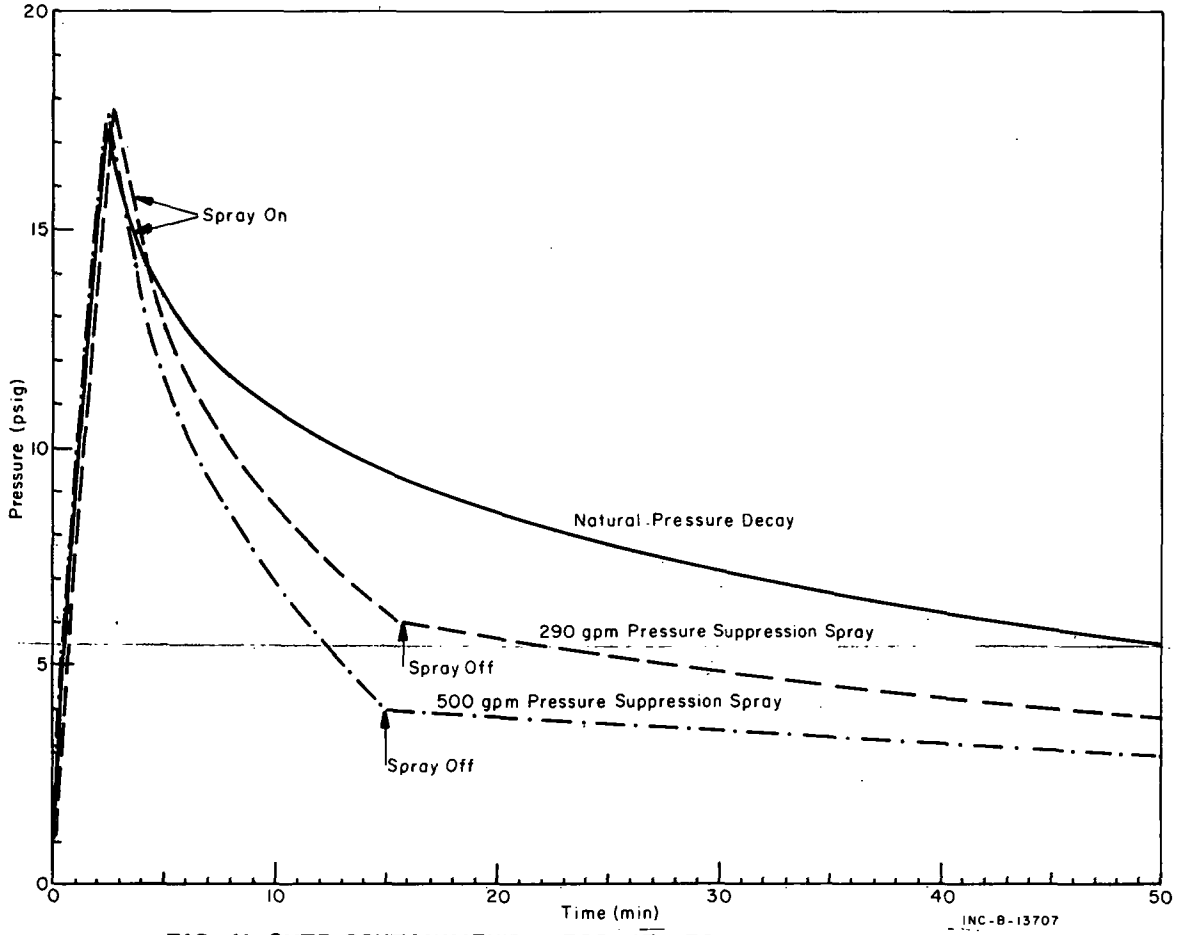

FIG. 11 CVTR CONTAINMENT PRESSURE RESPONSE -- HEISE GAUGE.

[a] No temperature correction data were available for one pressure transducer; therefore, the data from this transducer are not included in the pressure plots.

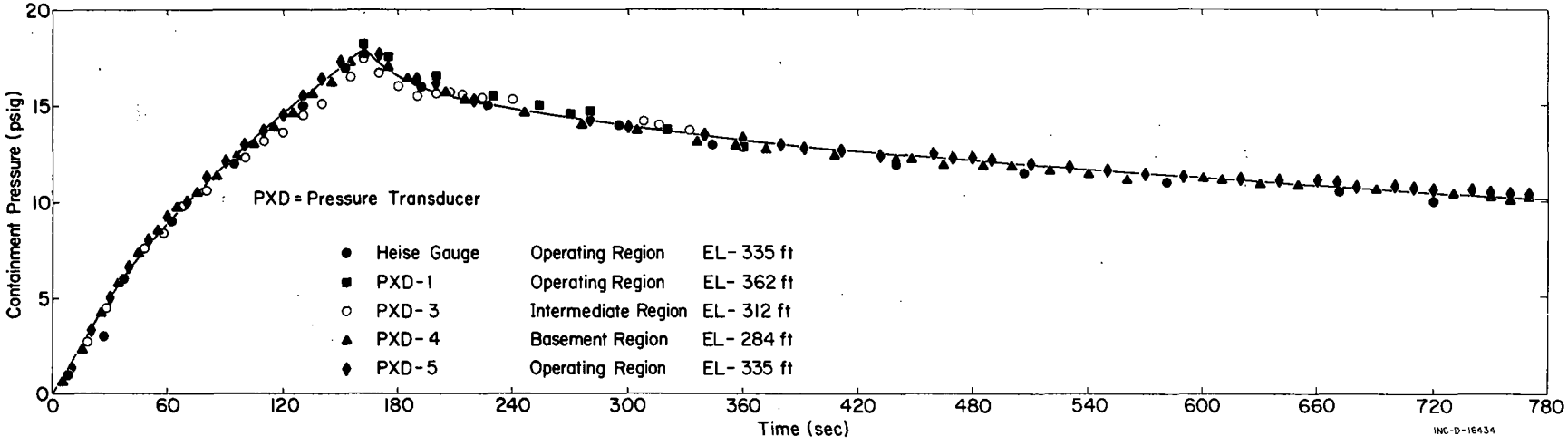

FIG. 12 CVTR CONTAINMENT PRESSURE RESPONSE -- PRESSURE TRANSDUCERS, TEST 3.

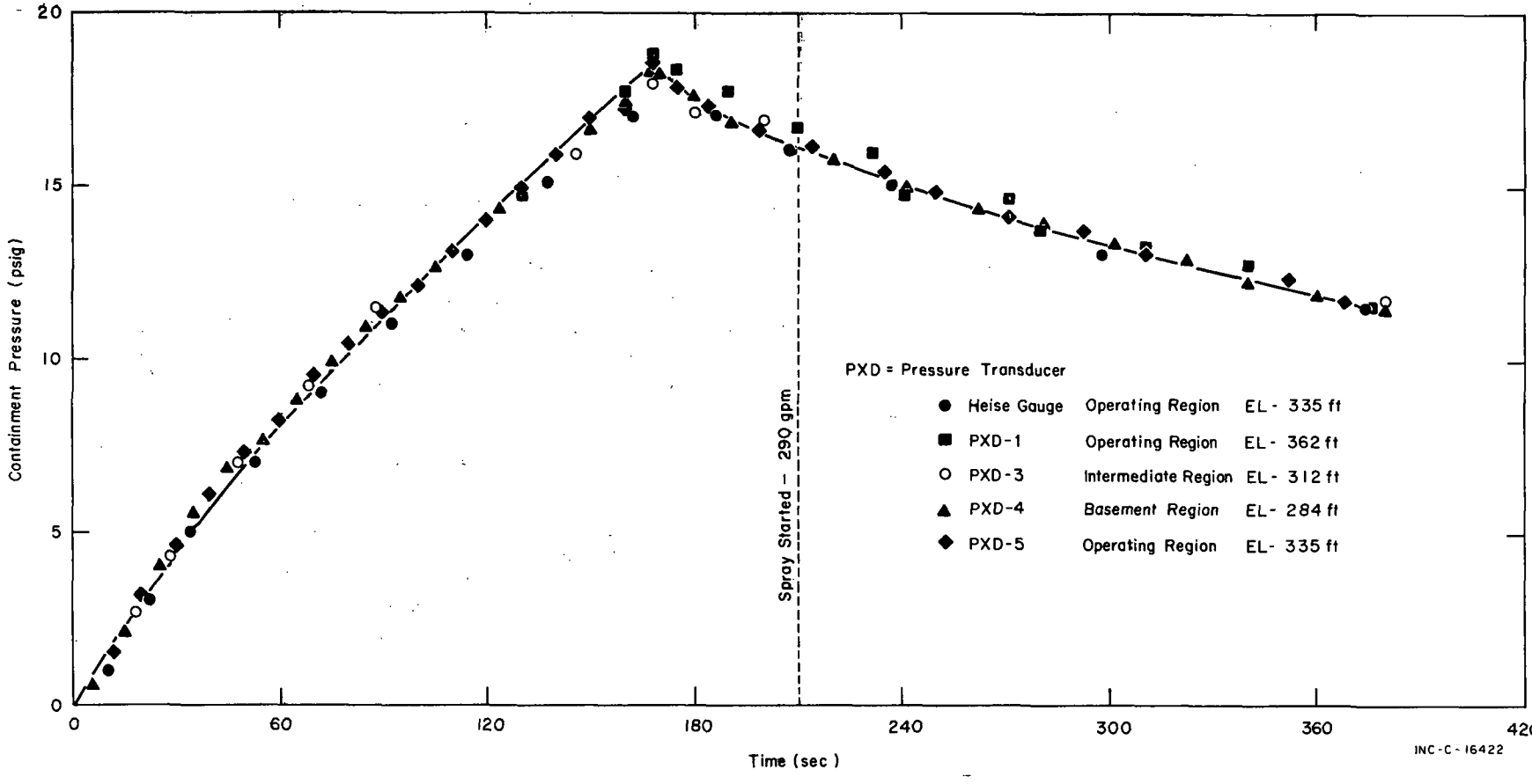

FIG. 13 CVTR CONTAINMENT PRESSURE RESPONSE -- PRESSURE TRANSDUCERS, TEST 4.

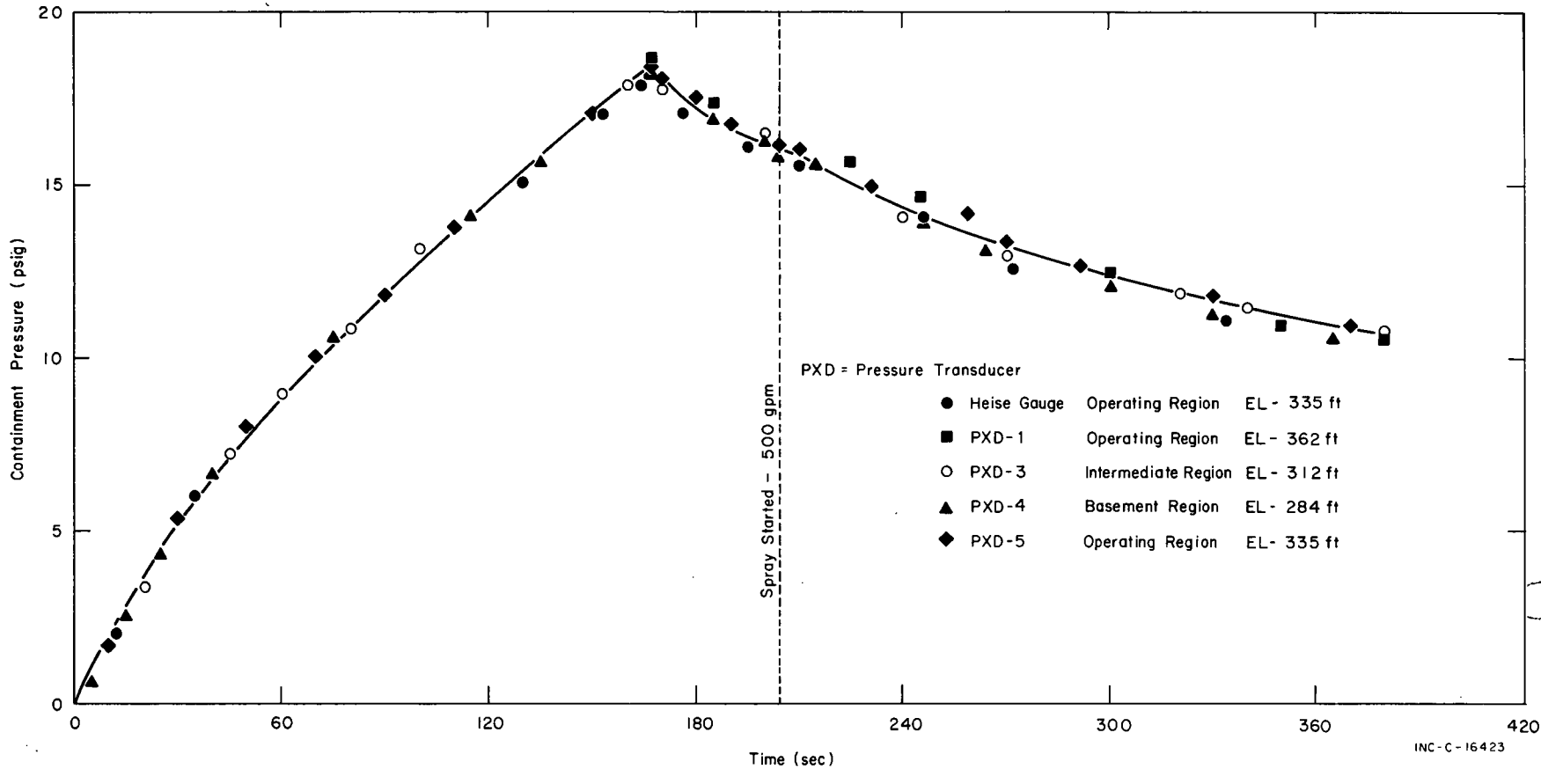

FIG. 14 CVTR CONTAINMENT PRESSURE RESPONSE -- PRESSURE TRANSDUCERS, TEST 5.

Pressure transducers were installed in the reactor header cavity and the fuel transfer canal to measure the pressure in those partially isolated volumes. An objective of those measurements was to determine whether any pressure or time of peak pressure differences existed between the partially isolated volumes and the main containment volume. The measurements for the header cavity, which had an almost unrestricted[a] flow area to the main containment volume of about 50 $in.^2$, showed essentially no difference in either peak pressure or time of peak pressure. In the fuel transfer canal, however, which had a connecting flow area of about 3 $in.^2$, a definite lag in time of peak pressure of about five seconds occurred during all three tests, which resulted in a pressure lag of approximately 1 psi. No differences in the magnitudes of the peak pressures were observed. The pressure lag indicates that for a highly compartmented containment with small connecting areas and a rapid blowdown situation, large pressure differences might result in structural damage.

The peak containment pressures produced during the steam tests, 17.9, 18.5, and 18.4 psig for Tests 3, 4, and 5, respectively, are reasonably proportional to the total amount of steam energy added and to the initial containment energy content (Table I). Test 5, which had a steam energy input slightly smaller than that of Test 3, resulted in a containment pressure about 0.5 psi greater than that of Test 3 because of the higher initial energy content of the containment. Previous steam tests caused an approximate 10°F higher initial temperature of the containment walls, liner, and internal structures for Test 5 than for Test 3.

3. TEMPERATURE HISTORY

During the steam injection tests, a number of containment measurements were made using thermocouples and resistance thermometers[b] to determine: (a) containment atmosphere vertical temperature profiles; (b) containment liner vertical temperature profiles; (c) containment horizontal temperature profiles (including the liner); (d) containment concrete surface temperatures at various locations; and (e) temperature of the partially isolated containment volumes (the header cavity and the fuel transfer canal).

3.1 Atmosphere Vertical Temperature Profile

Containment atmosphere vertical temperature profiles were determined by using data from temperature measuring devices that were positioned as nearly as possible at the same radius and angle from the containment center, but which were located at different containment elevations. The vertical temperature profiles for Steam Tests 3, 4, and 5, as determined by four thermocouples, are shown in Figures 15, 16, and 17, respectively. As can be seen,

---

[a] Absolute filters were installed above the header cavity so that all air passing to or from the header cavity had to pass through the filters. The filter area was 16 ft^2 and provided very little restriction to air flow.

[b] The exact locations of all temperature measuring devices are shown in Appendix A, Tables A-I and A-II.

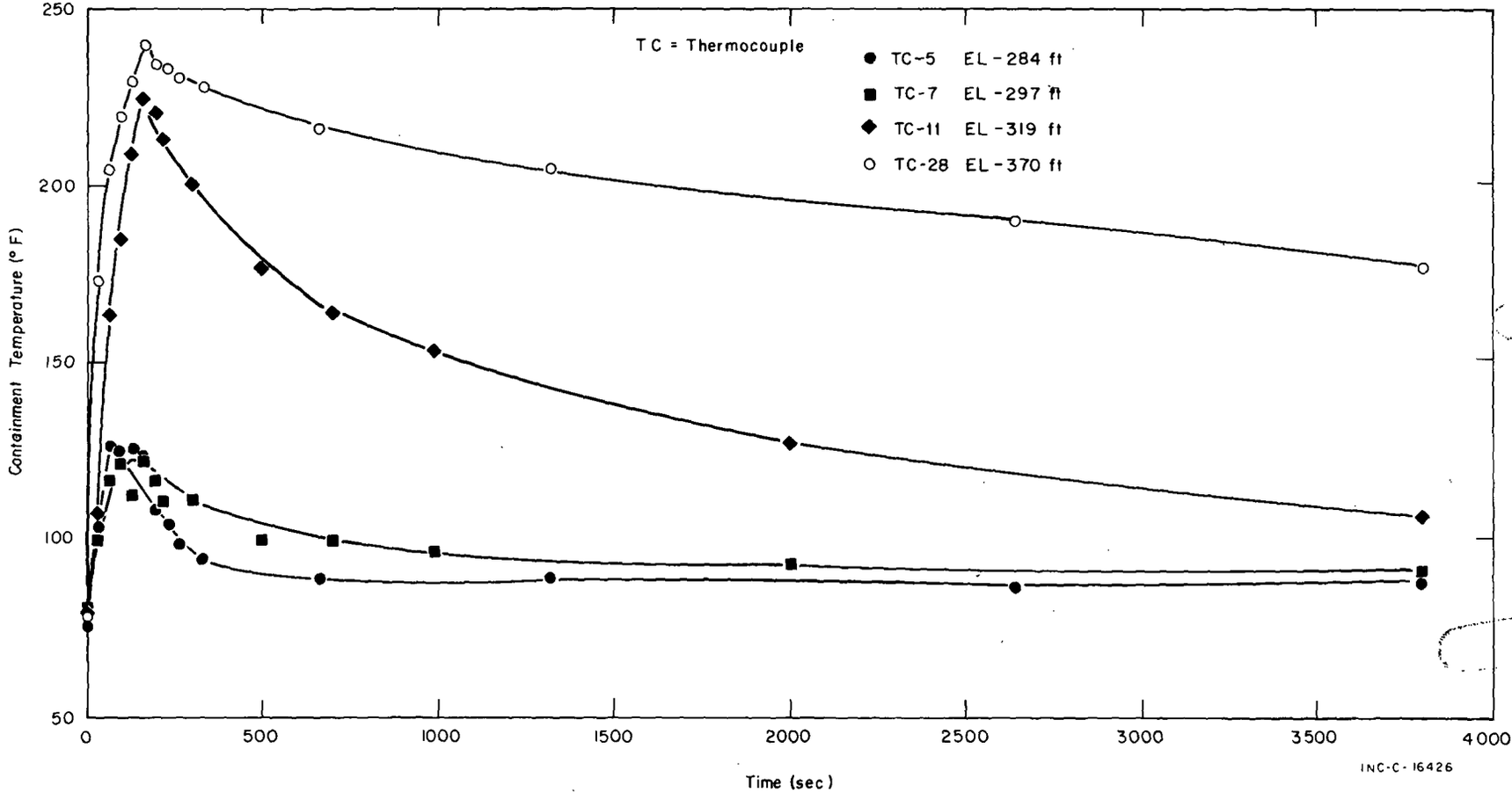

FIG. 15 ATMOSPHERIC VERTICAL TEMPERATURE PROFILE, TEST 8.

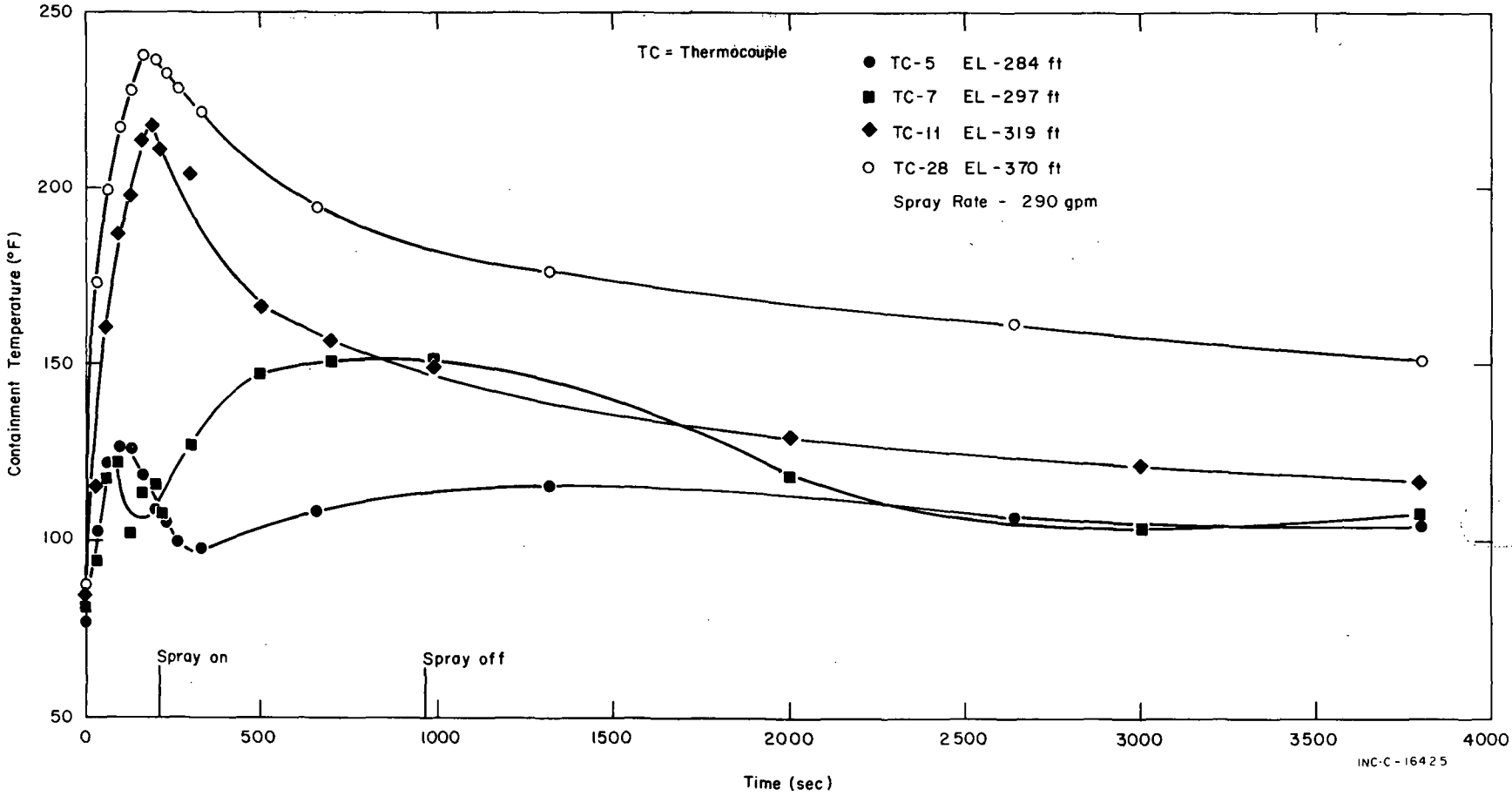

FIG. 16 ATMOSPHERIC VERTICAL TEMPERATURE PROFILE, TEST 4.

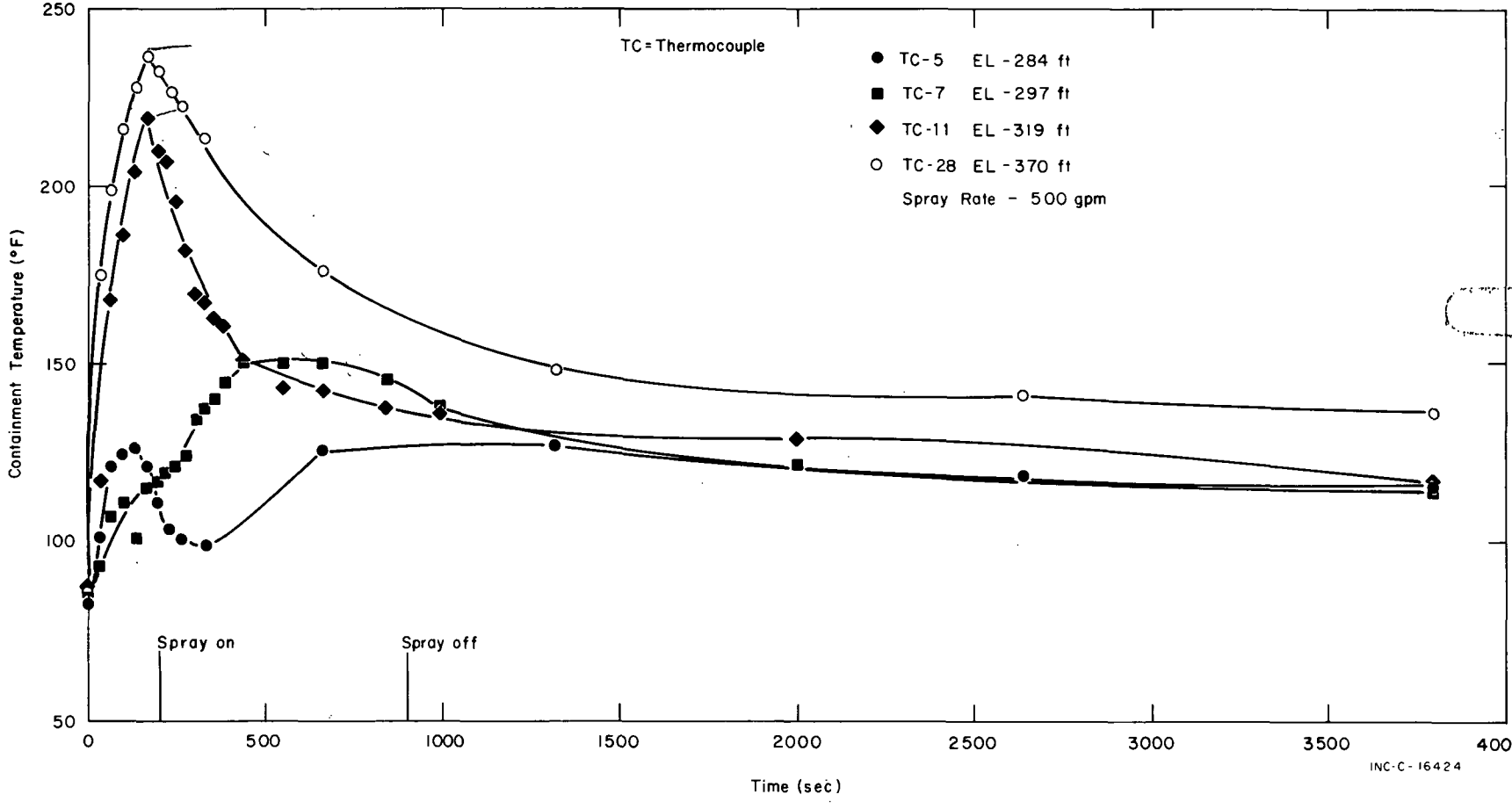

FIG. 17 ATMOSPHERIC VERTICAL TEMPERATURE PROFILE, TEST 5.

during steam injection the thermocouples showed essentially the same trend for all three tests; that is, the thermocouples exhibited rapid temperature rise with the operating region having the highest temperature and the basement region having the lowest temperature. Following steam injection, however, the temperature profiles become significantly different because of the activation of the containment spray systems during Tests 4 and 5. Without the spray, large containment temperature gradients existed for as long as data were taken (about two hours). The spray, however, tended to bring the entire containment to a uniform temperature[a], with the rate at which the temperatures approached uniformity dependent upon the spray rate. For example, as can be seen in Figures 15, 16, and 17, one hour after test initiation the maximum differential containment temperatures were approximately 90, 47, and 24°F for Tests 3, 4, and 5, respectively. The effect of the spray can be seen in Figure 18, which shows the containment dome temperature for Tests 3, 4, and 5. One hour following termination of steam injection, the dome temperature was approximately 177, 155, and 137°F for Tests 3, 4, and 5, respectively. Thus, for Test 5 in which the spray system was operated for 700 seconds, the containment temperature decreased an additional 40°F as compared to the temperature for the test without sprays (Test 3). About 1-1/2 hours after initiation of Test 3 the containment air recirculation system was activated to determine the effect on containment temperatures. The results of this test are shown in Figure 19. As can be seen, an air recirculation system, although not as effective as a spray system, has a pronounced effect on containment temperatures.

[a] The spray tended to equalize the containment temperature by decreasing the temperature of the operating region and increasing the temperature of the basement and intermediate regions.

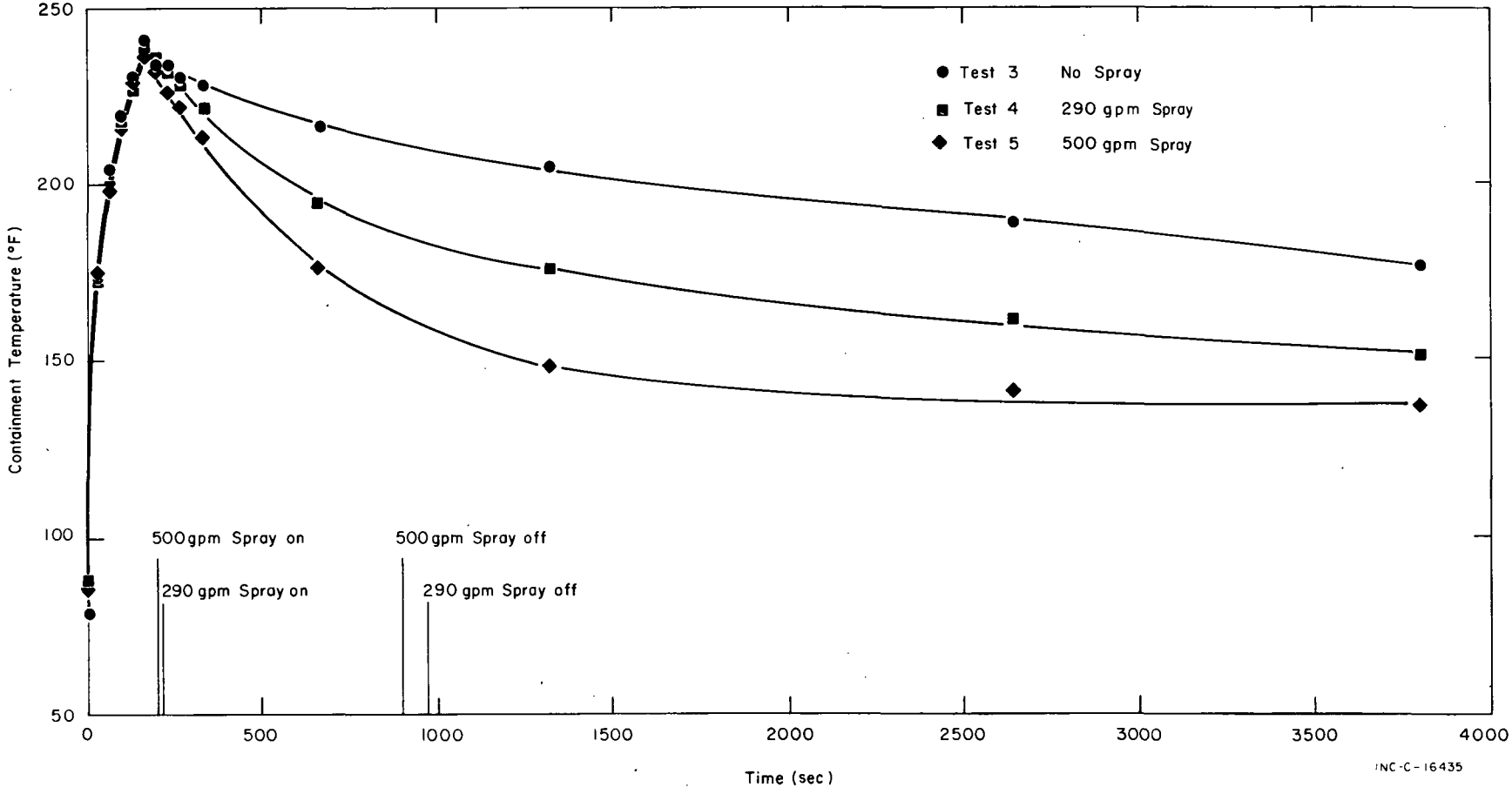

FIG. 18 CONTAINMENT DOME TEMPERATURES.

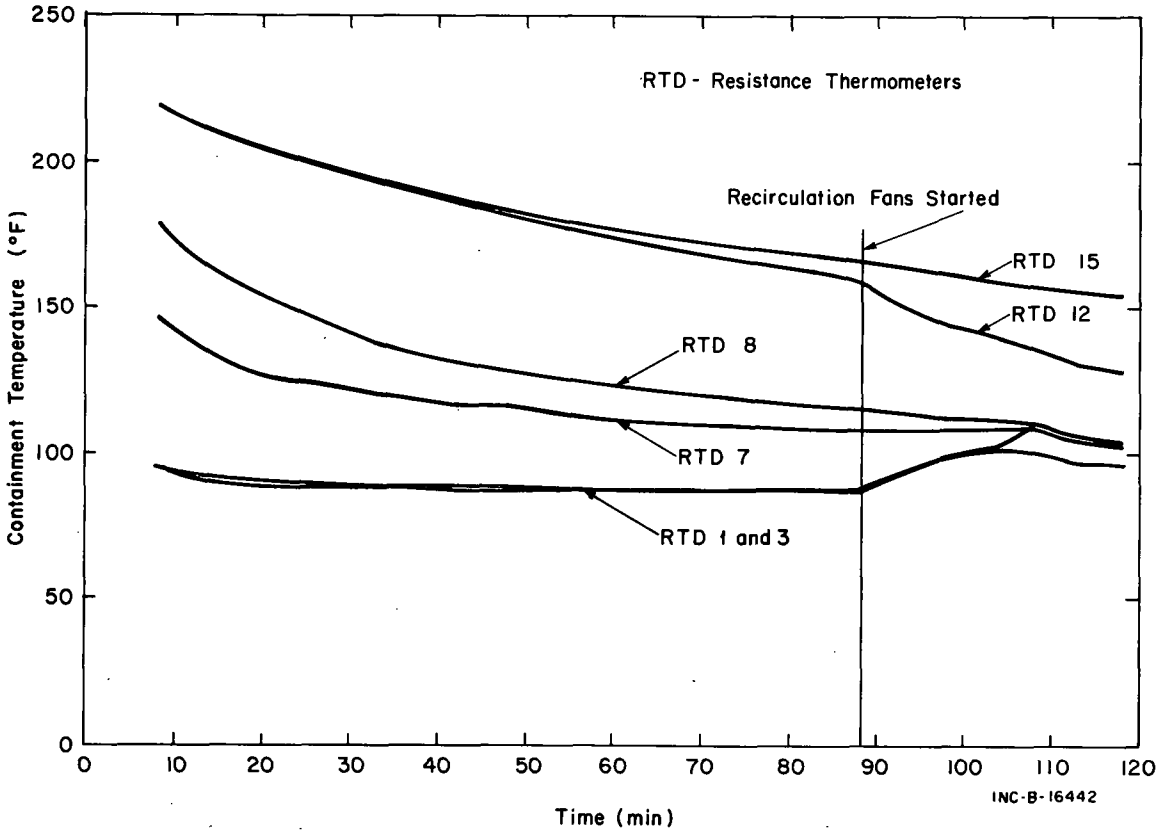

FIG. 19 TEMPERATURE EFFECT OF VENTILATION SYSTEM.

3.2 Liner Vertical Temperature Profile

Thermocouples were installed on the containment liner to provide liner temperatures during the steam tests. Data from these thermocouples were analyzed in a manner similar to that from the atmospheric thermocouples, with essentially the same results. That is, the higher the thermocouple was located in the containment, the higher the indicated liner temperature. In addition, each liner temperature was compared to an atmospheric temperature as obtained from an adjacent atmospheric thermocouple. These comparisons indicate that for the upper regions of the containment, the liner and atmospheric temperatures were almost identical. For the lower regions, however, as shown in Figures 20 and 21, the liner temperature exceeded that of the atmosphere. A possible explanation for the higher liner temperatures in the lower regions is that the steam, in moving from the operating region to the basement region, passed through the annulus surrounding the operating floor and down the containment wall, thus heating the wall rather than the atmosphere.

3.3 Horizontal Temperature Profile

Thermocouples in the operating region were arranged to provide a containment atmosphere horizontal temperature profile. Data from these thermocouples were analyzed to determine whether any horizontal containment temperature gradients existed either during or after steam injection. One hundred minutes of test data were analyzed with no significant temperature gradients or temperature trends identified.

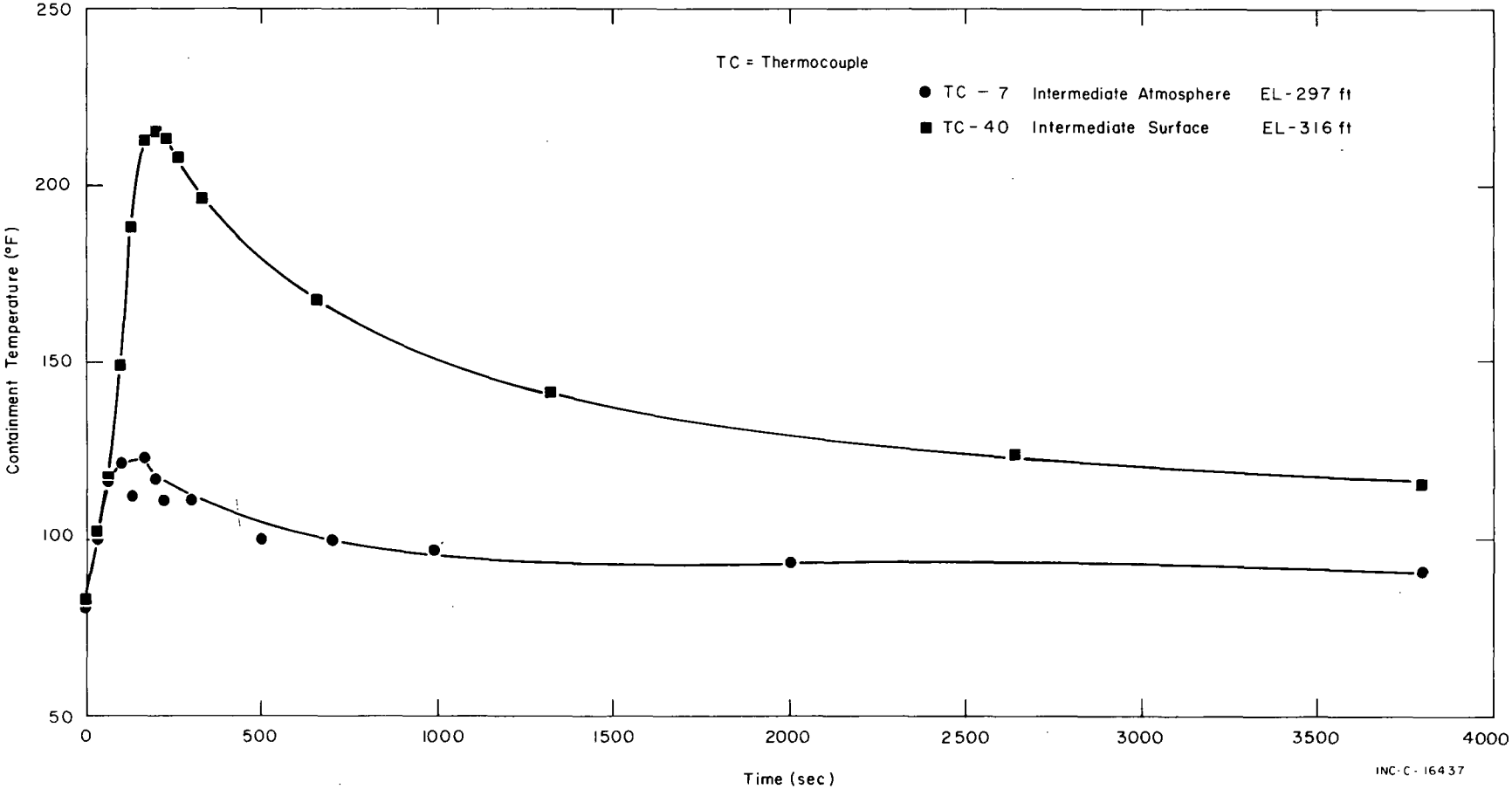

FIG. 20 SURFACE AND ATMOSPHERE TEMPERATURES — INTERMEDIATE REGION, TEST 3.

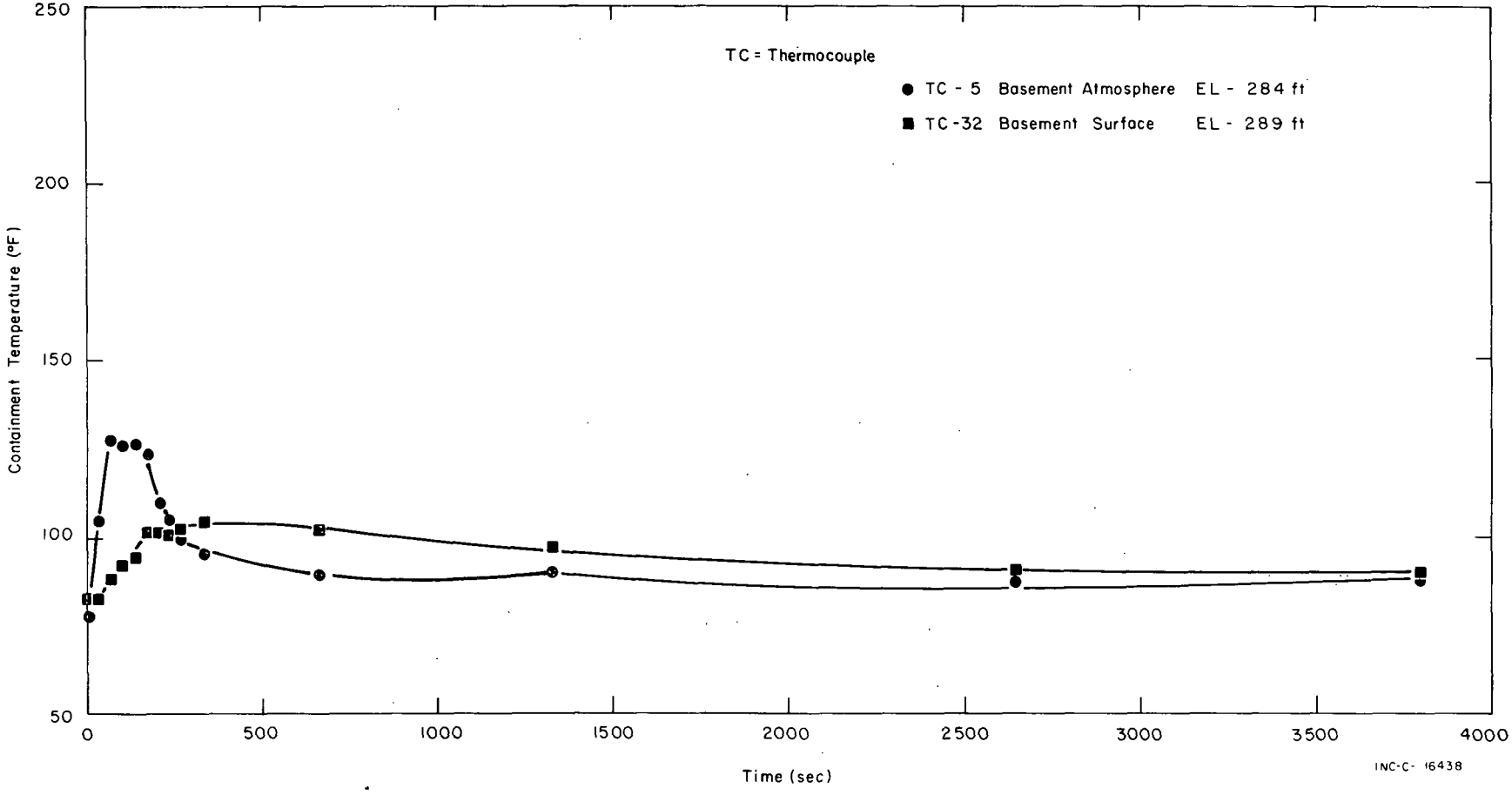

FIG. 21 SURFACE AND ATMOSPHERE TEMPERATURES -- BASEMENT REGION, TEST 3.

3.4 Concrete Surface Temperatures

Six thermocouples were embedded in concrete surfaces in the containment building to determine the response of these structures to steam injection. The concrete surfaces included the floor and a reactor support column in the basement, the wall of the fuel transfer canal, the reactor biological shield in the intermediate region, and the floor and the steam generator shield in the operating region. The data from these thermocouples, shown in Figure 22, indicated the same temperature pattern as the data from the atmospheric and liner thermocouples. That is, the operating region structures exhibited a large temperature increase, whereas the basement region structures exhibited essentially no temperature increase.

3.5 Isolated Region Temperatures

One thermocouple was installed in the reactor header cavity and another in the fuel transfer canal to monitor the temperatures of these partially isolated regions during the steam tests. For Test 3, the results obtained from these thermocouples are shown in Figure 23. As can be seen, only slight temperature increases were recorded in either region, and in both regions, the temperature rapidly returned to normal following termination of steam injection.

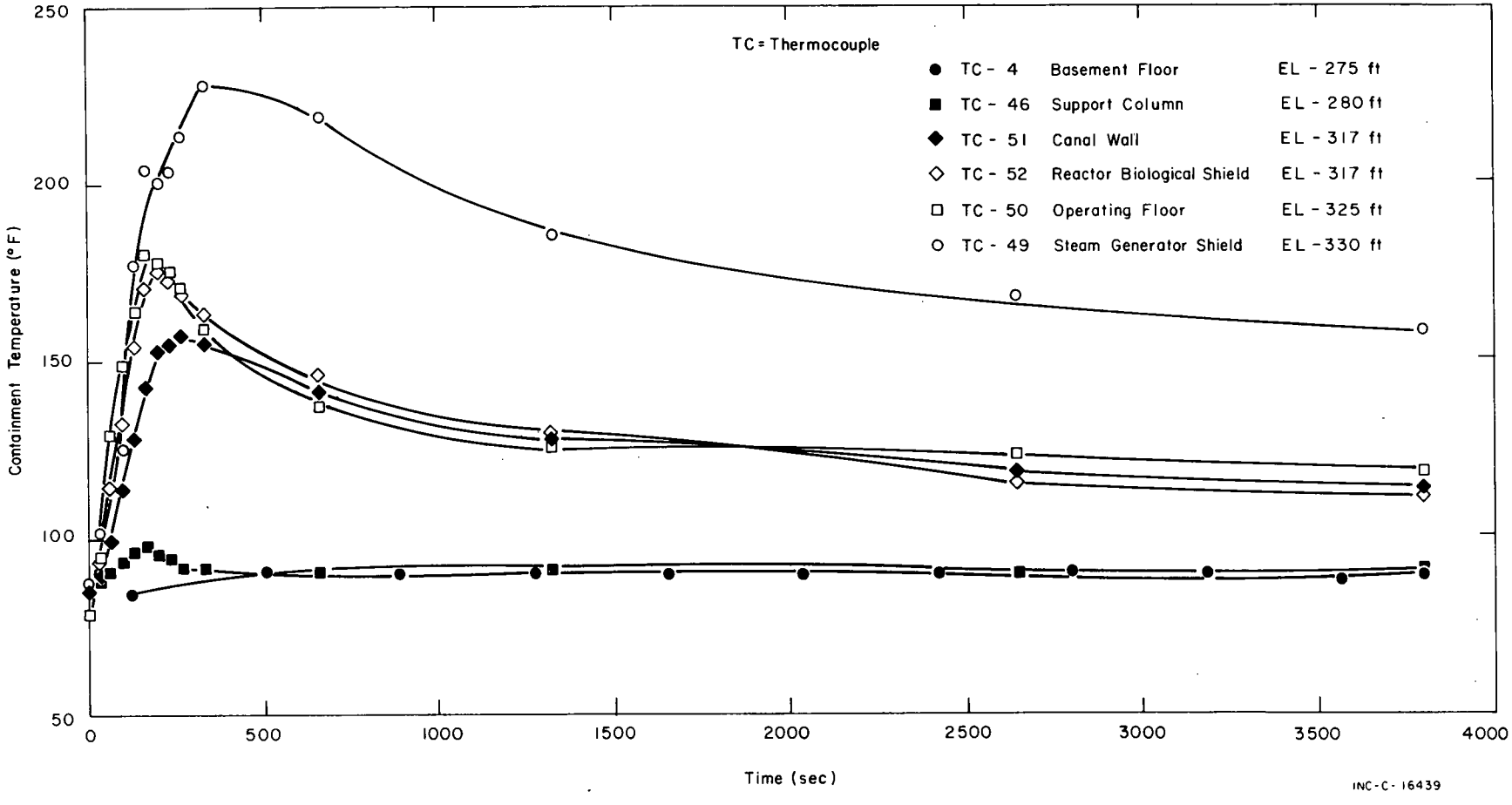

FIG. 22 CONCRETE SURFACE TEMPERATURES -- TEST 3.

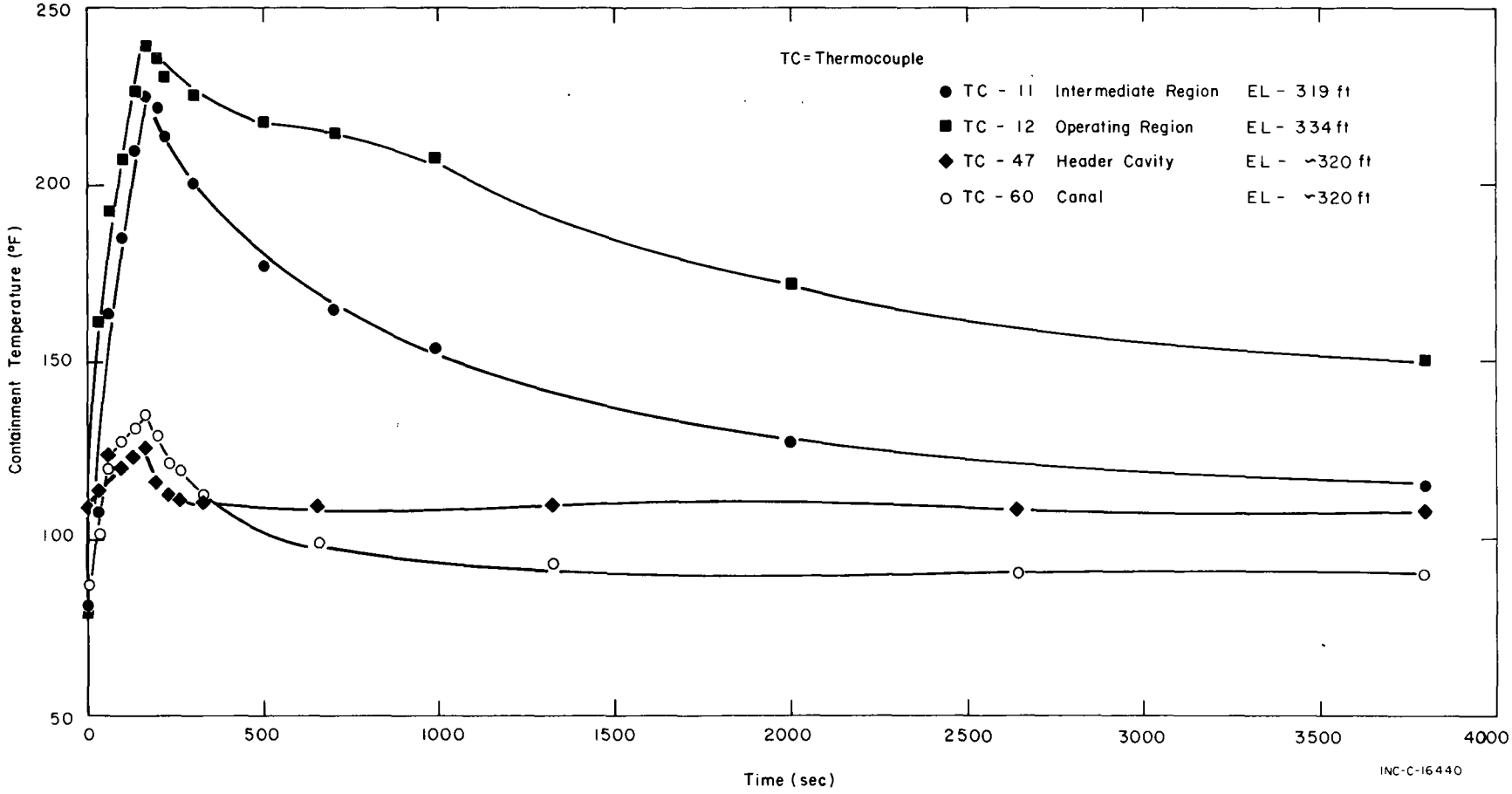

FIG. 23 ISOLATED CONTAINMENT REGION TEMPERATURES.

4. PRESSURE REDUCTION SPRAY

Objectives of the CVTR DBA tests were to determine the containment response to, and the effectiveness of, a containment pressure reduction spray system. To achieve these objectives, a containment pressure reduction spray system was installed in the CVTR containment vessel at the bend line (Figure 4), and was operated during Tests 4 and 5. The number and types of nozzles[a] used during each test are shown in Table II. The nozzle arrangement is discussed in Section II-2.2.

During Tests 4 and 5, the spray system was initiated about 35 seconds following termination of steam injection; the spray system was operated 12-1/2 and 11-3/4 minutes for Tests 4 and 5, respectively.

TABLE II

CVTR SPRAY NOZZLES

Nozzle (Spray Systems Company)	Number of Nozzles Test 4 (290 gpm)	Test 5 (500 gpm)
3/4-inch Type 7G3	8	16
1-inch Type 11-1/2 F18	4	8
1-1/2-inch Type F35	4	8

The approximate spray pattern was determined by arranging spray catch cans on two quadrants of the reactor operating floor (Appendix A-I.4), and by measuring the amount of water in each catch can following each test. Shown in Figures 24 and 25 are the spray distributions for Tests 4 and 5, respectively. As can be seen, both nozzle patterns provided good coverage of the containment. Isolated regions (generally adjacent to the containment wall) had less water coverage than average; however, the least coverage measured was still about 0.022 gal/ft^2-min. A slightly better spray coverage might have been obtained had the 3/4-inch nozzles been directed downward at an angle of 45° rather than at an angle of 30°.

Figure 26 illustrates the effect of the spray on the containment atmosphere temperature for the three DBA tests. Data from a single thermocouple located in the upper region of the containment volume (TC-23, at an elevation of 350 ft) were used for this figure and, as can be seen, the spray action significantly reduced the containment atmosphere temperature in this region with the rate of decrease almost directly proportional to the spray flow rate.

Figure 27 shows the effect of spray on the containment pressure decay for the three DBA tests. The spray was effective almost immediately in reducing the containment pressure, and continued to be effective throughout the operation of the spray system. As expected, the greater the spray flow rate the more rapid the pressure decrease.

[a] The spray system flow rate was determined by the number of nozzles installed on the spray header.

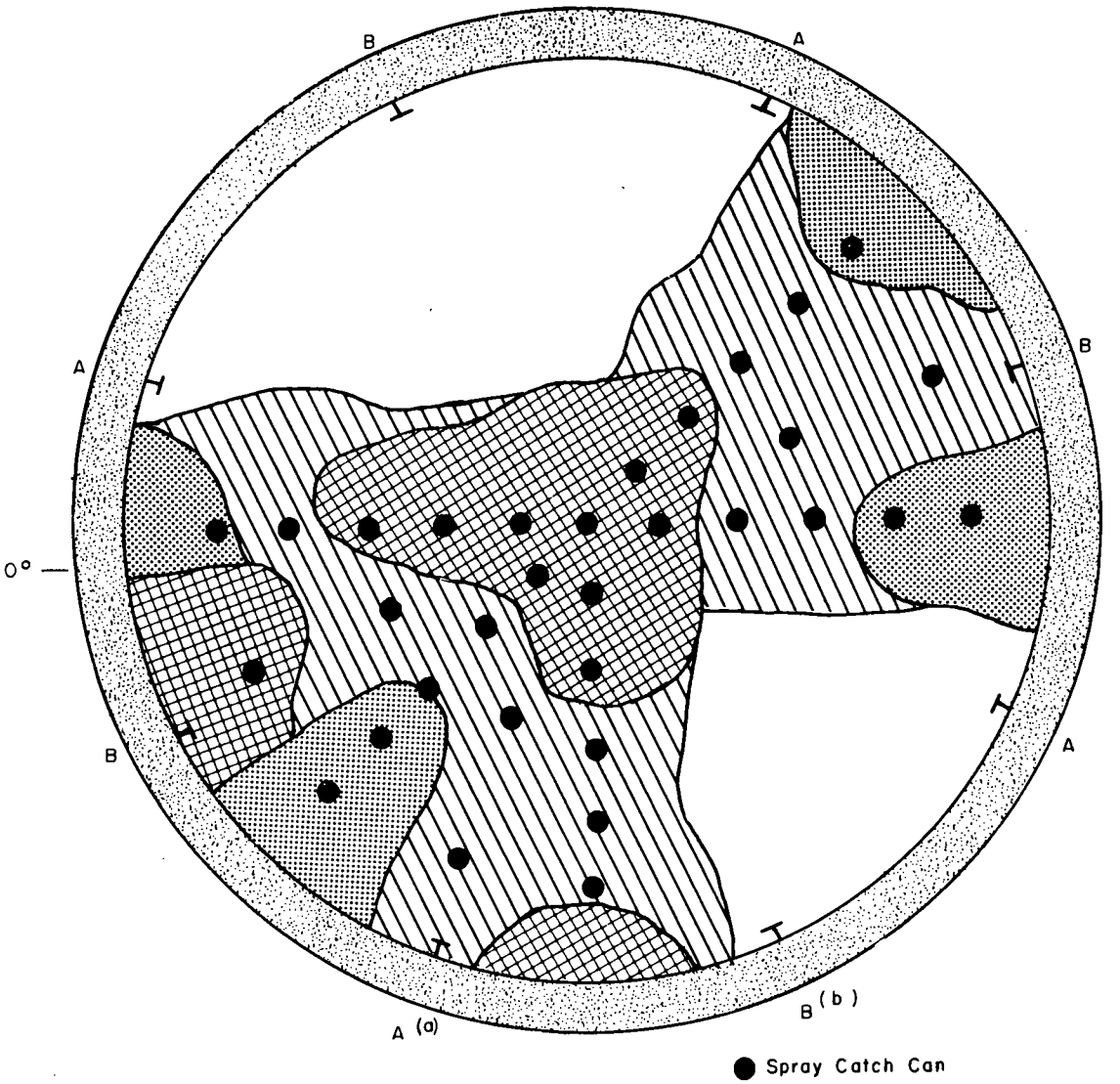

(a) A 3/4-inch Nozzle and a 1-1/2-inch Nozzle were Located at each A Nozzle Position

(b) A 3/4-inch Nozzle and a 1-inch Nozzle were Located at each B Nozzle Position

Light Spray – 0.021 to 0.077 gal/ft^2-min

Medium Spray – 0.077 to 0.23 gal/ft^2-min

Heavy Spray – >0.23 gal/ft^2-min

INC-A-16449

Area not Monitored

FIG. 24 SPRAY PATTERN, TEST 4.

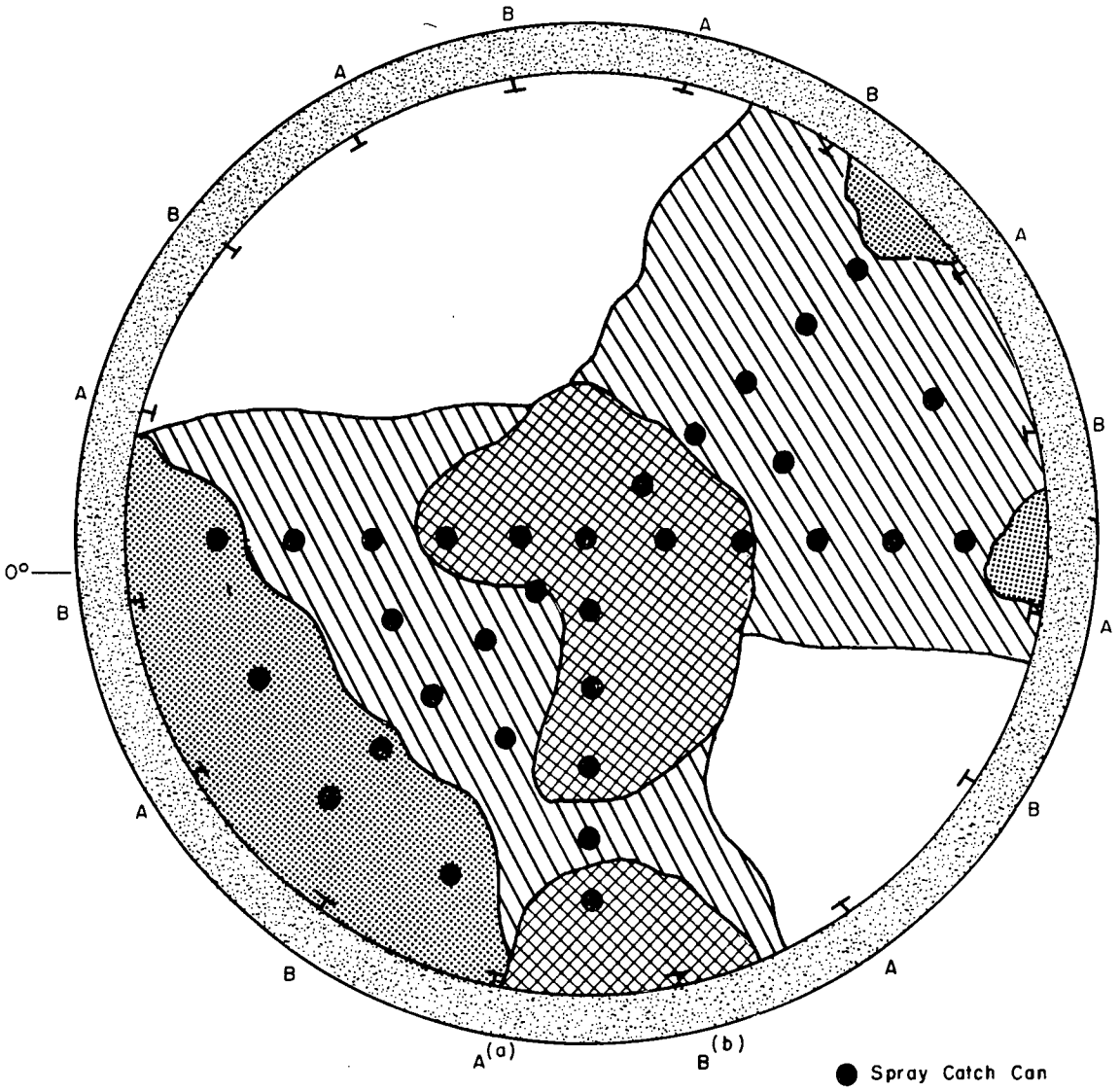

(a) A 3/4-inch Nozzle and a 1-1/2-inch Nozzle were Located at each A Nozzle Position

(b) A 3/4-inch Nozzle and a 1-inch Nozzle were Located at each B Nozzle Position

Light Spray – 0.053 to 0.13 gal/ft^2-min

Medium Spray – 0.13 to 0.35 gal/ft^2-min

Heavy Spray – >0.35 gal/ft^2-min

INC-A-16448

Area not Monitored

FIG. 25 SPRAY PATTERN, TEST 5.

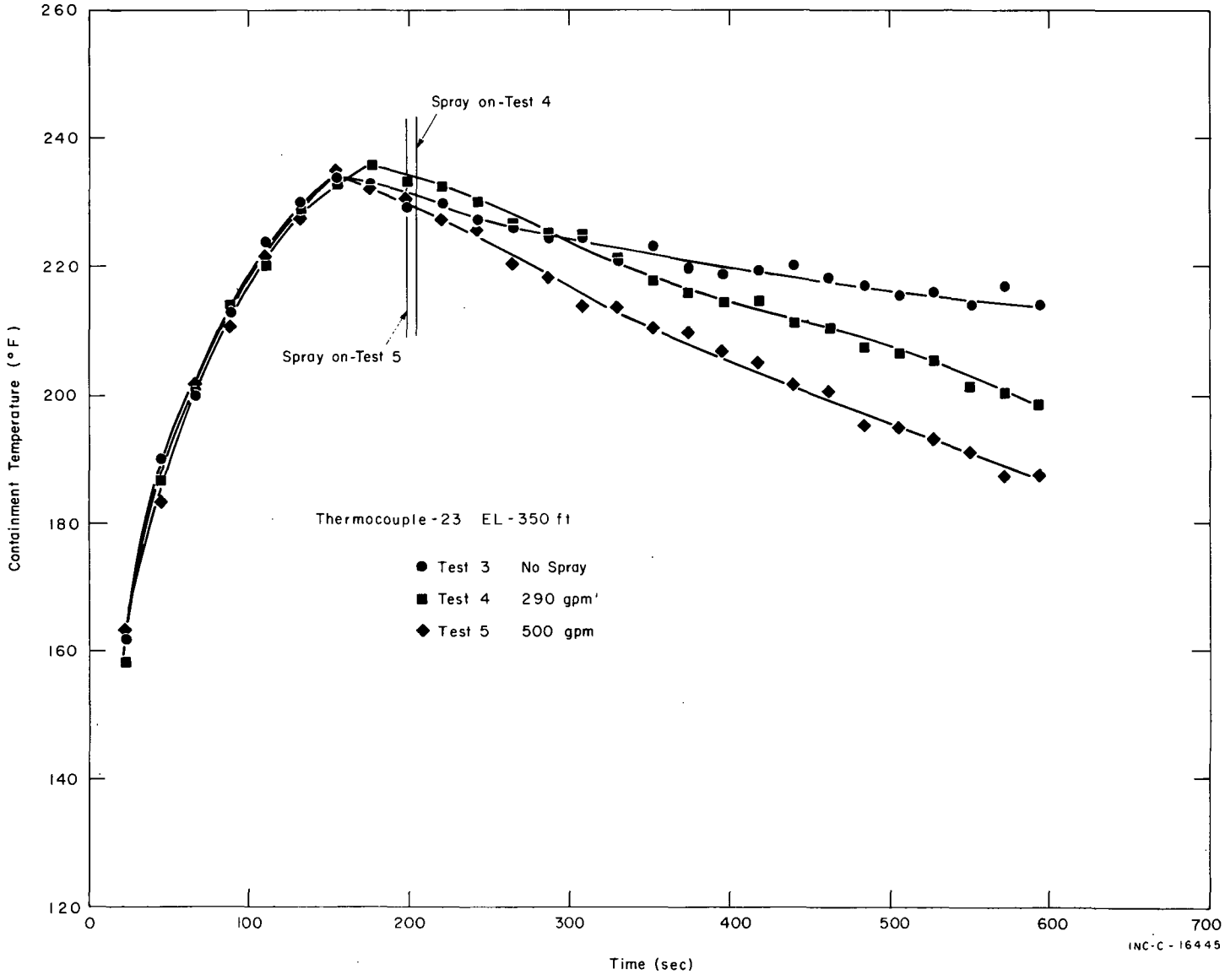

FIG. 26 CVTR SPRAY EFFECTIVENESS, TEMPERATURE.

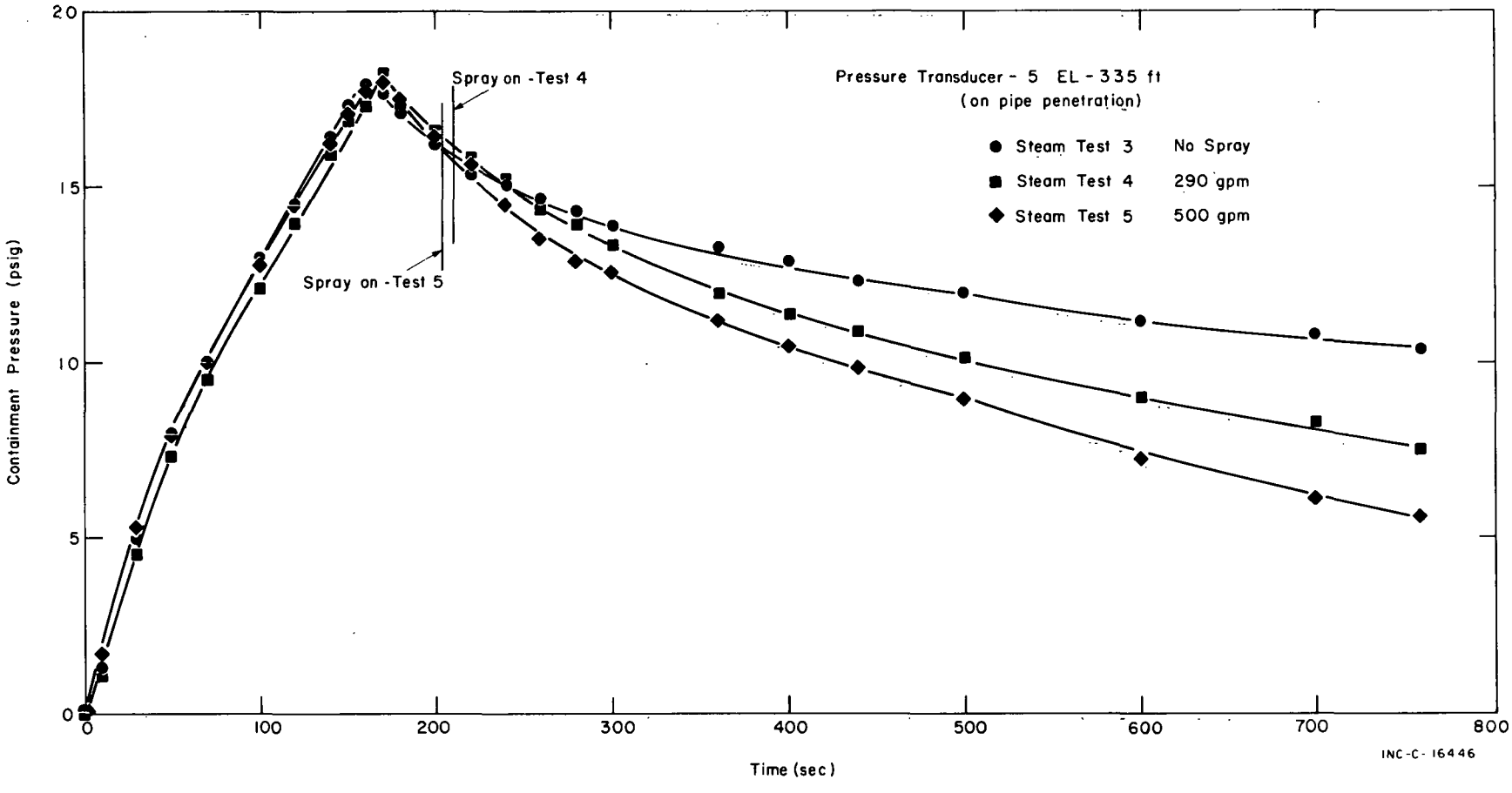

FIG. 27 CVTR SPRAY EFFECTIVENESS, PRESSURE.

The efficiency of the spray was determined by measuring the temperature of the spray at several heights in the containment operating region. Each temperature measurement was obtained from a thermocouple junction installed in the throat of a 4-in. funnel that was insulated with polyurethane to reduce the influence of atmospheric temperature. During spray system operation, as spray water was collected by each funnel, the temperature of the spray was measured by the thermocouple in the throat of the funnel. Five funnels were suspended at different heights in the operating region of the containment volume. Figure 28 shows a typical spray funnel.

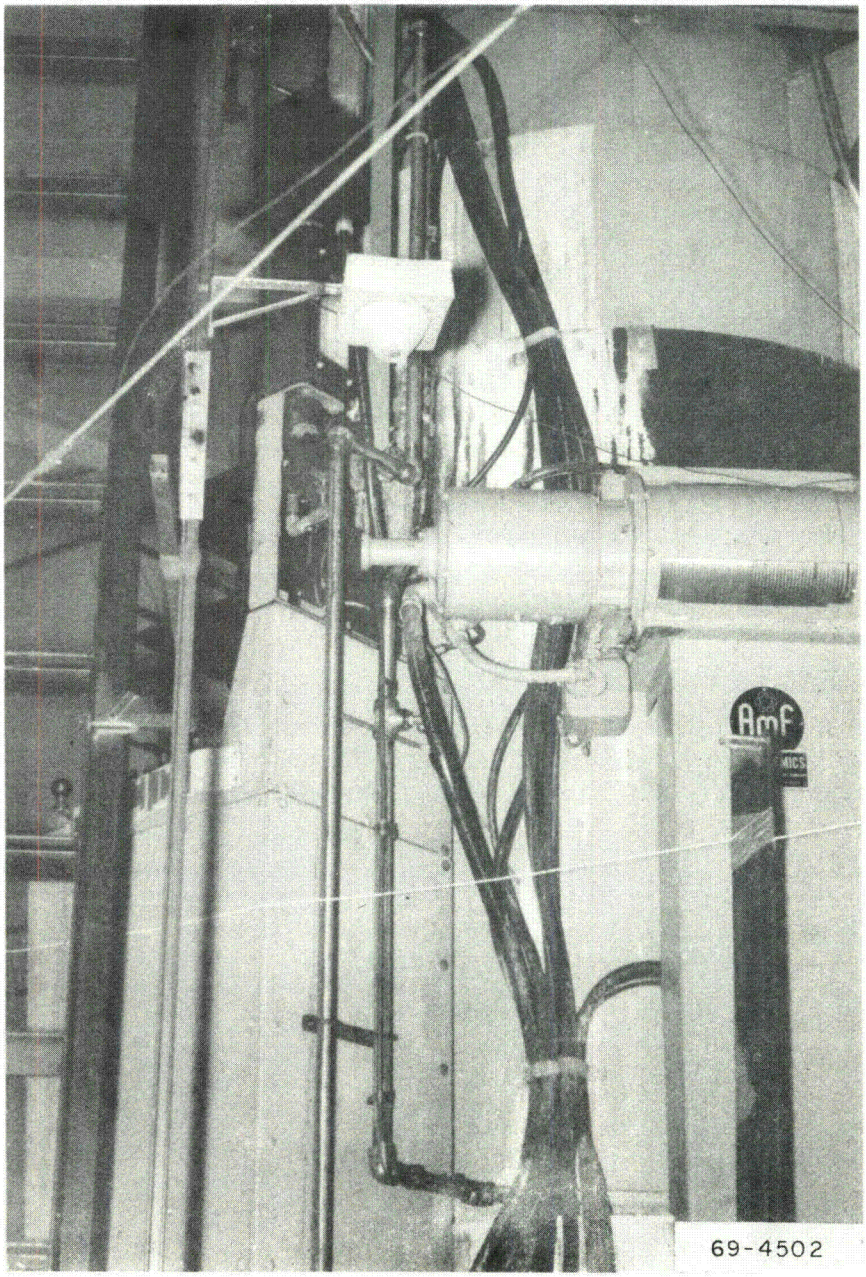

FIG. 28 TYPICAL FUNNEL ENCLOSING THERMOCOUPLE FOR DETERMINING SPRAY EFFICIENCY.

The temperature results of both spray tests indicate that the spray water was at thermal equilibrium with the containment atmosphere when it reached the nearest funnel, a distance of 31 ft. These results agree with reported heat transfer calculations[10], indicating that for 1000-micron droplets, 99% of thermal equilibrium is reached within a travel distance of 12 ft.

Figures 29 and 30 are plots of temperature versus time for the five thermocouples used to determine spray effectiveness and an adjacent thermocouple used to determine the temperature of the atmosphere during Tests 4 and 5, respectively. As can be seen, immediately following spray initiation the thermocouples for determining spray effectiveness indicated different temperatures and the temperature differences remained essentially fixed throughout the spray period. Also, the greater the spray rate, the smaller the temperature differences among the thermocouples. During the 290-gpm spray test, a temperature difference of 7.5°F was observed and during the 500-gpm spray test the difference was about 4°F. Thus, in addition to decreasing the containment temperature, spray also tends to equalize the containment temperature.

Nozzle plugging because of pipe scale was the only problem encountered during spray operation. During the semi-DBA test, performed about six months after installation of the spray system, the system was operated about 3 minutes. During this test, all of the 3/4-in. nozzles plugged with scale. The nozzles were removed from the spray header, the spray header was thoroughly flushed, the nozzles were cleaned, and a 40-mesh screen was installed in the body of each nozzle. Following the initial DBA spray test (Test 4, 290-gpm spray) all 3/4-in. nozzles were removed from the spray header and repositioned for Test 5. At this time two of the 3/4-in. nozzles were again found to be plugged and required cleaning. During Test 5 (500 gpm spray) nozzle plugging did not occur.

Because the CVTR spray system was temporary and was required to operate for only two tests, it was constructed of black-iron pipe. For permanent spray system installations, which may remain passive for years, the systems should be constructed of noncorrodable materials and should be kept dry during inactive periods.

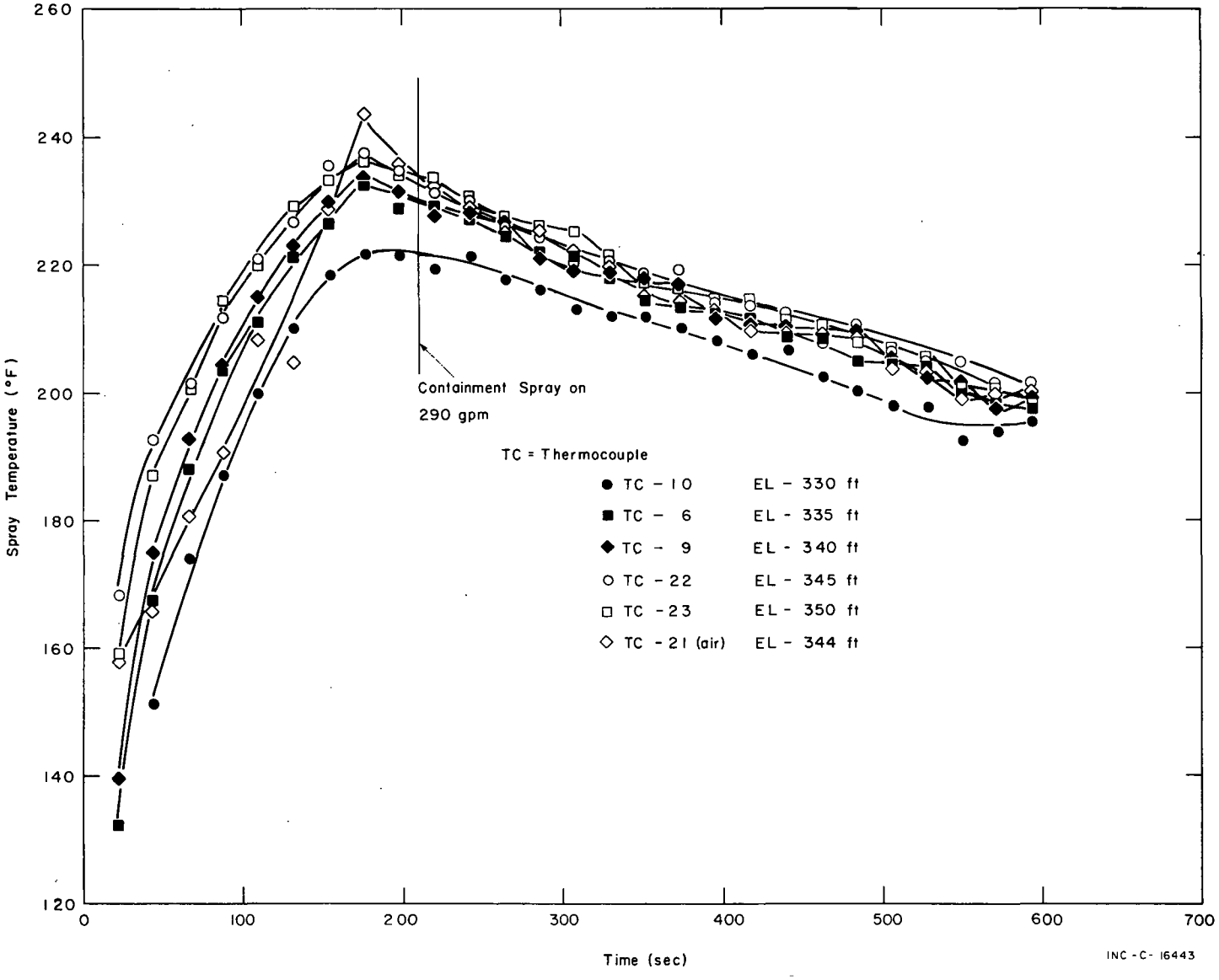

FIG. 29 SPRAY TEMPERATURES, TEST 4.

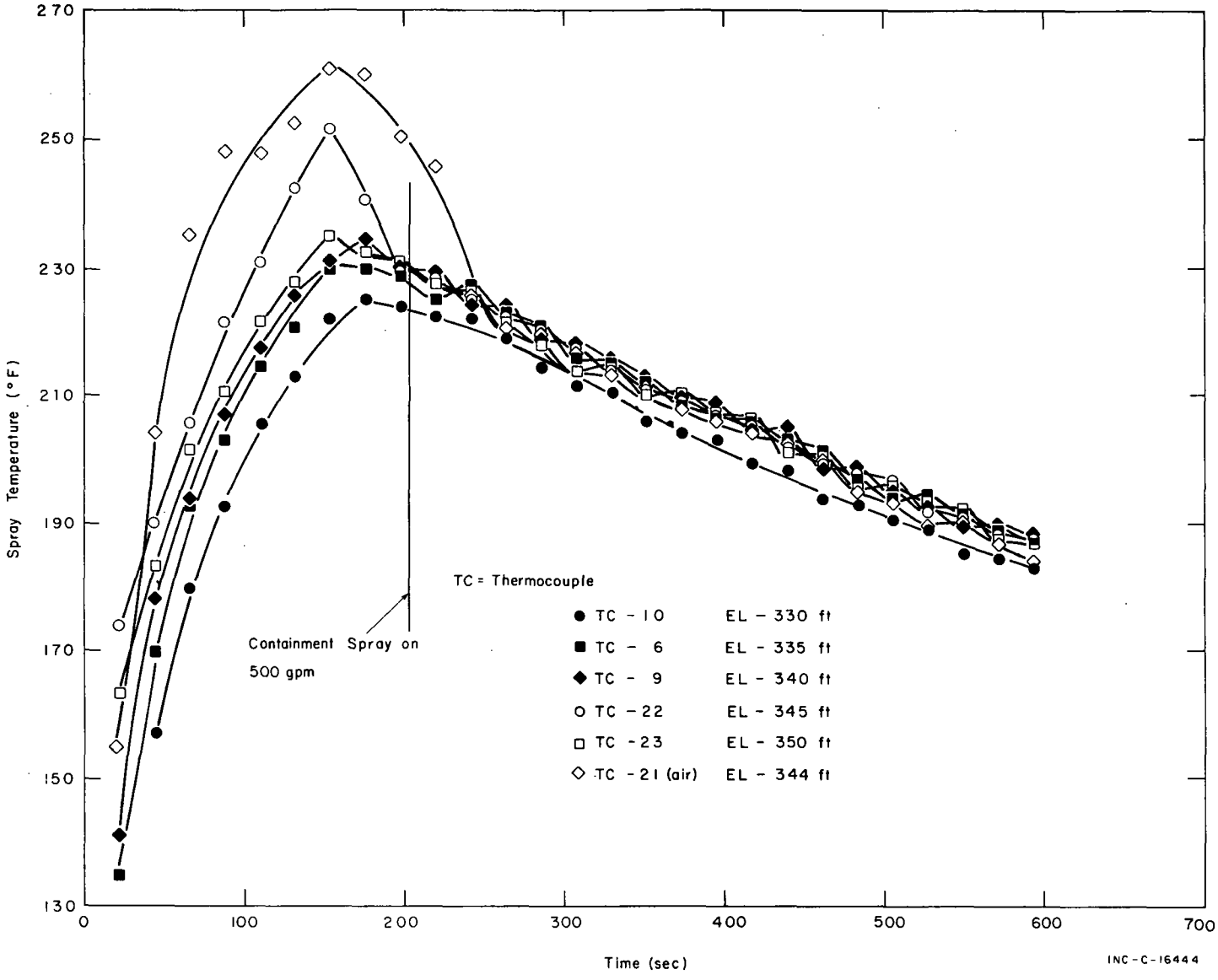

FIG. 30 SPRAY TEMPERATURES, TEST 5.

5. CONTAINMENT LINER STRAIN

Containment liner strain measurements were obtained at various conditions during the CVTR In-Plant Test Project. The measurements were made at 83 locations with three-component rosette strain gages. The primary purpose of the measurements was to provide backup data in the unlikely event of liner or containment failure because of testing. Although no failure occurred, some of the data were reduced and analyzed to determine strain magnitudes and stress patterns.

The CVTR containment is a reinforced concrete, right vertical cylindrical structure with a flat base and a hemispherical dome. Pressure retention is provided by the 2-ft-thick reinforced concrete walls of the cylinder section and by the 1/2-in.-thick steel dome. The cylinder walls and the flat base are covered with 1/4-in.-thick steel liner plates welded in 8-ft by 30-ft sections to metal support brackets fixed into the concrete structure. Each weld joint is covered by channel batten strips to insure leak tightness. The cylinder liner and the dome are sealed by a special transition section to make the containment volume vapor tight. The cylinder liner plates were installed following completion of the concrete structure. This construction technique resulted in gaps between the concrete wall surface and the liner plates, particularly in the central region of the plates.

5.1 Pressure Loading Analysis

Two separate analyses were performed to investigate the effects of pressure loading on the containment liner. The first method was a finite element axisymetric stress analysis using the computer code SAAS II[11]. For this analysis, the liner, reinforced concrete, and surrounding soil were assumed to act as a continuum (no gaps between materials or cracks in the concrete). The reinforcing was modeled as thin bonded plates located at radii corresponding to the rebar positions.

The second analysis assumed that the liner acted as a separate thin-walled cylinder. That is, sufficient gaps were postulated to exist between the liner and concrete for the liner to carry the entire pressure loading. The actual conditions of the structure varied between these two extremes, and thus, the analysis provided upper and lower bounds for the actual stress responses.

Figure 31 is a comparison of the analytical stress curves and experimental data representative of the stress on the cylinder liner plates. Experimental strain measurements near containment penetrations and joints were not considered in determining the indicated average stresses. As can be seen, the slope of the average experimental stress curve decreases with increasing pressure, indicating that the known gap between the central portions of the steel liner plates and the concrete walls is gradually closing as the pressure increases. Therefore, the CVTR strain measurements indicate that the liner initially assumed essentially the entire pressure loading for the structure. As the containment pressure increased, and the gap closed, the reinforced concrete began to assume a larger portion of the load.

The vertical bars on Figure 31 represent the range of data obtained from the strain gages examined. The large spread in data indicates the relative nonuniformity of the gap and other localized stress conditions.

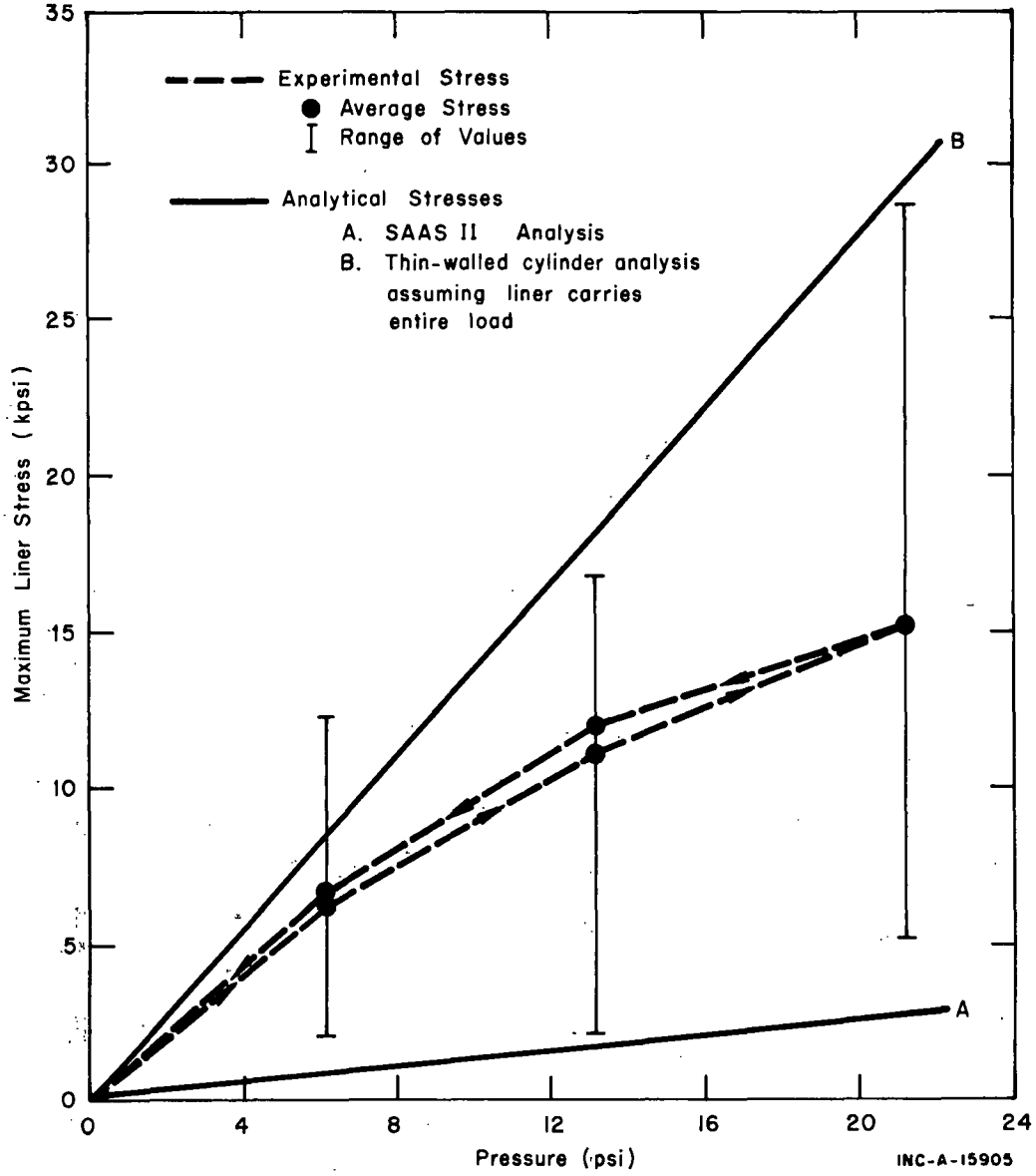

FIG. 31 COMPARISON OF ANALYTICAL AND EXPERIMENTAL MAXIMUM STRESSES IN THE CVTR LINER.

5.2 Dome-Cylinder Transition Loading

A theoretical analysis of the containment liner strain in the intermediate region of the transition zone[a] between the dome and the cylinder was performed through the use of the SAAS II computer program. No gap was assumed to exist between the liner and the concrete. The results of this analysis and the measured stress for a 21-psig containment leakage rate test[7] are shown in Table III.

---

[a] Data from seven strain gages were used for this analysis. Two gages were located on the 1/2-inch-thick dome plate about 3 and 6 inches above the dome-cylinder joint cover plate; three were located on the 1/4-inch-thick cylinder plate about 3 and 6 inches below the dome-cylinder joint cover plate; and two were located on the dome-cylinder joint plate which was welded over the dome-cylinder joint.

TABLE III

COMPARISON OF ANALYTICAL AND EXPERIMENTAL STRESSES FOR THE DOME-CYLINDER TRANSITION ZONE FOR A CONTAINMENT PRESSURE OF 21 PSIG

Strain Gage	Strain Gage Location	Experimental Stress (psi)	SAAS II Analysis (psi)
45	Dome	3815	1712
46	Dome	3379	1763
47	Transition region	3756	1335
48	Liner	7399	1656
49	Liner	7288	1689
52	Transition region	-2519	1335
53	Liner	3603	1656

The lack of agreement between the two values is attributed to gaps between the liner (dome and cylinder) and the concrete.

Because of the method of construction of the cylindrical section of the containment, and as observed when two holes were drilled through the liner for the heat plugs (Section II-5.4), gaps were known to exist in this section of the containment. Therefore, the assumption of gaps in this region of the containment to explain the discrepancy of Table III is considered valid. The transition region plate was also installed with a known air gap between it and the liner. Thus, the assumption is also valid for this region. The dome liner, however, was installed before the 20-inch concrete cover was poured, and any gap would be a result of concrete shrinkage upon curing. If a 1- to 20-mil gap is assumed to exist between the dome liner and concrete, the discrepancies of Table III can be explained. A gap of this size is considered not only feasible but probable. Thus, gaps are postulated to be the major reason for the discrepancies of Table III.

Calculations of the dome loading for a 21-psig pressure condition in which no concrete support was assumed resulted in a stress level of about 7,500 psi. Thus, the measured values again fall between the two boundary calculations.

5.3 Permanent Deformation

Through use of a Tresca (maximum shear stress) yield criterion, the experimental stresses were evaluated to determine which gage locations experienced local yielding. Initial stresses resulting from such features as welding and gage installation were not considered in the evaluation. No indication of yielding was obtained as a result of the ambient temperature-pressure loading. During pressure-temperature loading resulting from the

high temperature (about 200°F) leakage rate tests[7] in which the containment was slowly heated to about 200°F while a constant pressure of 21 psig was maintained, several gages appeared to have experienced some permanent deformation. The gages were randomly located, however, and no yield pattern was evident.

5.4 DBA Loading Analysis

The strain gage data from the containment liner obtained during the steam (DBA) tests were also examined. However, since analytical stress evaluations were not performed, only general observations are reported.

Liner stresses were found to be higher during DBA testing than the stresses measured at comparable pressures during the ambient temperature or the hot air leakage rate tests[7]. These higher stresses would be expected, however, since during DBA testing, the rapidly applied heat and pressure caused significant liner temperature gradients that added thermal stress effects to the loading. An examination of the stresses based on a Tresca yield criterion indicates that the higher stress levels produced yielding at all of the strain gage locations examined except one. The combined temperature-pressure stresses that exceeded the metal elastic limit probably explains why a large number of gages became inoperative following the first steam test.

Current reinforced concrete type containment structures are generally constructed by using the steel liner as the internal concrete form. (The CVTR liner, except for the dome, was welded in place after the concrete structure was completed). Use of the liner as a concrete form is expected to prevent large gaps between the liner and the concrete. However, concrete shrinks to some extent upon solidification and slight gaps will probably exist.

IV. CONTAINMENT HEAT TRANSFER PROPERTIES

The pressure, temperature, and structural response of a power reactor containment during or following a DBA will be a strong function of the heat transfer processes occurring within the containment. During the initial phases of the primary system blowdown, heat transfer to heat absorbing structures from the containment air-steam mixture is the principal heat transfer process and such heat transfer acts to limit the initial peak containment pressure. Later in the blowdown period, the operation of containment safety systems, such as pressure reduction sprays, fan coolers, and decay heat removal systems, also affects the containment pressure and temperature, but safety systems are usually incapable of reacting on a time scale sufficiently short to influence the magnitude of the initial pressure peak.

Although the CVTR DBA tests were directed toward investigation of the structural heat transfer process during blowdown, including the effect of heat transfer on the initial pressure peak, they also contributed information on structural heat transfer at later periods in the blowdown and on pressure reduction spray effectiveness.

The effect of heat transfer on pressure response was examined in a recent analytical study[12] for the PWR large break case, and when the results were compared with adiabatic pressurization, decreases in the calculated peak pressure of up to about 15% were indicated for a range of atmosphere-to-structure heat transfer coefficients between 0 and 290 Btu/hr-ft^2-°F. Thus, heat transfer is related to design limits, construction costs, and margin of safety considerations.

The heat transfer process is dependent on many variables such as steam concentration and distribution, condensation mode, thermal resistance of the condensate film, surface conditions, wall heights, condensing surface geometry, concentration of impurities and noncondensables, time after accident, and steam turbulence. Generally a detailed space-time solution for localized heat transfer coefficients is unachievable. A practice in containment response calculations for the safety analysis of power reactors is to use area-averaged heat transfer coefficients. The average coefficient permits estimation of total structural heat absorption and, consequently, the average containment pressure-temperature transient. However, the localized response may significantly differ from the average behavior. The possibility of local conditions exceeding design stress limits, pressures, or temperatures is of particular concern near the blowdown source.

Very little experimental heat transfer data exist that are directly applicable to large power reactor containments. Currently, heat transfer correlations that are based on data obtained from small-scale experiments or from analytical considerations are being used. Consequently, uncertainty exists as to the accuracy and applicability of these empirical correlations. For example, the Tagami correlation[13, 14] is often used for the maximum heat transfer coefficient during the steam blowdown or most turbulent period of a postulated DBA accident. However, the data from which this correlation was derived were obtained from a small-scale experiment atypical of large containments and the correlation was published with reservations as to the applicability for a different system.

A primary purpose of the CVTR simulated DBA tests was to examine heat transfer processes within a representative power reactor containment under conditions approaching those that might be encountered during a DBA occurrence. No attempt was made to duplicate any particular postulated CVTR accident; instead, the tests were designed to result in conditions that would be within those which the containment structure was designed to withstand (215°F, 21 psig). The steam injection system has been described (Section II); the injection time and steam conditions were noted to be about 170 seconds and 1200 Btu/lb, respectively.

The 10-in. steam injection line was dimensionally comparable to the 8- and 10-in. main coolant piping at CVTR and the injection time was also comparable to the predicted blowdown duration (about 100 sec) for a postulated CVTR pipe rupture. Thus, the tests were fairly representative of a possible CVTR pipe break or of an intermediate size break in other facilities. However, because of the large fluid enthalpy and long blowdown time, the tests are not necessarily representative of PWR large break, subcooled blowdowns. For large breaks, blowdown durations of about 15 sec and fluid enthalpies of about 550 Btu/lb are generally applicable. Mass expulsion properties, water carryover, condensation behavior, thermal stresses, dynamic effects and other characteristics of subcooled fluid expansion through a PWR large break are different from those of the saturated steam injection tests of the CVTR. Nevertheless, many of the trends in heat transfer behavior of the CVTR tests are expected to be applicable to the large break or fast blowdown case.

The principal measurements used to determine the heat transfer behavior in the CVTR containment are as follows:

(1) Containment wall interior temperature response (heat transfer assemblies)

(2) Steel liner surface - bulk atmosphere temperature differences

(3) Other heat sink surface temperatures

(4) Condensation rates

(5) Heat fluxes

(6) Energy addition versus pressure and temperature response (energy balance)

(7) Convective currents

(8) Pressure reduction spray efficiency and spray effectiveness (temperature and pressure response measurements)

(9) Steam migration times and steam distribution (high speed photography).

Detailed information related to the type and number of sensors and sensor locations is provided in Appendix A. The heat transfer measurements and results are discussed separately in following sections.

1. WALL INTERIOR TEMPERATURE RESPONSE

Measurements of temperature gradients within the liner and concrete provide a means for analytically determining the effective heat transfer co-

efficient and heat flux at the containment liner surface. This section presents a discussion of the measuring system, experimental data, and analytical approaches used to determine surface heat transfer from interior wall temperature data.

1.1 Heat Transfer Assemblies (Heat Plugs)

A representation of a section of the CVTR containment wall is shown in Figure 32. Pertinent dimensions are included on the figure with the exception

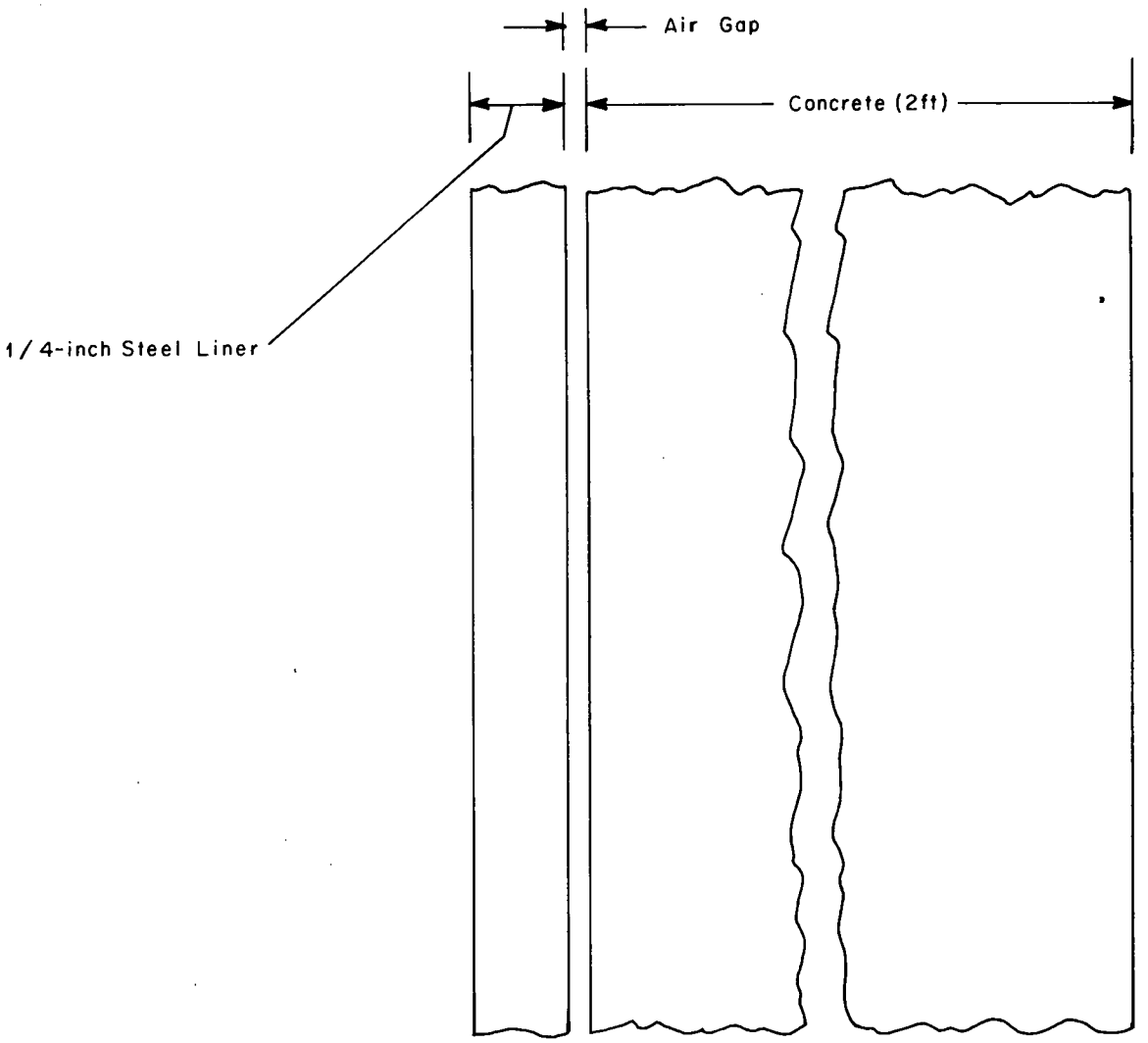

FIG. 32 SECTION OF CVTR CONTAINMENT LINER.

of an air gap of unknown dimension between the steel liner and concrete shell. The thickness of the air gap varies but was about 3/8 in. at the few spots checked.

As previously discussed, the heat transfer process at the surface consists of complex time-dependent phenomena as illustrated in Figure 33. Both dropwise and filmwise condensation processes are possible, but filmwise condensation is probably predominant. The containment bulk air-steam mixture is in contact with a gaseous layer of noncondensable gas (air) and vapor. Vapor in the gaseous layer is continually depleted by condensation such that the layer is in contact with a liquid condensate film of varying thickness depending

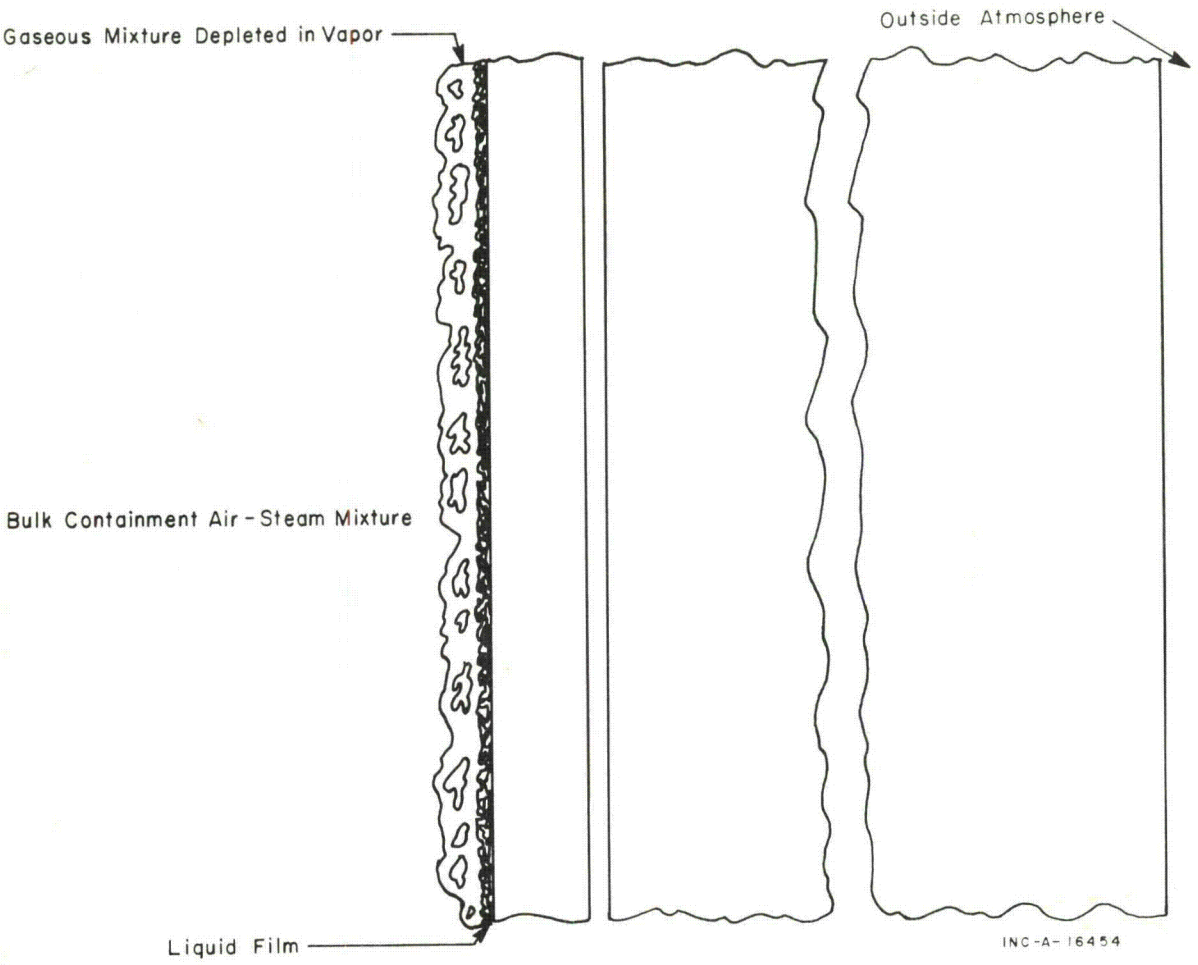

FIG. 33 CONTAINMENT WALL SURFACE PHENOMENA.

on the height of the wall. Turbulent flow of the condensate down the wall seems possible as will be discussed in a following section. Because of the difference in partial pressure of the vapor in the bulk air-steam mixture and at the liquid-gas film interface, the vapor diffuses from the bulk mixture through the gas film to liquify at the interface. The latent heat of condensation and the sensible heat lost by the vapor are transferred through the condensate layer to the structural heat sinks. Thus, the rate of condensation is a function of the diffusion of vapor through a film of noncondensable gas, conduction and convection through the liquid film, and conduction through the structural heat sinks.

Measurements sufficiently detailed to identify and determine all of the localized heat transfer behavior were not practicable. However, since the overall coefficient of heat transfer across the containment boundary is of primary interest for containment response analysis, two special assemblies (heat plugs) were installed to obtain temperature data from which to determine this coefficient. For each assembly, a circular 10-in. diameter segment was removed from the liner, a 1-in. hole was drilled through the concrete wall, and a concrete plug and replacement steel disc were installed as illustrated in Figure 34. Thermocouples were precisely located on the metal disc surfaces and in the atmosphere adjacent to the heat plug, as well as embedded in the replacement disc and plug. The steel disc was welded in place and the surface was finished to closely match the adjoining section of the liner. A typical installation is shown in Figure 35. Both installations were in the operating region with Heat Plug 1 being about 4 ft above the operating floor (elevation

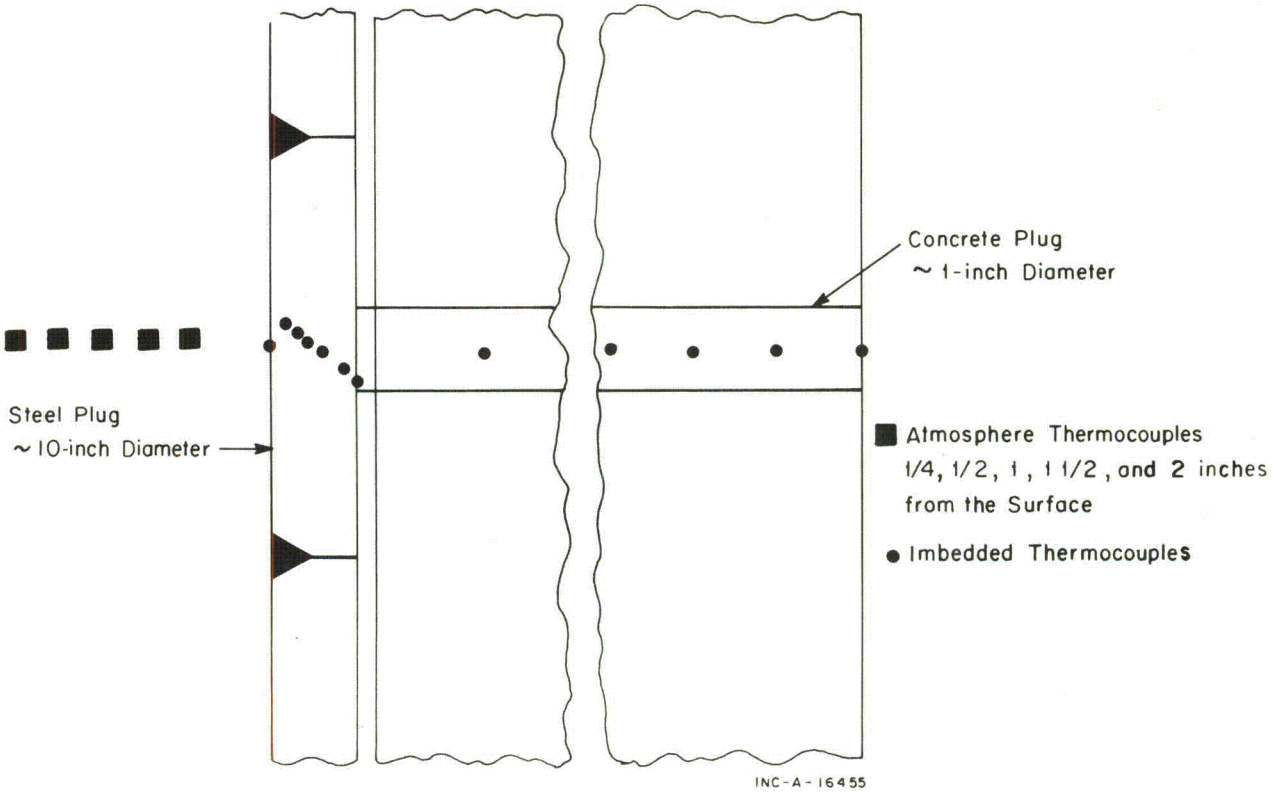

FIG. 34 HEAT TRANSFER ASSEMBLY.

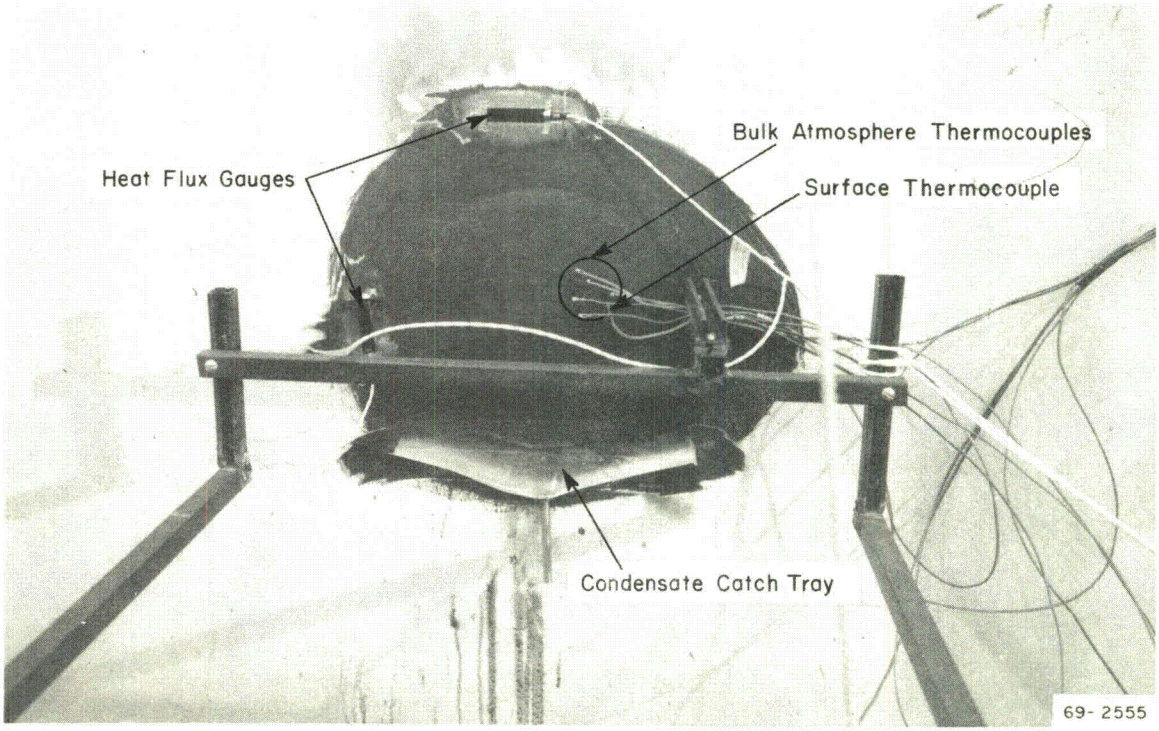

FIG. 35 BULK ATMOSPHERE THERMOCOUPLES AND SURFACE THERMOCOUPLES ON HEAT TRANSFER ASSEMBLY.

of 329 ft, 2 inches) and Heat Plug 2 some 20 ft higher on the wall (elevation of 348 ft, 4 inches) and nearer the level of major steam injection. Two heat flux gauges (discussed in Section IV-4) are also shown in this figure.

1.2 Experimental Data

A typical temperature profile across the surface films and containment wall is shown by the dashed line of Figure 36, which is for Test 3, Heat Plug 1 at a time of 60 seconds. A temperature difference of about 50°F between the bulk atmosphere and liner surface is noted at this time and is apparently the temperature drop across the liquid surface film and gaseous layer. The temperature difference from the surface to the first internal thermocouple of the heat plug is about 20°F. The first thermocouple is about 44-thousandths of an inch beneath the surface of this plug. Figure 37 illustrates part of the temperature history for Heat Plug 1 during Test 5. In this case, the temperature history for the metal surface, for the first point within the metal, and for the first point in the concrete, are compared with the average bulk atmosphere. The first concrete thermocouple is 3/16 of an inch from its junction with the steel liner. Additional heat plug thermocouple data for Tests 3 and 5 over part of the test period are tabulated in Appendix B-V. More detail on thermocouple locations within the heat plug is also given in Appendix B-V.

The closely spaced thermocouples within the metal liner section were intended to provide a temperature profile or gradient through the liner. The attempt to obtain this profile was, in general, unsuccessful because the differences between the readings of successive interior thermocouples were very small and were within the error band associated with the individual temperature measurements.

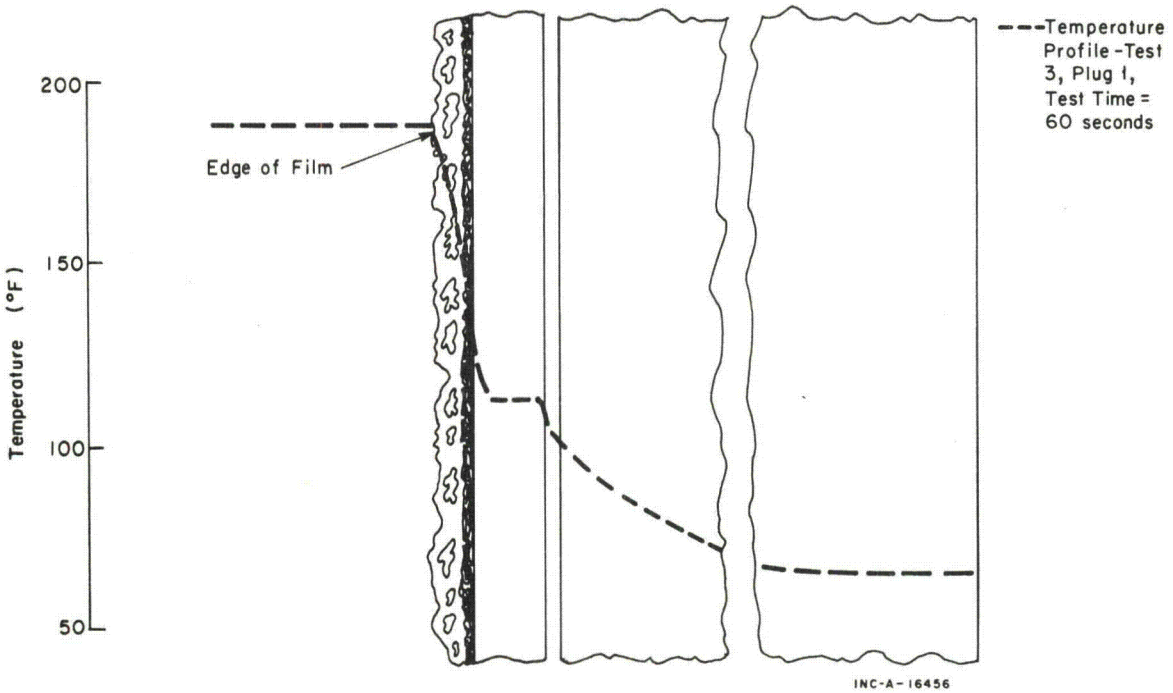

FIG. 36 TEMPERATURE PROFILE THROUGH HEAT TRANSFER ASSEMBLY.

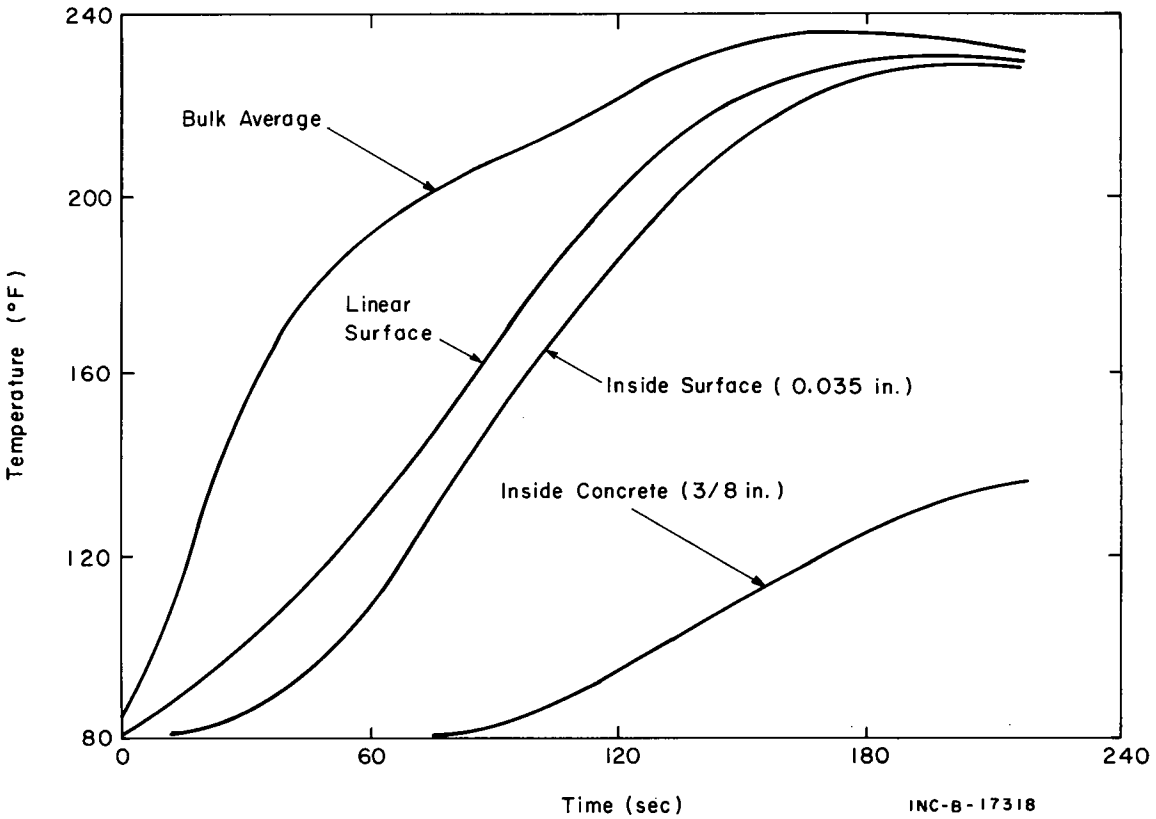

FIG. 37 TEMPERATURES DURING STEAM TEST 5, HEAT PLUG 1.

1.3 TAEH Heat Conduction Program

An inverse heat conduction code, TAEH, was developed in the CVTR program for analysis of the data from the heat plugs. A TAEH description, listing, and sample problem are provided in Appendix C. The code solves the inverse problem of heat conduction or the calculation of unknown surface conditions from known internal temperature behavior; which, in this case, is experimentally determined. In particular, Duhamel's theorem is solved by a numerical inversion technique (that is, an inverse solution of a convolution integral). The code calculates surface heat fluxes, temperatures, and effective heat transfer coefficients.

1.4 TAEH Calculation Results

Heat transfer coefficient curves, calculated by TAEH are shown for Test 3, Heat plugs 1 and 2, for Test 4 Heat Plug 2, and for Test 5, Heat Plugs 1 and 2 in Figures 38, 39, and 40, respectively. As can be seen, the heat transfer coefficients obtained from Heat Plug 2 peak earlier in all cases than those from Heat Plug 1; and, the peak occurs prior to termination of steam injection into the containment. This difference in behavior is attributed to the difference in heat plug locations. Heat transfer at Heat Plug 2 apparently reaches a limiting process prior to steam shut off. This limiting process may have been a result of either a conduction-limited heat transfer process occurring in the concrete or air gap behind the liner or a localized diffusion-limited mass transfer process occurring in the boundary layer. Also, the different time dependency for the formation of a condensate film and the different film thickness

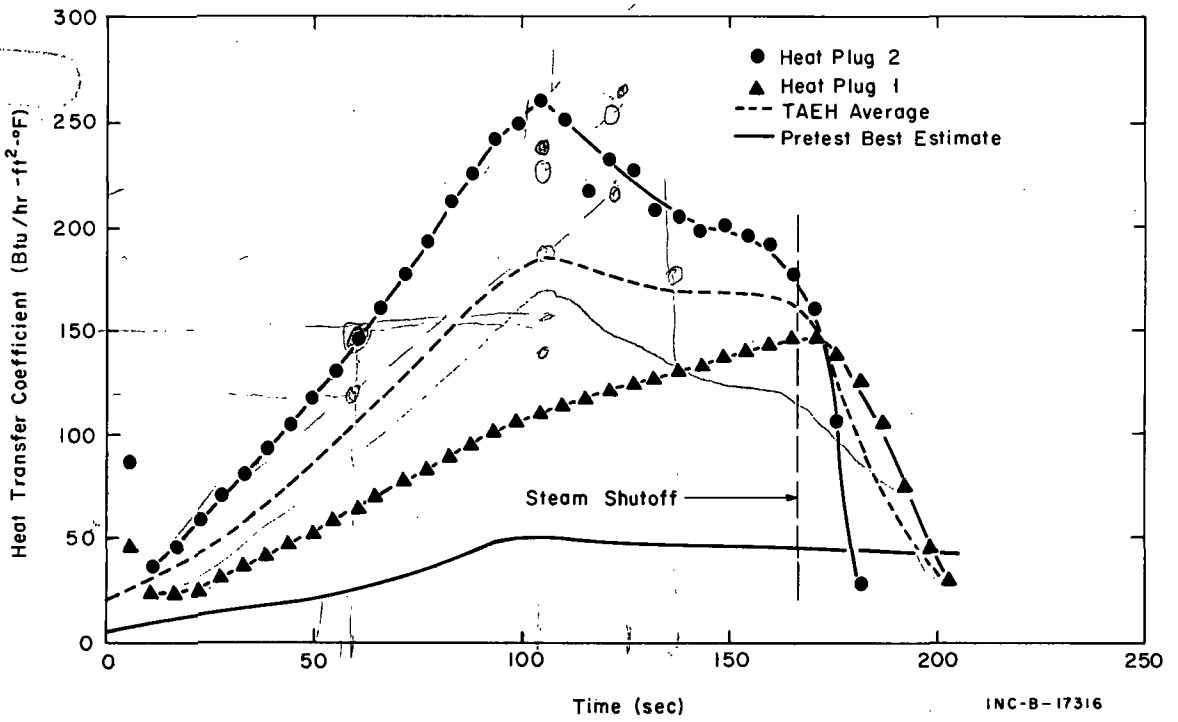

FIG. 38 TAEH-CALCULATED HEAT TRANSFER COEFFICIENT, STEAM TEST 3.

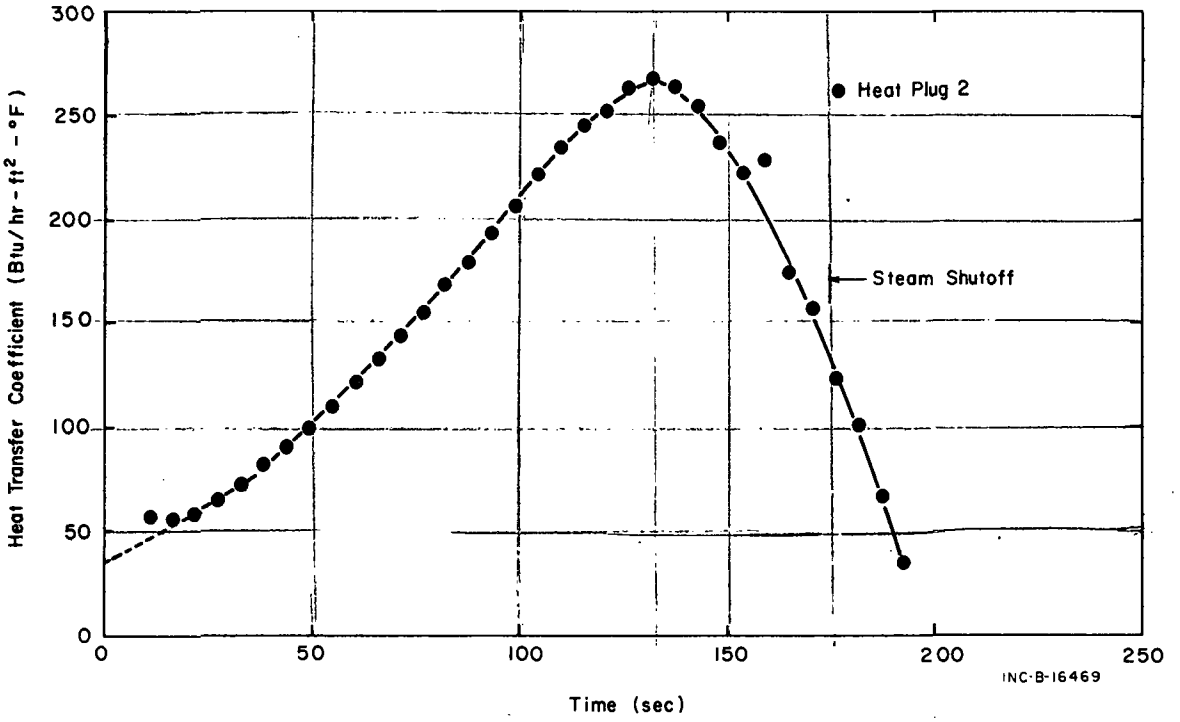

FIG. 39 TAEH-CALCULATED HEAT TRANSFER COEFFICIENT, STEAM TEST 4.

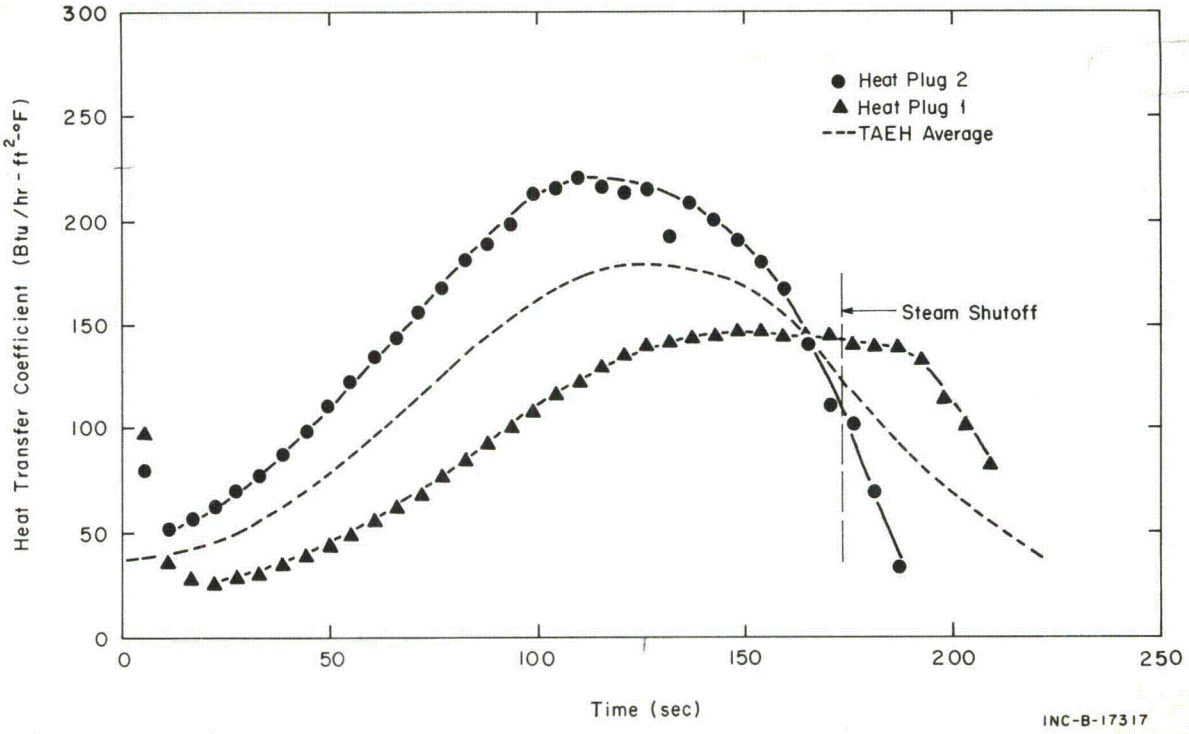

FIG. 40 TAEH–CALCULATED HEAT TRANSFER COEFFICIENT, STEAM TEST 5.

due to the difference in wall height influenced the observed temperature behavior between the two locations. In any event, the results indicate differences in heat transfer behavior for different locations even within the region of steam turbulence. As mentioned, Plug 2 was located about 20 ft higher on the liner wall of the operating region than Plug 1, and was nearly at the level of major steam exhaust from the diffuser section and apparently in a much more turbulent region of the steam-air atmosphere. Higher atmosphere and liner temperatures (approximately 20°F) were measured in the region of higher elevation near Heat Plug 2, the bulk atmosphere temperature reached a peak value sooner, liner temperatures increased more rapidly, and temperature differences between the bulk atmosphere and the liner decreased more rapidly.

As can be noted in the code description of Appendix C, the TAEH code was designed to analyze the temperature history at one or several internal slab spatial points, and the calculation can be performed using slab, cylindrical, or spherical geometry. The results in Figures 38, 39, and 40 are for cylinderical geometry and one average internal temperature. For Heat Plug 1, the internal temperature was the average of the data from the first five liner internal thermocouples, whereas generally for Heat Plug 2, an average of the data from only the first two internal thermocouples was used because of known uncertainties in the data from the other thermocouples. In all cases, an average of the bulk measurements near the face of the plugs was used for the bulk atmosphere temperatures. No significant change in results was noted from the calculation using a different code geometry, but the results are dependent on the meshpoint assignment for the average temperature. In general, the heat transfer coefficients will be larger by up to about 10% if the assignment is near the face of the liner or if the temperature history from the first thermocouple inside the liner is used.

The TAEH results are for point measurements at two locations in the containment. Heat transfer rate differences were noted and these differences appear dependent upon measurement locations relative to the steam exhaust. The dashed lines of Figures 38 and 40 are an attempt to form an average coefficient for the containment wall in the operating region based on these data and this average will be referred to later in this report. The solid line of Figure 38 is the pretest best estimate heat transfer coefficient based on the best available assumptions and common usage within the industry. This pretest estimate was used for pretest CVTR containment response predictions.

The TAEH calculation also produces calculated surface temperatures. Typical results for Test 3, Heat Plugs 1 and 2 are compared to measured surface temperatures in Figures 41 and 42, respectively. The agreement is good considering the usual difficulty associated with an accurate surface measurement (that is, in the transient state, measurements of the actual surface temperature, rather than some intermediate condition between the bulk atmosphere and surface, are inherently difficult).

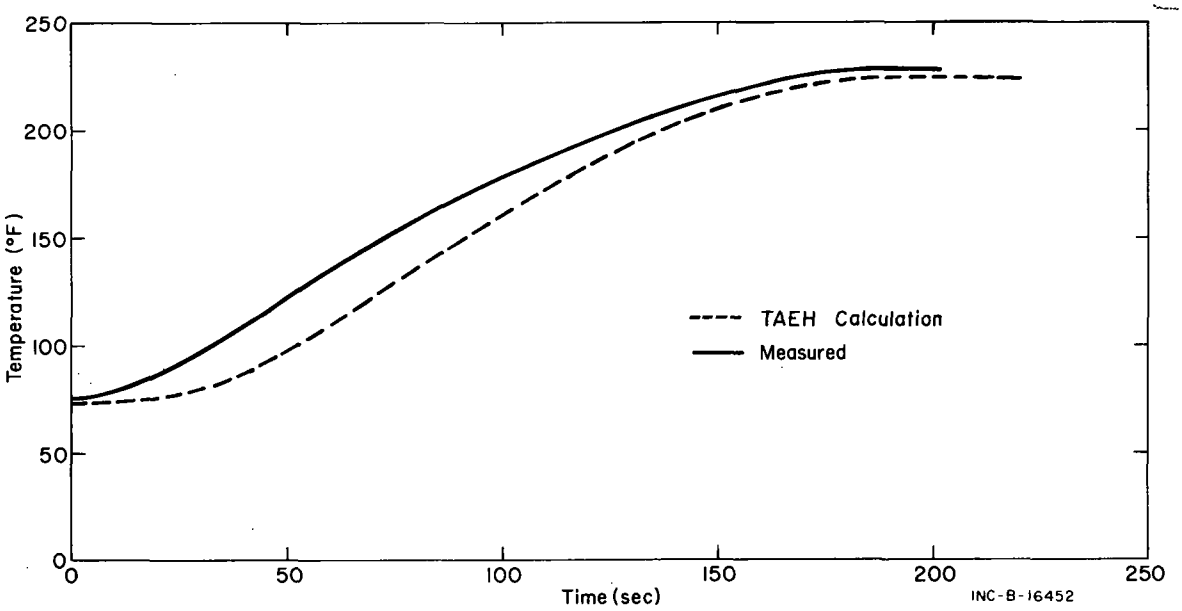

FIG. 41 COMPARISON OF EXPERIMENTAL AND CALCULATED SURFACE TEMPERATURES FOR TEST 3, PLUG 1.

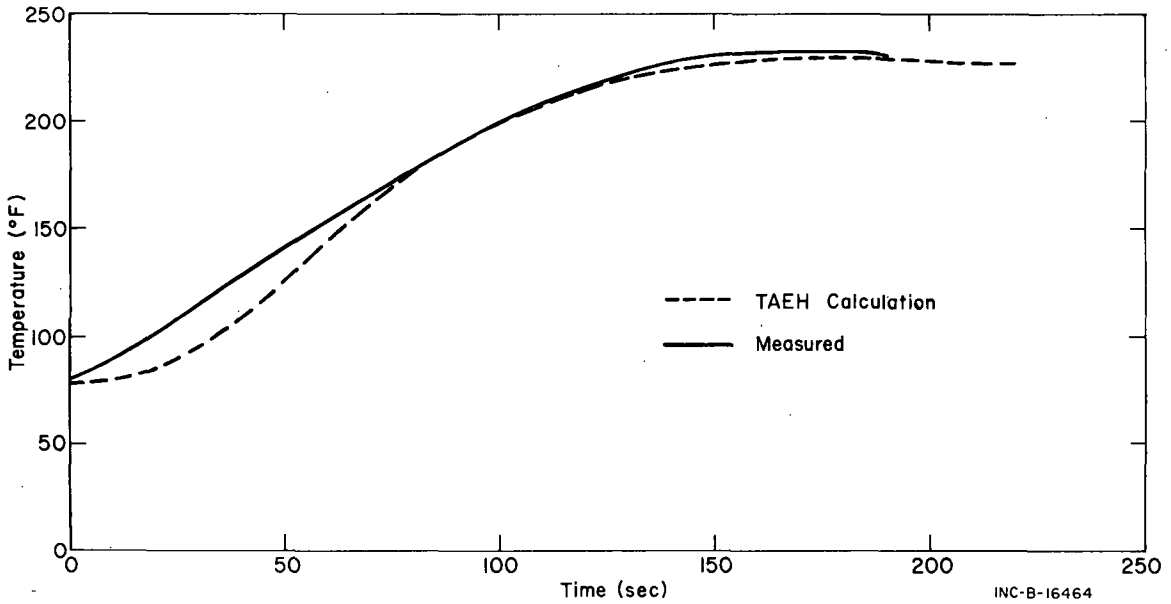

FIG. 42 COMPARISON OF EXPERIMENTAL AND CALCULATED SURFACE TEMPERATURES FOR TEST 3, PLUG 2.

1.5 Other Calculations

The TAEH approach to calculating heat transfer coefficients from the heat plug data is considered reliable within the limits of the measured temperature accuracies. However, other analytical approaches can be adopted and pursued as a check against the results. In particular, spot checks were made through use of the following three expressions for heat transfer:

$$h = \frac{k \cdot \Delta T/\Delta X}{T_a - T_s} \tag{1}$$

where

h = heat transfer coefficient
k = thermal conductivity of steel liner
$\Delta T/\Delta X$ = temperature gradient in steel liner
T_a = temperature of containment atmosphere
T_s = liner surface temperature.

$$h(t) = \frac{\rho C_p \cdot \Delta X \cdot dT_s/dt}{T_a - T_s} \tag{2}$$

where

$h(t)$ = time-dependent heat transfer coefficient
ρC_p = volumetric heat capacity (55 Btu/ft^3-°F)
ΔX = wall thickness (0.25 in.)
dt = time step (5.5 or 11 sec)
dT_s/dt = rate of temperature rise.

$$h(t)A(T_a - T_s) - \frac{kA(T_s - T_1)}{\Delta X} = \frac{A(\Delta X)(\rho C_p)(T'_{0.25} - T_{0.25})}{2\Delta t} \tag{3}$$

where A is the area, Δt is the time increment, and $T'_{0.25}$ and $T_{0.25}$ are the new and old temperatures, as shown in the following diagram.

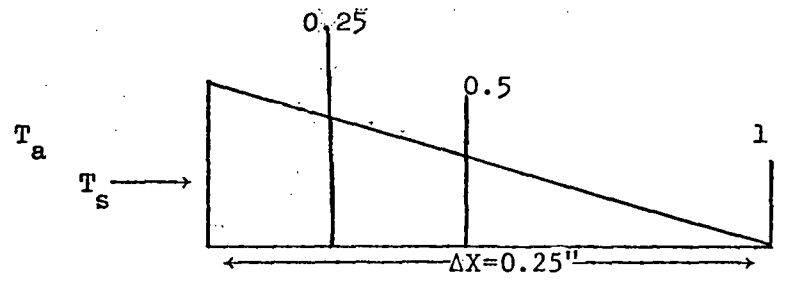

For Equation 1, $\Delta T/\Delta X$, T_a, and T_s were experimentally measured, but the expression does not adequately allow for conduction and storage in the interior of the wall. Equation 2 is a heat balance based on the assumption of a large liner thermal conductivity (liner surface and interior points not greatly different). Equation 3 is Dusinberre's numerical method. In general, the results from the spot checks were as large or larger than the TAEH-generated results for heat transfer coefficients.

1.6 Error Considerations

Any heat transfer calculations such as those of the previous section are tedious (unless performed by machine) and inherently subject to errors because division by the small difference between two large temperature values is required. Because of the high heat transfer rates, the temperatures of the steel liner closely followed the bulk air temperatures. Thus, differences between liner surface (or interior liner points) and the bulk atmosphere temperatures rapidly decreased to small values. Small uncertainties in liner temperature or bulk atmosphere temperature measurements then lead to large uncertainties in the calculated heat transfer coefficients. The temperature data used in these and all heat transfer calculations of the report were carefully corrected for all known recording, calibration, or data reduction errors. However, significant thermocouple temperature variations remained within the 366.6-millisecond time step over which data were recorded and apparently resulted from condensation behavior, steam jets, and mechanical vibration. To smooth the data, a least squares fitting program using a seventh order polynomial equation was applied to the temperature measurements used in the heat transfer calculations. Additional details on the fitting program and error analysis are given in Appendix A, Sections A-III and A-IV, respectively. The heat plug temperature data given in Appendix B-V are the smoothed data.

An indication of the uncertainty of the TAEH heat transfer coefficient calculations resulting from temperature uncertainties is given in Figure 43. For this case, Heat Plug 2 data from Test 3 have been used. The thermocouples associated with the liner have an uncertainty of about ±1.3°F whereas those associated with the bulk measurement have an uncertainty of about ±1.4°F. Thus, in the least squares sense, an error of ±2° is an acceptable estimate of the inaccuracy. Figure 43 illustrates the results of the heat transfer coefficient calculations with this error estimate assigned to the temperatures. This error band is also representative of other similar heat transfer evaluations. However, as previously mentioned, the large temperature variation from steam jet and other effects, are not accounted for by the error estimates. The data smoothing program helped reduce the effect of this type of uncertainty; however, the results also varied considerably depending on the location of the thermocouple relative to the steam exhaust. Standard deviations about the smoothed mean from one up to several degrees were calculated for different thermocouples. In general, thermocouples having large uncertainties either from the error analysis or the smoothing results were eliminated from the heat transfer considerations. Nevertheless, the extremes of the heat transfer calculations are questionable; that is, initially large and erratic bulk atmosphere temperature changes were recorded. Near the time of steam shutoff, bulk atmosphere-liner temperature differences are small and small temperature uncertainties result in large heat transfer uncertainties. Also following steam shutoff, liner temperatures exceeded bulk atmosphere temperatures in some instances (particularly for the spray tests) and both liner and bulk atmosphere temperatures decreased.

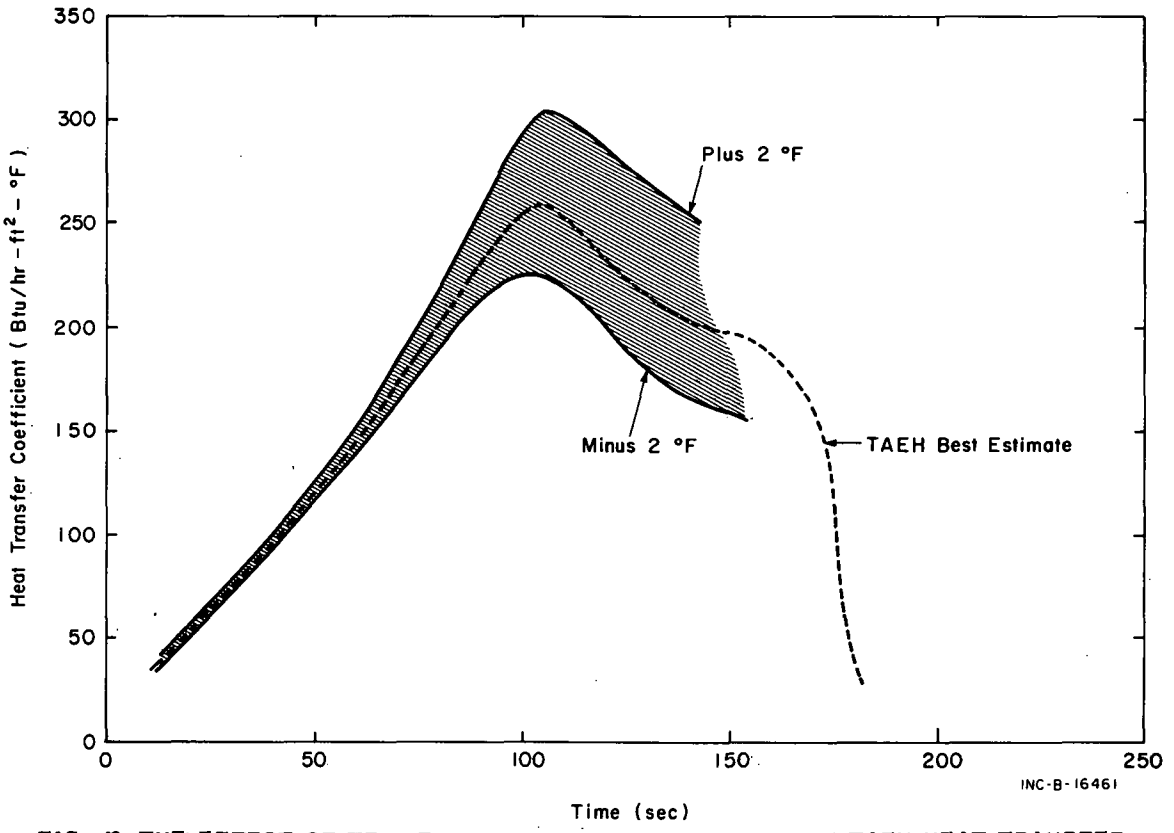

FIG. 43 THE EFFECT OF TEMPERATURE UNCERTAINTIES ON THE TAEH HEAT TRANSFER COEFFICIENT -- TEST 3, PLUG 2.

2. LINER SURFACE-BULK ATMOSPHERE TEMPERATURE DIFFERENCES

In addition to a liner surface temperature measurement at each of the heat plugs, temperatures of the liner surfaces were measured at various locations throughout the containment. Also, several bulk atmosphere temperatures were recorded in each region of the containment. These temperature measurements were used to determine heat transfer coefficients at locations in the containment other than at the heat plug points. The basis for determining these coefficients was comparison of both the time dependent differences of the liner and bulk atmosphere temperature with corresponding differences from the heat plugs and calculations described in the following section.

2.1 Temperature Data

To use the temperature data for calculations, approximations such as an average basement bulk atmosphere temperature or atmosphere temperatures measured in the proximity of a liner temperature were required. Because small changes in temperature differences heavily influence heat transfer calculations, these approximations should be recognized as potentially capable of leading to serious inaccuracies. For the previously discussed heat plug data and the TAEH calculations, this type of inaccuracy was reduced by using several bulk temperature measurements close to the face of the plug.

2.2 Calculations and Results

The calculational approach used for determining heat transfer coefficients from the experimental liner surface-bulk atmosphere temperature data involves the heat balance expression of Section IV-1.5 and repeated here:

$$h(t) = \frac{\rho C_p \cdot \Delta X \, dT_s/dt}{T_a - T_s} .$$

Results of Steam Test 3 are given in Figures 44 and 45 and are compared with the TAEH calculations for the heat plugs. The heat transfer coefficients of Figure 44 are a sample of a large number of such determinations for the operating region. Variations in rates of liner temperature increases within the operating region are indicative of significantly different heat transfer rates from point to point even within relatively open volumes. Some of these differences between heat transfer rates for this region can be correlated with impediments to steam distribution such as the refueling machine, crane structure, or distance from point of injection. The heat transfer coefficients for the basement region (Figure 45) are observed to be much smaller than those for the upper intermediate and operating regions and are in keeping with the restrictions to the flow of steam to the lower regions. In the intermediate region, the apparent discrepancy of higher heat transfer rates for the thermocouple located 9 ft under the operating floor compared with the rates for the thermocouple located 2 ft under the floor is due to the lower thermocouple being exposed more directly to steam through the annulus whereas the higher thermocouple was located near conduit, piping, and other structures.

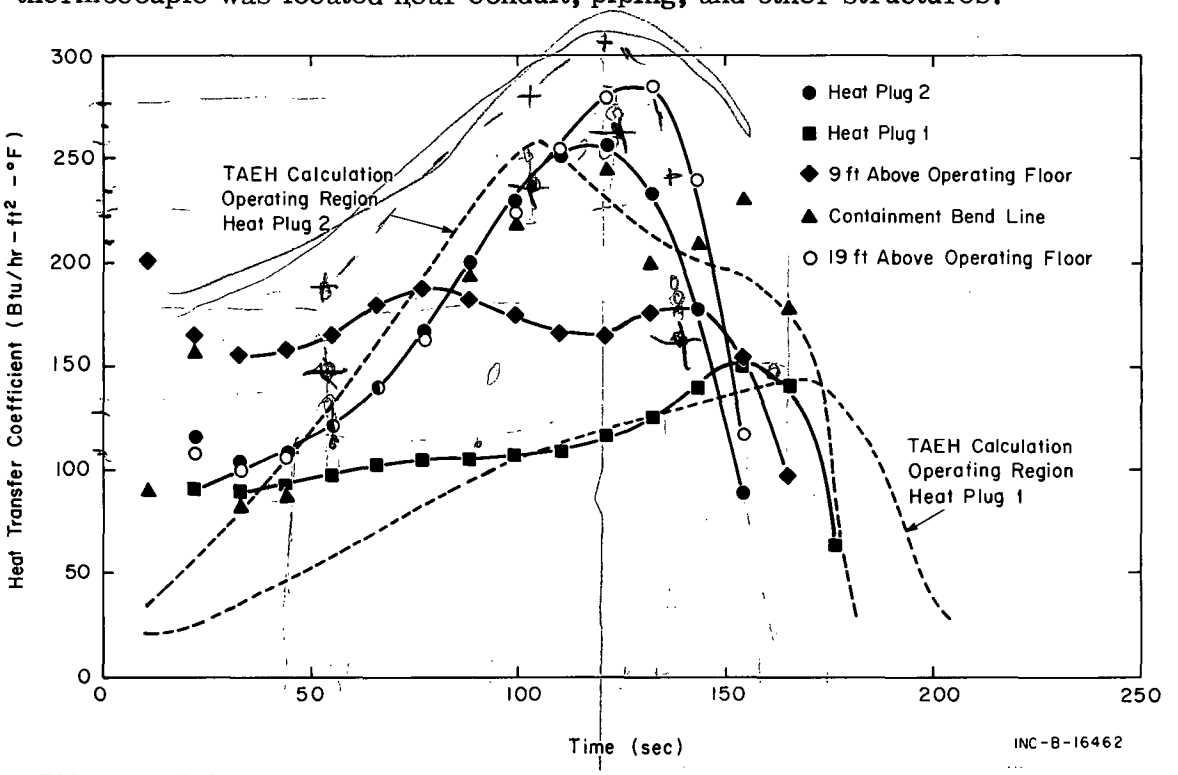

FIG. 44 OPERATING REGION HEAT TRANSFER COEFFICIENTS FROM LINER SURFACE-BULK ATMOSPHERE TEMPERATURE DIFFERENCES, TEST 3.

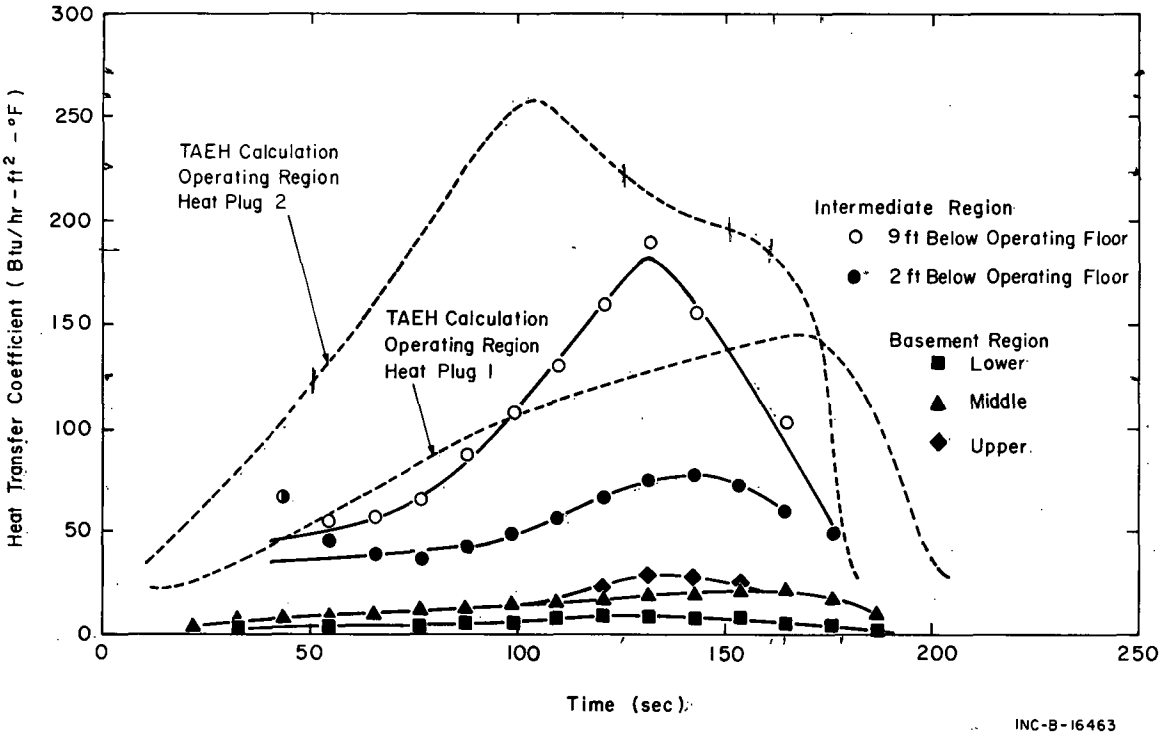

FIG. 45 BASEMENT AND INTERMEDIATE REGIONS HEAT TRANSFER COEFFICIENTS FROM LINER SURFACE–BULK TEMPERATURE DIFFERENCES, TEST 3.

3. CONDENSATION RATES

During the DBA tests, measurements were made to determine the rate at which condensation formed on the containment liner surfaces. These measurements were to aid in understanding the heat transfer process, and also possibly to be of potential value in other programs in understanding fission product washdown processes.

3.1 Condensate Collection and Measuring System

The collecting system consisted of 1-ft-wide troughs welded to the containment wall at selected locations. An area 1 ft wide extending from each trough location to the bend line of the containment (junction of cylindrical wall and dome) was bordered with a bead of Dow Corning Compound III. Condensate forming and running down the outlined area was routed through plastic tubing to catch cans. Additional details of the collection system are provided in Appendix A-I.

The rate measurement was provided by suspending the catch cans from specially designed load cells. As the condensate was collected, the output of the load cell was recorded on a multipoint strip chart recorder as a function of time. Also, at the completion of each test, the collected condensate was weighed as a check against the measuring system. Typical load cell and catch can installations are shown in Figures 46 and 47.

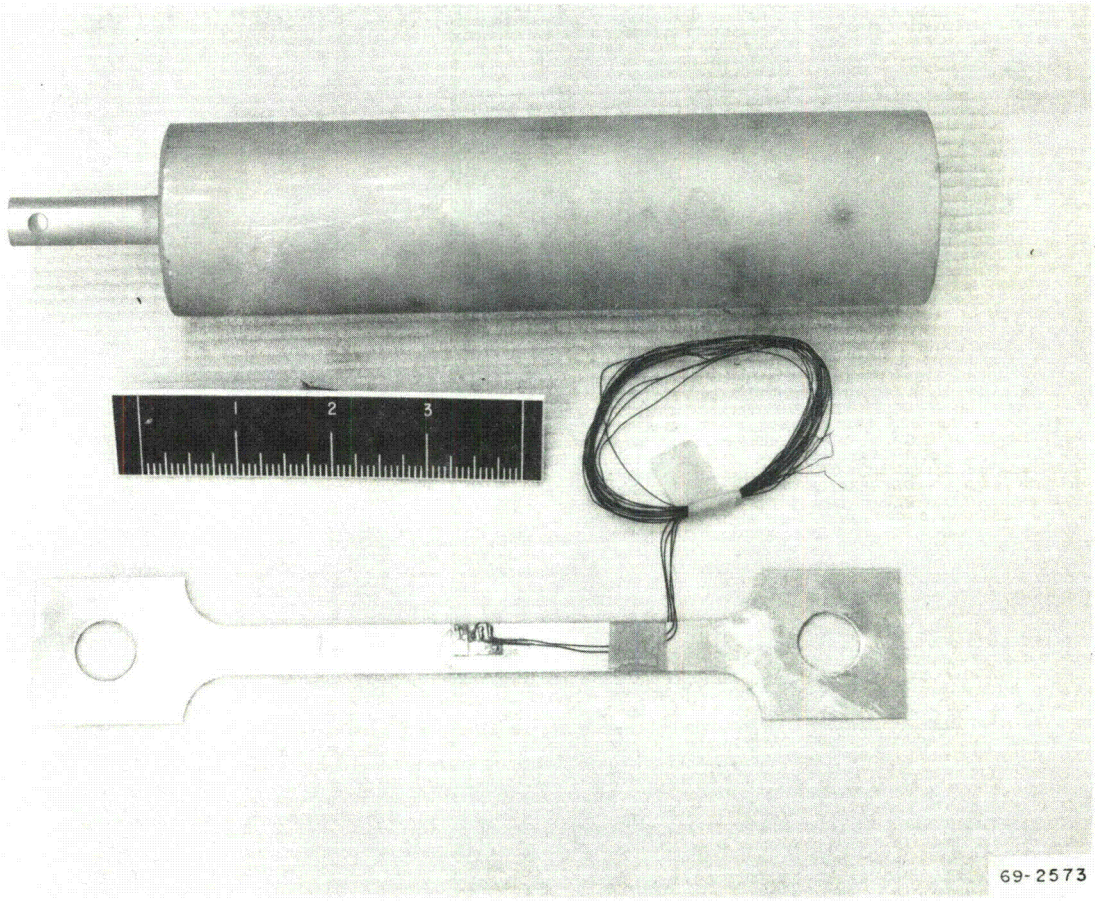

FIG. 46 CONDENSATE LOAD CELL.

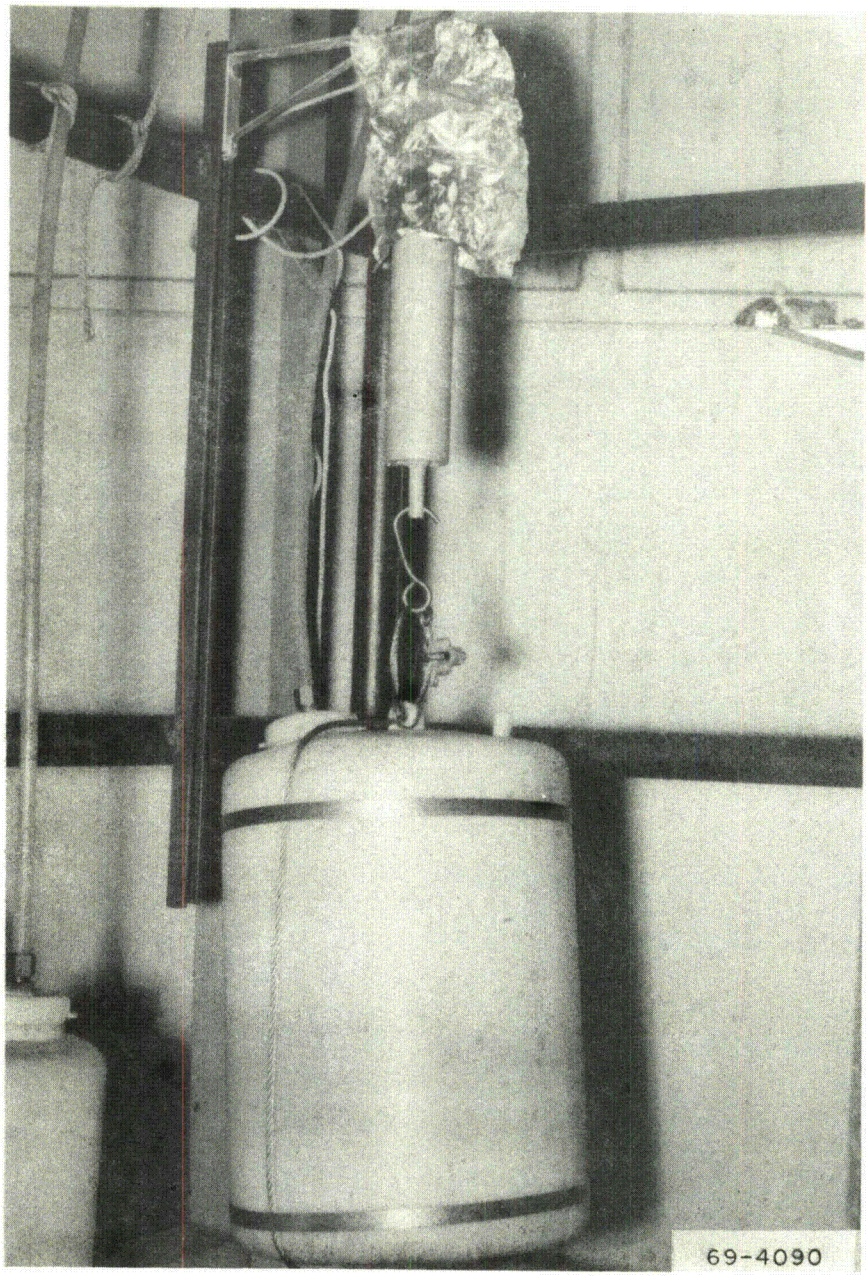

FIG. 47 CONDENSATE CATCH CAN INSTALLATION.

3.2 Calculations and Results

As described in Section 3.1 the condensation rates were obtained by collecting condensate from large surface areas. Thus the condensation rate measurements are distributed measurements. An accurate time correlation between the condensation rate data and the actual test time was not obtained. The difficulty in correlating the condensation rate with the test time basically involved the unknown time requirement for the formation of a film, flow down the wall, and flow through the trough and tubing of the collection system. Typical condensation rate results are shown in Figure 48 for Steam Test 3 with a best estimate for timing. The results are for Rate Gauge 4 which had a condensation area of 31 ft^2. Other data similar to those given in Figure 48 are provided in Appendix B-III. Condensation rates larger or smaller than those of Rate Gauge 4 were observed. The discrepancies apparently involve differences in orientation of the condensation surface with respect to the steam injection point and differences in the length and bends of tubing of the different gauges. Also, spillover or loss of condensate may have occurred. Reasonably high condensation rates are observed. At 15 minutes, the total condensate collected is 10,000 ml (22 lb) of water or well over 2 1/2 gallons for this 31-ft^2 strip. About 10,600 ft^2 of liner area for the containment cylindrical section is above the operating floor; therefore, on the basis of the data obtained from the areas sampled, about 850 gallons (7120 lb) of condensate formed on this area of the liner in the 15-minute test period. The total amount of water weighed following test completion for this strip was 12,700 ml which extrapolates to 9565 pounds of condensate for the upper liner surface area. A CONTEMPT[15] calculation with the TAEH average heat transfer coefficient (discussed in Section V-3) predicted the mass of condensate at 18 minutes to be about 12,000 pounds which agrees reasonably well with the experimental data. Of course, this cylindrical section is only a part of the total surface in the containment available for condensation, and the condensation rates will be heavily dependent on steam source condensation surface orientations. Photographic evidence from the behavior of condensation on the glass windows of camera boxes (discussed in Section IV-7) indicates that dropwise condensation may have occurred during the initial part of the CVTR tests. However, the special surface conditions, such as an oil film, necessary for promoting and maintaining this type of condensation, and the fact that these surface conditions may have been eliminated by the first presence of steam, strongly suggest that the predominant behavior was filmwise condensation.

Classically, the approach to analysis of filmwise condensation on vertical surfaces is the Nusselt Theory. However, the transient wall temperatures, the presence of noncondensable gas (air), the possible unstreamlined flow in the condensate film, the velocity of the vapor, and other characteristics of the CVTR heat transfer problem are departures from the assumptions common to the classical theory. Experimental investigations of the corrections needed for these departures from classical assumptions are incomplete. The findings of several investigators are summarized by McAdams[16]. Analysis patterned after recommendations by McAdams and Geidt[17] have been pursued to obtain an indication of the heat transfer coefficient from measured condensation rates.

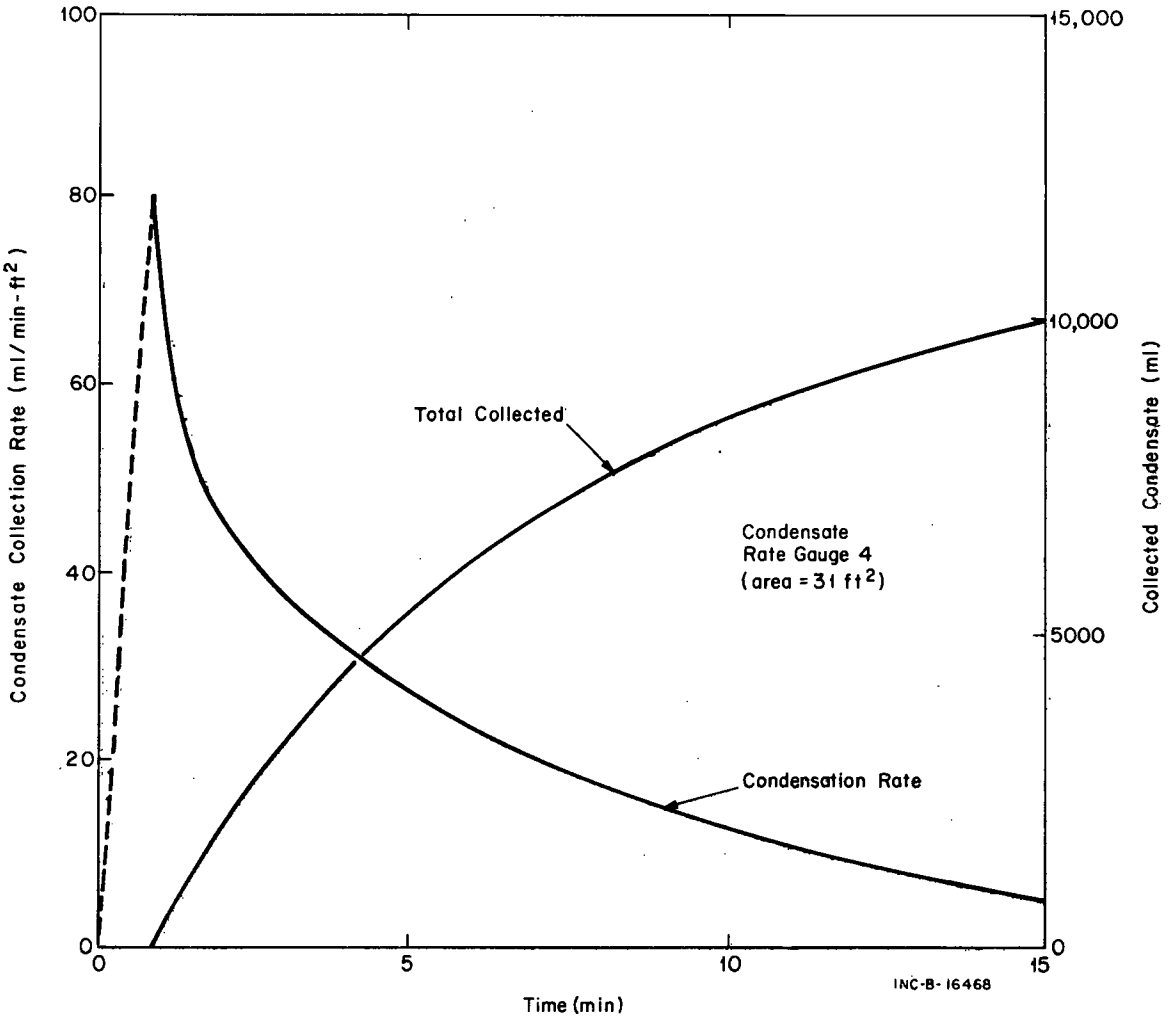

FIG. 48 CONDENSATION RESULTS FOR STEAM TEST 3.

With film condensation of vapor on tall vertical surfaces, condensation rates may easily be sufficiently large to cause turbulent flow in the film. Turbulent flow has been found to commence at a critical value of the Reynolds number for the film. The critical value is found to be about 1800 for vertical surfaces when the Reynolds number is defined as:

$$N_{Re} = \left(\frac{4W}{\mu g}\right)$$

where

W = mass flow rate of condensate from lowest point on condensing surface divided by the width (lb/hr-ft)

μ = dynamic viscosity of condensate film (lb-sec/ft^2) ($\simeq 6 \times 10^{-6}$ lb-sec/ft2 for water at 200°F)

=

1100. Consequently, turbulent flow for the condensate down wall surfaces may have been approached but not exceeded for any extensive period of time.

For N_{Re} = 1100, the Nusselt expression for the heat transfer coefficient h_{Nu} is:

$$h_{Nu} = 1.47 (N_{Re})^{-1/3} \left(\frac{\mu^2}{k^3 \rho^2 g}\right)^{-1/3}$$

where

h_{Nu} = Nusselt zero vapor velocity heat transfer coefficient (Mean value of h with respect to height of condensing surface)

k = thermal conductivity of condensate (0.39 Btu/hr-ft-°F for water at 200°F)

ρ = density ($\approx$1.87 slugs/ft^3).

Thus, h_{Nu} $\approx$810 Btu/hr-ft^2-°F. In practice, h is found to be larger than that of Nusselt. For low vapor velocities and N_{Re} $\leq$1800, McAdams recommends multiplication of h_{Nu} by 1.28, such that the predicted h would be about 1000 Btu/hr-ft^2-°F. As discussed in Section IV-6, steam flow velocities up to about 30 ft/sec were measured during the tests. The effect of vapor velocities on film condensation behavior is clearly dependent on whether vapor flow is up or down the wall, and local behavior is difficult to specify from the limited velocity measurements at CVTR.

The most serious deviation from Nusselt's assumptions is probably related to the presence of noncondensable gas that results in a significant decrease in heat transfer from predicted values. The temperature of the free surface of the liquid film, T_f, will be equal to the saturation temperature of steam at a pressure equal to the partial pressure of the steam at that surface. Since the saturation temperature of steam decreases considerably with pressure, the difference $T_f - T_s$ will become much smaller when the concentration of air is significant. Consequently, much less heat will be transferred, less condensation will occur, and the heat transfer coefficient predicted by the Nusselt relationship will be too large. During the course of a CVTR steam test, the concentration of noncondensable air varies widely. At the time of test initiation, the mass of air in the containment is 16,481 lb and the mass of vapor is 179 lb. Both results are from CONTEMPT containment response code calculations discussed in Section V-2. During the test, leakage out of the containment was essentially zero such that no loss of air occurred. However, the vapor concentration changes according to steam addition rates and condensation behavior. The CONTEMPT calculated results for condensation during Steam Test 3 serve as a guide. At a time of 97 seconds, CONTEMPT predicted about 5510 lb of vapor and 4130 lb of liquid condensate; at 169 seconds, or about steam shutoff time, the mass of vapor increased to about 8660 lb and the liquid to 8060 lb. Thus, at 97 seconds, the air concentration was about 75% air by weight from this calculation.

Experimental or analytical investigations for condensation in the presence of large concentrations of noncondensables are lacking. Generally, some form of empirical relationship is used to describe experimental results and the relationships are strictly applicable only to the particular experiment. In one set of results referred to in Jakob[18], air contents between 0.2 and 20% of the steam weight were investigated. The heat transfer coefficient decreased by a factor of about 5 over this range. McAdams reports a relationship, $h/h_{Nu} = 1.17/C^{0.11}$ which, however, is of questionable applicability since the air concentration C was restricted to a range of 0.2 to 4.0% air by weight. However, for the very large concentration of air associated with these tests, the predicted Nusselt heat transfer coefficient is much too large.

4. HEAT FLUX

Three commercially available heat flux gauges were installed for data acquisition during the steam tests. The gauges are identified as Hy-Cal Engineering Bi-Directional Calorimeters -- Model CCH-25G that operate on a thermopile principle. The gauges were installed at the heat plug locations, two at Heat Plug 1 and one at Heat Plug 2 as shown in Figure 35. Results from the gauges are somewhat uncertain but are reported for completeness.

4.1 Heat Flux Results

Heat flux results for Test 3 from one of the gauges located at the Heat Plug 1 position are shown in Figure 49. The fluctuating signal is probably a representative picture of actual heat transfer through the condensate film to the wall. The dashed lines of the figure are two possible interpretations of the signal for the purpose of heat transfer determinations. Bulk atmosphere-surface temperature differences from Heat Plug 1 data were used with the data from the heat flux gauges to calculate a heat transfer coefficient, and the results are shown in Figure 50. The heat transfer coefficients determined from the heat flux gauge are substantially smaller than determined in other ways as discussed in former sections, and the heat flux from this gauge is representative of the results obtained from the other heat flux gauges during the tests. Significant weight has not been assigned to the gauge results because of the following indeterminant effects. First, the gauges were clamped to the wall with a silicone-base grease around the edges for a moisture seal. Trapped air between the gauge and the liner may have resulted in a reduced flow of heat through the gauge. Second, the effective temperature difference driving the gauge is largely unknown but is less than the difference between the wall surface and bulk atmosphere temperatures. If a smaller temperature difference is correct, the heat transfer coefficients must be correspondingly larger than shown in Figure 50 for the measured heat flux. An arithmetic mean between the surface and bulk atmosphere temperatures for Heat Plug 1 might provide a conservative assumption which, of course, would result in heat flux gauge heat transfer coefficients of twice the magnitude in Figure 50.

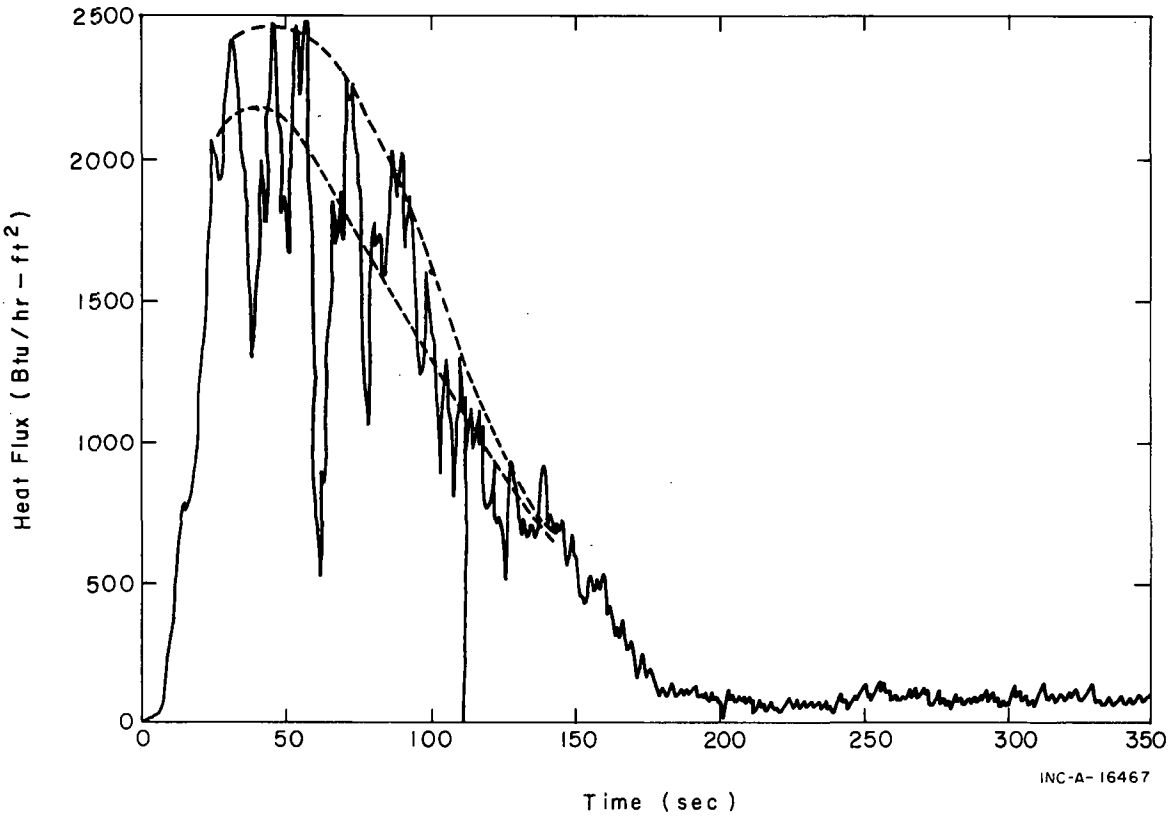

FIG. 49 HEAT FLUX RESULTS FOR STEAM TEST 3.

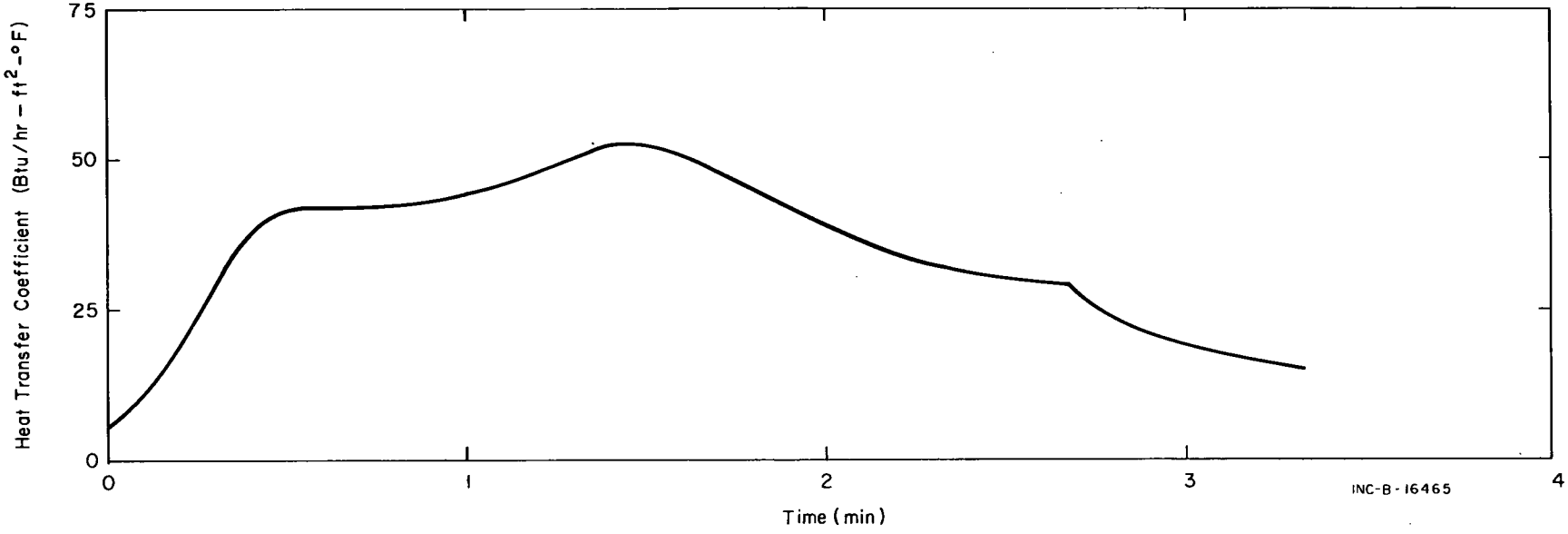

FIG. 50 HEAT TRANSFER COEFFICIENTS AS DETERMINED FROM HEAT FLUX GAUGES -- STEAM TEST 3.

4.2 Heat Flux Comparisons

Heat flux gauge results are compared to the heat flux derived from TAEH and condensate rate gauge measurements in Figure 51. The heat flux from condensation results was obtained by assuming that condensation must be accompanied by the transport of the latent heat of condensation to the wall. Fair agreement is achieved between the three methods in view of the usual difficulties with good heat transfer measurements and in view of the fact that the heat flux data and TAEH results are from point measurements, whereas the condensate rate result is from a distributed measurement.

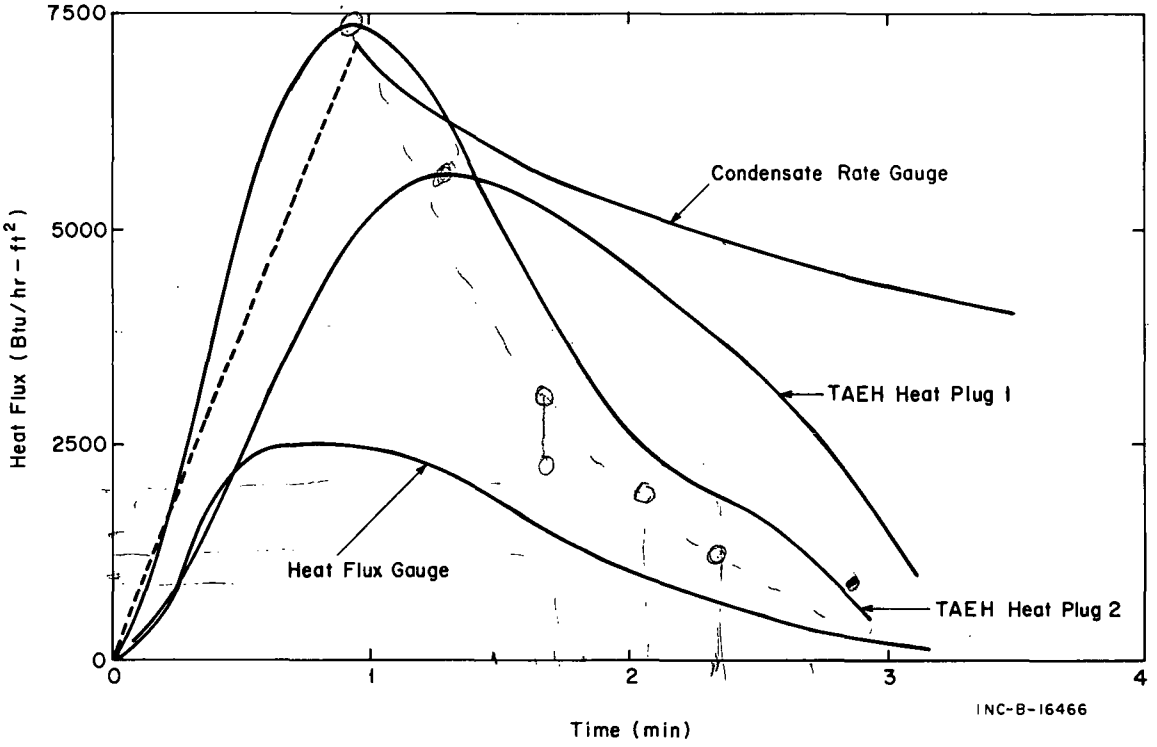

FIG. 51 HEAT FLUX VALUES FOR STEAM TEST 3.

5. ENERGY BALANCE

Time dependent energy absorption rates and average condensation heat transfer coefficients were also determined for the CVTR containment during steam tests from an energy balance. The energy balance for the system was obtained from calculations based on the measured containment temperature and pressure time history data compared to the known (measured) energy addition of the steam injection.

$q = h \Delta T$

5.1 RECACO Calculation[a]

A computer code RECACO (for recalculation of heat transfer properties) was developed to perform the energy balance calculations. The assumptions in the code are a homogeneous water-vapor-air mixture and thermodynamic equilibrium. The code will function with either saturated or superheated steam. Necessary input data are the initial containment atmospheric conditions, volume and condensing surface area, the steam addition rates and associated steam enthalpies, and the measured containment pressure, bulk atmosphere temperature, and liner surface temperature data. The RECACO code is classed as developmental because it has not been subjected to exhaustive evaluation. Consequently, the calculated results should be treated accordingly.

5.2 Energy Balance Calculation Results

The RECACO calculation produces an average heat transfer coefficient comparable to the usual assumptions for the coefficient in containment analysis (that is, an average overall coefficient).

Representative results for Tests 3, 4, and 5 are shown in Figures 52, 53, and 54, respectively. The heat transfer coefficients derived from RECACO are observed to be a factor of two or so larger than from the TAEH calculations.

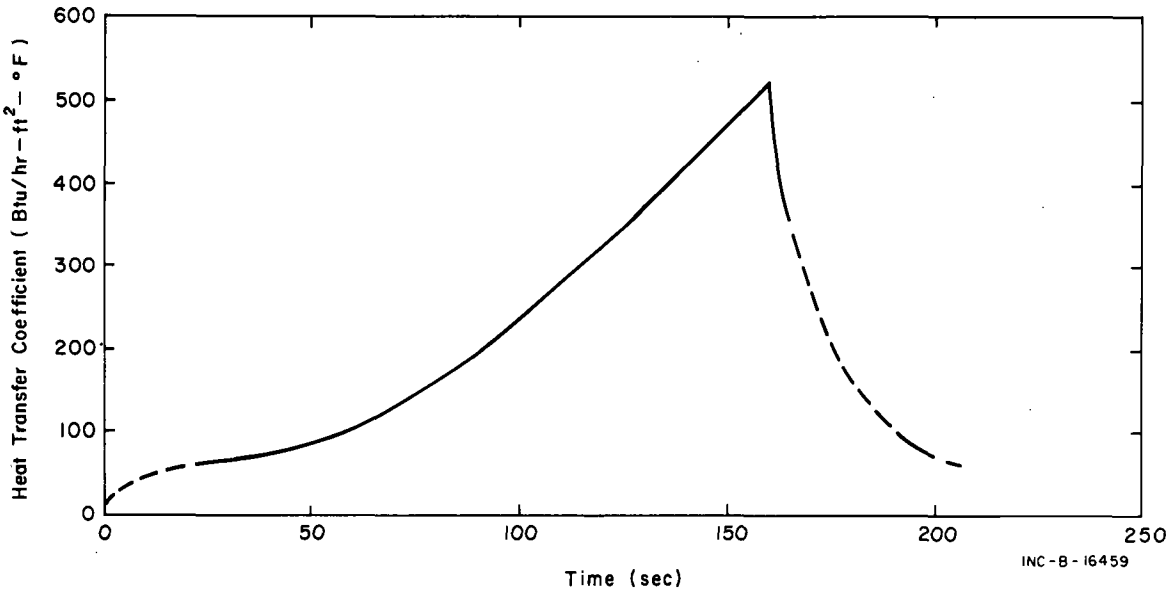

FIG. 52 RECACO RESULTS, TEST 3.

[a] The RECACO code was written by H. G. Seipel, a West German National formerly on temporary assignment to Phillips Petroleum Company through an AEC training agreement; the code utilized some portions of CONDRU II, a containment response code discussed in Section V-1.

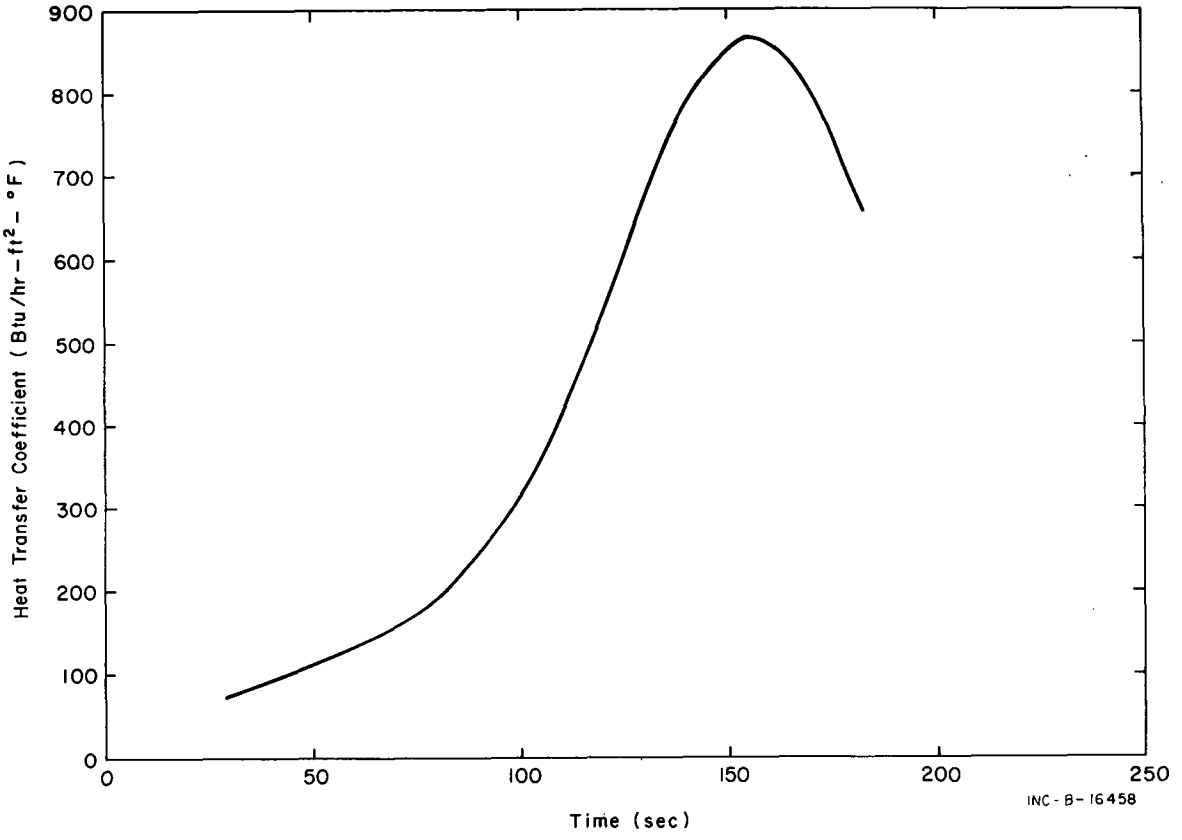

FIG. 53 RECACO RESULTS, TEST 4.

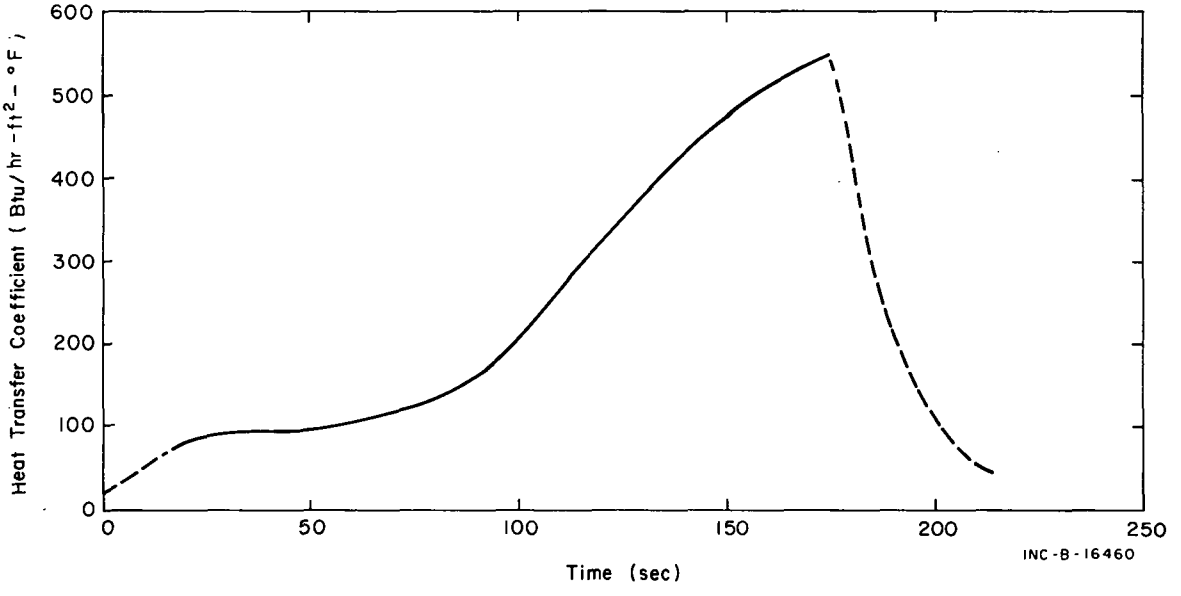

FIG. 54 RECACO RESULTS, TEST 5.

6. MISCELLANEOUS OBSERVATIONS

Several observations of a miscellaneous nature are briefly discussed in this section.

6.1 Pressure Reduction Spray

The pressure reduction spray system and some of the test results were discussed in Section III-4. However, additional comments related to the heat transfer process during spray operation are provided here.

The pressure behavior during spray operation was illustrated in Figures 11 and 27. From this behavior, the spray water was observed to be an effective heat sink. Calculated results discussed later in this report (Section V-3) indicate that shortly after steam shutoff and spray initiation, the heat transfer coefficient for heat transfer to containment structures rapidly approached a small value indicating that the spray water became the principal heat sink. Also, temperature measurements indicated temperature turnaround in the slabs shortly after spray initiation (that is, heat slab temperatures higher than those of the bulk atmosphere temperature were measured and suggest heat flow reversals).

The measured temperature behavior during the DBA tests shows that a result of spray operation is temperature redistribution throughout the containment volume or temperature equalization when compared with the stratification of the test without spray. This behavior was discussed in the preliminary DBA report[8] but is included here for completeness. The behavior is shown in Figure 55 for Tests 3 and 5. For this figure, the smoothed Heat Plug 2 bulk average data are used for the operating region and a smoothed average of four thermocouples for the basement. These smoothed data are in contrast to the point data of the earlier report, but the features of the data remain unchanged. The spray operation effectively increases the rate of temperature decay and apparently contributes to atmosphere mixing throughout the containment volume since the temperature of the basement region is convergent to a higher value earlier. The mixing mechanism is influenced by the transfer of energy to the lower regions by the migration of the spray water and condensate. Results for Test 4 converge similarly to the results shown for Test 5; however, the convergence is not as great.

6.2 Convective Currents and Photographic Results

The measured convective current behavior is discussed in Section VI-4 and photographic results are discussed in Section VI-5. Convective currents of approximately 30 and 15 ft/sec were noted for the wall and annulus locations, respectively. Times for steam migration to camera locations below the operating floor are given in Section IX. These data were significant in understanding the heat transfer process in that, when taken with other experimental data, an indication as to the degree of participation of the lower regions in heat transfer was obtained.

Also, photographic results of the operating region blowdown indicated early dropwise condensation behavior on the camera viewing windows. However, this behavior may have been restricted to the surface of the windows. Widespread

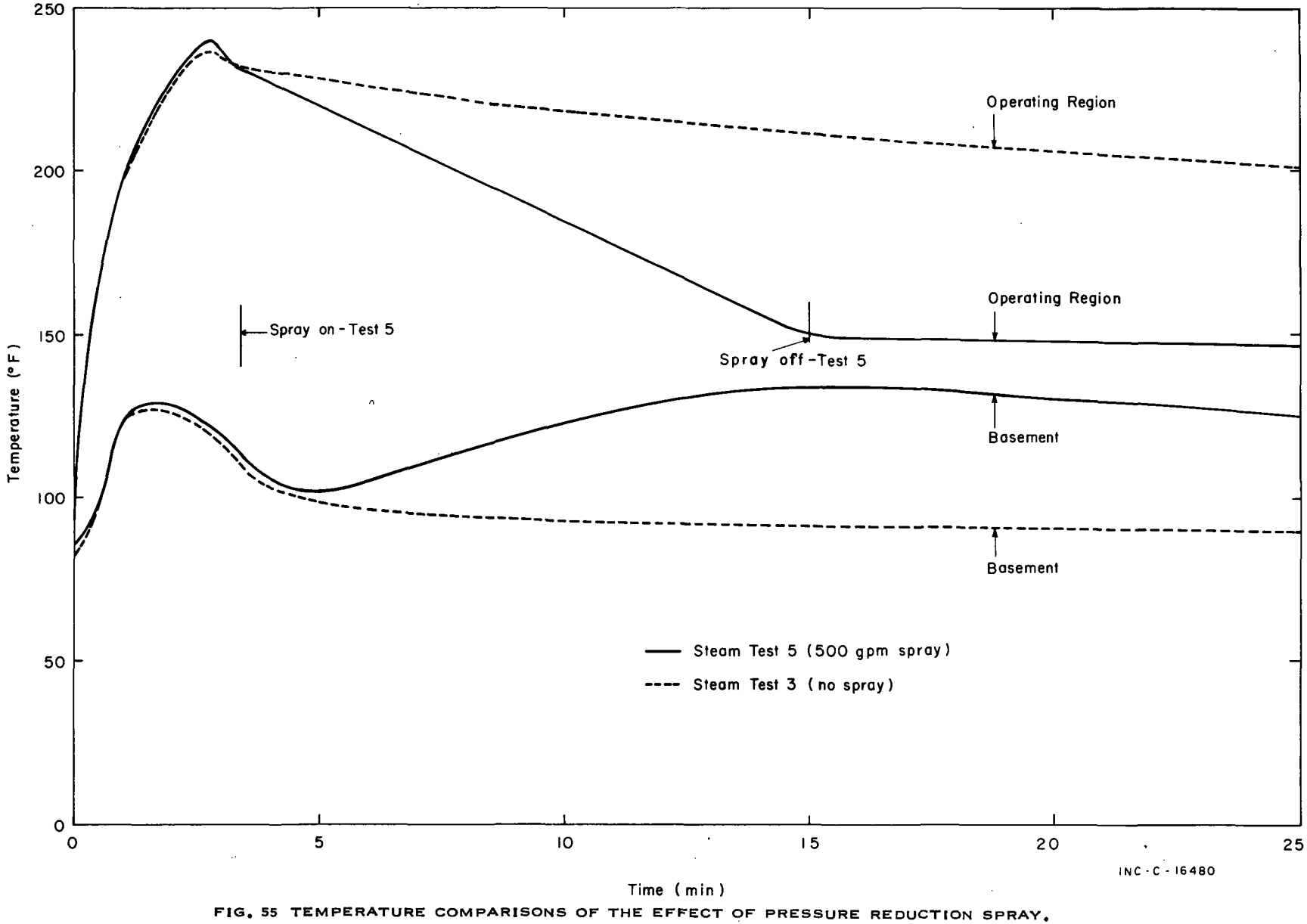

FIG. 55 TEMPERATURE COMPARISONS OF THE EFFECT OF PRESSURE REDUCTION SPRAY.

dropwise condensation behavior on the containment surfaces is considered highly unlikely. Conditions needed to promote dropwise condensation behavior are difficult to maintain and might have been destroyed by the first DBA test.

7. HEAT TRANSFER COEFFICIENT ESTIMATE

From the results and considerations of previous sections, an estimate of the CVTR heat transfer coefficient may be formed primarily for the purpose of necessary input data for the containment response analysis of Section V to follow. The reader is cautioned that the features of heat transfer discussed here are modified by the results of the analysis, and the best estimate for the heat transfer coefficient should be concluded following that discussion.

The heat transfer behavior obviously varied from location to location throughout the containment, apparently even in relatively open volumes. This behavior can be related to steam distribution and flow obstructions in many cases, and although the behavior may have been exaggerated by the CVTR geometry and steam injection system, it should be expected in varying degrees for any primary system blowdown into large containment volumes. Two approaches to a suitable heat transfer estimate can be taken: (1) an average coefficient uniformly assigned as is done in common usage, or (2) a more realistic model of the actual heat transfer distribution. For this report, both approaches are examined by the analysis in Section V. From former sections, the magnitude of the heat transfer coefficient has also been observed to differ among the different calculational methods. In most cases, the techniques gave values somewhat larger than the TAEH calculated values. However, the TAEH values are considered the most reliable, even though deficient, in that sampling at only two points was possible. For the operating region, the TAEH average coefficient is adopted as a first estimate of the behavior for the region. From the temperature data and heat transfer results, the heat transfer in lower regions is considerably reduced from that of the operating region. Time dependent coefficients of reduced magnitude for the intermediate and basement regions would be applicable but, as will be discussed, cannot be incorporated into the CONTEMPT containment code (Section V). Consequently, constant values for heat transfer coefficients for lower containment regions are assumed.

8. COMPARISON OF HEAT TRANSFER COEFFICIENT RESULTS WITH THOSE USED BY INDUSTRY

A review of heat transfer coefficients for condensing steam in a containment building following a loss-of-coolant accident has recently been completed [19]. The uncertainty that exists in the selection of an accurate empirical correlation for the heat transfer coefficients in large power reactor containments was underlined by this review. The Tagami correlation was recommended for use until improved data are available because of its apparent trend to conservatism.

For containment analysis, two separate time periods following a loss-of-coolant accident are often considered during which two different condensing steam heat transfer coefficient correlations are required. The first period is characterized by high turbulence caused by decompression of the primary coolant system and is often identified as the forced convection, turbulent, or blowdown period; that is, the transient state, the second period is the natural convection, postblowdown, or steady-state period during which turbulence is considerably reduced.

Current industry usage indicates a preference for a heat transfer model based on the Tagami correlation for the maximum coefficient on steel surfaces [19]. Various assumptions are used for a smooth transition from the preaccident steady-state coefficient to the maximum value predicted from the Tagami correlation. The natural convection data of Uchida[20], which are based on a weight ratio of air to steam is often used following the peak value from the Tagami correlation. Little information regarding heat transfer coefficients on concrete surfaces exists, and a value of 40% of the steel values and other estimates believed to be conservative are often used.

The Tagami correlation can be expressed as follows:

$$h_{max} = 72.5 \left(\frac{Q}{V \cdot t_p}\right)^{0.62}$$

where

h_{max} = the maximum heat transfer coefficient during blowdown (Btu/hr-ft^2-°F)

Q = the total energy released from the primary system during blowdown (Btu)

V = the free volume of the containment vessel (ft^3)

t_p = the time interval until peak pressure (sec).

For Steam Test 3, $Q \simeq 1.97 \times 10^7$ Btu, $V \simeq 141 \times 10^3$ ft^3 (above the operating floor), and $t_p \simeq 167$ sec such that the Tagami correlation predicts a maximum heat transfer coefficient of about 65 Btu/hr-ft^2-°F. The choice of volume in this case corresponds more closely with the blowdown, or turbulent region. The normal assumption of total free containment volume would result in a lower predicted maximum heat transfer.

The Uchida coefficients can be determined from estimates of the air-to-vapor weight ratios. The weight of air initially in the containment was approximately 1.64×10^4 lb and leakage of air during the test period was assumed to be negligible. The amount of vapor in the containment is calculated by CONTEMPT (Section V-2). The amount of vapor, air-to-steam ratio, and corresponding predicted coefficients from Uchida data are given in Table IV for a few time points from a typical calculation for Steam Test 3. The mass of vapor from CONTEMPT depends heavily on assumed heat transfer coefficients and Table IV reflects calculations using the TAEH average heat transfer from the previous section.

TABLE IV

UCHIDA HEAT TRANSFER COEFFICIENTS

Time (sec)	Steam (lb)	Ratio of Air to Steam[a]	Uchida Coefficients (Btu/hr-ft^2-°F)
3.6	240	68.3	2
10.8	718	22.8	7
18.0	1395	11.7	12
25.2	2011	8.2	16
39.6	3036	5.4	20
61.2	4120	4.0	24
90.0	5248	3.1	29
118.8	6469	2.5	34
165.6	8805	1.9	44
327.6	6597	2.5	34
471.6	5854	2.8	31
615.6	5520	3.0	29
759.6	5207	3.1	28.5
903.6	4888	3.4	27
1047.6	4574	3.6	26

[a] Basis -- CONTEMPT calculation for Test 3; TAEH average heat transfer coefficient with uniform assignment and initial conditions of 1.642×10^4 pounds of air, 1.79×10^2 pounds of water vapor, and no containment leakage.

The heat transfer coefficients determined from the Tagami correlation and Uchida data for CVTR are representative in magnitude to values which would be predicted by common practice in the industry. Clearly, the predicted coefficients are smaller than those derived from the CVTR measurements.

V. CONTAINMENT RESPONSE ANALYSIS

The state-of-the-art for containment response calculations has advanced steadily during recent years as a result of the growth in nuclear power facility usage and the accompanying need for accurately predicting facility behavior for all phases of postulated accidents. Generally, the advance has been commensurate with the developing ability to utilize digital computing techniques in the solution of complex heat transfer problems. A common assumption is that containment response calculations are sufficiently accurate to require little additional attention; however, as discussed in this report (Sections V-3, -4 and VII), the calculations may be significantly inaccurate as a result of unsatisfactory analytical models for the complex geometry of some containment structures, incorrect material properties, or inadequately understood heat transfer behavior, particularly during the pressure-temperature transient typical of a design basis accident. Assessment of the adequacy of containment response calculations has been hampered by the limited availability of representative test data for comparison with analytical predictions. An important objective of the CVTR DBA tests was to provide an assessment of state-of-the-art response analysis by using experimentally determined heat transfer behavior, thus allowing increased confidence in applying similar analysis for the safety evaluation of nuclear power plants. The analytical models used for the CVTR calculations, pretest predictions, and posttest calculational results are discussed in the following sections.

1. ANALYTICAL MODELS

Three containment response codes were employed for the CVTR calculations: CONTEMPT[15] and CONDRU I and CONDRU II[a].

Principal differences among the codes involved assumptions made in developing and using mathematical models. The different model assumptions between the codes are discussed in the following sections to aid in understanding the comparison of results but no attempt is made to provide complete code descriptions. The CONDRU codes are classed as developmental and only a brief description is included in this report.

1.1 CONTEMPT

The CONTEMPT computer program was initially developed to predict the pressure-temperature response of a dry containment building to a loss-of-coolant accident (current versions of CONTEMPT also include the option of calculations for a pressure suppression containment). The analytical model assumes that the loss-of-coolant accident can be separated into phases such that the results of the analysis of one phase serve as the initial conditions or the

[a] The CONDRU codes were written by H. G. Seipel, a West German National on assignment to Phillips Petroleum Company through an AEC training agreement, and are an extension of earlier work by Mr. Seipel and others.

time dependent input to the next phase. The model is concerned only with the pressure and temperature response of the containment volume and the temperature throughout the containment structure. The computer program input has provision for the description of several heat absorption slabs and for the description of the discharge of coolant, the boiling of residual water by decay heat, the superheating of steam passing through the core, and metal-water reactions. The program also calculates the effect of building leakage and the effects of engineered safety devices such as pressure reduction spray.

CONTEMPT uses a single-node analytical model such that a single bulk atmosphere temperature and pressure prediction representative of the average response behavior is provided at each calculation time point. The code differs from most other containment response codes in that it does not assume thermodynamic equilibrium between water and vapor in the containment. For CONTEMPT, the containment volume is separated into a liquid region and a vapor region. Each region is assumed to have a uniform temperature, but the temperatures of the two regions may be different. For each time step, energy in expelled coolant or other energy is commonly added to the vapor region. Pressure and temperature in this region are calculated by standard methods for energy and mass balances that include energy absorption by the walls and internal structures. From a mass balance and calculated quality value, the amount of water in the vapor region is determined. This water is transferred to the water region and the temperature of the water region is calculated by an energy balance.

1.2 CONDRU I

In comparison with CONTEMPT, CONDRU I is a fairly simple single-node model that uses the more conventional assumption of a homogeneous mixture and equal temperature of water, vapor, and air throughout the containment volume. Similarly to CONTEMPT, CONDRU I considers heat exchange between the containment atmosphere and walls or internal structures and calculates pressure and temperature after each time step from a mass and energy balance for the total system.

1.3 CONDRU II

CONDRU II is a two-node modification of CONDRU I with the capability of calculating the pressures and temperatures in a containment made up of two volumes (compartments) connected by a flowpath. Pressure and temperature in both compartments are evaluated in the same way as in CONDRU I. In the first compartment, an energy addition from the coolant blowdown, the chemical reaction, or the spray water addition can be considered by input tables. In either compartment, heat exchange among an artibrary number of structures is allowed. To account for separate vapor-to-air ratios, each compartment can have a different table of heat transfer coefficients. The flow area between the compartments can be changed either as a function of time or pressure. Either an isentropic or quasi-steady state flow calculation is made for the vapor, water, and air vent flow between the two compartments.

Thus, CONDRU II can evaluate pressure differentials in a two-compartment system and simultaneously consider energy addition, water spray addition, and heat exchange among internal structures.

1.4 Calculation Input Data

In the CVTR calculations much of the CONTEMPT code capabilities are not utilized. Specifically, such calculations as for the heat exchanger, fan cooler, metal-water reaction, liquid region heat or water addition are not required, and thus, entries controlling these calculations are zero. The principal inputs to the code for CVTR calculations were specifications of the initial containment environmental conditions, the composition of the heat conducting structures, including material types, dimensions and heat transfer coefficients, and the enthalpy, rate and duration of the steam addition. Additional input was required when a pressure suppression spray or some other special effect was calculated.

Input quantities common to all codes used in the CVTR calculations are listed in Tables V, VI, and VII. Each code has the capability of handling twenty heat sink structures, and these have been assigned to the most prominent features in the CVTR containment as listed in Table VI. A typical containment system contains a large number of minor heat sinks. For CVTR calculations, the additional material in the sinks was lumped and assigned to one of the heat slabs as additional material and in some cases varied as a parameter.

TABLE V

CODE INPUTS

Containment free volume - 226,920 ft^3
Bulk temperature - 80°F (Test 3, 80°F; Test 4, 82°F; Test 5, 84°F)[a]
Outside air temperature - 64°F (75°F)[a]
Slab geometry for heat conducting structures
Thermal conductivity for steel - 25 Btu/hr-ft-°F (26.1 Btu/hr-ft-°F)
Thermal conductivity for concrete - 0.8 Btu/hr-ft-°F
Volumetric heat capacity for steel - 55 Btu/ft^3-°F
Volumetric heat capacity for concrete - 30.2 Btu/ft^3-°F
Spray flow rates - 150,000 or 300,000 lb/hr (Test 4, 145,000 lb/hr; Test 5, 252,000 lb/hr)
Initial spray water temperature - 60°F

[a] Values in parentheses indicate revised values or values based on measured data.

TABLE VI

CVTR CONTEMPT CODE HEAT SINKS

Number	Title	Material	Area (ft^2)	Thickness (in. or ft)	Volume (ft^3)
1	Cylindrical shell	Steel	15,470	0.25 in.	332
		Concrete		2.0 ft	30,940
2	Dome of shell	Steel	5,370	0.50 in.	224
		Concrete		1.75 ft	9,400
3	Foundation mat	Concrete	2,640	4.5	11,880
4	Operating floor	Concrete	2,478	2.50 ft	6,195
5	Header cavity	Concrete	1,305	4.0 ft	5,220
6	Reactor compartment	Concrete	1,660	4.75 ft	7,880
7	Fuel canal	Concrete	1,600	2.0	3,200
8	Fuel canal support	Concrete	280	1.0 ft	280
9	Floor of reactor compartment	Concrete	143	3.0 ft	429
10	Concrete supports	Concrete	960	2.5 ft	2,400
11	Steam generator shield	Concrete	400	2.0 ft	800
12	Moderator overflow tank	Steel	552	0.75 in.	34.5
13	Pressurizer	Steel	176	4.5 in.	66
14	Pressurizer discharge tank	Steel	227	0.5 in.	9.5
15	Steam generator	Steel	513	3.0 in.	128.2
16	Moderator coolers	Steel	280	0.25 in.	5.8
17	Shutdown coolers	Steel	66	0.12 in.	0.7
18	Pumps, primary and injection	Steel	250	1.0 in.	20.8
19	Fuel handling apparatus	Steel	500	0.94 in.	39.0
20	"I" beams	Steel	2,250	1.62 in.	303.8

TABLE VII

PRETEST ESTIMATES

Input Quantity	Best Estimate	Upper and Lower Estimates	
Volume (ft^3)	226,920	238,226 215,574	+5% -5%
Surface Area (ft^2)			
Steel	25,654	38,481	+50%
Concrete	13,943	15,337	+10%
Steam Injection Rate (lb/hr)	400,000	424,000 376,000	+6% -6%
Steam Injection Enthalpy (Btu/lb)	1,188	1,200 1.176	+1% -1%
Heat Transfer Coefficient ($Btu/hr\text{-}ft^2\text{-}^oF$)	Time-dependent from 6.13 to 49.5 $Btu/hr\text{-}ft^2\text{-}^oF$; An average ≃ 23.55 $Btu/hr\text{-}ft^2\text{-}^oF$	81.92 16.38	

The best pretest estimate and upper and lower limit estimate values for several code input quantities are given in Table VII. The data and other code inputs were altered as more reliable information, particularly as data on steam flow rates, enthalpies, and heat transfer coefficients, became available after the CVTR Tests.

2. PRETEST PREDICTIONS

Pretest CVTR containment calculations were performed for design of the DBA experiments, for test safety considerations, and for comparison with measured results.

2.1 Calculation Summary

Summarized in Figures 56 and 57 are sample CVTR CONTEMPT pretest calculations of pressure and temperature. The calculations, which do not account for pressure suppression spray, were made through use of the best estimate of the code input quantities. The steam injection time was 99 seconds for these calculations on the basis of an estimated 400,000 lb/hr steam flow rate from the Parr Station boilers. Figure 56 gives details on behavior during the steam injection period and Figure 57 extends the prediction to one hour. Figure 58 is a comparison of CONTEMPT and CONDRU I predictions for the pretest best estimate data. The small differences between the predictions from the two codes are caused by the slightly different starting pressures and temperatures. Potential deviations from the best estimates are indicated by Figures 59 and 60. Either positive or negative deviations from the best estimate data were summed to indicate an overall potential deviation. Thus, the CVTR response was expected to fall within the limits of these calculations. However, the steam flow rate and enthalpy could not be accurately predicted and actual experimental conditions were significantly different from the 400,000 lb/hr, 99-second best estimate used for these calculations. The ±6% and ±1%, respectively, for steam flow and enthalpy reflect the instrument measurement capability and do not account for steam supply differences. Preliminary steam line checkout tests and Steam Test 2, a steam injection of reduced duration, were used to more accurately define these quantities for additional calculations and for sizing the full-scale DBA tests. The checkout tests indicated flow rates of about 370,000 lb/hr whereas Test 2 resulted in about 326,000 lb/hr. For Test 2 the steam injection time was 46 seconds, and a peak pressure of about 7.6 psig was reached. CONTEMPT calculations based on the 326,000 lb/hr measured flow rate and 46 second injection time resulted in a peak pressure of about 9 psig which indicated a margin of safety for continuing to full-scale steam test work. Test 2, being a checkout test, is not discussed further in this report.

2.2 Geometry Considerations

The CONTEMPT and CONDRU I results are indicative of the predictive capabilities of typical state-of-the-art containment response codes within the limits of the input quantity uncertainties. CONTEMPT has some special features with regard to separation of liquid and vapor and both the CONTEMPT

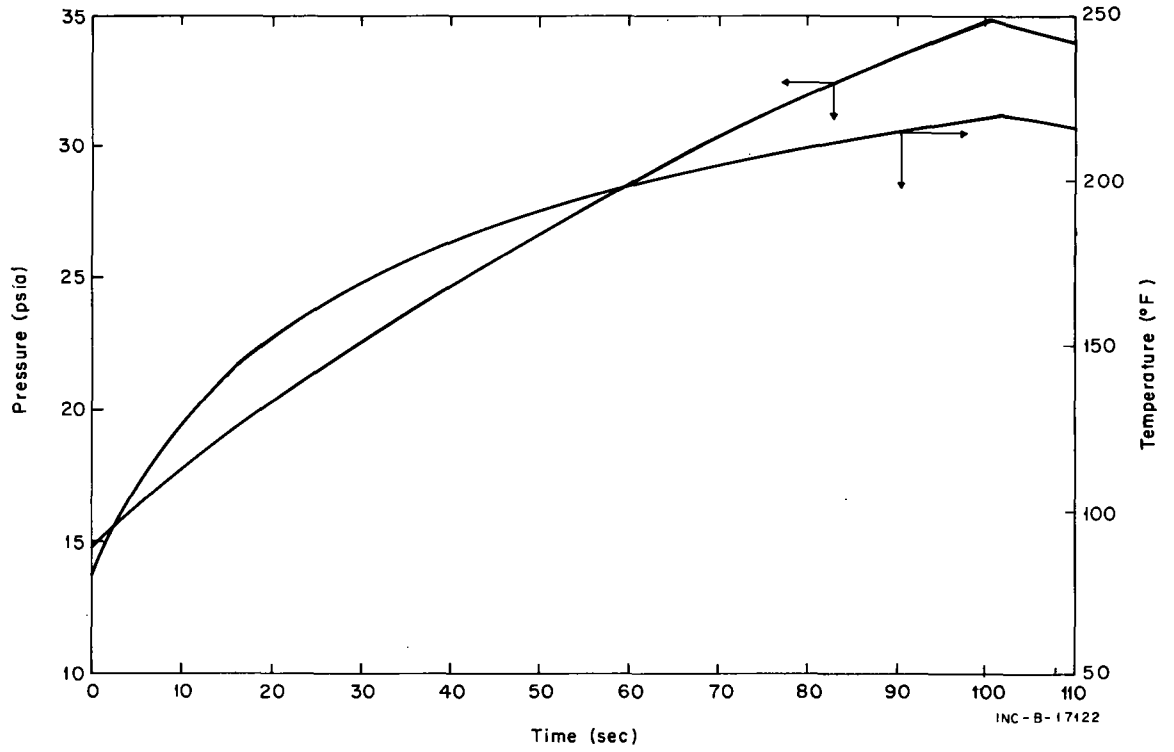

FIG. 56 CONTEMPT PRETEST BEST ESTIMATE.

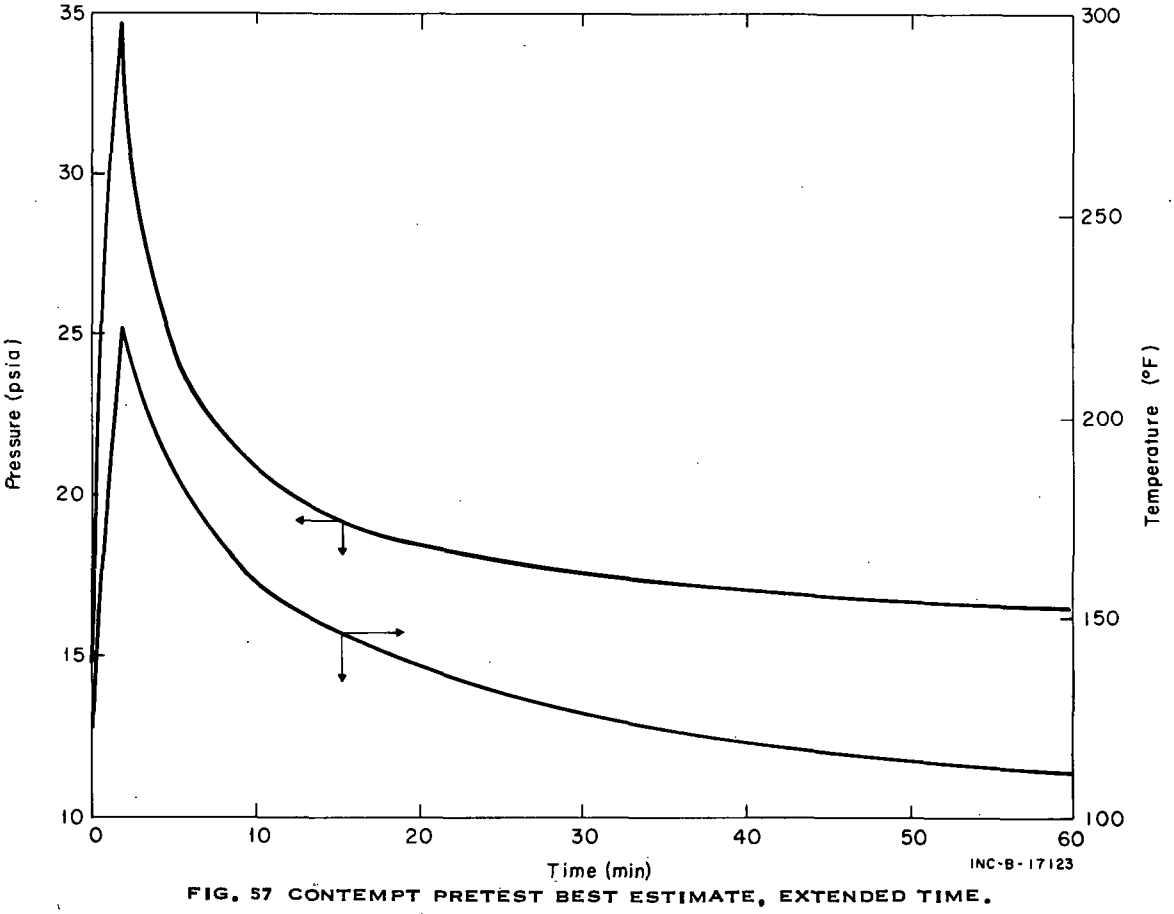

FIG. 57 CONTEMPT PRETEST BEST ESTIMATE, EXTENDED TIME.

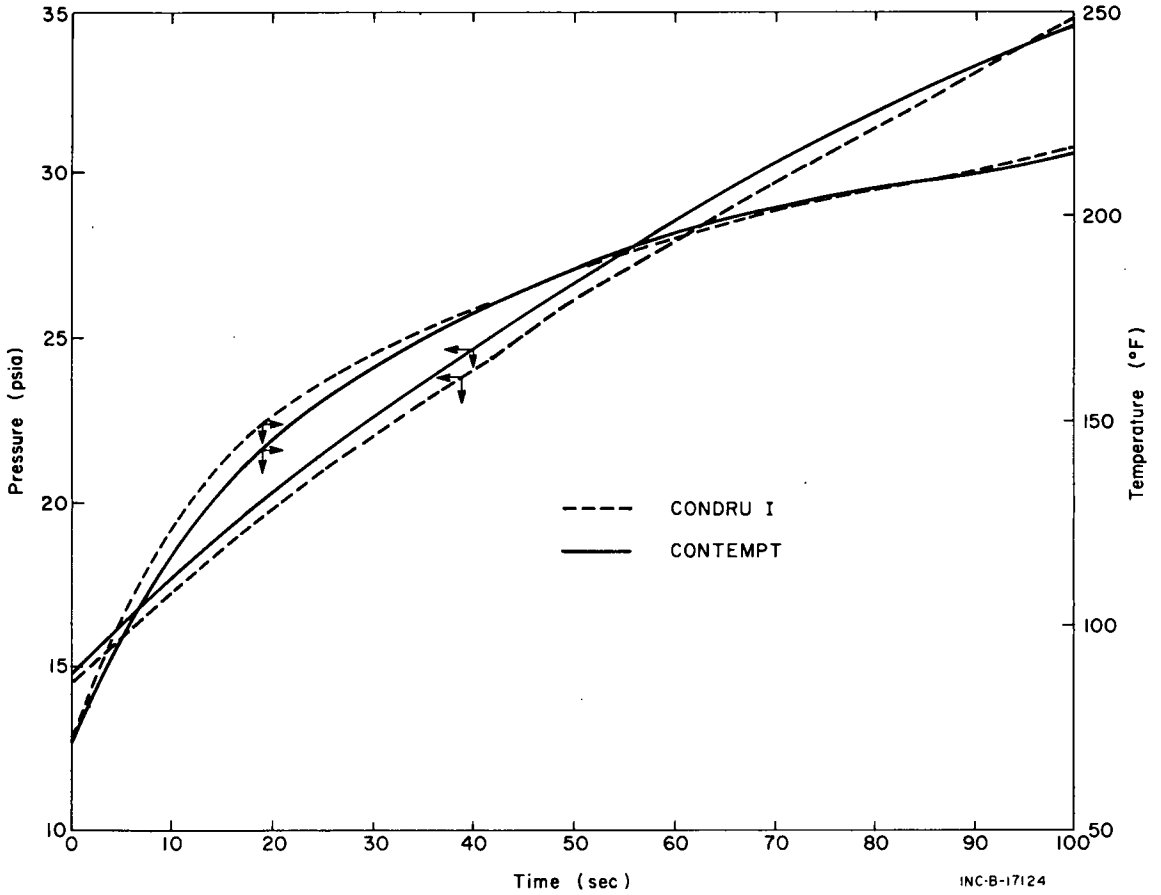

FIG. 58 COMPARISON OF CONTEMPT AND CONDRU I PREDICTED PRESSURE.

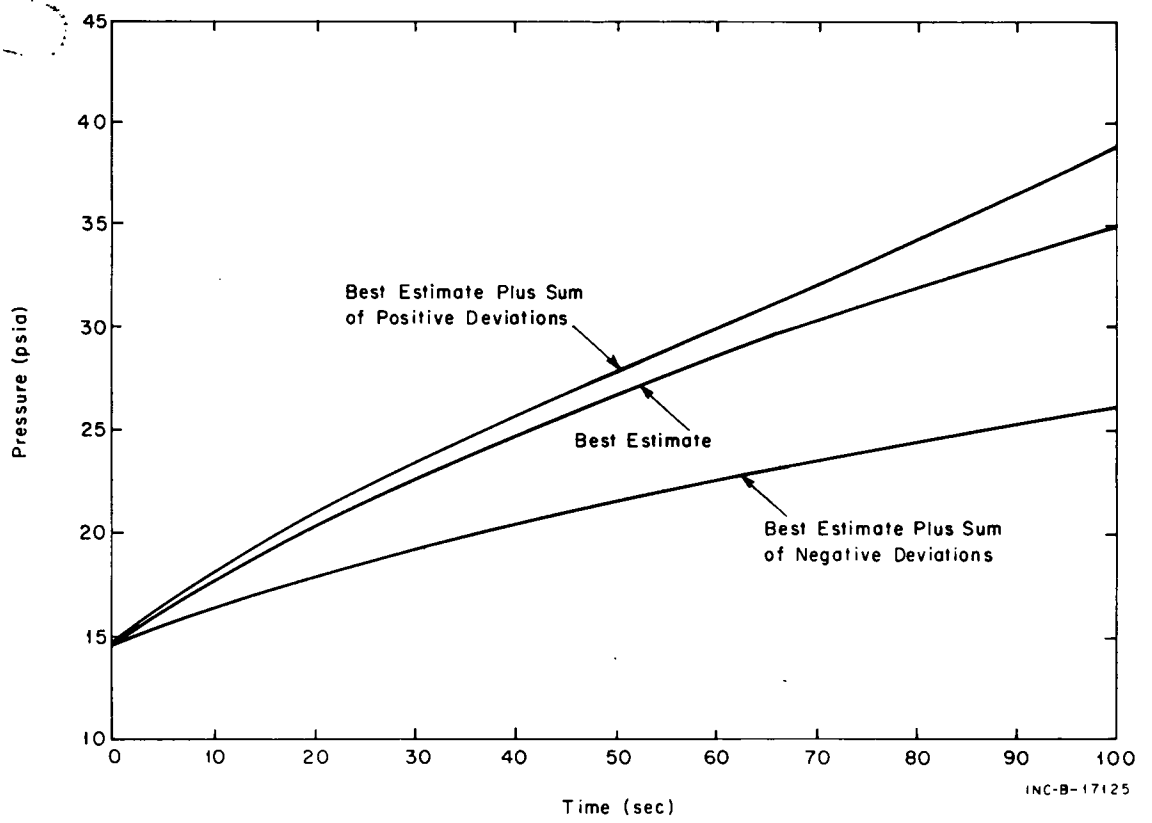

FIG. 59 EFFECT ON PRESSURE OF VARYING CONTEMPT INPUT QUANTITIES.

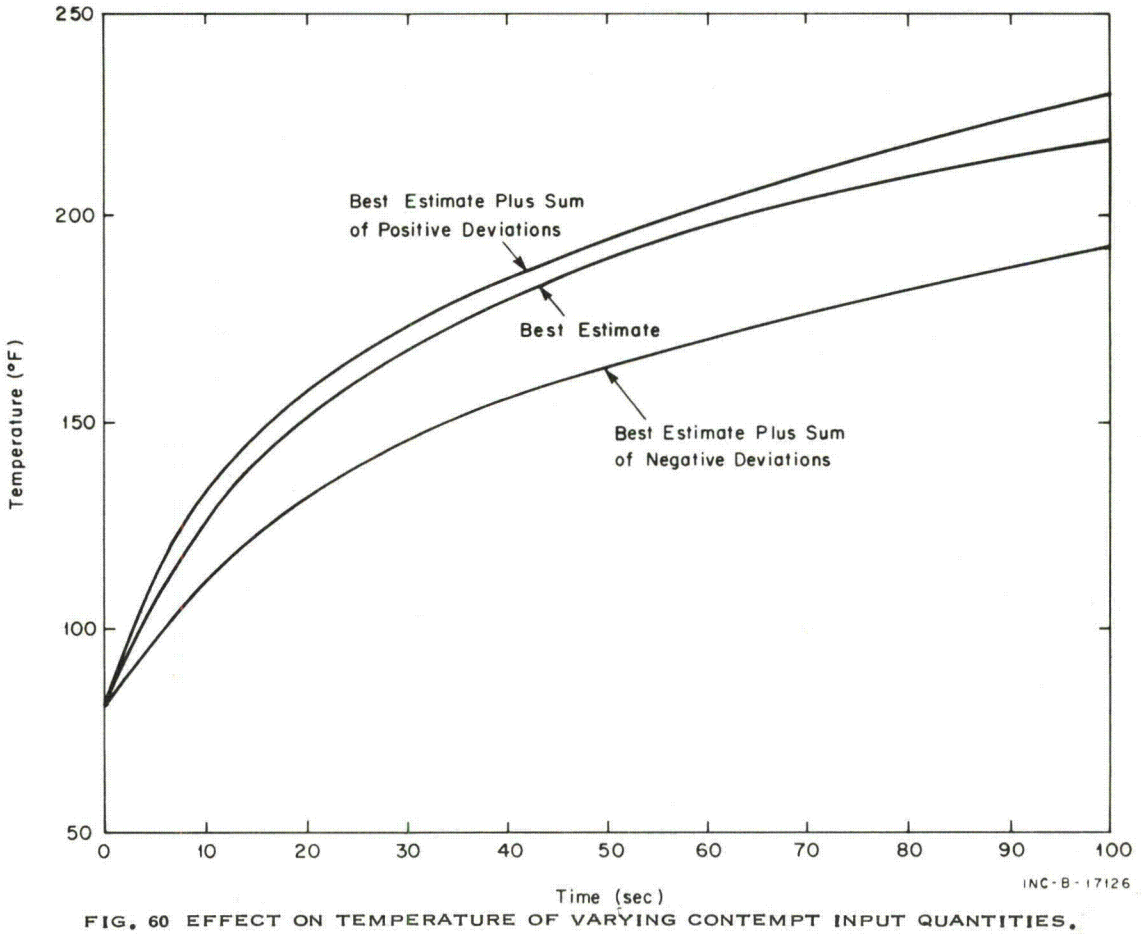

FIG. 60 EFFECT ON TEMPERATURE OF VARYING CONTEMPT INPUT QUANTITIES.

and CONDRU I codes account for superheated steam, but otherwise they are basically one-volume codes. The CVTR is divided by an operating floor into two distinct volumes or compartments with an interconnecting flow path (as discussed in Section II-1). The upper and lower volumes are 141,328 ft^3 and 85,590 ft^3, respectively, and the flow path is 329 ft^2. Thus the CVTR geometry is representative of containment compartmentation into large volumes. The CONDRU II code, described in an earlier section, was developed as part of the CVTR work to more realistically represent the CVTR containment and examine compartmentation response.

CONDRU II temperature predictions for the best estimate quantities are compared with the CONDRU I average temperature of the containment given in Figure 61. The probability of significant temperature differentials between the upper and lower regions was clearly indicated. Because of the relatively slow steam injection rate available for these tests, no significant differential pressure between the two volumes was predicted. However, decreasing flow path sizes, increasing steam injection rates, or decreasing the size of compartment volumes may lead to significant differential pressures that should not be ignored in containment response analysis.

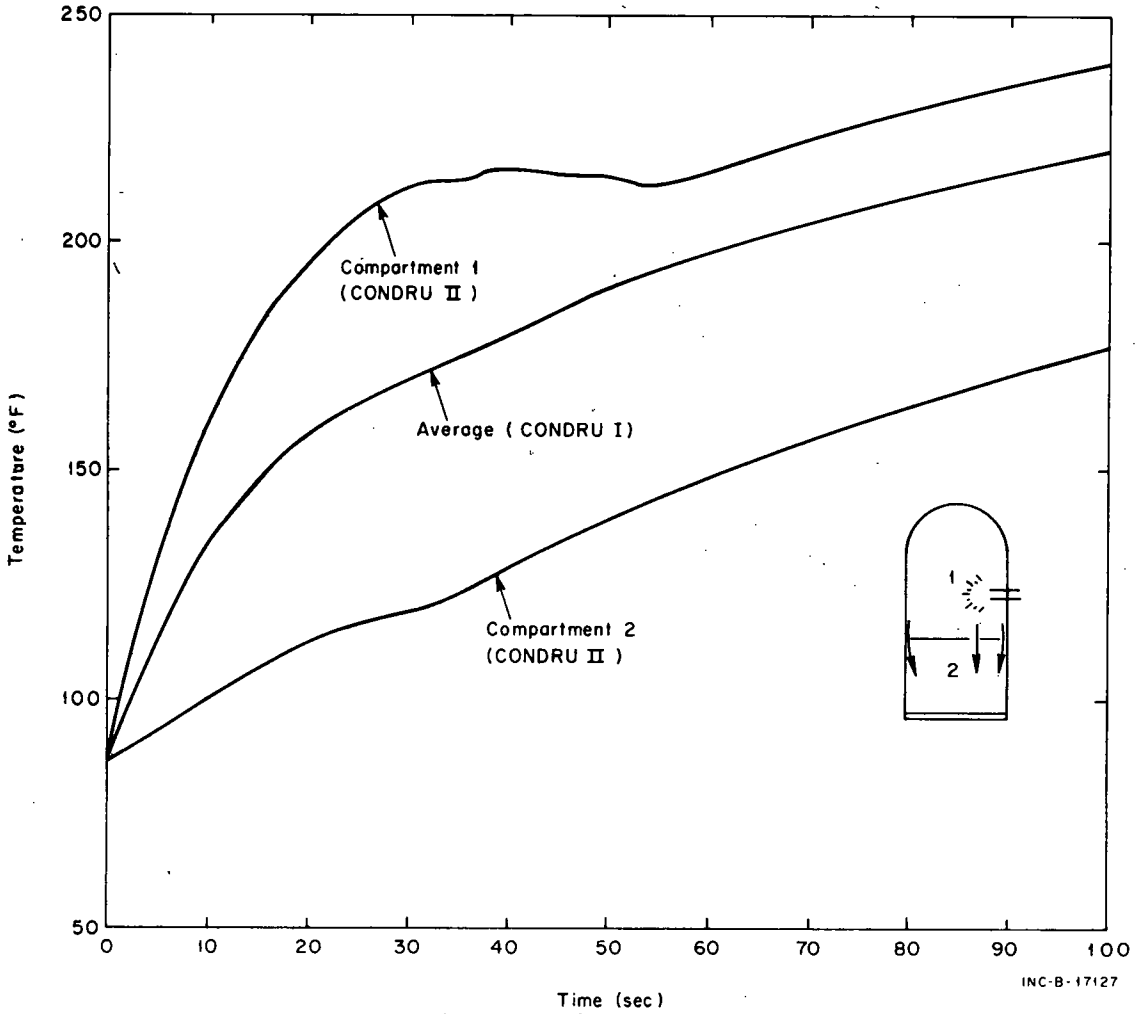

FIG. 61 CONDRU II BEST ESTIMATE FOR CVTR COMPARTMENTS.

2.3 Calculations with Spray

The effect of a pressure suppression spray is indicated by Figure 62 in which pressure behavior from CONTEMPT calculations using the pretest best estimate data are given. Spray is initiated at the time of steam shutoff and continues for 28.5 minutes. The initial temperature of the spray water was 60°F and a spray efficiency of 100% was used in these particular calculations[a]. For posttest calculations, an efficiency of 90% was used.

---

[a] For a spray system using an external water supply, the efficiency of the spray water droplets, E_s, are defined in CONTEMPT as:

$$E_s = \frac{T_f - T_{hout}}{T_a - T_{hout}}$$

where

T_f = temperature of the spray droplets after heat transfer to the containment atmosphere

T_{hout} = temperature of the water at the spray head

T_a = containment atmosphere temperature.

An efficiency of 100% corresponds to $E_s = 1.0$.

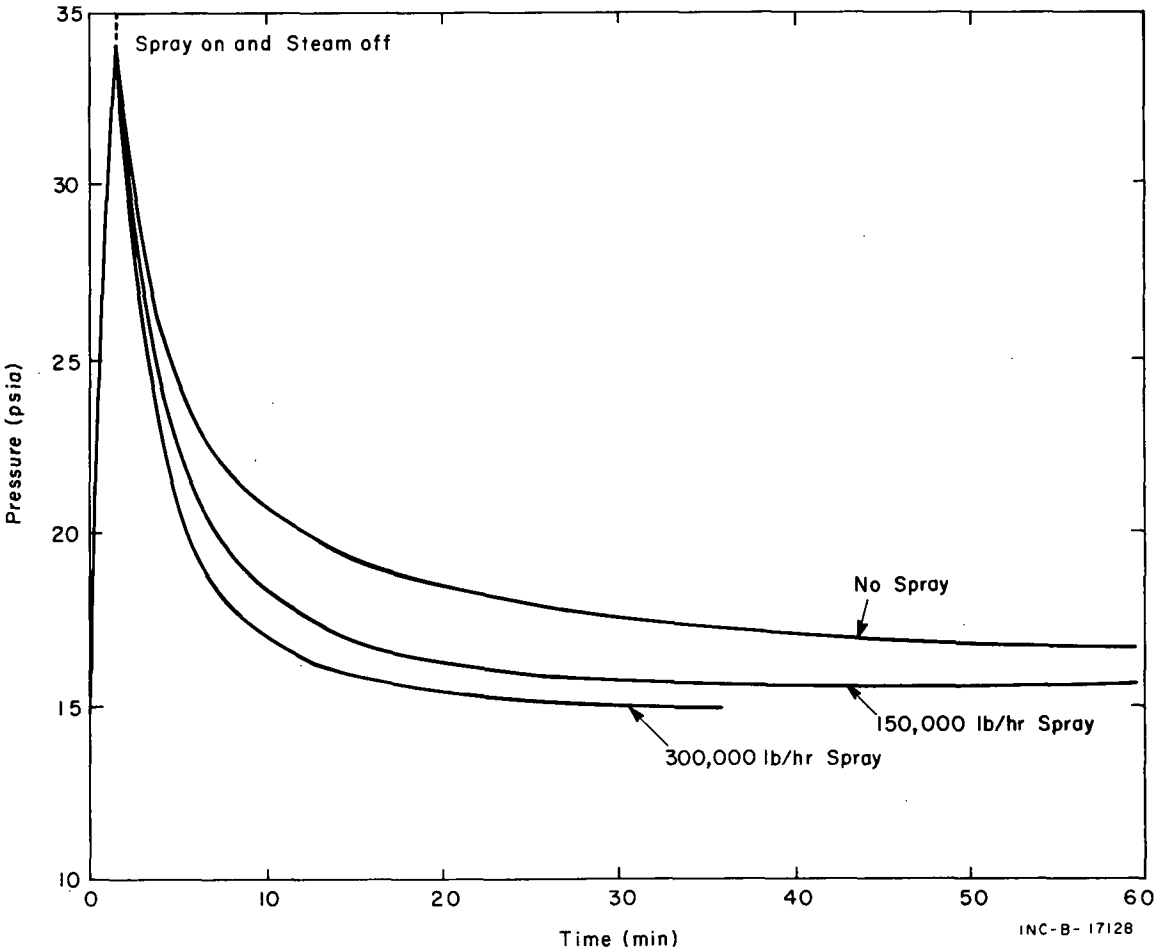

FIG. 62 CONTEMPT BEST ESTIMATE EFFECT FOR PRESSURE SUPPRESSION SPRAY.

3. POSTTEST CONTEMPT CALCULATIONS

As discussed in Section I-2, an important objective of the CVTR test program is the assessment of representative containment response analytical models by comparing the predicted CVTR containment response with experimental response measurements.

The CONTEMPT code has been the principal analytical model evaluated during the CVTR work because of its widespread usage. The opportunity for other organizations to evaluate other containment codes was provided under an industrial participation program.

For evaluation of CONTEMPT, necessary code input data, such as heat transfer coefficients or steam injection rates, were derived from measured data and used in obtaining response predictions. The predicted responses, such as pressure and temperature were compared with corresponding measured response data. In some cases in which obvious differences occurred between the calculated and measured response, such differences were evaluated in terms of whether the fault was in the code or in the input data. Thus, to a limited degree, CONTEMPT was also used as an investigative tool to aid in defining the heat transfer properties. A large number of posttest CONTEMPT calculations were performed and representative results are included in this section. The discussion of the results is centered around heat transfer considerations and the reader is referred to Section IV in which many of the heat transfer considerations were presented.

3.1 Pressure Calculations

The containment pressure for Steam Test 3 is given in Figure 63 for various heat transfer coefficients. For Figure 63, the upper trace represents a calculation in which the pretest heat transfer coefficient used was that illustrated in Figure 38 of Section IV. The steam injection rate and steam conditions used in this calculation are the measured values. As compared to the measured pressure history (also included on the figure), the calculation with the pretest heat transfer coefficient overpredicts the pressure peak by about 8 pounds, or 45%.

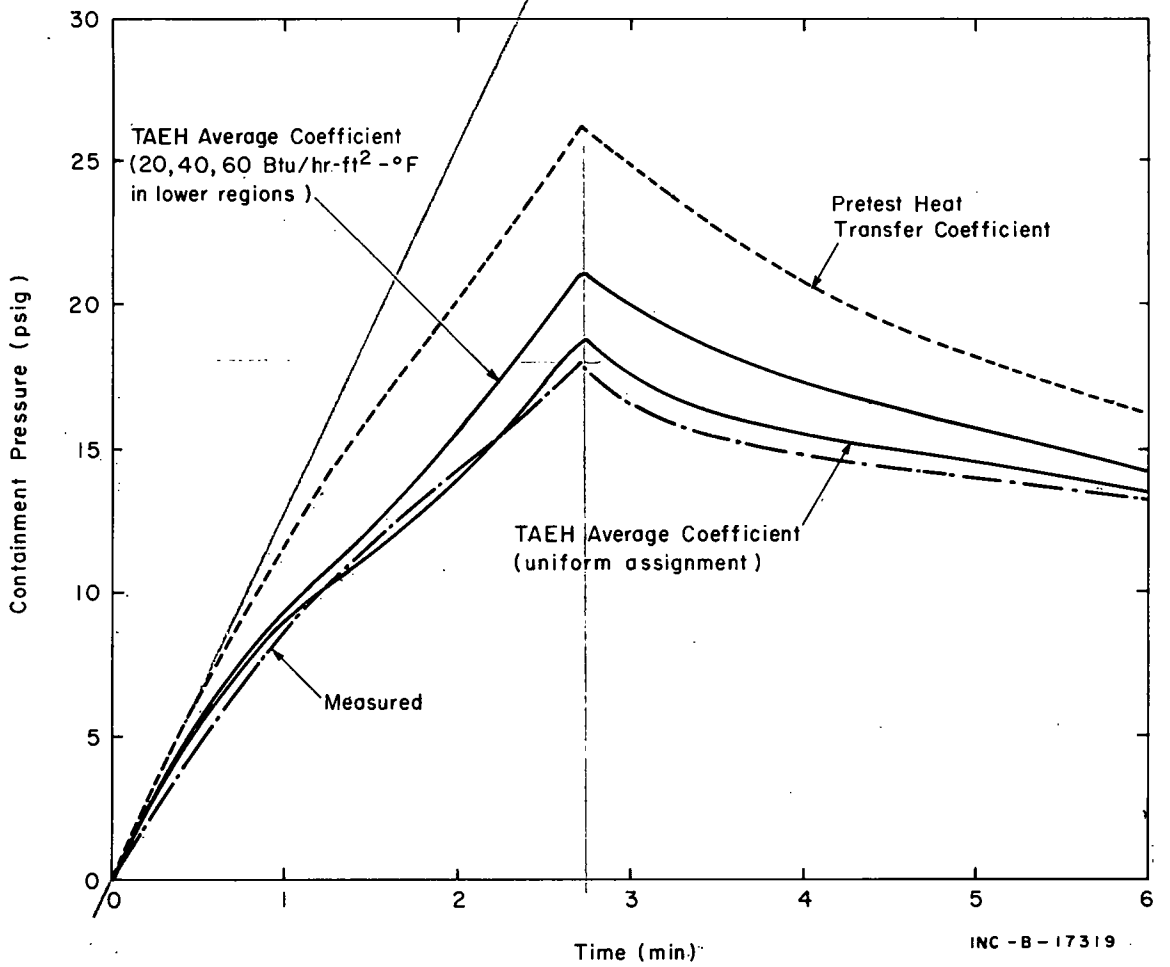

FIG. 63 STEAM TEST 3, PRESSURE CALCULATIONS -- 0 TO 6 MINUTES.

The pressures calculated for the time dependent TAEH average heat transfer coefficient in the operating region and constant values for heat transfer in lower regions are also shown on the figure. From Section IV, the heat transfer to the lower regions was found to be time dependent but of reduced magnitude as compared with that of the operating region. A deficiency of the CONTEMPT code is the inability to include more than one time dependent heat transfer coefficient. The restriction is in keeping with the single-volume model assumption. With this restriction, the assignment of constant values for the heat transfer coefficient of 20, 40, and 60 Btu/hr-ft^2-°F to the concrete in all lower regions, steel in the basement, and steel in the intermediate region,

respectively, was an attempt to more accurately model the heat transfer distribution of the containment. As seen from Figure 63, the calculated pressure still exceeds the measured data by about 3 pounds, or 17%, at the peak.

Finally, Figure 63 presents calculated results for uniform assignment of the TAEH average heat transfer coefficient to all heat absorbing structures. This heat transfer assumption is identical to common practice in containment analysis but is surely erroneous for the CVTR case because of the known reduced heat transfer in the lower regions. Nevertheless, the agreement between calculated and measured results is considerably improved.

To illustrate another feature of the calculation with the average TAEH heat transfer coefficient assigned uniformly, the results are extended in time to 18 minutes and are presented in Figure 64. For the lower curve, the heat transfer coefficient has been held at a constant value of 30 Btu/hr-ft^2-°F commencing at a time of about 200 seconds. From Table IV, Section IV, this assumption would seem to correspond fairly well with the Uchida data for the air-to-steam ratios of the test. However, apparently, such an assumption is

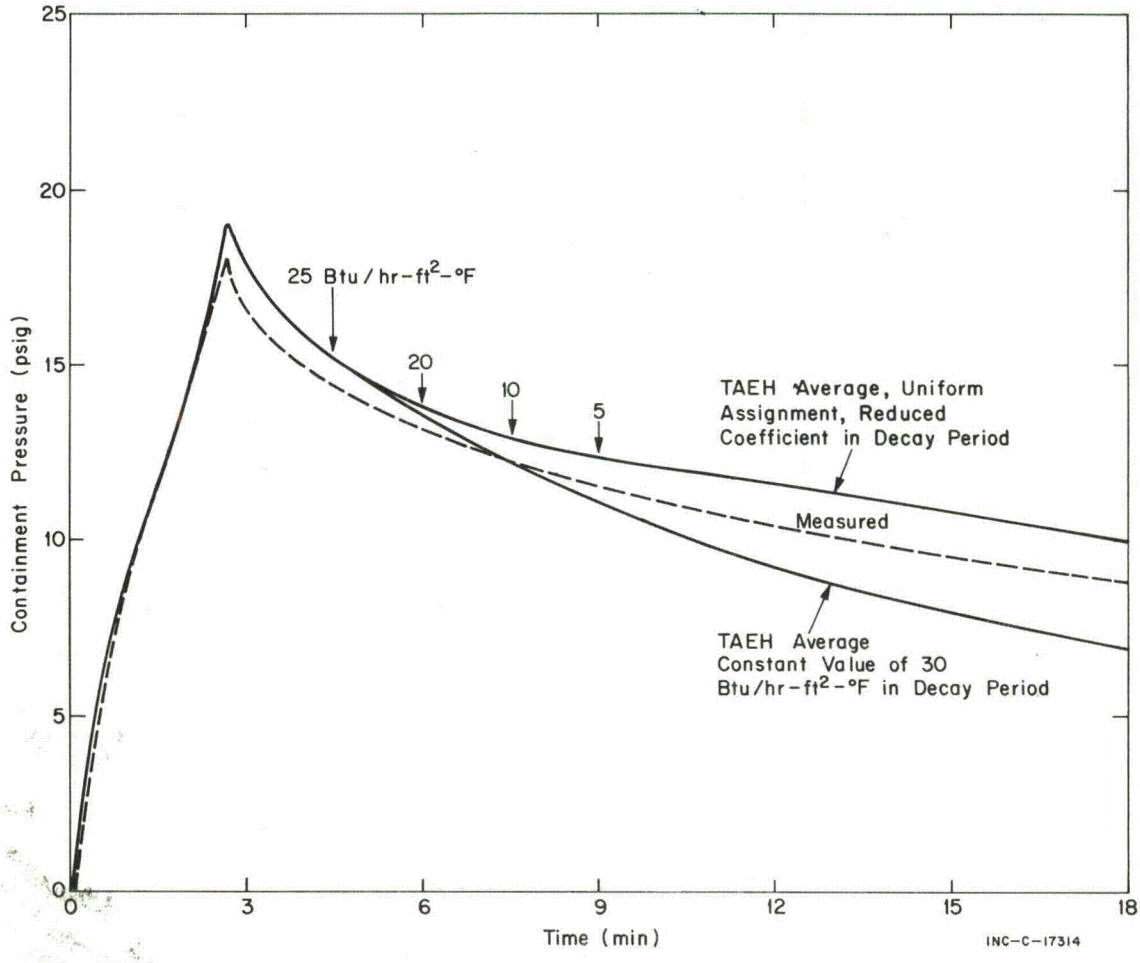

FIG. 64 STEAM TEST 3, PRESSURE CALCULATIONS -- 0 TO 18 MINUTES.

incorrect for the case of CVTR and will result in the actual pressure being underestimated over the long time period. For the top trace of Figure 64, the heat transfer coefficient has been reduced in the pressure decay period as indicated. For example, at a time of 9 minutes, the heat transfer coefficient was assigned a value of 5 Btu/hr-ft^2-°F until termination of the calculation. The shape of the curve indicates that this heat transfer coefficient is more nearly correct; however, it possibly should have been assigned at a time later than 9 minutes.

The TAEH average heat transfer coefficient with uniform assignment has been shown (Figure 63) to give a reasonable approximation to the measured pressure curve. However, as discussed, the heat transfer in lower regions for the CVTR tests obviously should be reduced in magnitude compared to that of the upper region. Also from Figures 63 and 64, a suitably large heat transfer coefficient for calculated and measured peak pressure agreement has not been achieved. Two possibilities are that the heat transfer in the upper region is somewhat larger on the average than that given by the TAEH average data, or, that the amount of steel in the containment has been underestimated. This latter possibility is a very real one in that the large amount of piping, ventilation ducts, gratings, tanks, and miscellaneous gear are difficult to estimate or incorporate as heat slab code input data in an accurate fashion. The procedure was simply to incorporate only major components and to use the added steel as a parameter. Additional calculations, the results of which are shown in Figure 65, were performed for Test 3 to investigate these possibilities. The upper curve is from a calculation in which the TAEH-generated heat transfer coefficient is from Heat Plug 2 and corresponds to an increase in the heat transfer in the upper region. The constant heat transfer coefficient assignment to the lower regions is identical to that of the earlier discussion. Some improvement in the agreement between the calculated and measured peak pressures is observed by comparison with the similar run with the TAEH average coefficient of Figure 64. However, the improvement is small such that increases in the heat transfer coefficient of the upper region would appear to be an unlikely solution. An additional observation is that the constant heat transfer coefficient assignment for the lower regions is a poor assumption in the long time sense as indicated by the incorrect calculated pressure decay curve.

To investigate the effect of underestimating the amount of steel in the containment, the quantity of steel was increased by 20% in the operating regions and by 50% in the lower regions. These increases are considered to be the upper limit of possible inaccuracy in determining the quantity of steel in the containment. For both the operating and lower regions, the steel increase was assigned as an increase in the area of an existing heat absorbing steel slab and given a thickness of 1/2 in. Calculated results for the case of increased steel are shown in Figure 65.

The peak pressure agreement is improved but the pressure during the decay period is obviously in error. The erroneous pressure during this period is believed to be primarily due to the constant heat transfer assignment in the lower regions. For the case in which the TAEH average heat transfer coefficient was assigned uniformly to all regions along with the increase in steel heat slabs, too much heat transfer is exhibited.

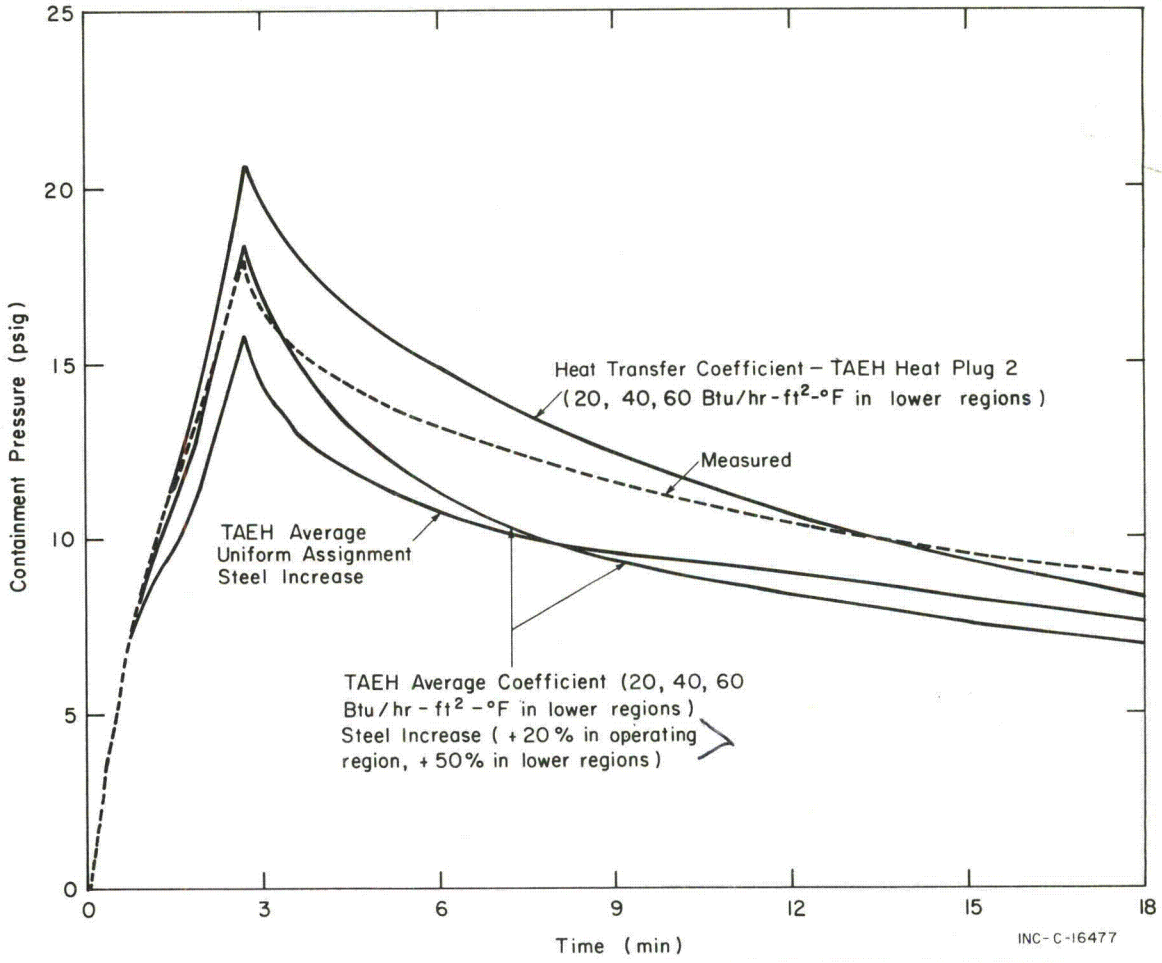

FIG. 65 STEAM TEST 3, PRESSURE CALCULATIONS WITH STEEL CONSIDERED.

Figure 66 shows the results of two calculations compared to the experimental data for Steam Test 4. For Test 4, only Heat Plug 2 was functioning, thus, the calculation uses the TAEH determined heat transfer coeffficient from Plug 2 with uniform assignment to all regions. The upper trace was obtained by using the measured steam flow rate data. The lower trace shows the results obtained by assuming a 2-1/2% inaccuracy in the steam flow rate measurements. As given in Table VII, Section V-1.4, the inaccuracy of the steam flow measurement could be as great as 6%.

Again, from the results of Test 4, very little heat transfer in the decay period is indicated by the values at the 6- and 7-1/2-minute times. For this calculation, the coefficient was about 4 Btu/hr-ft^2-°F at 18 minutes and was reduced to 3 Btu/hr-ft^2-°F at 30 minutes. The code performed a tabular interpolation for needed values at other times. Even at these low values the heat transfer coefficients are too large in the decay period for this test. Apparently, the pressure suppression spray water employed for this test acted as an effective heat sink such that heat transfer to structures was reduced nearly to zero.

A similar calculation for Steam Test 5 is given in Figure 67. The TAEH Heat Plug 2 data are used for the heat transfer coefficient in the upper region and the constant heat transfer coefficient is assigned to the lower regions. As can be seen, the calculated results for Test 5 indicate the same general trends as have been commented on in the preceding discussions.

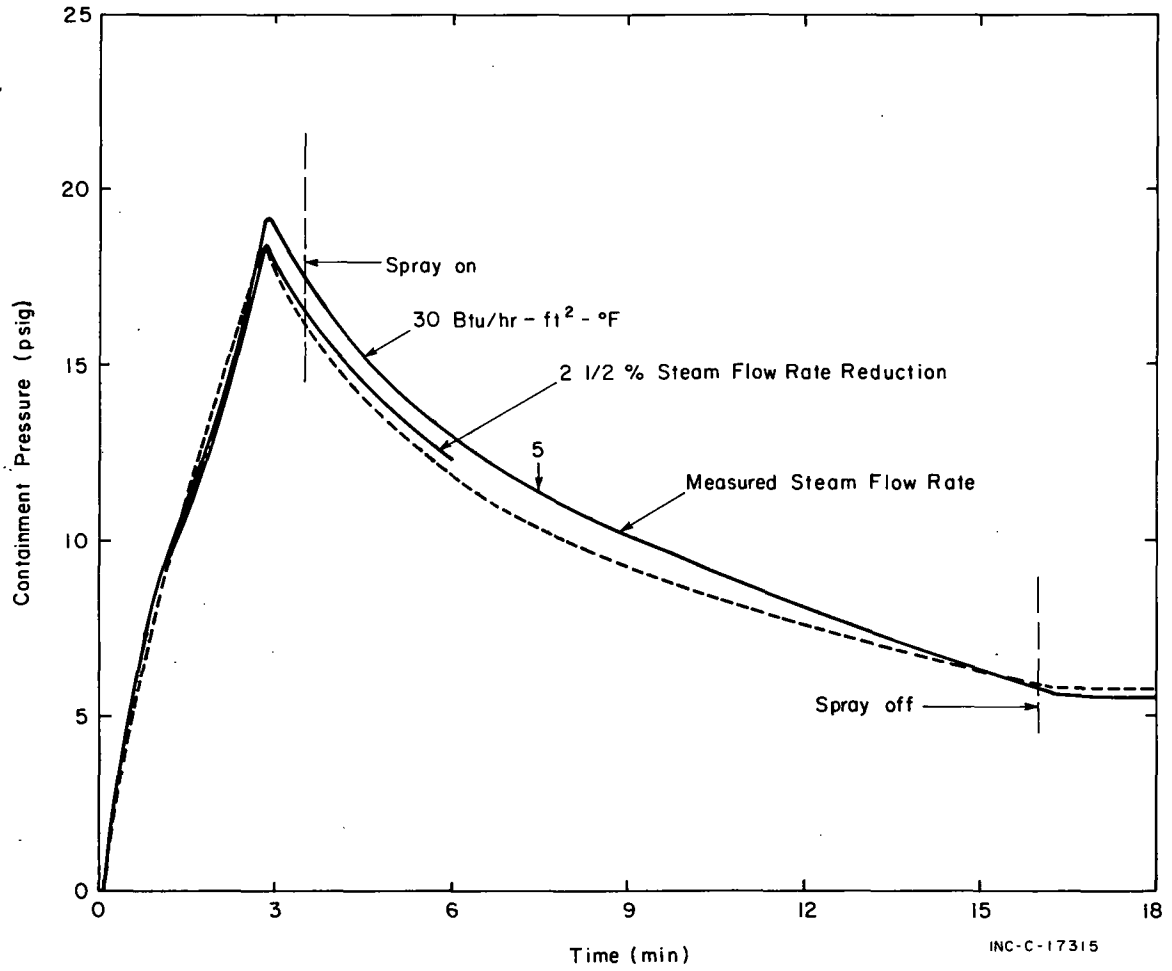

FIG. 66 STEAM TEST 4, PRESSURE CALCULATIONS.

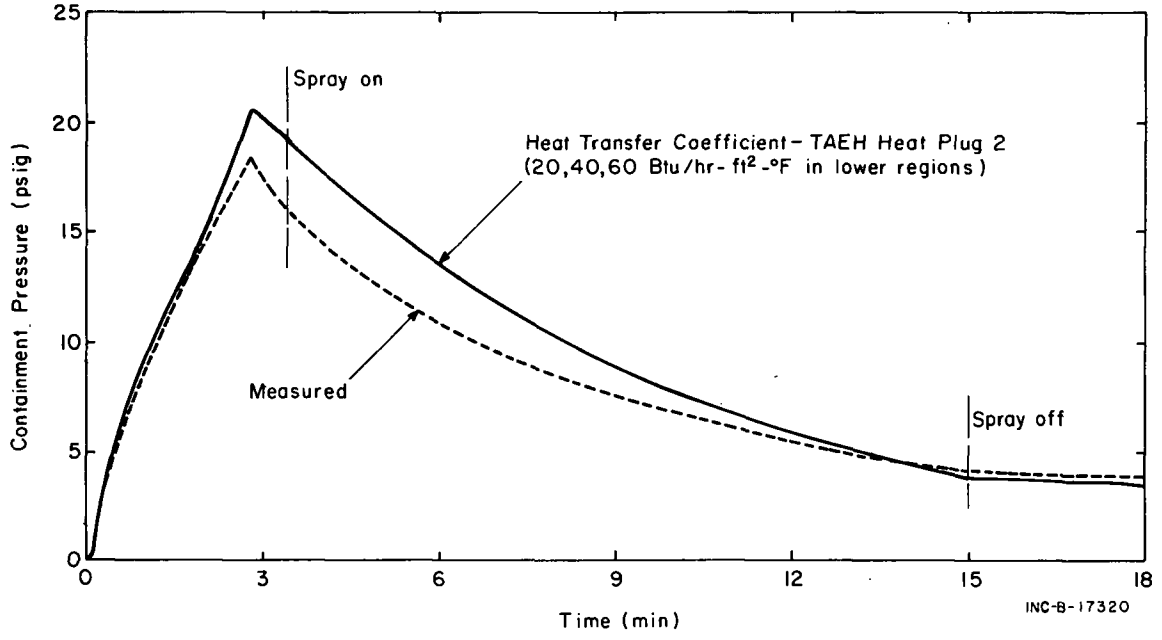

FIG. 67 STEAM TEST 5, PRESSURE CALCULATIONS.

3.2 Temperature Calculations

CONTEMPT-calculated temperature results are compared with experimental data from Steam Test 3 in Figure 68. The experimental bulk atmosphere and surface temperatures for the operating region shown in this figure are from Heat Plug 2 and are nearly representative of the average behavior for the operating region. (However, higher temperatures were recorded at some points in the region.) Temperatures at two locations in the intermediate region are shown on the figure to illustrate the large differences noted in this region. The temperature of the basement region is representative of the average behavior in this region. CONTEMPT, being a single volume code, calculates a single temperature, shown by the dashed line in Figure 68, which in this case is approximately a volume-weighted average of the temperature behavior throughout the containment. As can be seen, the experimental maximum temperatures are underestimated by CONTEMPT. This underestimation was not particularly serious in the case of CVTR because the temperature of the injected steam was relatively low (about 380°F), the injection rates were low, the volumes relatively open, and interconnecting flow paths large. However, for fast blowdowns of high temperature water (approximately 600°F) and blowdowns in smaller volumes, or blowdowns for which more serious flow restrictions exist, temperature predictions may be seriously in error and localized heating exceeding design limits may result.

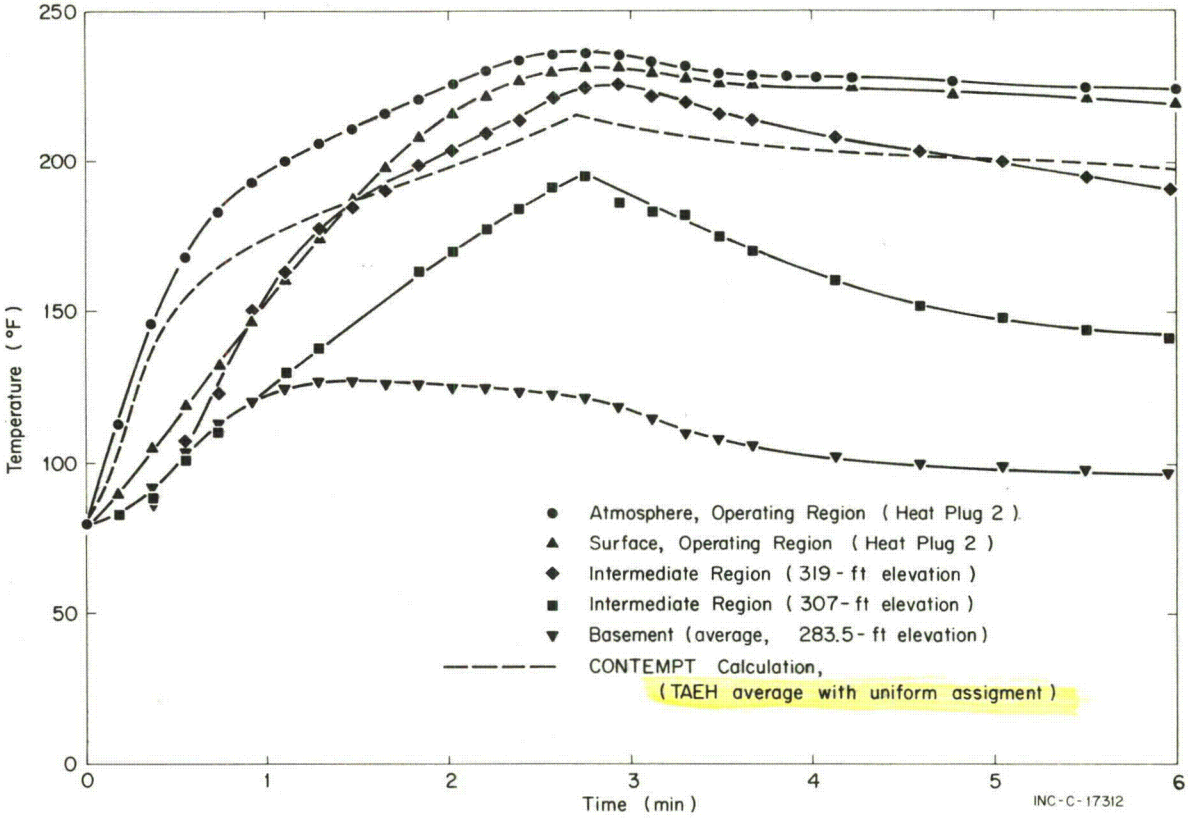

FIG. 68 STEAM TEST 3, TEMPERATURE RESULTS.

The calculated temperature behavior is dependent on the heat transfer assumptions used in the calculation. Calculated temperatures based on the various heat transfer assumptions that have been discussed in previous sections are compared in Figure 69 for Test 3. As can be seen, the effect of heat transfer over the range investigated has relatively small effects on the calculated average temperature.

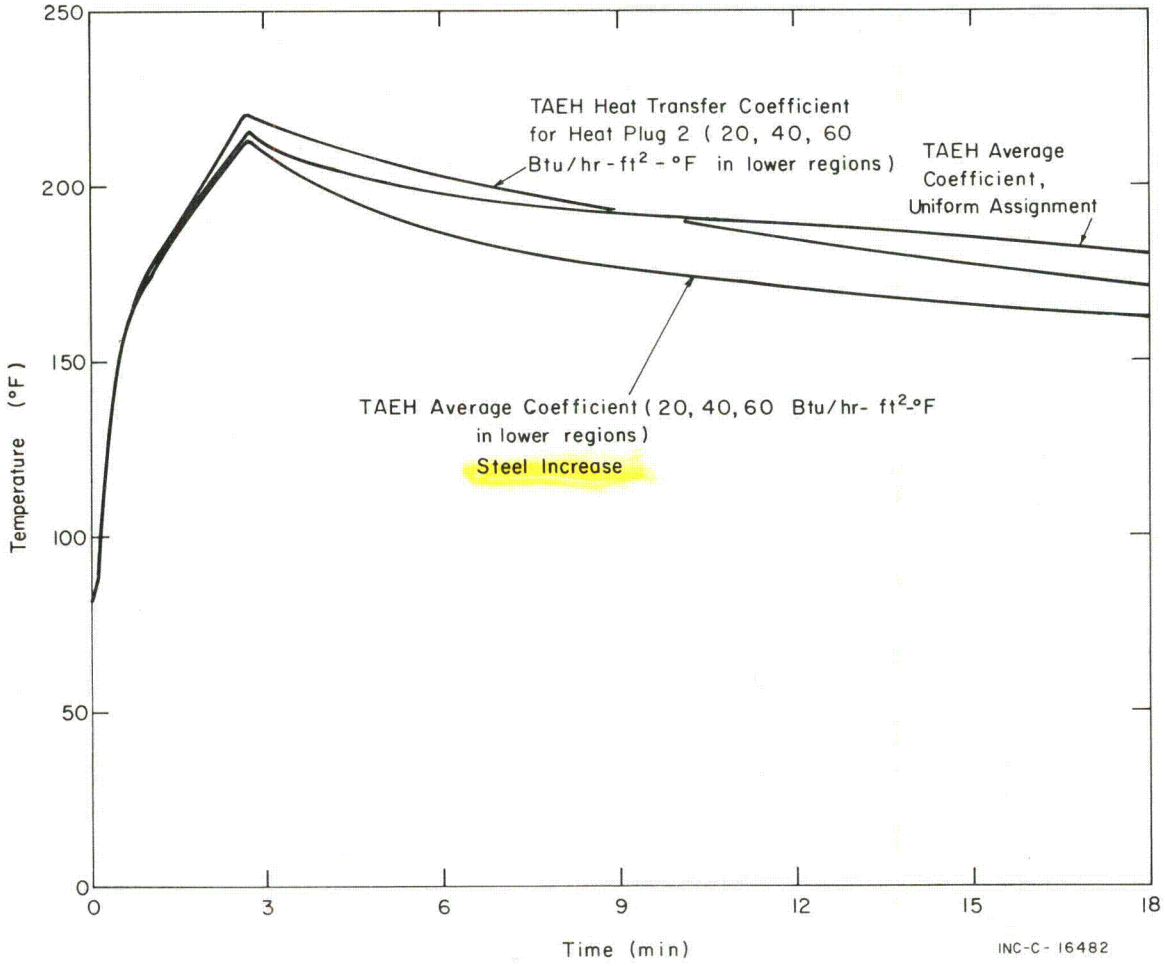

FIG. 69 STEAM TEST 3, CONTEMPT-CALCULATED TEMPERATURES FOR VARIOUS HEAT TRANSFER ASSUMPTIONS.

4. CONDRU II CALCULATIONS

As noted in the previous discussions, actual steam injection conditions result in special temperature (and pressure) gradients that need to be taken into account in the plant design. The two-node code, CONDRU II (Section V-1.3) was developed to predict pressure and temperature gradients in containment systems. Results of CONDRU II posttest calculations are shown in Figures 70 through 73. For these calculations, the TAEH average heat transfer coefficient was assigned to the operating region (Compartment 1) and a second time-dependent heat transfer coefficient was assigned to the lower regions (Compartment 2). The heat transfer coefficient for Compartment 2, which was nearly the average of the two curves shown for the intermediate region in Figure 44, had a peak value of 115 Btu/hr-ft^2-°F at about 135 seconds.

Calculated temperatures are compared with measured values for Tests 3 and 5 in Figures 70 and 71, respectively. Good temperature agreement is noted for the operating region whereas poor agreement is evidenced for the lower regions. Again, the one node assigned to the lower region was found to be insufficient for accurate representation of the CVTR temperature distribution and the need for development of a several-node model is indicated.

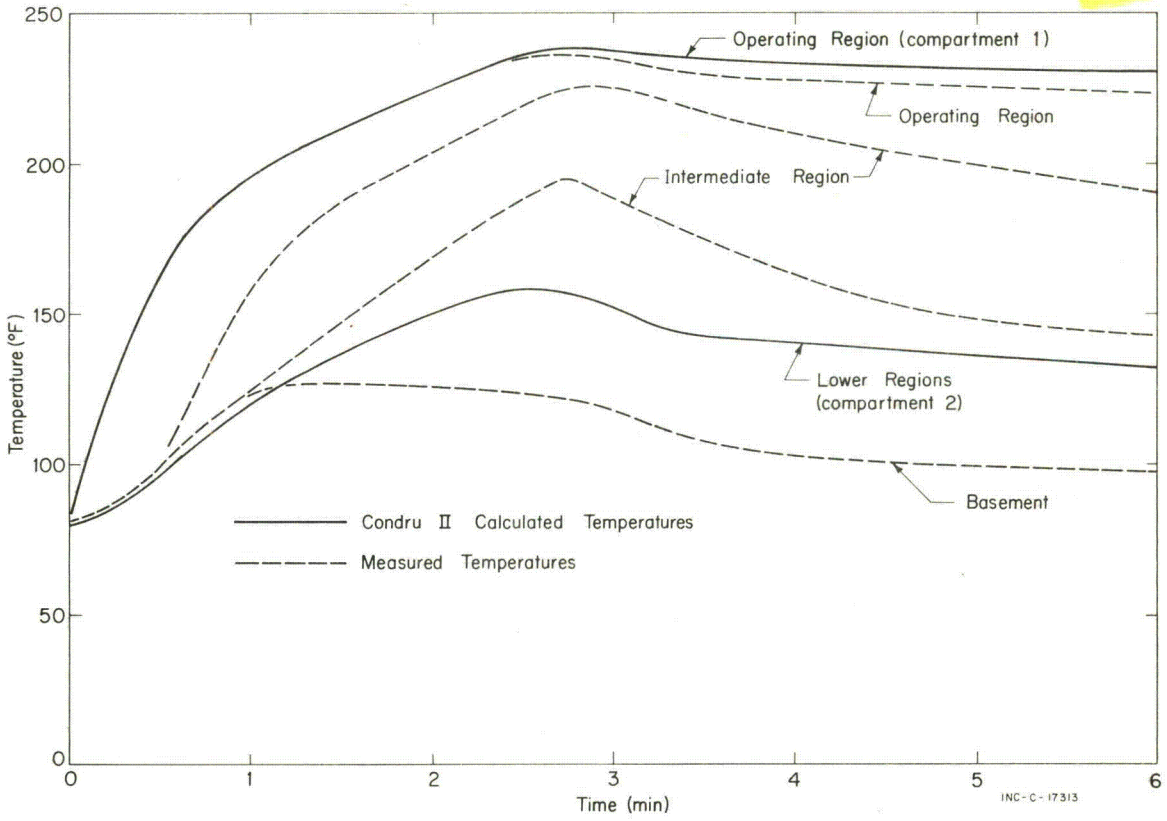

FIG. 70 CONDRU II TEMPERATURE CALCULATION RESULTS FOR STEAM TEST 3.

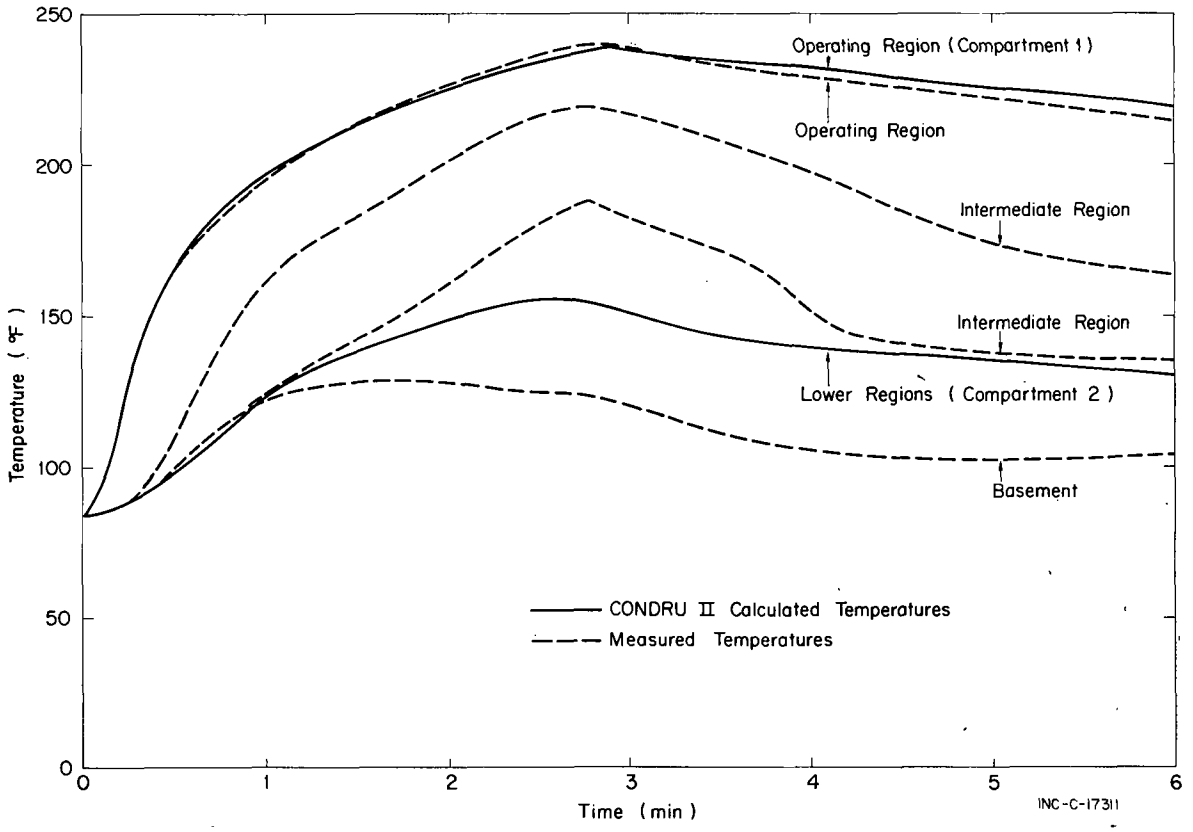

FIG. 71 CONDRU II TEMPERATURE CALCULATION RESULTS FOR STEAM TEST 5.

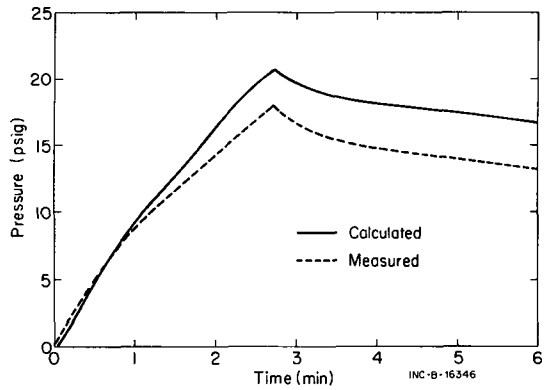

FIG. 72 CONDRU II PRESSURE CALCULATION RESULTS FOR STEAM TEST 3.

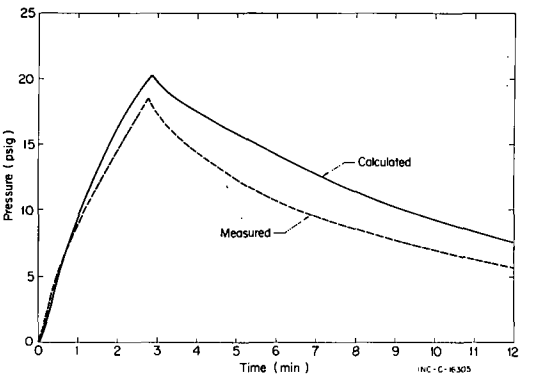

FIG. 73 CONDRU II PRESSURE CALCULATION RESULTS FOR STEAM TEST 5.

CONDRU II pressure calculation results are shown in Figures 72 and 73 for Steam Tests 3 and 5, respectively. The CONDRU II calculated pressures are 15 and 10% too high for the two tests but the shape of the curves is approximately correct, particularly in the decay portion. This behavior is attributed to the more nearly accurate representation of the heat transfer in the lower region provided by the second time-dependent heat transfer coefficient assignment.

VI. MISCELLANEOUS RESULTS

Experimental information concerning containment insulation, containment coatings, a fixed leak system, containment convective currents, and the gross effects of DBA testing on the containment was obtained during the DBA tests.

1. POLYURETHANE INSULATION

Reinforced-concrete containment vessels used for nuclear power reactors frequently are provided with thermal insulation on the bottom 20 feet of the inside surface of the liner to reduce the stress contribution from thermal effects at the junction of the wall and base slab in the unlikely event of an accident. To examine the effectiveness of this technique, an 8-ft high by 30-ft long section of the CVTR containment liner, between elevations of 287 and 295 feet, was insulated with a 2-inch-thick sheet of polyurethane (U-200, $\rho = 2.8$ lb/ft^3). Thermocouples and strain gauges were placed on the liner surface under the insulation and also on an adjacent uninsulated section of the liner.

Figure 74 presents liner surface temperature data obtained during DBA Test 3 for two thermocouples positioned under the insulation and one thermocouple on the adjacent uninsulated liner. As can be seen, the insulation resulted in a reduced temperature. Had the insulation been located in the operating region where a much higher containment temperature was obtained, a much more significant effect would have been observed. The results from the strain gages located beneath the polyurethane also indicated a reduced strain when compared with results from gages installed on the bare liner. Thus, insulation provides protection to the liner from DBA effects. The more rapid the atmospheric temperature increase and the higher the peak temperature value, the greater the potential protective effect of the insulation.

The insulation will reduce the total energy absorbed by the liner and thus cause a higher peak containment pressure during a DBA. A trade-off evaluation is thus required to determine the optimum design.

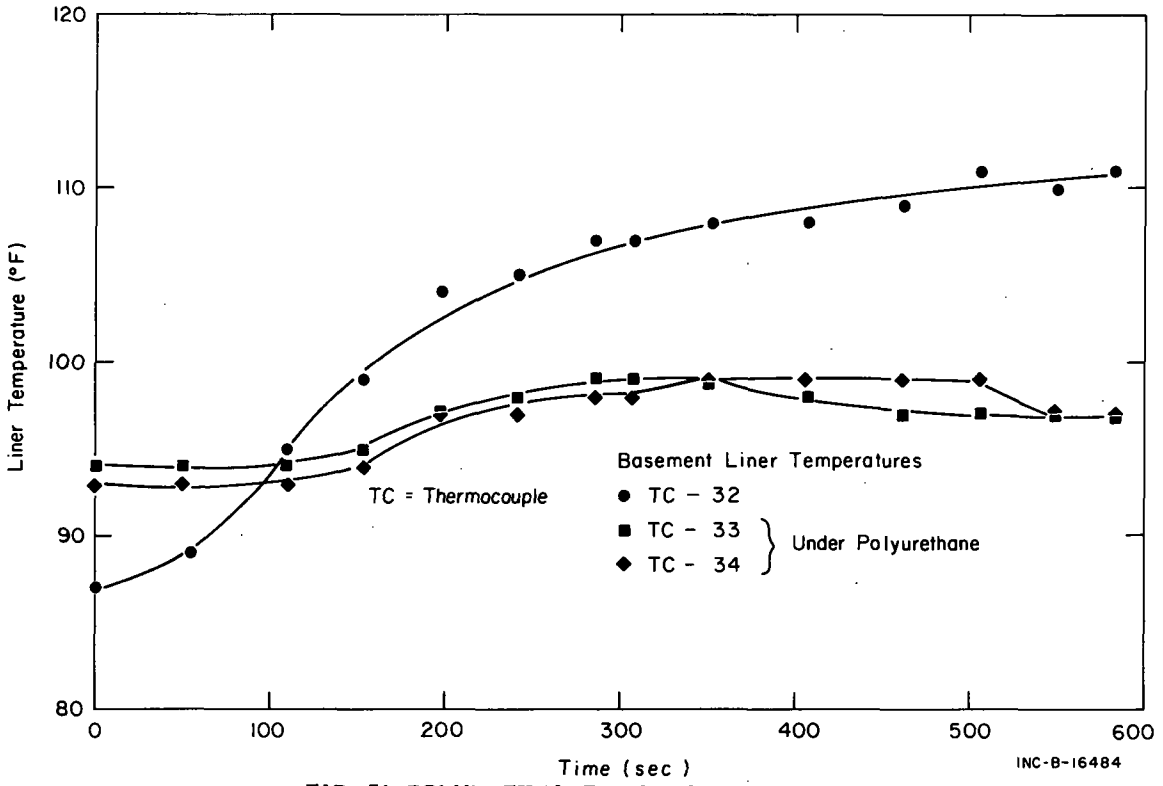

FIG. 74 POLYURETHANE INSULATION EFFECT.

2. PAINT SAMPLES

In cooperation with the Oak Ridge National Laboratory[21], paint samples were installed in the CVTR containment operating region for exposure during the steam injection tests to determine the effects of DBA testing upon various paint samples. The samples, shown in Figure 75, consisted of about 160 commercial paint samples from 12 paint manufacturers, and 20 experimental paint samples designed primarily for fission product retention. The paint samples represented various paints, different thicknesses of paint, different methods of application, and different types of prime coats. The commercial paint was applied to 6-inch square coupons, some of which were steel and some of which were concrete. The experimental paint was applied to 1-inch square coupons.

The effects of DBA conditions upon some of the paint samples is shown in Figure 76. As can be seen, after one steam test the experimental paint samples showed chipping, cracking, and blistering. Most of the commercial paint samples, however, showed little, if any degradation. Following the DBA tests, the paint samples were shipped to ORNL for final evaluation. Information on the results of this evaluation can be found in Reference 21.

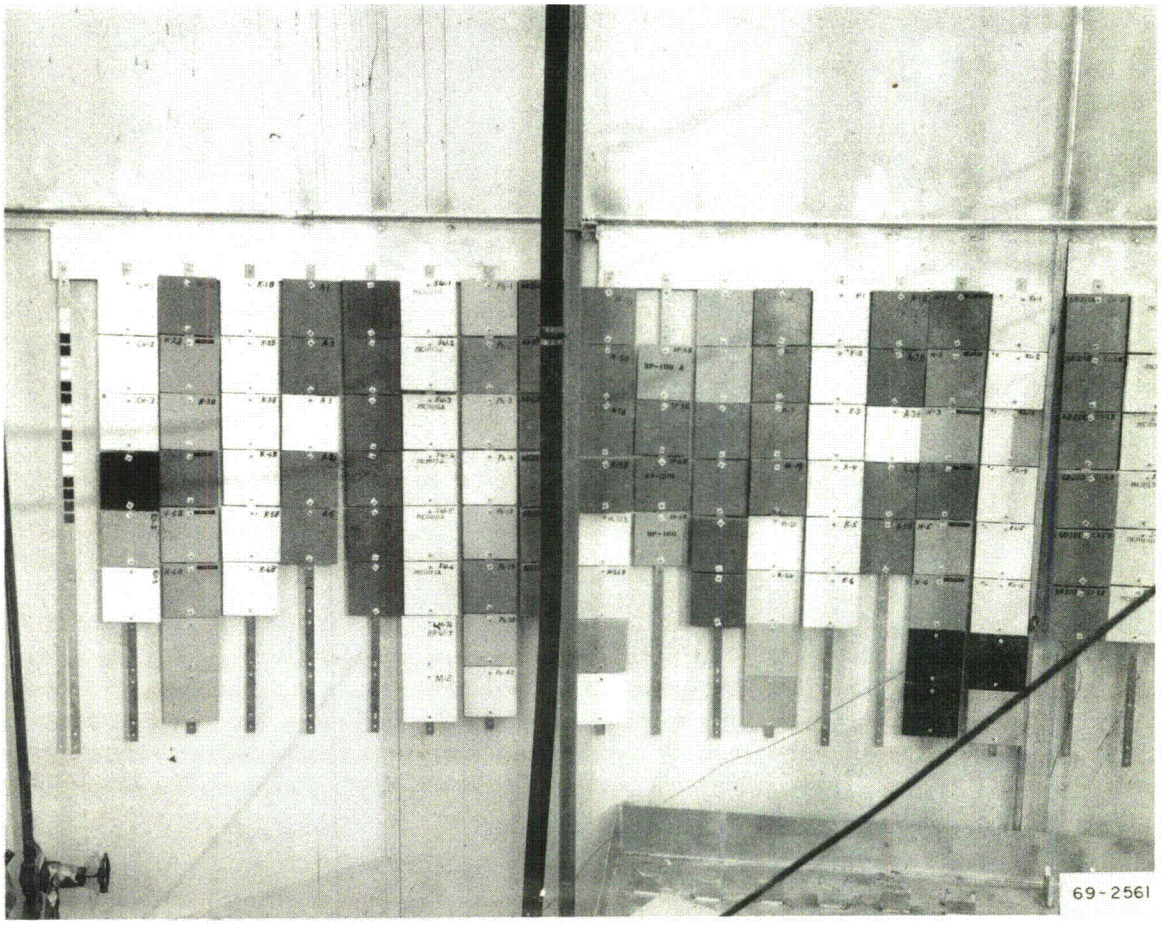

FIG. 75 ORNL PAINT SAMPLES.

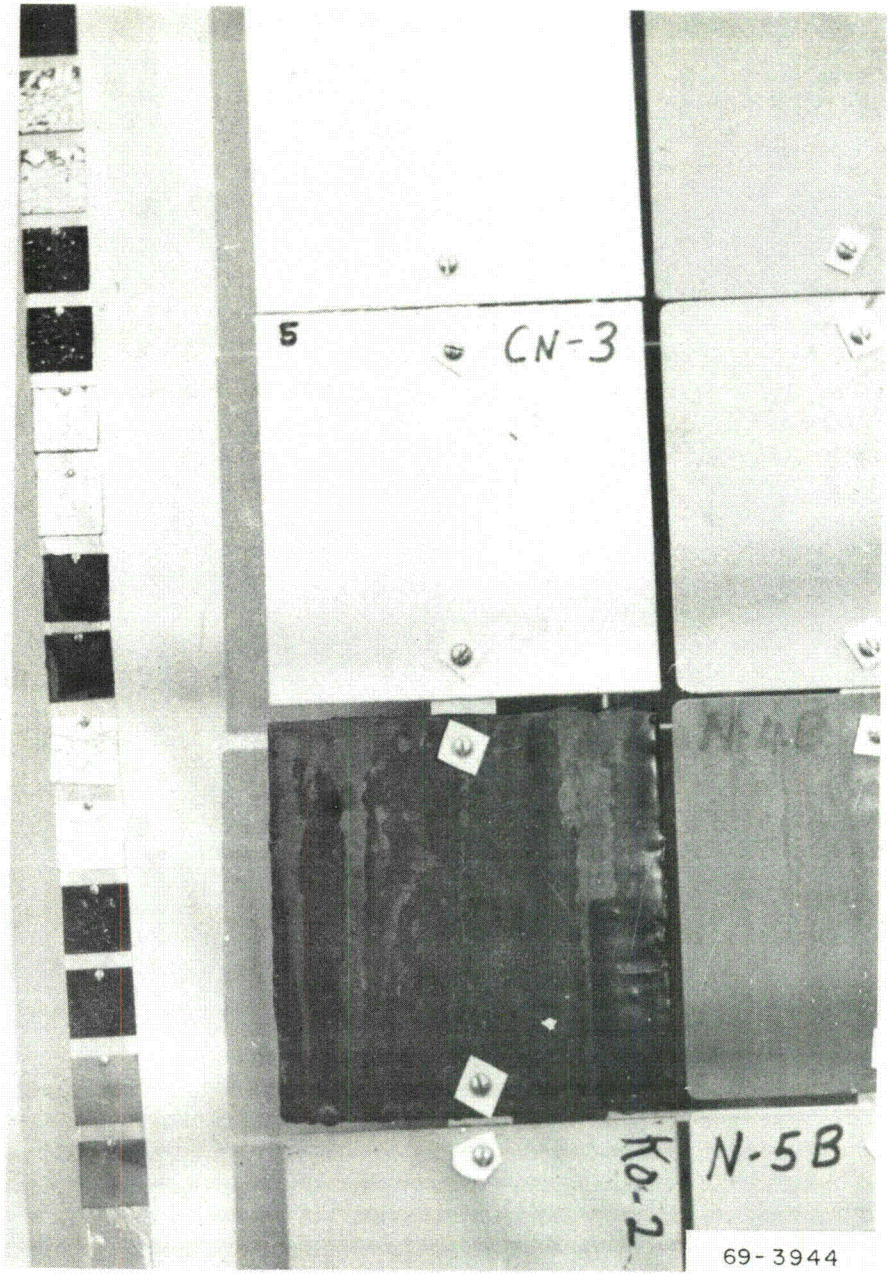

FIG. 76 ORNL PAINT SAMPLES FOLLOWING STEAM TEST 2.

3. FIXED LEAK DATA

A fixed leak system was installed in the CVTR containment to determine the influence of pressure, temperature, and DBA conditions on the leakage rate through a fixed leak path. This system, shown in Figure 77, consisted of a one-inch-diameter pipe, 48 inches long, 40 inches of which were filled with crushed concrete. A four-inch-thick stainless steel wool plug was installed at each end of the pipe to hold the concrete in position. The entire assembly was welded into an existing containment penetration and vented to the stack.

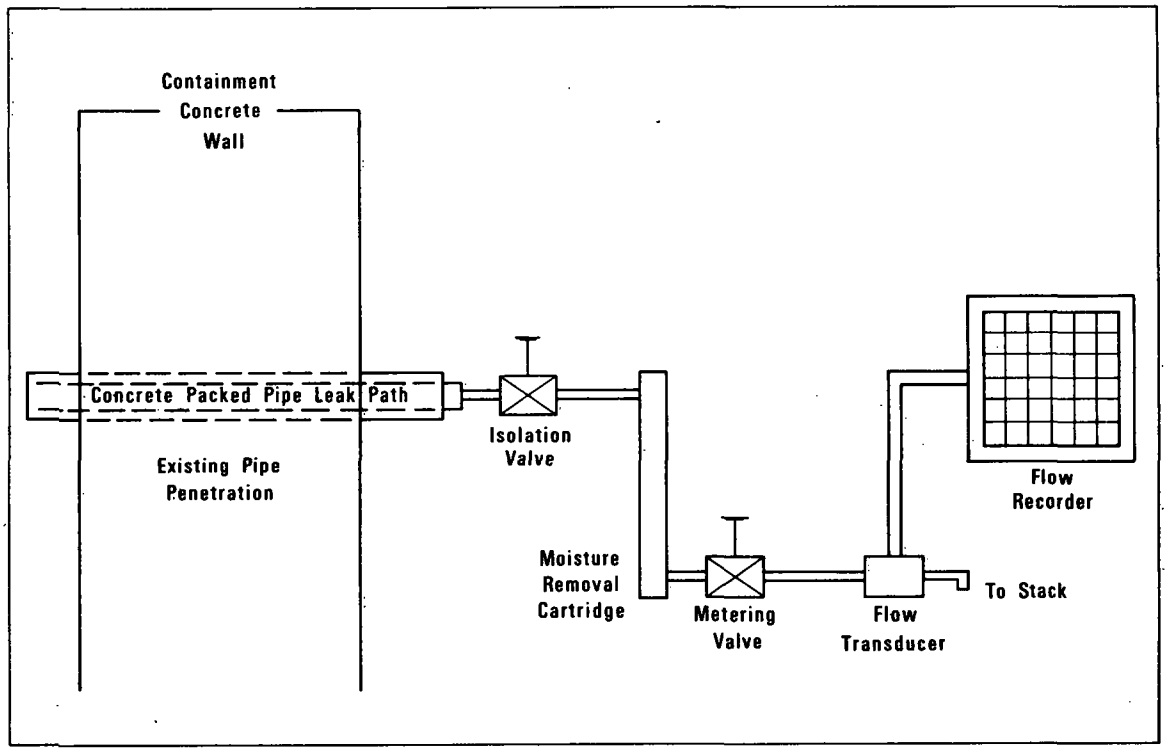

FIG. 77 FIXED LEAK SYSTEM.

At a pressure of 6 psig and at ambient temperature, a flow rate of about 100 cm^3/min was established with the metering valve. A fixed flow path was provided by operating an isolation valve at the fully on or off position. The air passed through a Drierite cartridge in which moisture was removed and then through a Hastings mass flowmeter by which flow rate was determined.

The results of this experiment indicate that although the flow rate changed with pressure about as expected, no significant change could be attributed to either temperature or steam conditions. That is, for the same containment pressure, the flow rate during the steam tests remained the same as that observed during the ambient temperature leakage rate tests[7]. Thus, for this particular experiment, DBA conditions did not change the leakage rate.

4. CONVECTIVE CURRENTS

Three ultrasonic anemometers developed by Phillips Petroleum Company[22] were installed inside the CVTR containment vessel for testing and evaluation and for sampling the CVTR containment air flow. Two of the anemometers were located in the vicinity of one of the heat transfer assemblies approximately 2-3/8 inches and 7/8 inches from the liner as shown in Figure 78. The third anemometer was located in the annulus between the operating floor and the containment liner. One of the anemometers on the wall failed during the CVTR leakage rate tests[7], however, and was not used during the steam tests. The data from the two operating anemometers have been

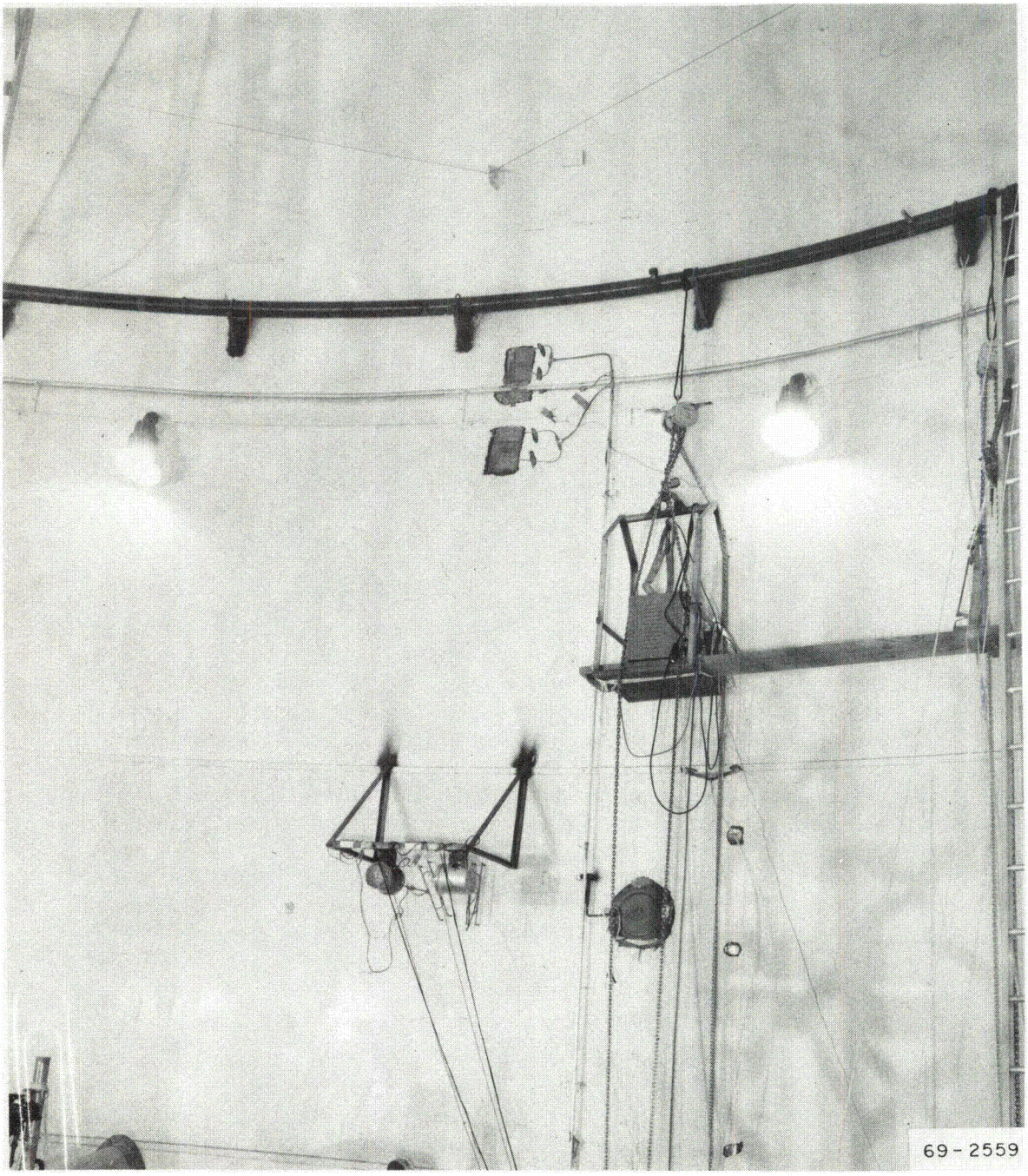

FIG. 78 ULTRASONIC ANEMOMETERS.

evaluated for Steam Tests 3 and 5. The maximum air current velocities of about 30 and 15 ft/sec measured by the anemometers on the wall and in the annulus, respectively, appear reasonable. The indicated directions of flow, however, are inconclusive because the anemometers indicated frequent changes in direction of flow, even following steam injection when containment conditions should have stabilized.

Problems associated with these instruments and their use were:

(1) Insufficient sampling points (devices)

(2) Equipment failure under steam conditions

(3) Insufficient data recording channels

(4) Instabilities in anemometer triggering under DBA conditions.

5. PHOTOGRAPHIC RESULTS

Four movie cameras were used to record the injection of steam into the containment building during the CVTR DBA tests. Three of the cameras were located inside the containment and one was located outside the containment. All four cameras were Photosonics 16-1B with 400-foot magazines of 16-mm film. The locations and running conditions of the cameras are shown in Table VIII.

To protect the cameras from the DBA test conditions, each camera was mounted in a waterproof aluminum box as shown in Figures 79 and 80. Each box contained a glass viewing window and each was installed on a camera tripod for ease of alignment. Twenty 1000-W photographic lamps were positioned to illuminate the containment during steam injection.

The three cameras inside the containment were started by a test sequence timer about eight seconds before initiation of steam injection. The fourth camera, located outside the containment as shown in Figure 81, and the camera lights were turned on manually about 30 seconds before initiation of steam injection. All cameras were allowed to run until they were out of film.

The lights were turned off immediately following camera run-out to reduce the heat addition to the containment atmosphere.

A typical steam injection sequence, as recorded by Cameras 1 and 2 is shown in Figures 82 and 83, respectively. These photos obtained during Steam Test 3 show events typical of all DBA tests. These figures indicate the extensive turbulence and mixing that occurred during steam injection and that aided heat transfer to the containment liner, floors, and interior equipment.

Camera 3 was located in the intermediate region at an elevation of 295 feet for Test 3, and at an elevation of 317 feet for Tests 4 and 5. Analysis of the films from this camera indicate that steam first reached the different containment elevations at the times and containment pressures shown in Table IX.

TABLE VIII

CVTR CAMERA SUMMARY

Camera	Location	Lens	Speed (frames/sec)	Running Time (min)
1	Inside containment at elevation of 345 ft. Recorded steam flow from the diffuser.	5mm	80	2.5
2	Inside containment at elevation of 325 ft. Recorded steam flow from the diffuser.	13mm	80	2.5
3	Inside containment at elevations of 295 ft (Test 3) and 317 ft (Tests 4 and 5). Recorded condensation on electrical penetrations and conduit.	2 in.	40	5
4	Outside containment at elevation of 535 ft. Recorded steam valve action.	1 in.	40	5

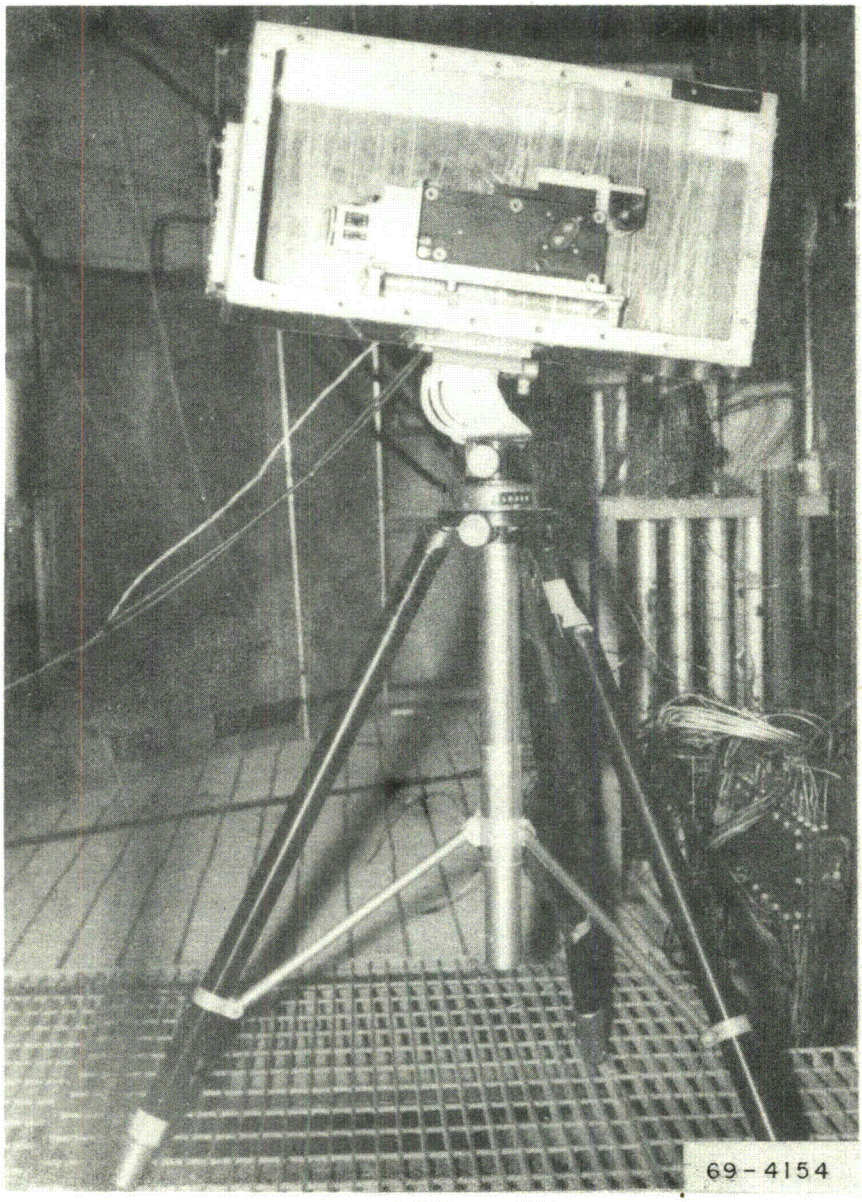

FIG. 79 CVTR CAMERA 3.

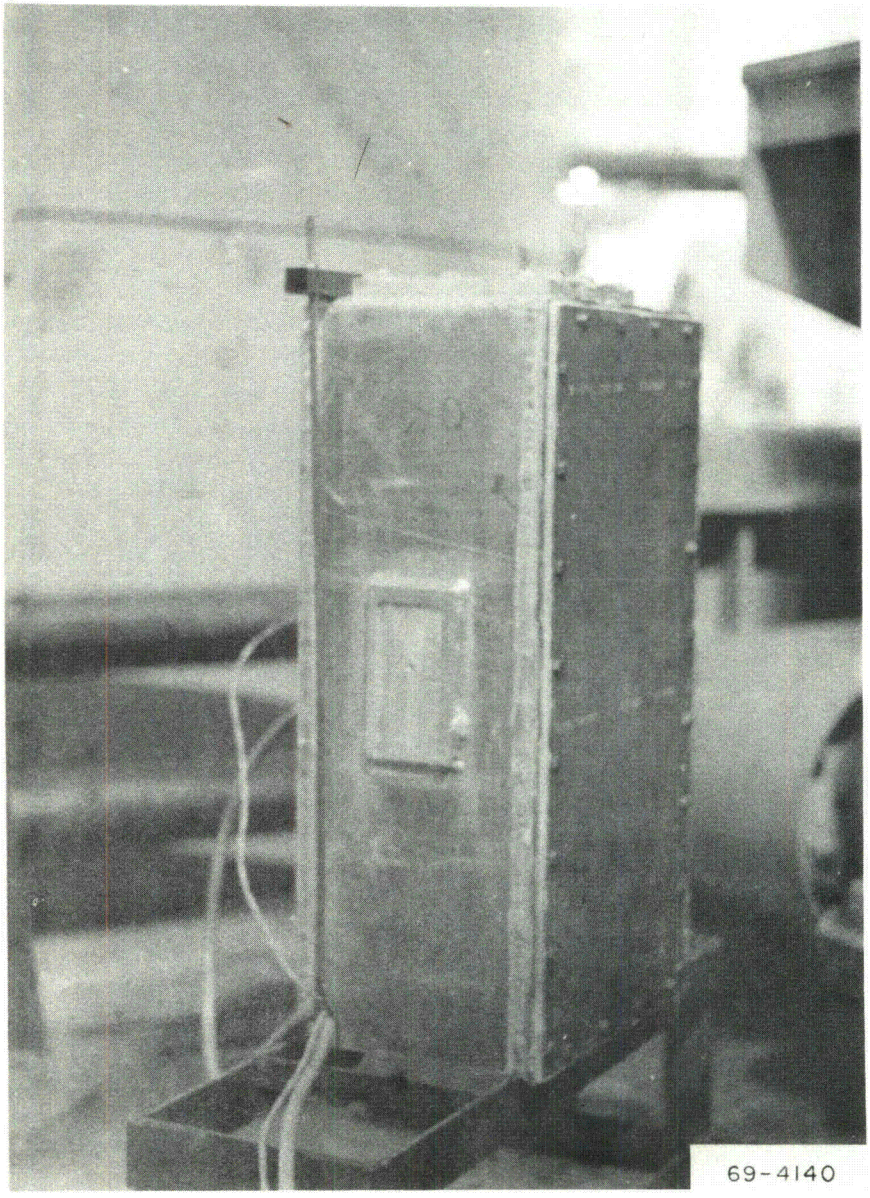

FIG. 80 CVTR CAMERA 2.

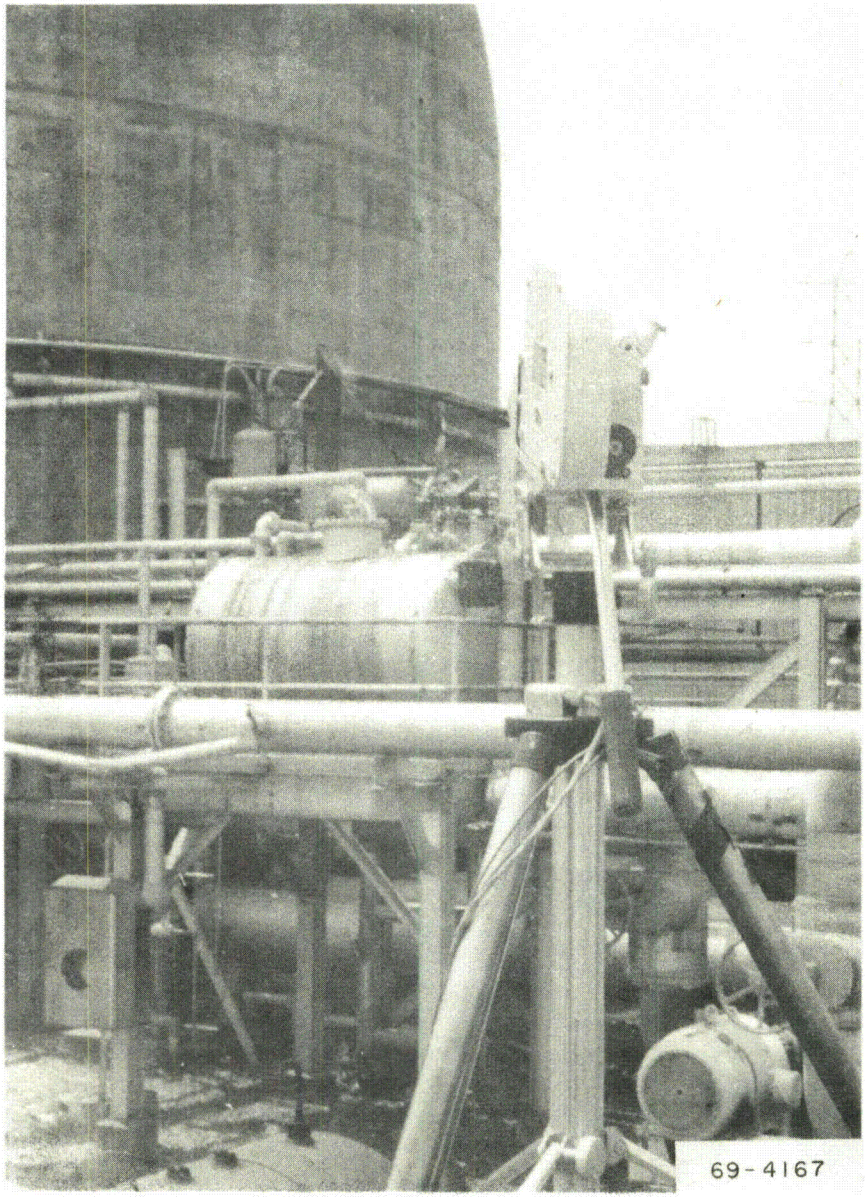

FIG. 81 CVTR CAMERA 4.

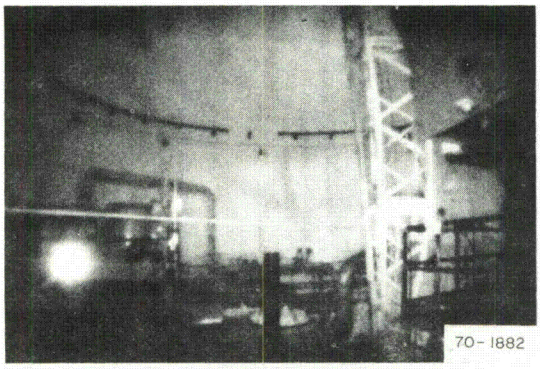

(a) t = 0 sec, Pressure = 0 psig

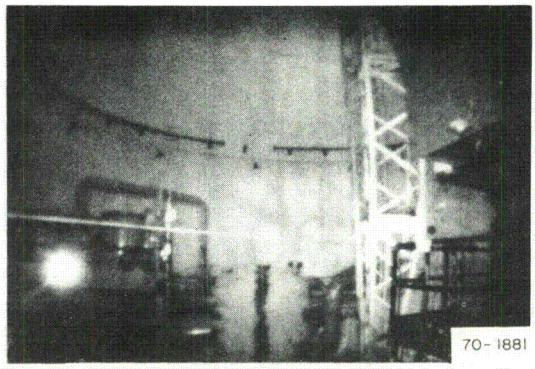

(b) t = 1.5 sec, Pressure = 0 psig

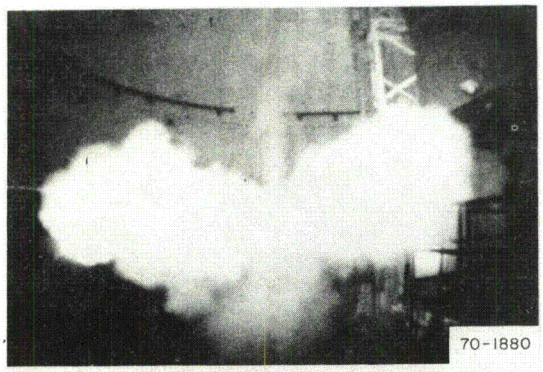

(c) t = 2 sec, Pressure = 0.1 psig

(d) t = 5 sec, Pressure = 0.9 psig

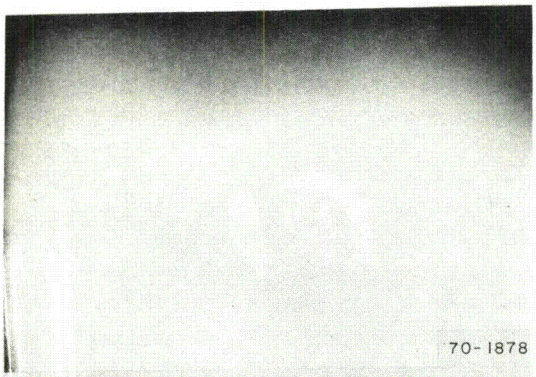

(e) t = 9 sec, Pressure = 1.4 psig

FIG. 82 STEAM TEST 3 PHOTOGRAPHIC SEQUENCE, CAMERA 1.

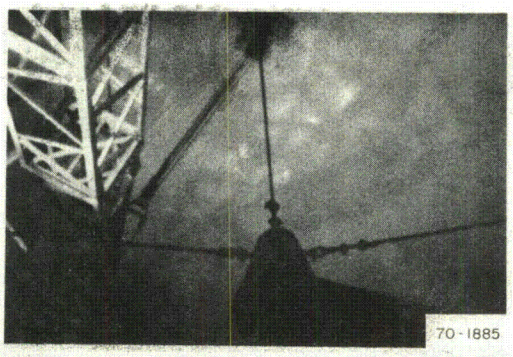

(a) t = 0 sec, Pressure = 0 psig

(b) t = 0.8 sec, Pressure = 0 psig

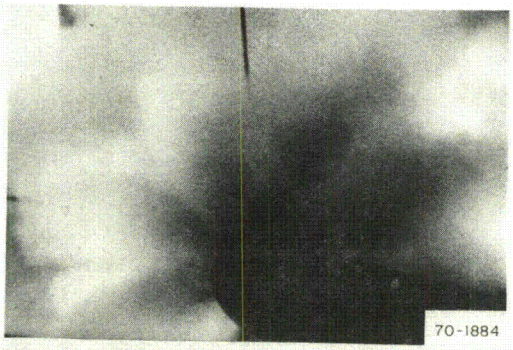

(c) t = 1.3 sec, Pressure = 0.3 psig

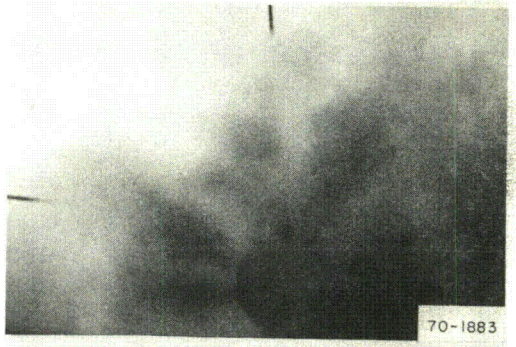

(d) t = 9 sec, Pressure = 1.4 psig

FIG. 83 STEAM TEST 3 PHOTOGRAPHIC SEQUENCE, CAMERA 2.

TABLE IX

CONTAINMENT STEAM DISTRIBUTION[a]

Elevation (ft)	Test Time (sec)[b]	Containment Pressure (psig)
317	13	2.8
295	44	7.3
275	[c]	10.8

[a] Steam injected at 335-ft elevation.

[b] t = 0 sec was the time the charge valve started to open.

[c] The time at which steam reached the 275-ft elevation was estimated to be 75 seconds on the basis of data from the 295-ft elevation during Test 3, and from the 317-ft elevation during Tests 4 and 5.

6. EFFECTS OF DBA TESTING ON THE CONTAINMENT

Visual observations and photographic records were made of the containment to evaluate degradation effects associated with DBA testing. Two major effects were noted, neither of which compromised the containment integrity and both of which are primarily associated with subjection of the containment to elevated temperature.

First, hair-line cracking on the outside concrete surface was observed during the 21-psig, 200°F hot-air leakage rate tests[5]. (Cracking was not evident during ambient temperature, 21-psig leakage rate tests.) The cracks were noticeably larger during the DBA tests and the more extensive cracking at this time is attributed to the higher temperature (~240°F) associated with the DBA tests. Figure 84 shows typical vertical cracking observed in the upper cylinder region of the containment structure. Since concrete has very little tensile strength, hair-line surface cracks were anticipated prior to testing because of the expected thermal expansion associated with the elevated internal temperatures of the hot-air leakage tests and the DBA tests.

External visual measurements with a theodolite, internal mechanical deflection measurements, and external containment wall surface expansion measurements with SR4 Type A-9, six-inch-long strip strain gages were made to determine containment growth during the leakage and DBA testing. Indications from these measurements were that the vessel cross sections elongated in the east-west direction with little or no growth in the north-south direction and that the maximum elongation was less than 0.5 inch. A vertical growth measurement with the theodolite was also made but the results were unreliable.

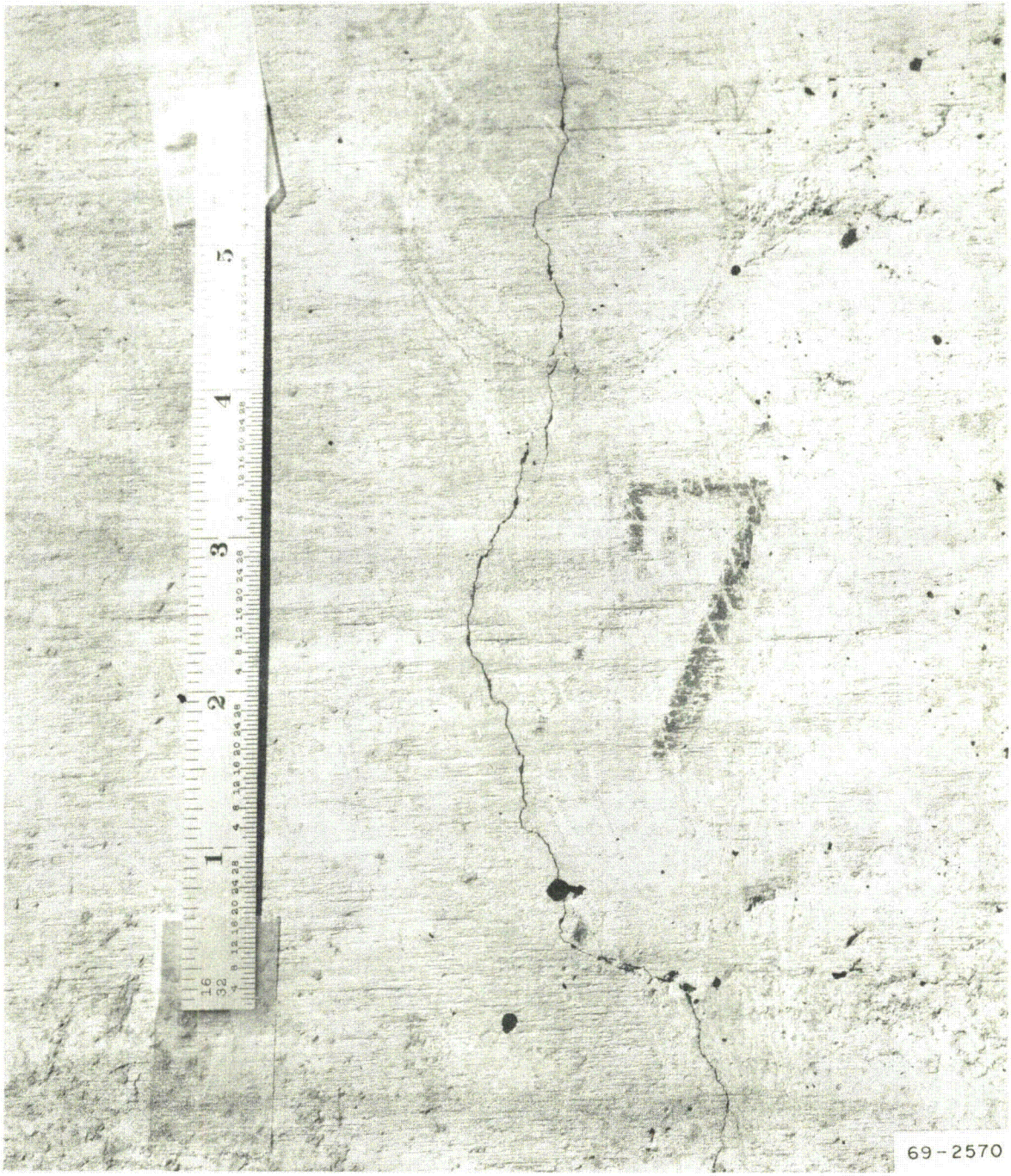

FIG. 84 TYPICAL CONCRETE CRACK.

The second containment degradation effect observed was blistering and peeling of paint on inside surfaces of the containment. Figure 85 shows typical blistering of the paint on the steel liner surface following DBA testing. Blistering and sagging of liner surface paint occurred mainly in the region of the containment above the operating floor. This type of paint degradation was apparently the result of steam or water penetrating the paint at a weak spot or pin-hole type inclusion and running down under the temperature-softened enamel coating. Blistering was also noted in the paint covering the concrete floor surfaces. These concrete paint blisters first appeared after the hot air leakage rate tests and are believed to be a result of temperature-related off-gassing of the concrete. DBA testing caused additional blistering of these surfaces, particularly on the operating floor that was exposed to high temperatures ($\sim 240°F$) during the DBA tests.

Other temperature-related degradation occurred to neutron moderator material in the refueling machine and ionization chambers. Figure 86 shows residue from one of the ionization chambers after exposure to the hot air leakage rate test series[5]. A large pool of wax-like material was noted under the refueling machine following the hot-air tests.

Following the DBA test series, an ambient temperature, 21-psig integrated leakage rate test, was performed to determine the effects of the DBA tests upon the leak tightness of the containment vessel. The results of this test[7] indicate that the DBA tests had no effect upon the containment integrity.

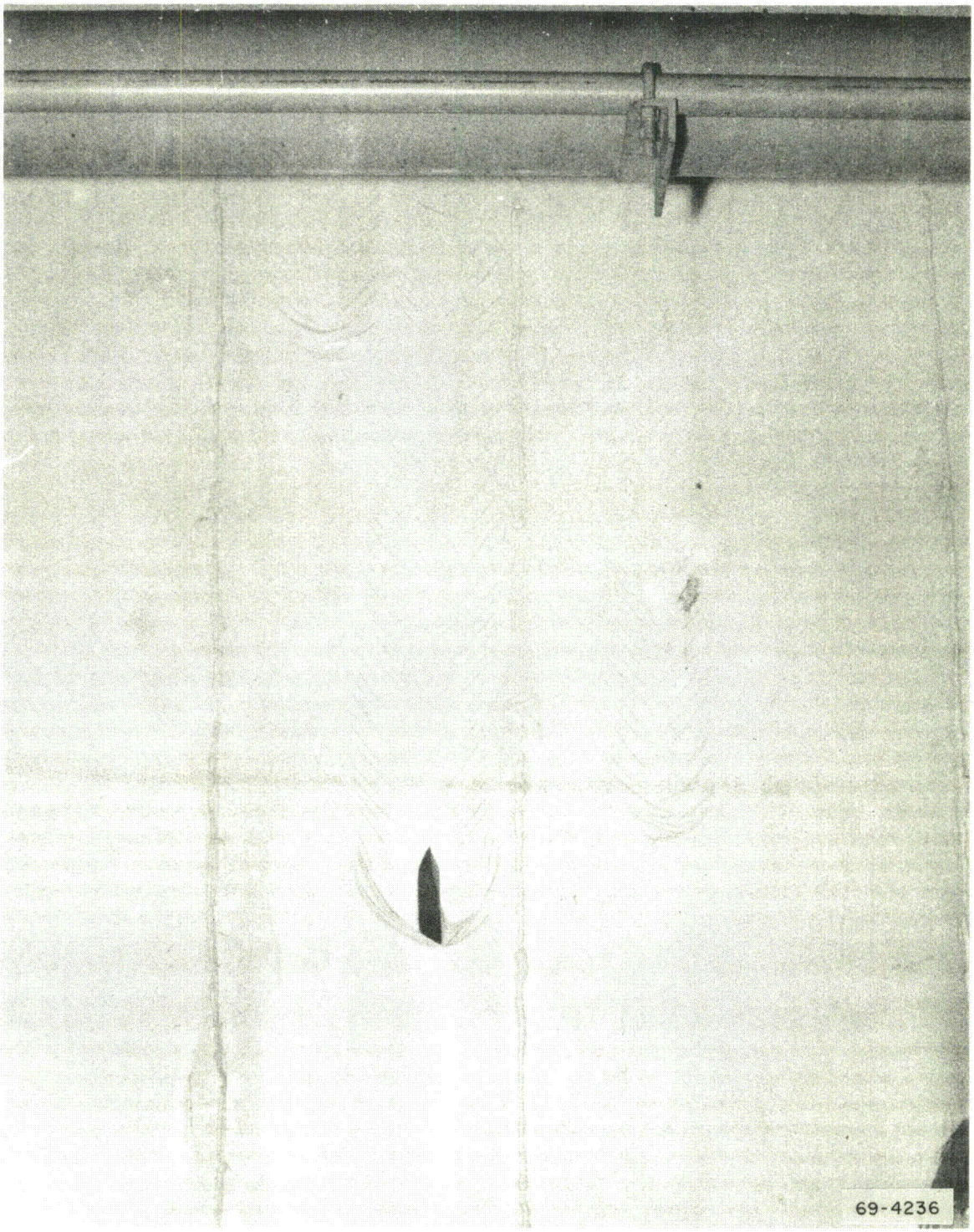

FIG. 85 BLISTERS IN CONTAINMENT LINER PAINT.

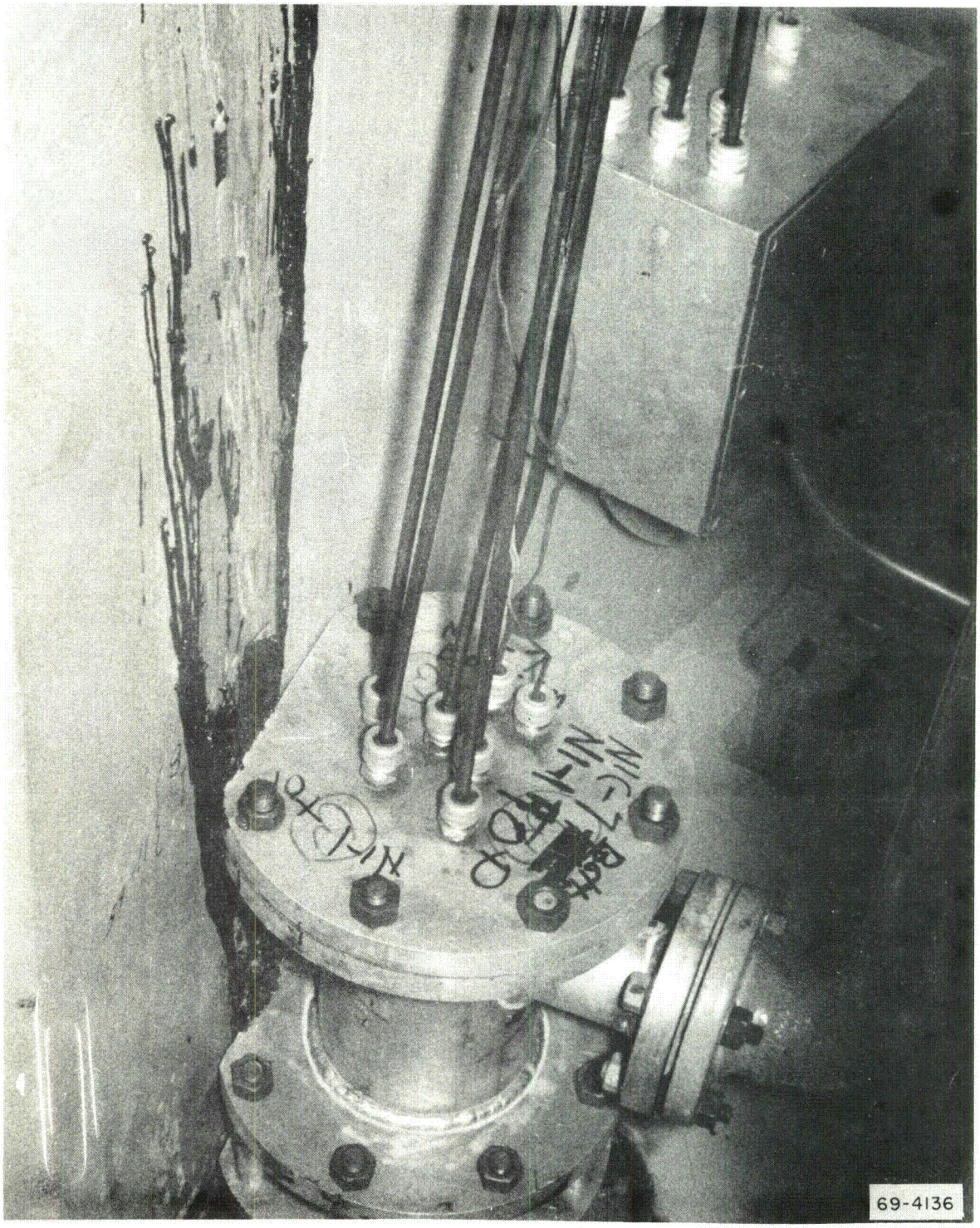

FIG. 86 NEUTRON MODERATOR MATERIAL FOLLOWING EXPOSURE TO HOT AIR LEAKAGE RATE TEST SERIES.

VII. CONCLUSIONS

The principal conclusions derived from the CVTR containment DBA tests involve the condensing steam heat transfer behavior, containment compartmentation, pressure suppression spray results, containment integrity, and the evaluation of current analytical practices. Also, the need for additional analytical and experimental efforts was concluded if an improved assessment of the safety margin of reactor containment systems is required.

1. HEAT TRANSFER BEHAVIOR

Maximum values for the condensing steam heat transfer coefficients were experimentally determined from the DBA tests, to be a factor of three to five larger than would be predicted from the often-used Tagami correlation[13]. These coefficients were subsequently substituted into CONTEMPT and the CONTEMPT response calculations obtained using the coefficients agreed with the measured response thereby verifying that the coefficients were of the right magnitude. Following steam shutoff and during pressure decay, the heat transfer coefficient rapidly decreased to values significantly less than those predicted for these conditions from the commonly-used Uchida data[20]. Otherwise, the heat transfer behavior was consistent with common assumptions used in the nuclear industry (that is, the heat transfer coefficient is initially small and increases rapidly to a maximum value during blowdown as mixing and turbulence develops, followed by a rapid decrease to low values after completion of blowdown).

2. CONTAINMENT COMPARTMENTATION

The potential importance of compartmentation in containment response analysis was re-emphasized by this work (that is, containment response may not only be dependent on the total energy addition and addition rates, but also on blowdown locations and orientations). Temperature differences between regions and within regions were recorded during the CVTR tests. This phenomenon occurred even though the steam injection was comparatively slow and the CVTR containment volume is relatively open with reasonably large connecting flow paths. These experimental results indicate that fast blowdowns in relatively isolated volumes within a containment may lead to localized heating. Another potential concern in compartmentation is that fast blowdowns in enclosed volumes or volumes with restricted flow paths may lead to differential pressures. However, no significant differential pressure behavior was noted in the CVTR results.

3. PRESSURE REDUCTION SPRAY

The pressure reduction spray was demonstrated to effectively lower the pressure and temperature of the containment atmosphere following the simulated DBA steam injection. Experimental temperature behavior showed that the spray effectively promoted atmosphere mixing and temperature equalization throughout the containment. From comparisons between CONTEMPT calculated response behavior and experimental behavior, and from spray efficiency temperature measurements, spray efficiencies were determined to be very large initially (nearly 100%). Although spray efficiency probably decreases as a function of time and temperature reduction in the containment, such decreases were not detected by the CVTR temperature measurements.

4. CONTAINMENT INTEGRITY

Containment integrity was not compromised by these tests. In fact, leakage rate tests performed at the conclusion of DBA testing indicated that the leakage rate may have been slightly reduced by the DBA tests. However, strain gage measurements of the containment liner during the DBA tests indicated that the liner yield stress was approached. This behavior is thought to be associated with the manner in which the liner was erected (concrete poured first), and the consequent air gaps existing behind the liner. Thus, portions of the liner carried a significant amount of the load associated with containment pressurization instead of the reinforced concrete as intended. The current practice in constructing reinforced concrete containment is to first erect sections of the liner and then to pour the concrete. A smaller air gap between the liner and concrete would be expected through use of this procedure such that the liner loading, and stress, would be reduced.

5. EVALUATION OF CURRENT ANALYSIS

The evaluation of current analytical practices was based on the results of CONTEMPT containment response calculations. CONTEMPT is considered to be representative of the state-of-the-art in the industry.

The CVTR DBA tests and analysis have demonstrated that the CONTEMPT containment response analytical model will predict reasonably accurately the containment atmosphere pressure-temperature response provided correct assignment of condensing steam heat transfer coefficients and other key parameters are made. But, when common assumptions currently used for the heat transfer coefficient (Tagami) or similar were employed, the CVTR DBA test results indicated that the peak pressure prediction obtained from CONTEMPT was conservative by about 45%. However, the magnitude of the overprediction of pressure depends on the blowdown conditions and other factors such that for a large pipe rupture (or fast blowdown), underestimating the heat transfer coefficient probably has a lesser effect on the peak pressure predictions (15% or less from Reference 12).

CONTEMPT, being a single-node model, provides an average temperature and pressure response prediction. For calculations of the CVTR test temperature, CONTEMPT significantly underestimated the actual peak temperature in the operating region but overestimated the temperatures in the lower region. No pressure differential behavior was noted for the CVTR steam injection conditions and the single pressure prediction capability of CONTEMPT was sufficient to accurately describe the measured results.

6. ADDITIONAL ANALYTICAL AND EXPERIMENTAL REQUIREMENTS

The CVTR DBA tests have provided information related to containment response, heat transfer behavior, and response analysis generally applicable to a DBA resulting from a medium-sized pipe rupture. However, similar representative containment response and heat transfer data are also needed for the large pipe rupture or fast blowdown case if an improved assessment of response predictions is required. Heat transfer behavior different from that of CVTR tests could be encountered for fast blowdown conditions such that a strict extrapolation of CVTR data to analysis of containment response for a large pipe rupture case is difficult. Also, the potential problem area of differential temperature and pressure conditions under fast blowdown conditions may be significant. Pressure differentials may be limited by engineering good flow communication between volumes but localized heating effects may be unavoidable.

The CVTR DBA tests have pointed to the possible improvements a multinode analytical containment response model could provide for accurate assessment of containment response and margin of safety in containment design. The success of the CONDRU II model that was developed and utilized with the CVTR work, has indicated the feasibility of the multinode model approach. However, to adequately describe all complex features of containment response may require many nodes, and a model incorporating such nodes could become undesirably complex. Thus, some limitation on this approach is implied.

Uncertainties in containment response analysis surely exist as has been purposely pointed out in this report. Furthermore, these uncertainties exist even though much of the input information needed for CVTR analysis, such as the steam injection history, were relatively well known from experimental measurements. Also, the reported analytical results for the CVTR response are a summary of many calculations investigating the influence of all applicable parameters. As a result of these observations, similar analyses done for other facilities are expected to have comparable (or possibly greater) uncertainties.

Finally, these tests have indicated probable conservatism in the practices currently employed for containment response. Localized behavior exceeding design limits is a possible exception. Some indication of the possibility of excessively high localized temperatures was provided by CVTR results; however, additional effort in containment response investigation could be expected to benefit the designer in terms of relaxed design restrictions or increases in margin of safety.

VIII. REFERENCES

1. J. A. Norberg, Carolinas Virginia Tube Reactor (CVTR) In-Plant Testing Project, IDO-17258H (April 1969).

2. Earth Sciences, Ambient Vibration Survey and Mathematical Analysis of the Carolinas Virginia Tube Reactor, Contract No. C-638 T.A. No. 1 (September 1968).

3. R. B. Mattheisen and G. B. Smith, Forced Vibration Tests of the Carolinas Virginia Tube Reactor (CVTR), UCLA Report No. 69-8 (February 1969).

4. R. C. Schmitt, Evaluation and Comparison of Structural Dynamics Investigations of the Carolinas Virginia Tube Reactor Containment, IN-1372 (May 1970).

5. G. E. Bingham et al, Preliminary Results and Test Experience of the Carolinas Virginia Tube Reactor Containment Leakage Rate Tests, IN-1326 (December 1969).

6. K. A. Dietz (ed.), Quarterly Technical Report -- Nuclear Safety Program Division -- July 1 - September 30, 1969, IN-1319 (May 1970).

7. G. E. Bingham, Final Results of the Carolinas Virginia Tube Reactor Containment Leakage Rate Tests, IN-1399 (June 1970).

8. J. A. Norberg et al, Simulated Design Basis Accident Tests of the Carolinas Virginia Tube Reactor Containment -- Preliminary Results, IN-1325 (October 1969).

9. Carolinas Virginia Nuclear Power Associates, Inc., Final Hazards Summary Report, CVNA-90 (January 1962), Vols. I-IV.

10. TROJAN NUCLEAR PLANT. Preliminary Safety Analysis Report, Vol. 2. (Portland General Electric Co., Oregon) (June 25, 1969) p 425.

11. R. M. Jones and V. G. Crose, SAAS II, Finite Element Analysis of Axisymmetric Solids, with Orthotropic, Temperature - Dependent Material Properties, Aerospace Corporation, Aerospace Report No. TR-0200 (S49 80) (September 1968).

12. D. C. Slaughterbeck, Pressure Response of PWR Containments -- A Parametric Analysis, IDO-17300, June 1969.

13. Takashi Tagami, "Interim Report on Safety Assessments and Facilities Establishment Project in Japan for Period Ending June 1965 (No. 1)", Unpublished Work, 1965.

14. H. Fujie, A. Yamanonchi, N. Sagawa, H. Ogasawara, and T. Tagami, "Studies for Safety Analysis of Loss-of-Coolant Accidents in Light Water Power Reactors", Japan Atomic Energy Research Institute, NSJ-tr-112, (March 1968).

15. L. C. Richardson et al, CONTEMPT -- A Computer Program for Predicting the Containment Pressure-Temperature Response to a Loss-of-Coolant Accident, IDO-17220 (June 1967).

16. William H. McAdams, Heat Transmission, 3rd Edition, McGraw-Hill Book Company, Inc., 1954, Chapter 13.

17. Warren H. Giedt, Principles of Engineering Heat Transfer, D. Van Nostrand Company, Inc., 1957, pp. 221-229.

18. Max Jakob, Heat Transfer, Volume I, John Wiley and Sons, 1948, pp. 691-692.

19. D. C. Slaughterbeck, Review of Heat Transfer Coefficients For Condensing Steam In A Containment Building Following A Loss-of-Coolant Accident, IN-1388, (September 1970).

20. H. Uchida, A. Oyama, and Y. Togo, "Evaluation of Post-Incident Cooling Systems of Light-Water Power Reactors", in Proceedings of the Third International Conference on the Peaceful Uses of Atomic Energy Held in Geneva, August 31 - September 9, 1964, Vol. 13, New York: United Nations, 1965, pp. 93-104, (A/CONF. 28/P/436). (May 1964).

21. J. C. Griess et al, Design Considerations of Reactor Spray Systems -- Part V, Protection Coating Tests, ORNL-TM-2412 (July 1970).

22. A. E. Arave, An Ultrasonic Anemometer for Measuring Steam Convection Currents, IDO-17293 (January 1969).

APPENDIX A -- INSTRUMENTATION AND DATA ACQUISITION AND REDUCTION

APPENDIX A -- INSTRUMENTATION AND DATA ACQUISITION AND REDUCTION

A primary objective of the simulated DBA tests was to measure and evaluate the containment response to rapid steam injection, and to relate the experimental response to that calculated by current analytical techniques. To accomplish this objective, the containment and the process systems were heavily instrumented to measure temperature, pressure, flow rate, condensate rate, and strain. A comprehensive discussion of the measurement methods and associated instrumentation systems was reported previously[8]. The following section presents additional details of the instrument locations and summarizes the measurement systems used in the performance of these tests.

A-I. INSTRUMENTATION

The main CVTR DBA instrumentation consisted of devices to determine temperature, pressure, condensation rate, and spray distribution.

1. CONTAINMENT TEMPERATURES

The containment atmospheric and surface temperatures were obtained during the simulated DBA tests by two independent temperature measuring systems: (a) 15 platinum resistance thermometers; and (b) 59 Chromel-Alumel thermocouples. (Thirty-six thermocouples measured atmospheric temperatures, 23 measured surface temperatures.)

1.1 Resistance Thermometers

During the steam tests, the resistance thermometers were positioned as shown in Table A-I and Figures A-1 through A-6. The sensors were positioned as much as possible to obtain representative measurements in all regions of the containment volume. Data from the resistance thermometers were recorded through the use of a manual switch-timer unit and a digital voltmeter with a digital printer. Readings were initiated immediately following completion of steam injection and were repeated every five minutes throughout the containment pressure decay period.

Prior to installation at CVTR, each resistance thermometer was calibrated in a standards laboratory through use of instrumentation having calibrations traceable to the National Bureau of Standards (NBS). A calibration of the complete resistance thermometer system was performed in a standards laboratory following completion of the CVTR tests to determine the measurement error. Section A-IV discusses the error analysis.

1.2 Thermocouples

Fifty-seven thermocouples were used to measure containment temperature during the DBA tests. In addition, two thermocouples (one in the header cavity and one in the fuel transfer canal) were used. Thirty-six of these thermocouples monitored containment atmospheric temperature and 23 monitored various containment surfaces, as shown in Table A-II and Figures A-1 through A-4 and Figures A-7 through A-10. The thermocouples were located so that all representative regions and surfaces of the containment were sampled.

Thermocouples measuring concrete surface temperatures were installed in small diameter holes drilled into the concrete surfaces and sealed with epoxy. Liner surface thermocouples were installed in a similar manner, except the thermocouples were held in place by peening.

Five thermocouples were installed to measure the temperature of the spray water as it passed through the containment atmosphere to aid in determining the thermodynamic effectiveness of the spray system. These measurements were accomplished by installing a thermocouple junction in the throat of a 4-in. funnel and positioning the funnels approximately 5 ft apart between the

TABLE A-I

RESISTANCE THERMOMETER LOCATIONS DURING DBA TESTS

Resistance Thermometer	Elevation[a] (ft)	Radius[b] (ft)	Orientation[c] (degrees)	Containment Region
1	281	16	285	Basement
2	283	22	165	Basement
3	284	19	45	Basement
4	295	16	330	Intermediate
5	298	24	150	Intermediate
6	305	24	30	Intermediate
7	306	18	185	Intermediate
8	316	17	270	Intermediate
9	319	24	90	Intermediate
10	334	18	350	Operating
11	339	13	90	Operating
12	343	27	120	Operating
13	350	6	225	Operating
14	370	5	270	Operating
15	375	0	Containment center	Operating

[a] The elevation of the containment basement floor is 275 feet.

[b] The radius was measured from the containment center. The radius of the containment vessel is 30 feet.

[c] 0° was arbitrarily designated as shown in Figure A-1.

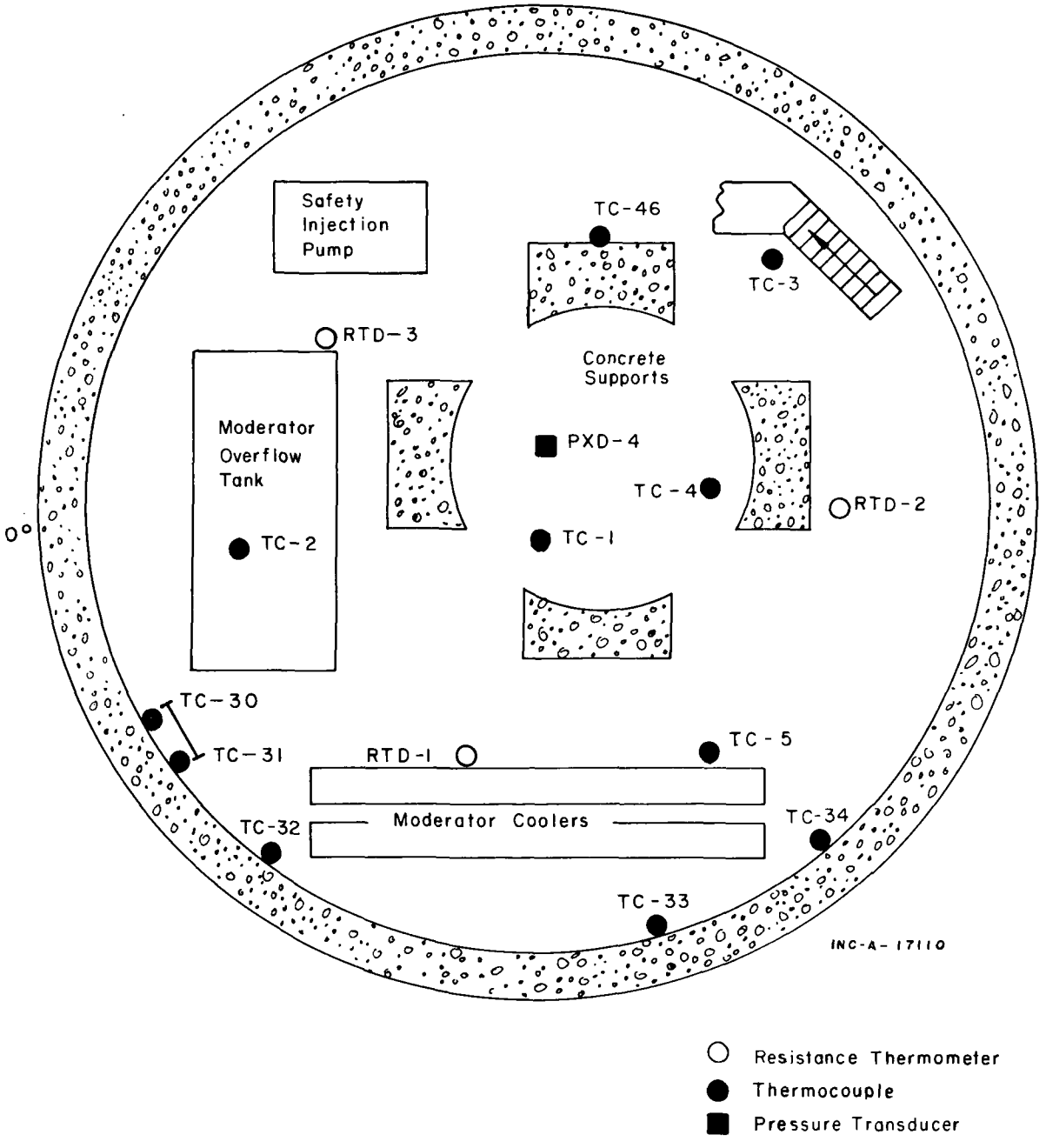

FIG. A-1 RESISTANCE THERMOMETER, THERMOCOUPLE AND PRESSURE TRANSDUCER LOCATIONS -- 284 FEET.

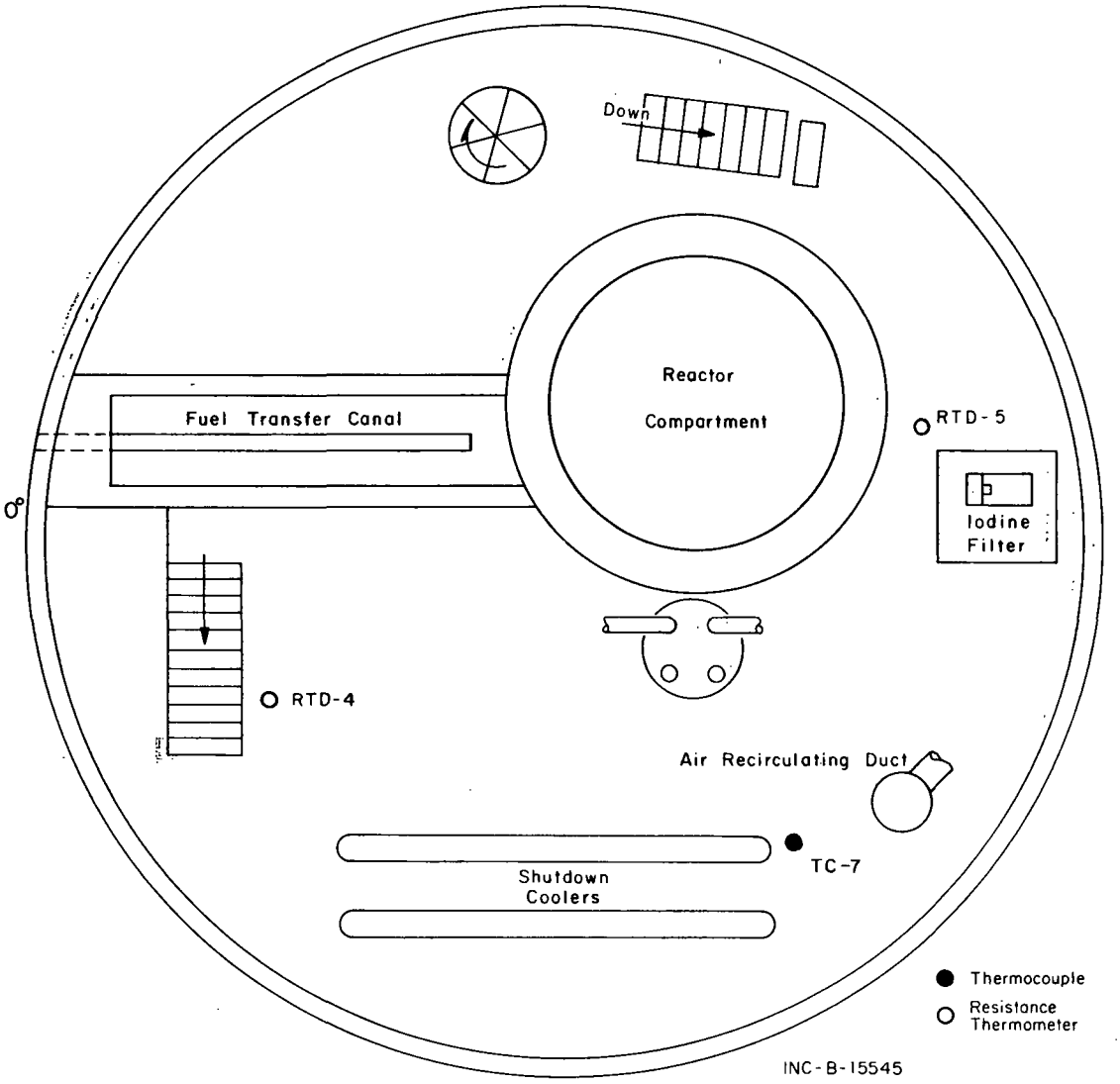

FIG. A-2 RESISTANCE THERMOMETER AND THERMOCOUPLE LOCATIONS -- 297 FEET.

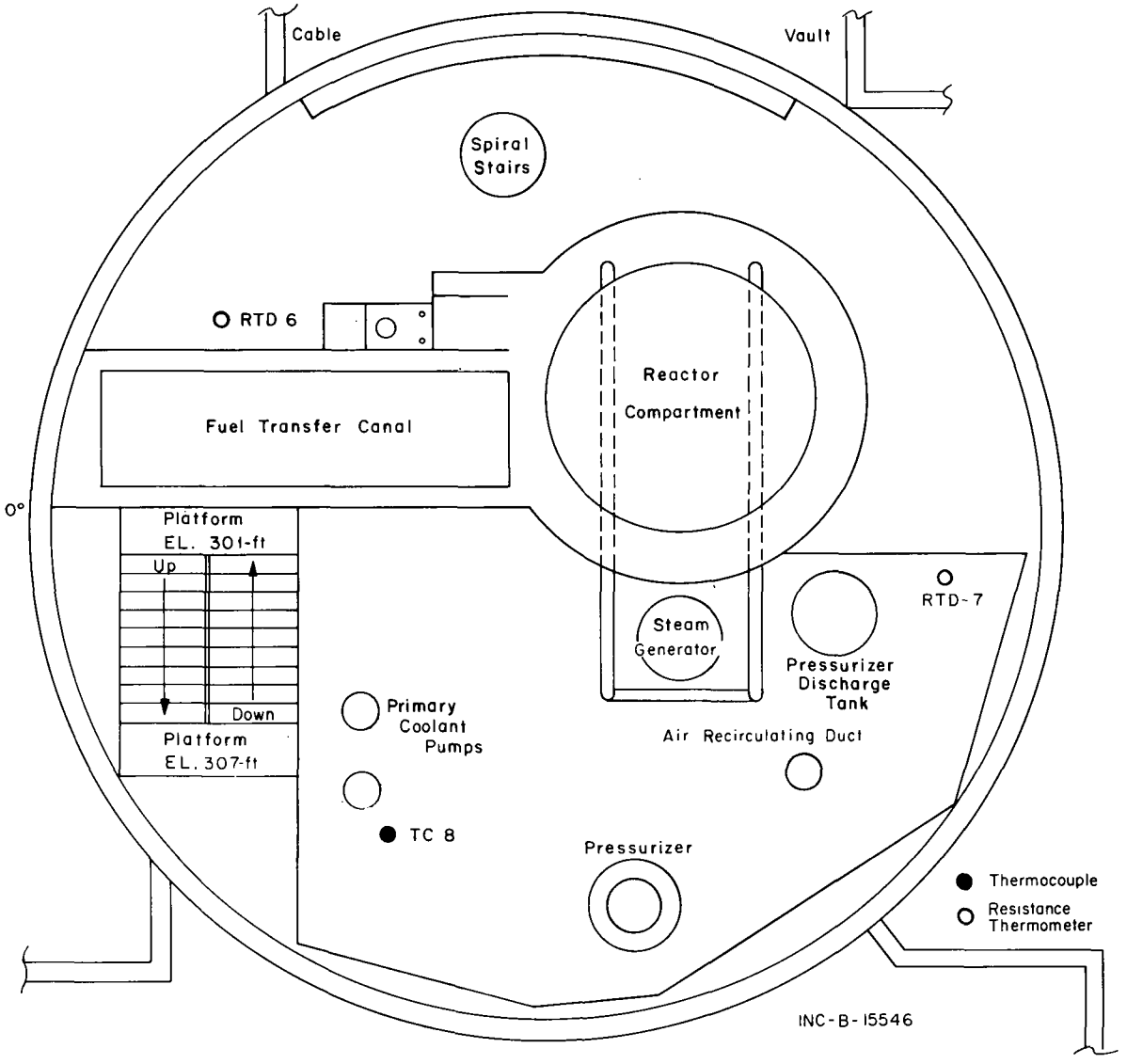

FIG. A-3 RESISTANCE THERMOMETER AND THERMOCOUPLE LOCATIONS -- 307 FEET.

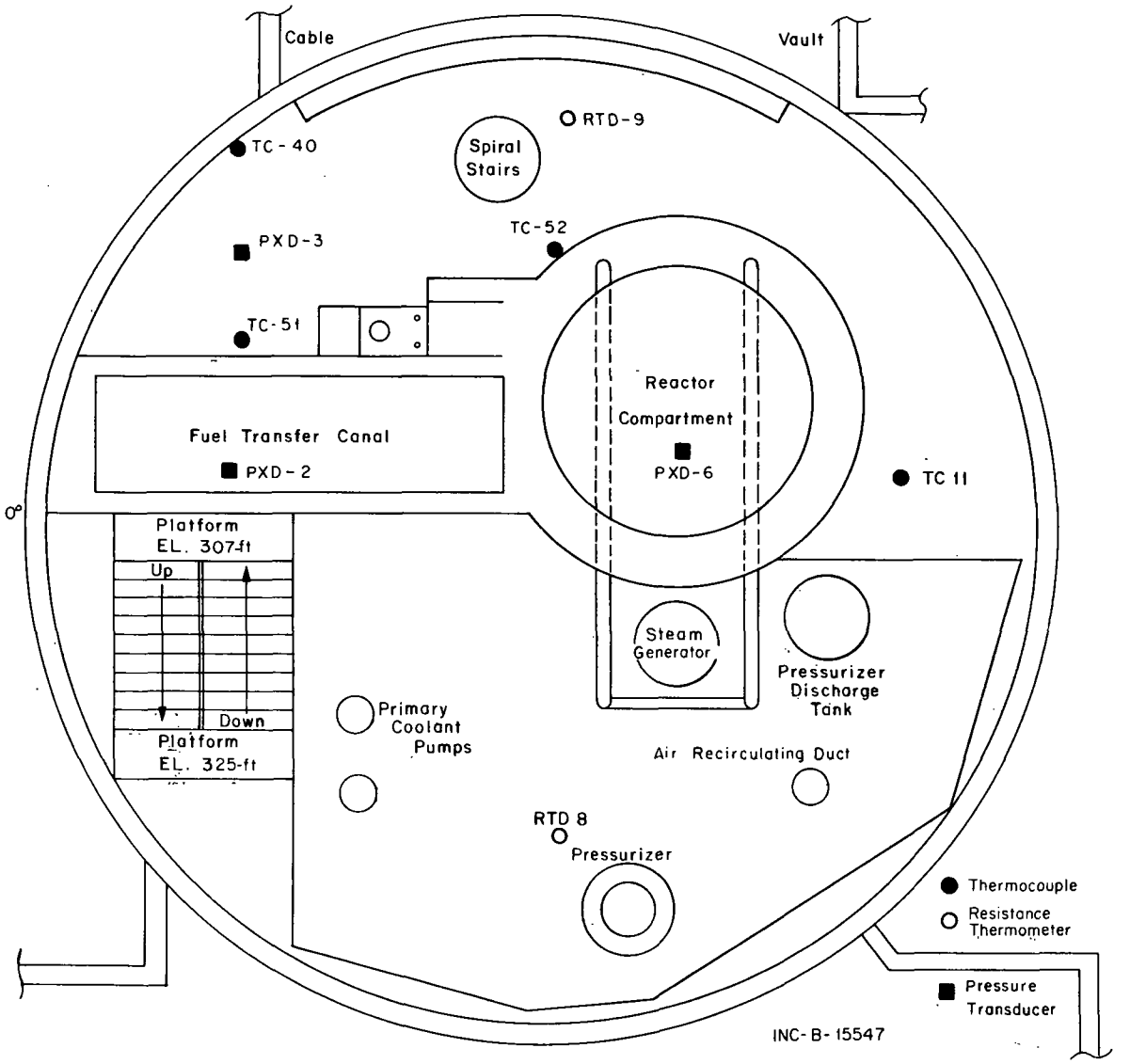

FIG. A-4 RESISTANCE THERMOMETER AND THERMOCOUPLE LOCATIONS -- 319 FEET.

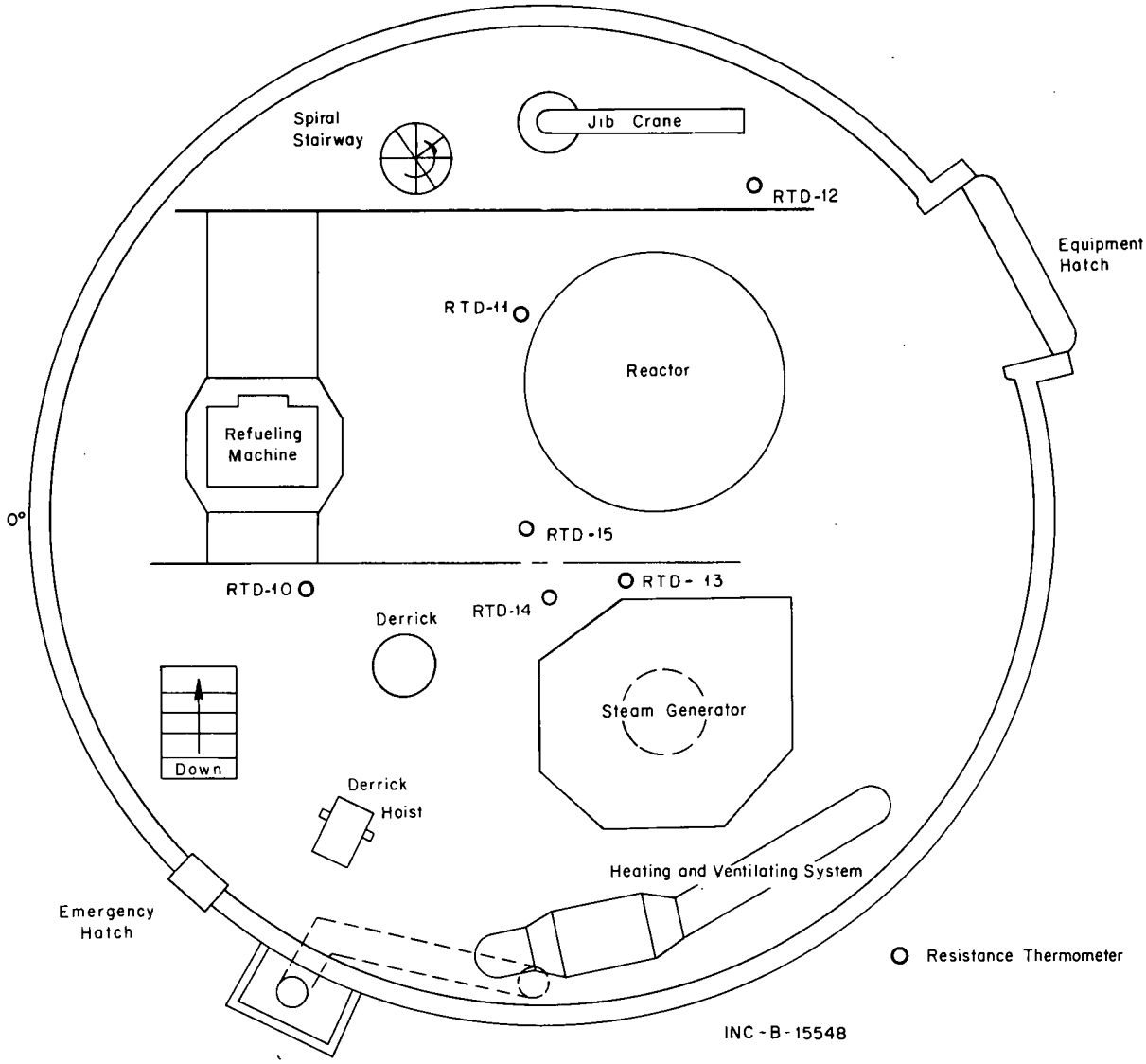

FIG. A-5 RESISTANCE THERMOMETER LOCATIONS -- OPERATING REGION, PLAN VIEW.

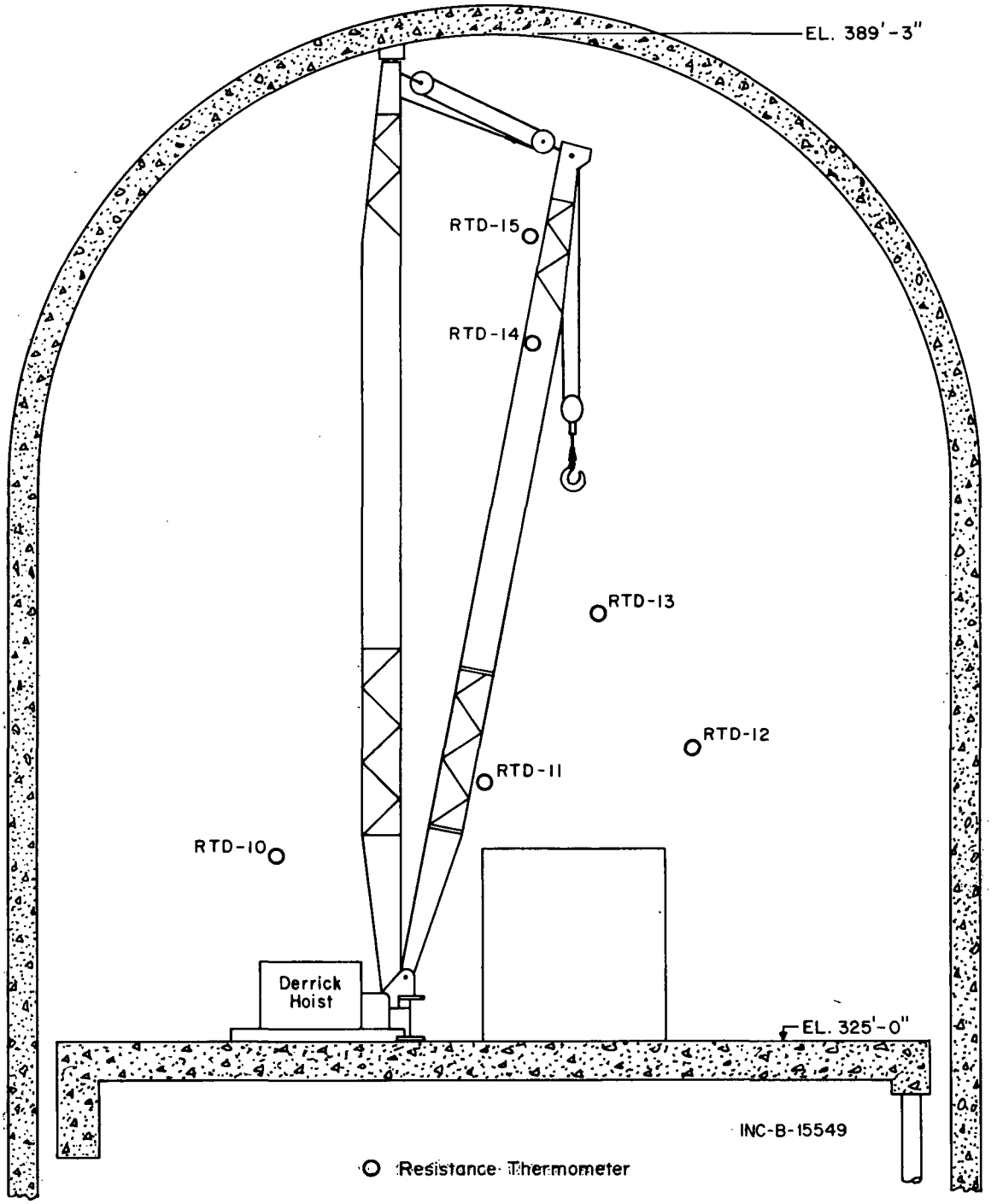

FIG. A-6 RESISTANCE THERMOMETER LOCATIONS -- OPERATING REGION, ELEVATION VIEW.

TABLE A-II

THERMOCOUPLE LOCATIONS DURING DBA TESTS

Thermocouple	Elevation (ft)[a]	Radius (ft)[b]	Orientation (degrees)[c]	Containment Region	Medium Measured
1	283	0	Containment center	Basement	Atmosphere
2	284	20	0	Basement	Atmosphere
3	284	21	120	Basement	Atmosphere
4	275	10	180	Basement	Concrete basement floor
5	284	21	240	Basement	Atmosphere
6	335	8	120	Operating	Spray
7	297	24	240	Intermediate	Atmosphere
8	307	24	300	Intermediate	Atmosphere
9	340	8	120	Operating	Spray
10	330	8	120	Operating	Spray
11	319	24	180	Intermediate	Atmosphere
12	334	0	Containment center	Operating	Atmosphere
13	334	10	350	Operating	Atmosphere
14	334	18	350	Operating	Atmosphere
15	334	22	170	Operating	Atmosphere
16	334	0	Containment center	Operating	Atmosphere
17	344	18	350	Operating	Atmosphere
18	344	20	170	Operating	Atmosphere
19	344	10	350	Operating	Atmosphere
20	334	11	170	Operating	Atmosphere
21	344	9	170	Operating	Atmosphere
22	345	8	120	Operating	Spray
23	350	8	120	Operating	Spray
24	348	29	318	Operating	Atmosphere (heat plug profile)
25	348	29	318	Operating	Atmosphere (heat plug profile)

TABLE A-II (Contd.)

THERMOCOUPLE LOCATIONS DURING DBA TESTS

Thermocouple	Elevation (ft)[a]	Radius (ft)[b]	Orientation (degrees)[c]	Containment Region	Medium Measured
26	348	29	318	Operating	Atmosphere (heat plug profile)
27	348	29	318	Operating	Atmosphere (heat plug profile)
28	370	5	270	Dome	Atmosphere
29	375	0	Containment center	Dome	Atmosphere
30	299	29	324	Basement	Liner
31	283	29	324	Basement	Liner
32	289	29	304	Basement	Liner
33	291	29	265	Basement	Liner[d]
34	291	29	237	Basement	Liner[d][e]
35	360	29	313	Operating	Liner
36	337	29	175	Operating	Liner
37	344	29	142	Operating	Liner
38	334	29	127	Operating	Liner
39	323	29	133	Intermediate	Liner
40	316	29	44	Intermediate	Liner
41	331	29	52	Operating	Liner
42	347	29	77	Operating	Liner
43	355	29	52	Operating	Liner
44	330	29	350	Operating	Liner heat plug
45	348	29	318	Operating	Liner heat plug
46	280	21	90	Basement	Concrete
47	~315	10	180	Header cavity	Atmosphere (header cavity)
48	332	29	90	Operating	Atmosphere
49	330	15	270	Operating	Concrete
50	325	25	90	Operating	Concrete

TABLE A-II (Contd.)

THERMOCOUPLE LOCATIONS DURING DBA TESTS

Thermocouple	Elevation (ft)[a]	Radius (ft)[b]	Orientation (degrees)[c]	Containment Region	Medium Measured
51	317	22	30	Intermediate	Concrete
52	317	26	90	Intermediate	Concrete
53	348	29	318	Operating	Atmosphere (heat plug profile)
54	330	29	350	Operating	Atmosphere (heat plug profile)
55	330	29	350	Operating	Atmosphere (heat plug profile)
56	330	29	350	Operating	Atmosphere (heat plug profile)
57	330	29	350	Operating	Atmosphere (heat plug profile)
58	330	29	350	Operating	Atmosphere (heat plug profile)
59[f]	---	---	---	---	---
60	320	10	0	Canal	Atmosphere (fuel transfer canal)

[a] The elevation of the containment basement floor is 275 feet.

[b] The radius was measured from the containment center. The radius of the containment vessel is 30 feet.

[c] 0° was arbitrarly designated as shown in Figure A-1.

[d] Thermocouple and liner insulated with a 2-inch polyurethane sheet.

[e] Thermocouple moved to steam line for final steam test.

[f] Thermocouple 59 was a steam line process thermocouple.

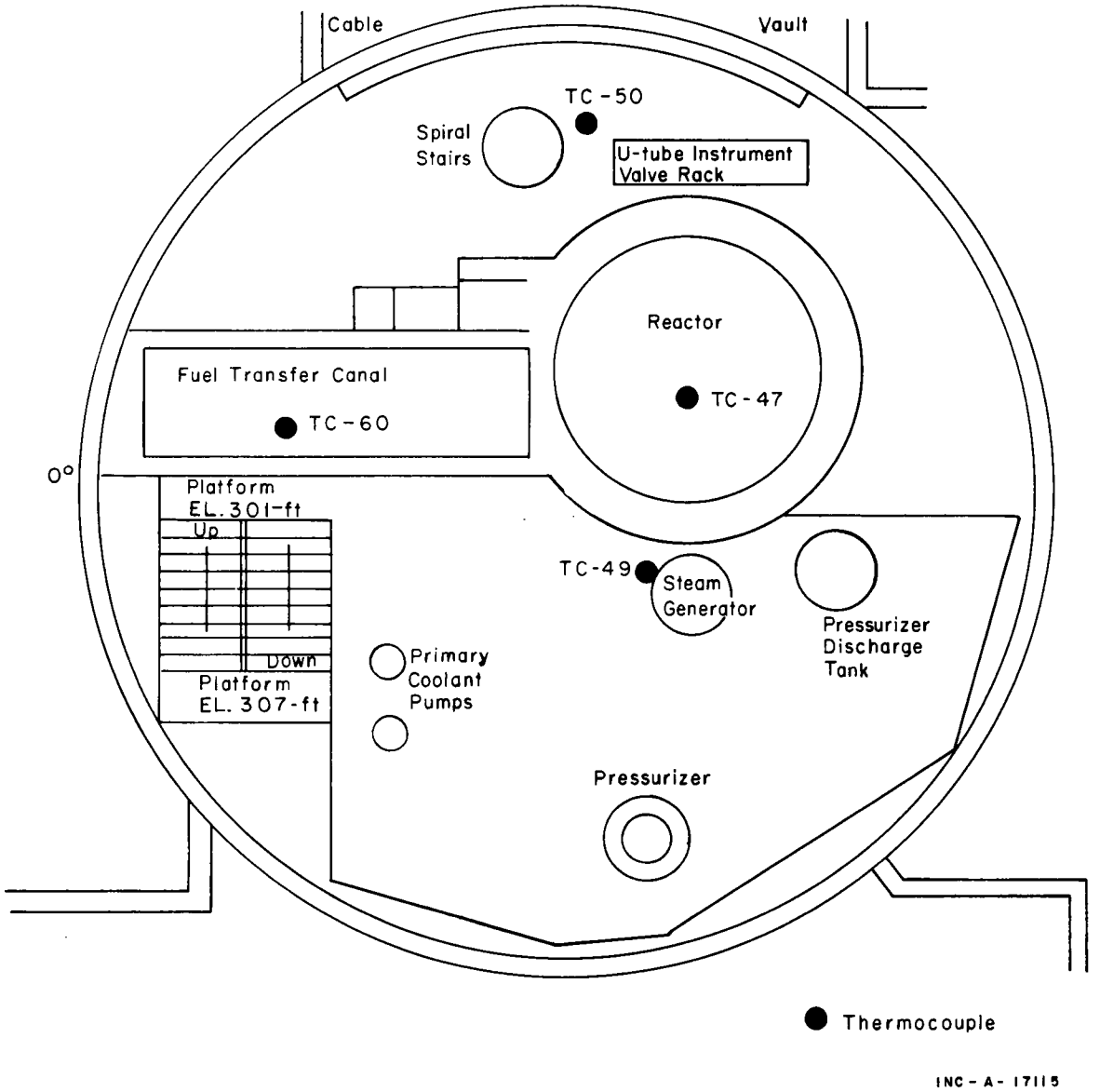

FIG. A-7 THERMOCOUPLE LOCATIONS -- 325 FEET.

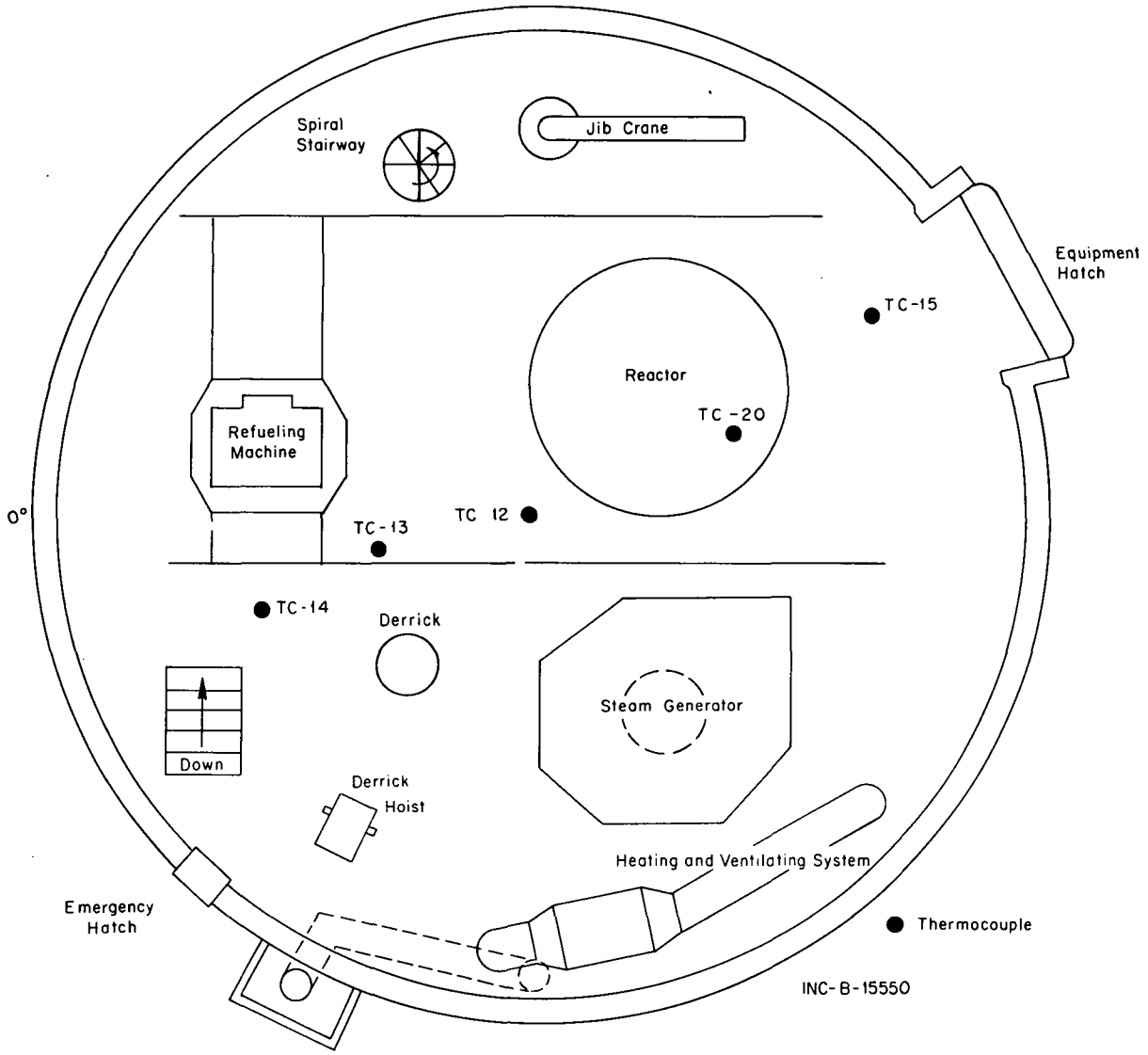

FIG. A-8 THERMOCOUPLE LOCATIONS -- 334 FEET.

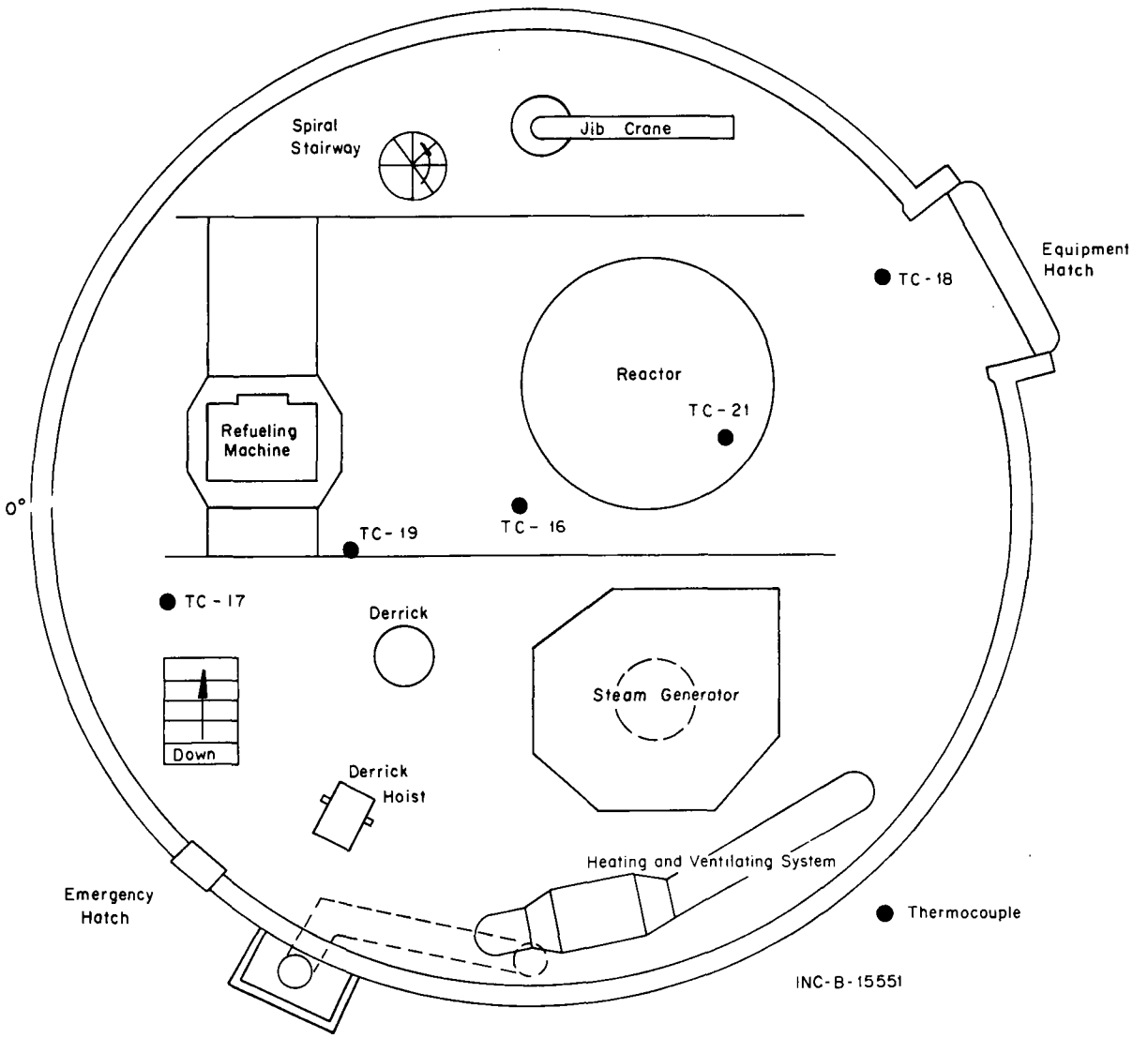

FIG. A-9 THERMOCOUPLE LOCATIONS — 344 FEET.

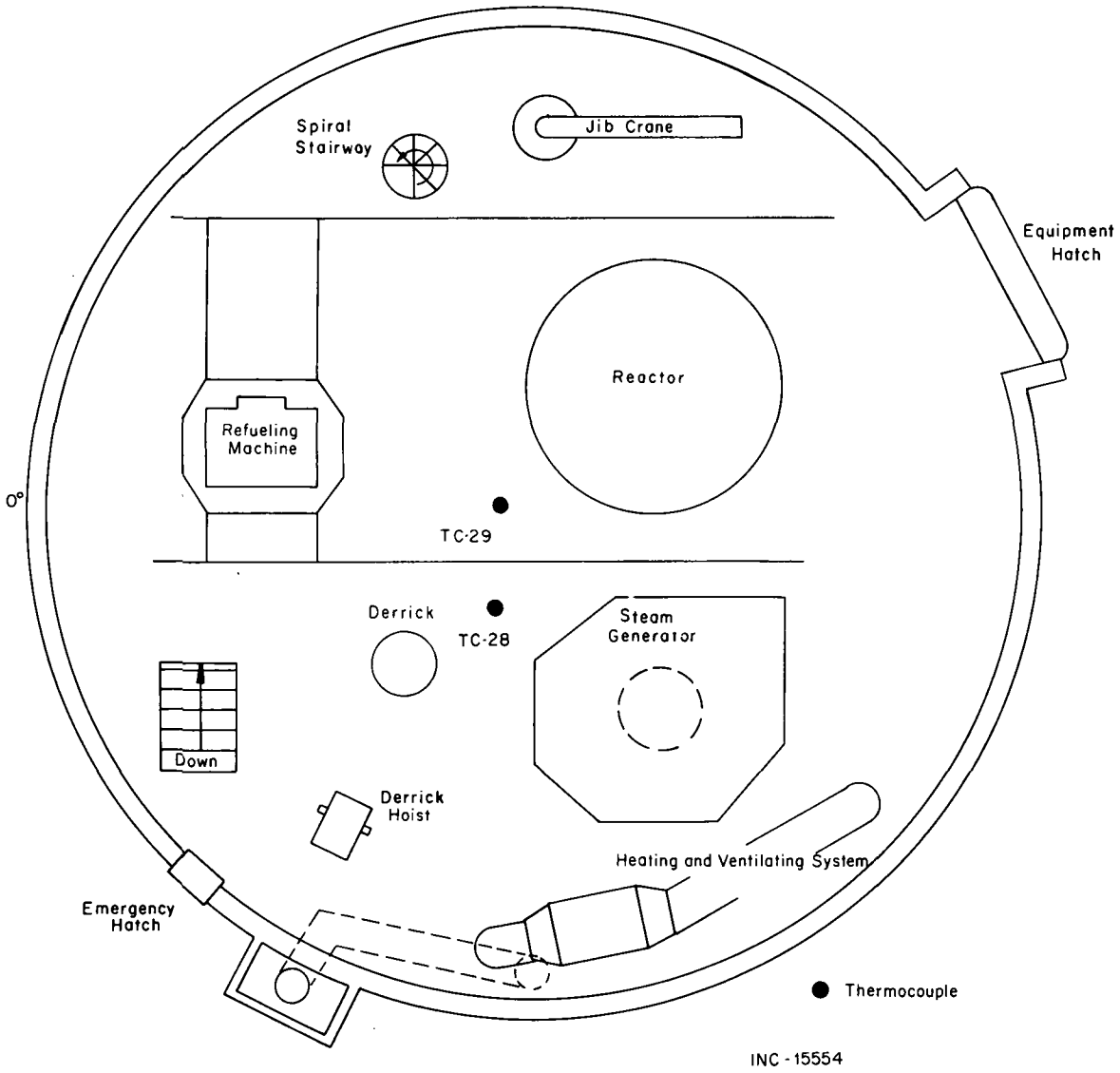

FIG. A-10 THERMOCOUPLE LOCATIONS -- 375 FEET.

containment elevations of 330 to 350 ft, as shown in Table A-II and Figure A-11. During spray operation, spray water and condensate that entered the funnel, passed over the thermocouple junction which provided a record of water temperature as a function of time and containment elevation.

Five thermocouples were used with each of the two heat transfer assemblies to measure the atmospheric temperature profile adjacent to the assemblies. The thermocouples were positioned at 1/4, 1/2, 1, 1-1/2, and 2 in. from the face of the assembly. In addition, a thermocouple was attached to the surface of each assembly to measure the temperature of the containment liner. The thermocouples in each heat transfer assembly provided a detailed temperature profile which extended from 2 in. in the containment atmosphere to 5 in. into the concrete containment wall.

All thermocouples were fabricated at CVTR from premium grade Chromel-Alumel, Teflon-insulated Teflon-jacketed wire. Each thermocouple junction was made by fusing the Chromel and Alumel leads into a 3/16-in. diameter bead. Existing Chromel-Alumel electrical penetration assemblies were used to bring the thermocouple leads through the containment wall. Chromel-Alumel thermocouple wire was also used between the electrical penetration and the 150°F reference junctions located in the reactor control room. Shielded two-conductor copper cables were used to connect the leads from the reference junction box to the data acquisition systems.

Leads from the thermocouples imbedded in the steel liner sections and the concrete plugs of the special heat transfer assemblies were routed on the outside of the containment to the 150°F reference junctions.

The temperatures of the reference junctions were recorded throughout the DBA tests to allow correction of any temperature changes associated with the junctions. Figure A-12 is a general schematic diagram of the thermocouple system.

An in-place calibration was performed on the complete temperature measuring system (thermocouples, leads, reference junction box and data acquisition system). The atmosphere and surface thermocouples were calibrated by inserting the thermocouple junctions into a controlled temperature water bath, increasing the temperature of the bath in 5°F increments from 60 to 200°F, and recording the output from the thermocouple. The water temperature was measured with an accurate (±0.01°C) quartz crystal thermometer.

The heat transfer assemblies were calibrated prior to installation in the containment wall. This calibration was performed by heating the assemblies in a controlled temperature oven and obtaining data at five temperatures between 65 and 185°F.

A least-squares fitting technique was applied to all calibration data to obtain an equation correlating millivolts output to degrees Fahrenheit.

The thermocouple data were recorded on the analog data multiplexing system (fast scan), the digital data acquisition system (slow scan), or the oscillograph system, depending on test requirements.

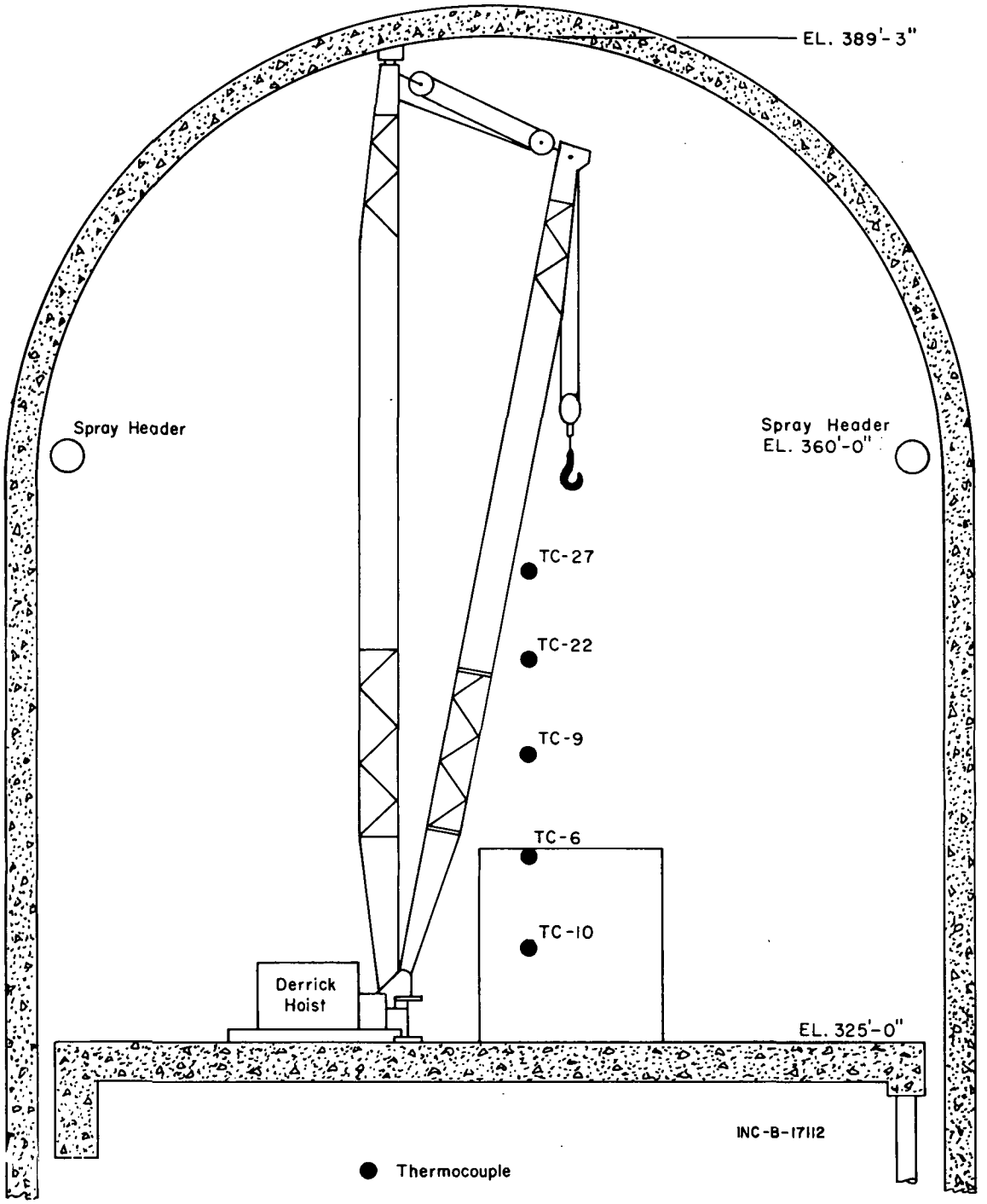

FIG. A-11 LOCATIONS OF THERMOCOUPLES FOR DETERMINING SPRAY EFFECTIVENESS.

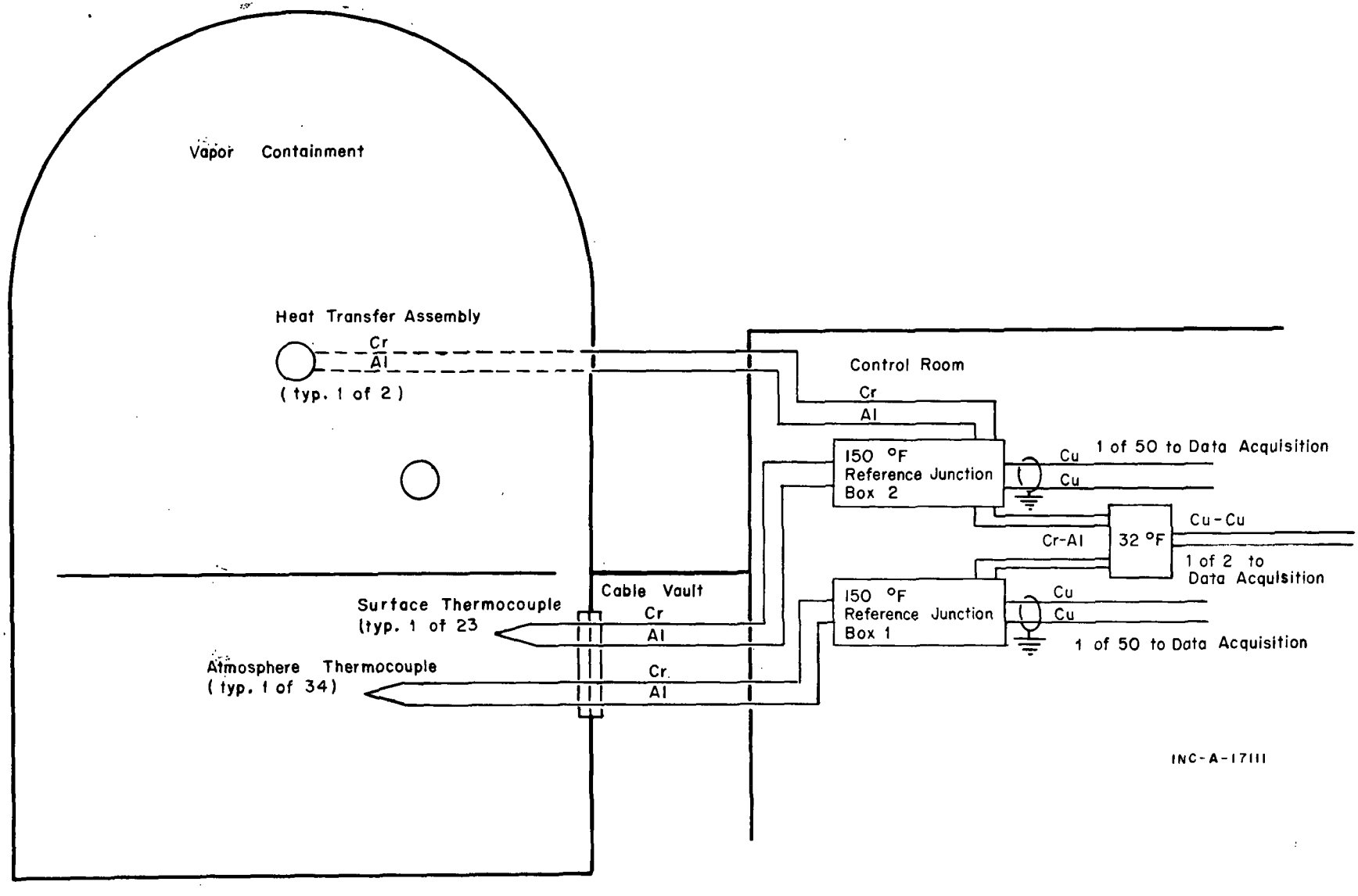

FIG. A-12 THERMOCOUPLE SCHEMATIC.

2. CONTAINMENT PRESSURE

The time-dependent pressure response of the containment atmosphere was measured with seven 0 to 25 psig, fast response, Norwood Model 141 pressure transducers. The transducers were located as shown in Table A-III and Figures A-1, A-4, and A-13.

TABLE A-III

PRESSURE TRANSDUCER LOCATIONS DURING DBA TESTS

Pressure Transducer	Elevation (ft)	Measurement Location
1	362	Operating region
2	310	Reactor header cavity
3	312	Intermediate region
4	284	Basement region
5	335	Operating region[a]
6	325	Fuel transfer canal
7	345	Operating region

[a] The transducer was installed outside the containment on the end of a pipe that penetrated the containment wall.

Prior to installation, the transducers were calibrated through use of a mercury manometer. During the ambient temperature and hot air leakage rate tests[4], in-place calibration data were obtained through use of the Texas Instrument precision absolute pressure gauge. These data were used for temperature corrections of the steam test data. The pressure transducer data were recorded on the oscillograph system.

In addition to the pressure transducers, a 0- to 30-psig Heise gauge located in the reactor control room was used to monitor the containment pressure. The Heise gauge was connected to the containment through a 1/2-in. copper tube (Figure A-13). Data from the Heise gauge were obtained during the leakage rate tests and compared to the data from the precision pressure gauge to determine the accuracy of the Heise gauge. In addition, prior to the steam tests the accuracy of the Heise gauge was checked with a mercury manometer.

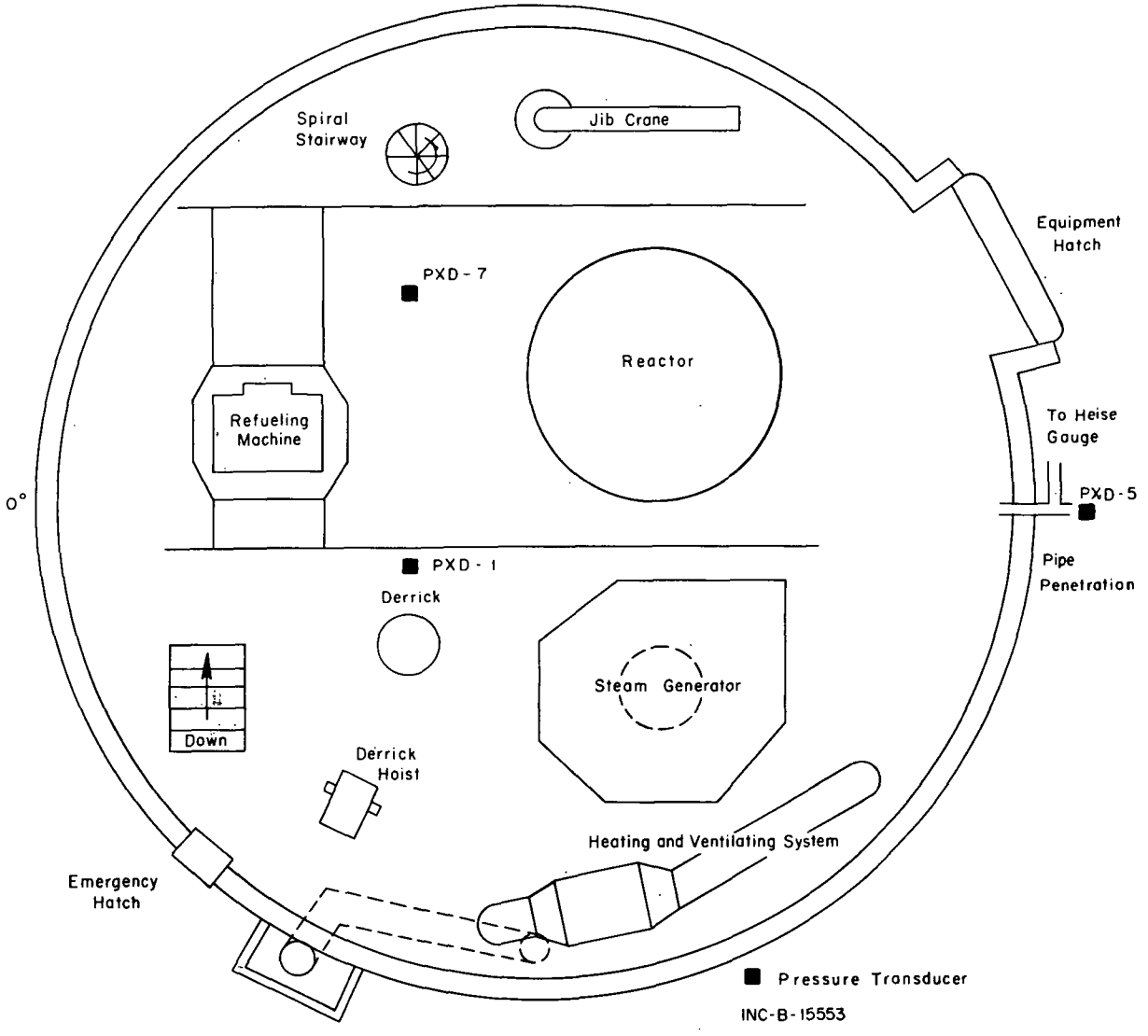

FIG. A-13 PRESSURE TRANSDUCER LOCATIONS -- OPERATING REGION.

3. CONDENSATE CATCH CANS

Eleven condensate measuring devices (Section IV of the body of this report) were installed in the CVTR containment to determine the rate of condensate formation and the total condensation on specific areas of the containment liner during the steam injection tests. A bead of Dow Corning Compound III was placed on the containment liner to define a specific condensate collection area for each gauge. The location and area of the liner monitored by each catch can is shown in Table A-IV.

TABLE A-IV

CONDENSATE CATCH CANS

Catch Can	Elevation (ft)	Area (ft^2)[a]
1	359	1
2	351	9
3[b]	343	17
4	335	25
5	327	33
6[b]	319	41
7	311	49
8[b]	303	57
9	295	65

Rate Gauge	Elevation (ft)	Area (ft^2)[a]
1	348	12
4	331	29

[a] The area is defined only to the containment bend line (elevation 360 feet).

[b] These catch cans were also rate gauges.

Each rate gauge was calibrated in-place by filling the catch can with water (1000 ml increments) and recording the millivolt signal from each load cell at each increment.

4. SPRAY DISTRIBUTION CANS

Thirty-two catch cans were positioned on two quadrants of the reactor operating floor to collect spray water and provide information on the general distribution of the spray within the containment. The spray catch cans were about 13 1/2-in. in diameter and were positioned on approximately 5-ft centers, as shown in Figure A-14. Following each steam test, the amount of water contained in each can was measured.

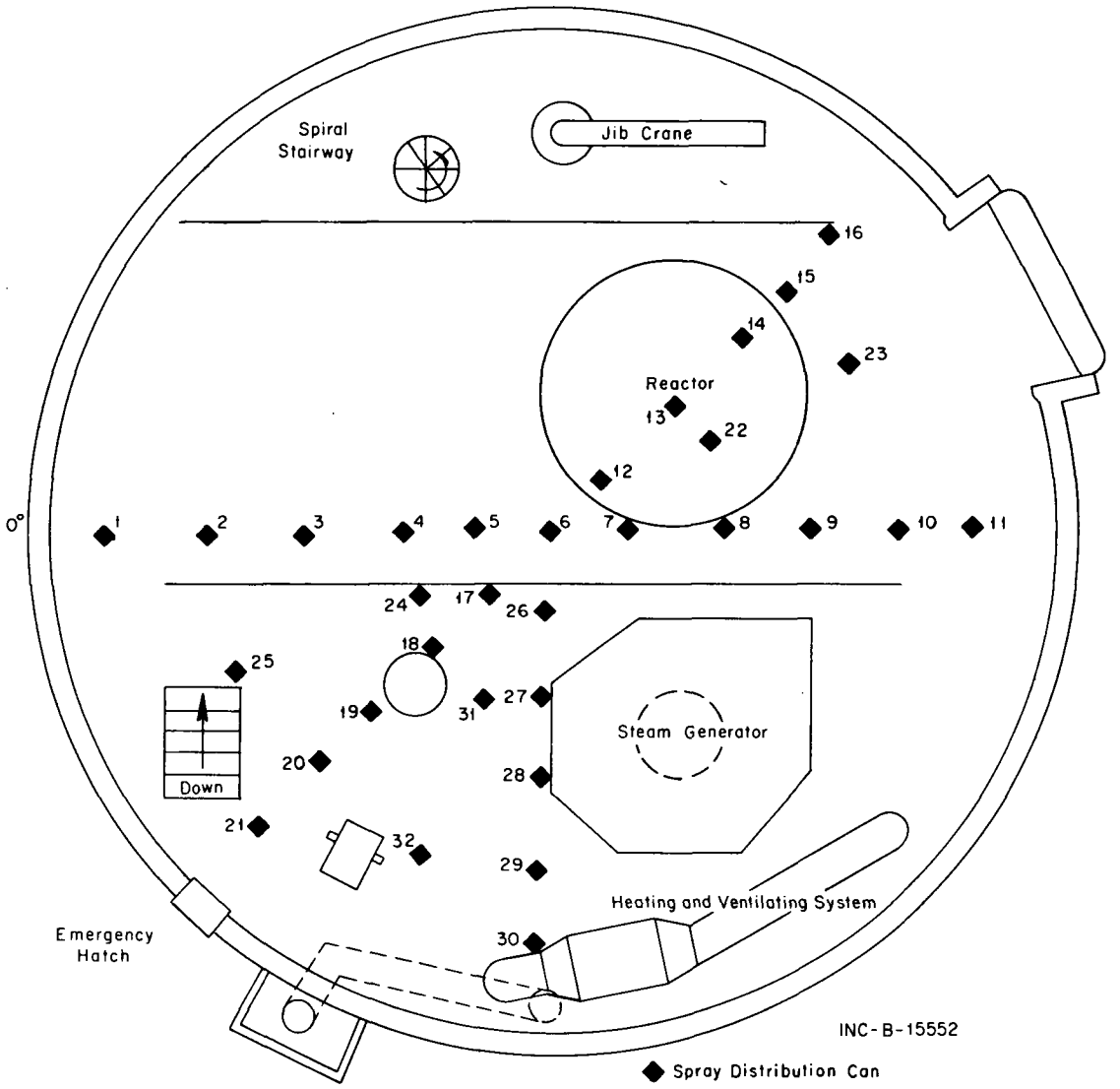

FIG. A-14 SPRAY DISTRIBUTION CAN LOCATIONS.

A-II. DATA ACQUISITION SYSTEMS[8]

The principal CVTR data acquisition systems consisted of a digital data acquisition system (slow scan), an analog data multiplexing system (fast scan), a digital voltmeter with a digital printer, an oscillograph system, and various process instrument recorders.

1. DIGITAL DATA ACQUISITION SYSTEM (Slow Scan)

The digital data acquisition system provided the capability for scanning and recording data from 198 channels of low-level dc signals. The output signals from the sensors were scanned sequentially and the analog output converted to digital form by a digital voltmeter. A visual digital display of the input signal was provided by the voltmeter that also provided an output signal to a digital recorder (paper tape printer) or to a paper tape perforator. A time code generator was connected to the system so that time was recorded digitally once during each scan cycle. Data were recorded by this system at the rate of one point every two seconds. Figure A-15 shows a functional block diagram of the digital data acquisition system.

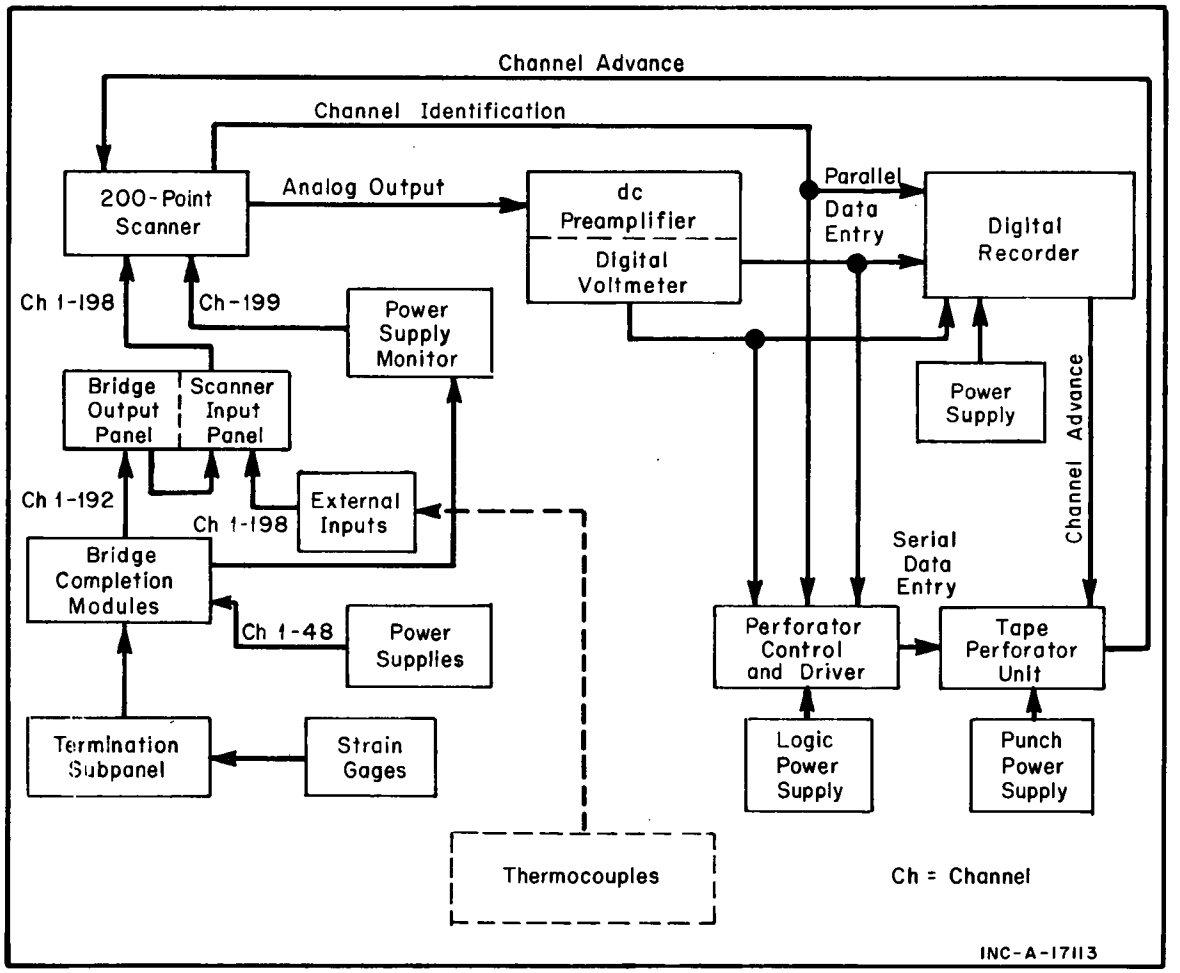

FIG. A-15 DIGITAL DATA ACQUISITION SYSTEM.

2. ANALOG DATA MULTIPLEXING SYSTEM (Fast Scan)

The analog data multiplexing system was capable of scanning, conditioning, and recording 90 analog input signals. Figure A-16 shows a simplified block diagram of the analog data multiplexer. Input signals were multiplexed in groups of ten channels with respect to the output of the multiplexer. That is, each of the ten multiplexed output channels contained ten input signals. Each multiplexer output channel was conditioned by a separate low-level amplifier. The ten amplified outputs were channels of a 14-channel magnetic tape recorder. Channel 14 of the tape recorder was used for channel identification and time synchronization with the multiplexer inputs. Each input signal was recorded about three times per second. A millivolt calibration box with an accuracy of 0.1% of full range was used to calibrate each channel of the multiplexer prior to each DBA test.

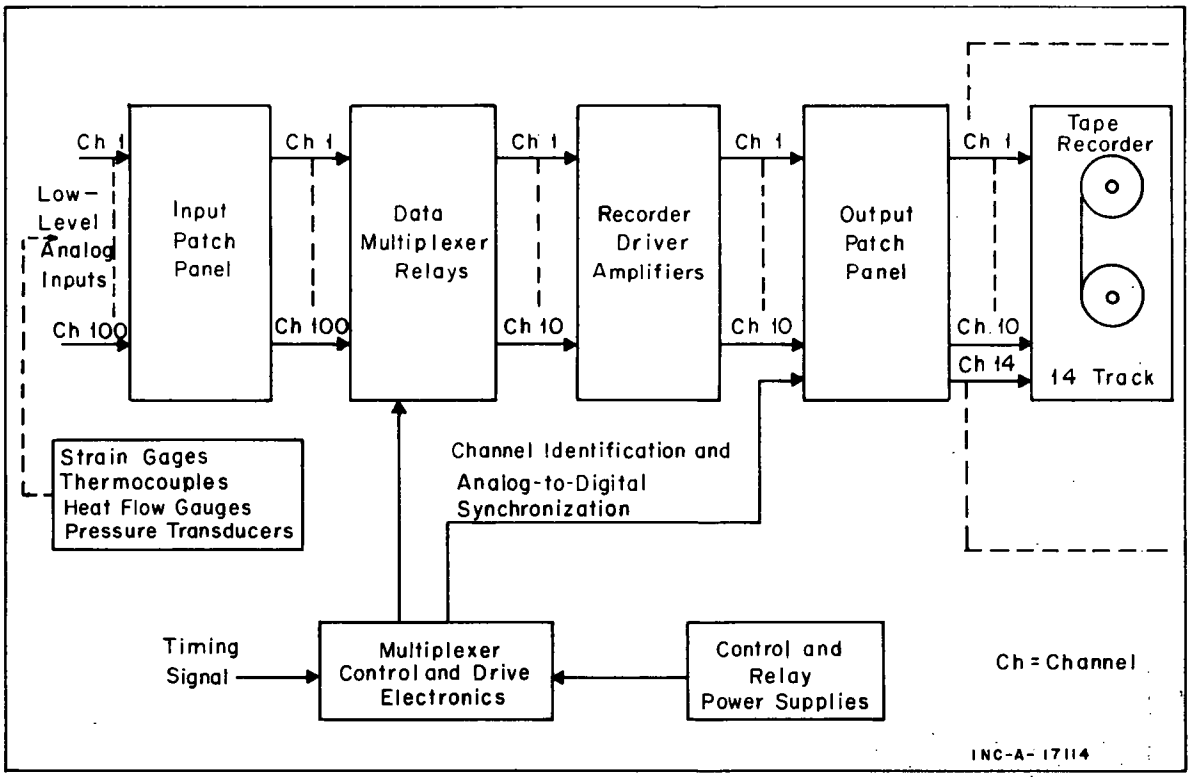

FIG. A-16 ANALOG DATA MULTIPLIER SYSTEM.

3. DIGITAL VOLTMETER SYSTEM

The digital voltmeter with the digital printer was capable of recording in digital form one channel of data at a rate of five times a second. The system accepted low-level millivolt signals directly and was equipped with an ohms-to-volts converter so that it could be used for readout of resistive devices such as resistance thermometers. A manual switch-timer unit permitted manual scanning and recording of up to 15 channels of resistance thermometer data. Figure A-17 is a block diagram of this system.

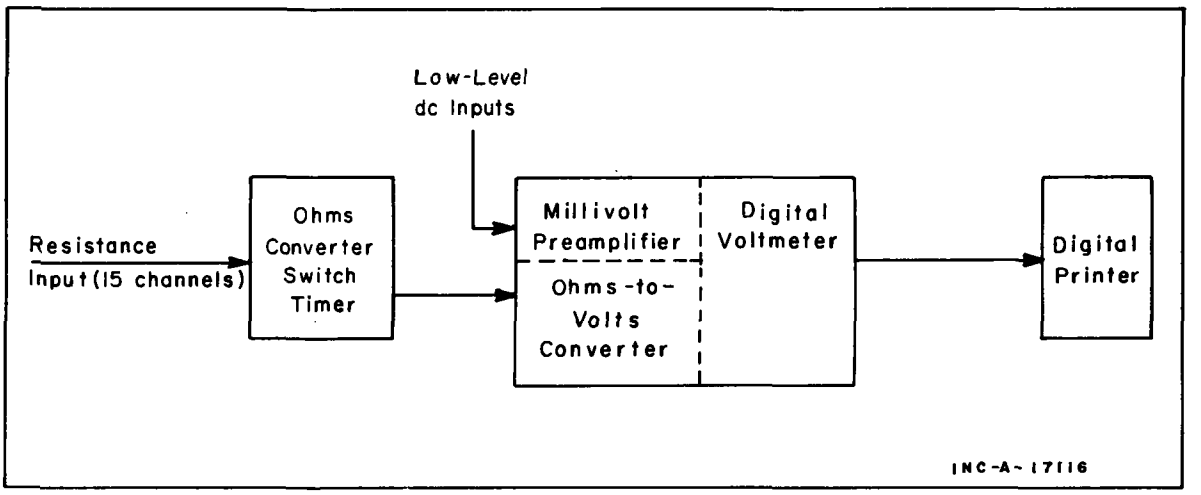

FIG. A-17 DIGITAL VOLTMETER AND DIGITAL PRINTER SYSTEM.

4. OSCILLOGRAPH SYSTEM

The oscillograph system provided capabilities for signal conditioning and continuous recording of 36 channels of low-level signals. Figure A-18 shows a block diagram of this system. Low-level dc signals were amplified and fed into the oscillograph to provide a permanent record of the input signal. A low-level calibration source, with an accuracy of ±0.1% of full range, was used to calibrate each channel of the system prior to each test.

For the DBA tests, the oscillograph system was used to record key process conditions (temperature, pressure, and flow) and representative containment pressures and temperatures to permit rapid and accurate on-site data reduction and evaluation.

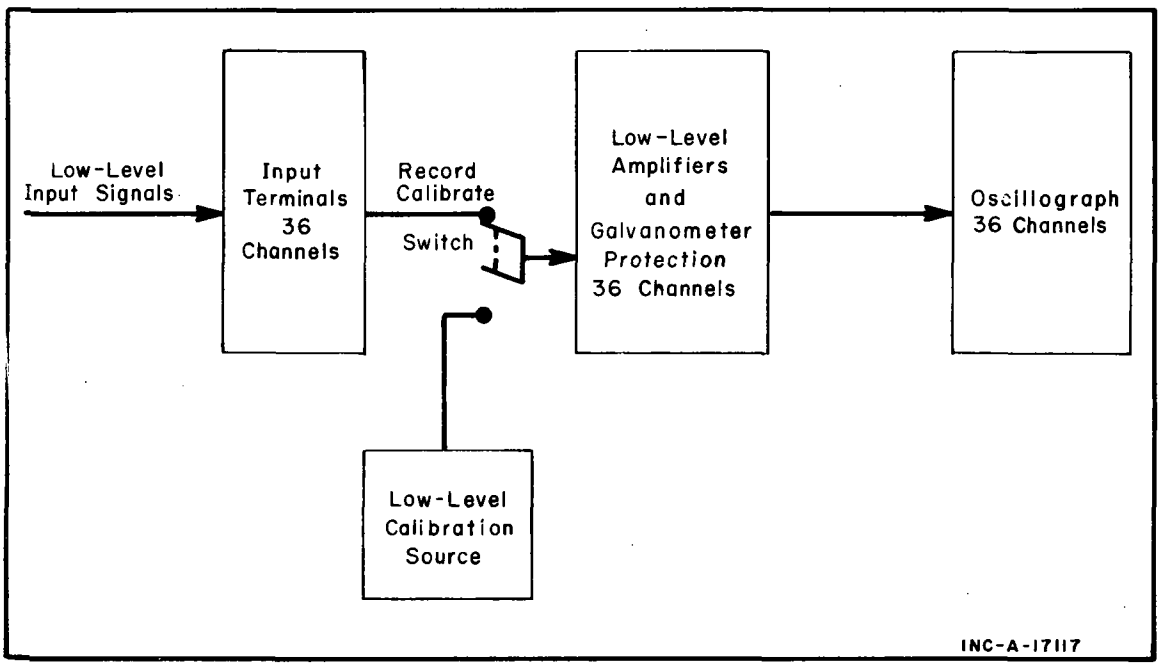

FIG. A-18 OSCILLOGRAPH SYSTEM.

5. PROCESS INSTRUMENT RECORDERS

Conventional process instrument strip chart recorders and indicators were used to obtain process data not recorded on the oscillograph system. The data from the condensate rate gauges were recorded on a multipoint recorder such that each point represented data from one rate gauge. Data from the ultrasonic aneometers were recorded on a special time-sharing duel-pen strip-chart recorder system.

Prior to the initial DBA steam test, the process instrumentation was checked out and calibrated through use of standard techniques and calibration equipment. The condensate rate gauges and the ultrasonic anemometers were calibrated and subjected to environmental testing in laboratories at the NRTS prior to shipment to CVTR.

A-III. DATA REDUCTION PROCESS

The instrumentation for DBA data acquisition was briefly described in previous sections of this appendix. Elements of the data reduction process are discussed in the following sections as an aid to understanding the test results.

1. SLOW SCAN - PAPER TAPE PRINTER - PAPER TAPE PUNCH

The sensing devices assigned to channels of the slow scan system were generally of a backup nature or, alternately, were monitoring instruments expected to respond slowly, such as thermocouples in the concrete. Since for the containment response-heat transfer studies, interest was primarily centered on the transient or short term behavior, the slow-scan system data were primarily used for spot checks or for long temperature-time behavior. Data from the slow-scan system were recorded by a paper tape printer or paper tape punch both of which were part of the slow-scan system.

2. FAST SCAN

Pressure transducers, heat flux gauges, test timing, some strain gages, most of the heat plug thermocouples, and many other thermocouples were assigned to fast scan channels. The resulting magnetic tape was of the frequency modulated, multiplexed, analog form. Reduction was through the use of existing SPERT [a] data reduction equipment and suitably modified SPERT data reduction programs. Essentially, a typical analog-to-digital conversion routine was employed to produce millivolt plots and to transfer the data to a seven-track tape. This tape was then transferred to the NRTS IBM-360 system and the data were stored on a nine-track storage tape. Knowledge of file index numbers, digitizing intervals, and calibration numbers permitted any given data record or portion thereof to be retrieved and converted to engineering units by use of a CVTR data code (TCDUMP) briefly discussed in Section A-III-4.2. The SPERT system produced 2000 digitized bits of data having a digitizing interval variable from 366.6 milliseconds to 3.3 seconds.

3. OSCILLOGRAPH AND RECORDERS

The oscillograph data were used primarily for test control. Key process conditions were recorded on the oscillograph and were reduced immediately following such tests. Sufficient data were reduced to permit an understanding of, and confidence in, the test results and to serve as a basis for the following DBA test.

---

[a] SPERT - Special Power Excursion Reactor Tests.

Oscillograph data were the basis of the preliminary CVTR report[8]. For this report the oscillograph and strip chart data were more carefully reduced through use of a Computer Industry Inc. data digitizer and tracing machine that converted analog data to digital form on punch cards. The punched cards were then used as input to an existing SPERT data program that produced plots and listings in engineering units.

4. CVTR DATA CODES

The CVTR data codes were written specifically for the CVTR In-Plant Testing Project to aid in data reduction. Since the codes were tailored to the CVTR data acquisition system and the SPERT program formats they are not generally applicable to other work. Thus, only general features of the codes are discussed.

4.1 FSCAN

The FSCAN program rearranged the SPERT digitized data tape in a suitable manner for direct input into such analytical programs as TAEH. The philosophy was complete machine manipulation of the large amount of data on the storage tapes. However, because of various difficulties with changes in formats and number of sensors from test-to-test, difficulties with the FSCAN program were encountered and the program was little used.

4.2 TCDUMP

The TCDUMP program simply listed the stored nine-track IBM-360 storage tape. Specifications on channels, timing, and calibration could be applied to obtain any desired part of a record from any sensor. Generally, all 2000 digitized data bits or the complete record of a given sensor were listed. The program was used particularly for data from thermocouples. Pretest thermocouple calibration information was applied to obtain the output in engineering units.

4.3 LSPF

The LSPF program was a standard least-squares polynomial fitting program available from the NRTS library of operational codes. The code was used for smoothing the CVTR thermocouple data, particularly the data associated with heat transfer calculations. However, certain modifications were necessary before the code could be used for the CVTR data. Since each thermocouple was digitized in terms of 2000 data points and a number of thermocouples were used for heat transfer calculations, normal preparation of LSPF input data on cards was not feasible. Consequently, the TCDUMP program was altered to create a temporary data set in which the LSPF control parameters were included. Subsequent smoothing of the 2000 data points or any portion thereof was possible for any specified thermocouple. In practice, the data were smoothed by parts. The first part commensed at the time of charge valve actuation and continued for 220 seconds; the second part commensed at 220 seconds and continued to test termination. Seventh order polynomials were

used uniformly. Printout was for every 15 time-steps (5.5 seconds). The LSPF program also produced data on uncertainties such as standard deviations and variance.

4.4 CVSTRS

A special computer program was written to analyze the millivolt output data obtained from the 83 three-gage rectangular strain rosettes. Input to the program consisted of parametric and control data, and millivolt data that could be read from any desired medium; that is, from punched and paper tape from the slow scan data system, or from magnetic tape from the fast scan data system.

A rectangular rosette consists of three overlapping strain gages mounted at orientations of 0, 45, and 90 degrees. The millivolt output of each arm is a function of gage factor, bridge circuit exitation voltage, and strain as given in the following equation:

$$mv = \frac{GF\ (EX)\ E}{4 \times 10^{-3}} \qquad \text{(B-I)}$$

where

mv = output (mV)

GF = gage factor

EX = excitation voltage (volts)

E = strain (μin./in.)

By utilizing the input data and the strain gage millivolt data, the program calculated the strain for each of the three arms of the rosette. From these values, the program determined the maximum and minimum principal strains, the maximum shearing strain, the corresponding stresses, and the strain orientations. Any number of strain gages and data sets could be processed in one run.

A-IV. INSTRUMENT UNCERTAINTIES

In any measuring system inaccuracies and uncertainties exist. Usually the inaccuracy resulting from systematic errors or bias and corrections can be determined. Other errors are those of a random nature which, unlike the bias, are not always of the same magnitude or in the same direction. Corrections for random errors are not possible, but an estimate of the uncertainty often can be accomplished as described in the following discussions. Finally, uncertainties can result from such things as imprecise positioning of sensing elements, steam jet effects, air currents, or other mechanical effects. These uncertainties are not adaptable to error analysis, but some of the effect can be reduced by suitable smoothing such as is done by the LSPF program.

Data uncertainties in this section result from the combined data acquisition and reduction systems and similarly corrections or random error estimates refer to the entire system.

1. SYSTEMATIC ERRORS

For the CVTR tests some of the systematic errors were determined, and corrections to the data were made for the following:

(1) Zero shift in electronic amplifiers that occurred after instrument calibration

(2) Temperature shift in the thermocouple reference junction box

(3) Amplifier gain variations.

A zero trace was established for each channel prior to each test, and in addition for the fast scan system, the zero was recorded continously during the course of a test. Data from the zero trace were reduced and the average zero offset was calculated. Corrections were applied to the test data for zero offset.

Similarly, corrections were made for temperature shifts in the 150°F thermocouple reference junction box temperature.

An instrumentation system calibration with a known input source was made prior to each CVTR test. Data from the calibration were reduced to obtain an average output for each channel. The average output was compared with the known calibration input such that a gain correction was obtained and applied to test data.

2. RANDOM ERROR

Statistical techniques were used to establish the random error in the CVTR data associated with the combined acquisition and data reduction systems. For example, the standard deviation from some of the averages in the previous

section provided a random error uncertainty. Also, a calibration was made on each thermocouple and pressure transducer prior to testing, and a standard deviation for each thermocouple was calculated from the calibration data.

By using standard error propagation techniques, the standard deviations of the instrumentation zero, calibration output, and thermocouple output were combined to provide the overall maximum uncertainty to which the instrumentation system contributed. Tables A-V and A-VI show the maximum uncertainty from random errors of each channel of the oscillograph and multiplexer instrumentation systems, respectively. The maximum estimated error associated with pressure measurements is ±5% and is attributed primarily to transient temperature effects on the individual transducers.

TABLE A-V

UNCERTAINTY IN MULTIPLEXED THERMOCOUPLE DATA

Channel	Thermocouple	Maximum Uncertainty[a,b] (^{o}F)	Amplifier Gain
1	2, 3, 5, 6, 9, 10 13, 17, and 18	± 5.7	200
2	20, 21, 22, 23, 24 25, 27, 27, 30	± 1.4	200
3	31, 32, 33, 34, 36, 37 38, 39, 40	± 3.3	200
4	42, 43, 44, 45, 46 47, 48, 49, 50	± 1.3	200
5	51, 52, 53, 54, 55 56, 57, 58, 60	± 1.2	200
6	61, 62, 63, 64, 66 67, 68, 85, and 86	± 1.3	200
7	88, 90, 91, 92[c]	± 8.0	50
8	14, 15, 19, 28, 82	± 1.0	200

[a] Maximum uncertainty at one standard deviation determined using standard error propagation techniques.

[b] This uncertainty was calculated at approximately 230^{o}F in all cases; the uncertainty is correspondingly less at lower temperatures.

[c] Channel 7 thermocouples were eliminated from heat transfer coefficient calculations because of the large uncertainties; the uncertainty resulted from the gain setting which was necessary for other large signal output instruments such as heat flux gauges assigned to this channel.

TABLE A-VI

UNCERTAINTY IN OSCILLOGRAPH DATA[a]

Channel	Maximum Uncertainty	Amplifier Gain
1, 2, 6, 8, 9, 10, 11	± 0.59% of reading (1.36°F at 230°F)	200
3, 4, 5	± 0.46% of reading	100
15, 16, 17, 18, 19, 20, 21, 25, 26	± 0.2% of reading	50
14, 23, 24, 28, 29, 30, 31	± 0.21% of reading	20

[a] As reduced with the SPERT data digitizer.

APPENDIX B -- DATA SUMMARY

APPENDIX B -- DATA SUMMARY

This appendix presents a summary of the data obtained during the simulated DBA tests. A primary purpose of this data summary is to provide other interested organizations with a means of performing analyses of the CVTR tests. A particular objective is to present data that can be used for comparing and evaluating analytical models used for predicting containment response to accident conditions.

B-I. CONTAINMENT ATMOSPHERE PRESSURE

Although containment pressure was measured by seven pressure transducers, the most accurate pressure data were obtained from the Heise gauge having a readout system in the control room. As a DBA test progressed, the Heise gauge was observed and the containment pressure was recorded as a function of time. When the Heise gauge indicated a containment pressure of about 17.5 psig, the steam injection was terminated. The data from the Heise gauge (containment pressure versus time) for Steam Tests 3, 4, and 5 are shown in Table B-I.

Because of the effect of temperature on the pressure transducers, the data from these instruments had to be corrected through use of information obtained during the hot air leakage rate tests. The uncorrected and corrected data from the pressure transducers are shown in Table B-II.

TABLE B-I

HEISE GAUGE PRESSURE SUMMARY

Pressure (psig)	Test Time (min) Test 3	Test 4	Test 5
0	0	0	0
1	0.133	0.167	0.1
2	0.216	0.250	0.2
3	0.283	0.366	0.283
4	0.316	0.449	0.367
5	0.517	0.566	0.467
6	0.615	0.670	0.583
7	0.75	0.882	0.717
8	0.882	1.00	0.867
9	1.033	1.20	1.033
10	1.183	1.366	1.217
11	1.384	1.533	1.4
12	1.565	1.716	1.567
13	1.75	1.899	1.767
14	1.965	2.1	1.967
15	2.166	2.283	2.167
16	2.333	2.5	2.367

TABLE B-I (Contd.)

HEISE GAUGE PRESSURE SUMMARY

Pressure (psig)	Test Time (min) Test 3	Test 4	Test 5
17	2.537	2.67	2.55
17.6	2.60[a]	----	----
17.75	----	----	2.733[a]
17.8	----	2.83[a]	----
17	2.616	3.1	2.934
16	3.2	3.449	3.25
15	3.781	3.949	3.667
14	4.584	4.40	3.934
13	5.735	4.949	4.35
12	7.333	5.75	4.867
11	9.683	6.80	5.567
10	13.0	8.00	6.467
9	17.367	9.449	7.467
8	23.350	11.283	8.583
7	31.266	13.283	9.844
6	42.350	15.68	11.4
5	58.25	27.916	13.117
4	81.95	45.0	15.133
3		75.283	46.533

[a] Maximum pressure.

TABLE B-II

MAXIMUM PRESSURES AS OBTAINED FROM PRESSURE TRANSDUCERS

Transducer	Location	Pressure (psig)					
		Test 3		Test 4		Test 5	
		$\hat{P}$	Corrected $\hat{P}$	$\hat{P}$	Corrected $\hat{P}$	$\hat{P}$	Corrected $\hat{P}$
1	Operating region, elevation of 370 ft	21.5	18.3	22.0	18.8	21.8	18.6
2	Canal, elevation of 325 ft	20.7		19.2		18.5	
3	Intermediate region, elevation of 319 ft	17.5	17.5	18.0	17.9	18.2	
4	Basement region, elevation of 283 ft	17.7	17.7	18.3	18.3	18.2	18.2
5	Operating region (outside containment), elevation of 335 ft	18	18.0	18.5	18.5	18.4	18.4
6	Header cavity, elevation of 319 ft			18.6		18.6	
7	Operating region, elevation of 340 ft	22.5		20.6		20.3	

B-II. STEAM TEST SUMMARY

Table B-III summarizes the results of the three DBA tests and includes the total steam injection time, peak containment pressures reached, pressure reduction spray system flow rate, and total spray operation time. The total steam injection time is calculated from the time the charge valve starts to open to the time the charge valve is closed. The initial temperature of the spray water for all three tests was 67°F.

TABLE B-III

SUMMARY OF STEAM TEST PROCESS

Test	Total Steam Injection Time (sec)[a]	Peak Pressure (psig)	Spray Rate (gpm)	Total Spray Rate (min)
3	166.4	17.6	0	0
4	174.7	17.8	290	12.5
5	173.1	17.75	500	11.7

[a] Injection time was measured from the time the charge valve started to open until it closed again.

B-III. CONDENSATE

The condensate calculation areas and the total condensate collected by each catch can is shown in Table B-IV. The areas associated with each can were designated by beads of Dow Corning compound. The areas were 1 ft wide and extended from the collection tray to the bend line.

The total condensate collected was determined after each test by pouring it into a graduated cylinder.

TABLE B-IV

CONDENSATE CATCH CAN RESULTS

Condensate Catch Cans	Liner Area (ft^2)	Test 3 (No Spray)	Test 4 (290 gpm Spray)	Test 5 (500 gpm Spray)
7	1	7,330	6,000	8,640
2	9	640	670	720
3 (Rate Gauge 3)	17	6,850	3,960	4,760
4	25	5,990	5,800	5,360
5	33	5,050	4,000	2,130
6 (Rate Gauge 2)	41	15,520	18,000[a]	14,100
7	49	3,550	2,530	1,830
8 (Rate Gauge 5)	57	3,420	3,100	2,330
9	65	4,350	[b]	2,730
Heat plug 1 (Rate Gauge 4)	31	12,700	2,860[c]	18,000[a]
Heat plug 2 (Rate Gauge 1)	13	18,000[a]	8,900	9,950

[a] Full catch can.

[b] Catch can detached from mounting.

[c] The hose from the tray to the catch can became disconnected during test.

B-IV. SPRAY DISTRIBUTION

The distribution of the pressure reduction spray water within the containment is shown in Table B-V. The data are for Tests 4 and 5 that had a spray rate of 290 and 500 gpm, respectively. The amount of water in each can was measured after each test by pouring it into a graduated cylinder.

TABLE B-V

SPRAY DISTRIBUTION

Spray Distribution Cans	Water Collected (ml)	
	Test 4 (290 gpm Spray)	Test 5 (500 gpm Spray)
1	2,110	3,100
2	6,850	8,750
3	14,640	9,100
4	14,600	15,300
5	18,000	24,000[a]
6	19,740	24,000[a]
7	16,940	24,000[a]
8	6,730	14,600
9	4,800	12,000
10	760[b]	[b]
11	2,020	7,000
12	17,230	18,000
13	15,460	11,500
14	9,390	8,150
15	7,760	9,600
16	3,790	7,420
17	9,220	12,000
18	6,440	8,650
19	5,500	8,250
20	1,910	2,400
21	1,400	2,040
22	8,740	11,200
23	6,620	9,450
24	6,000	9,300
25	16,440	2,680
26	15,000	24,000
27	12,000	24,000[a]
28	6,340	18,400
29	8,030	12,480

TABLE B-V (Contd.)

SPRAY DISTRIBUTION

Spray Distribution Cans	Water Collected (ml)	
	Test 4 (290 gpm Spray)	Test 5 (500 gpm Spray)
30	9,140	17,500
31	6,000	9,800
32	4,020	2,200

[a] Full Can.

[b] Can damaged during test.

B-V. TEMPERATURE

Temperature data for the CVTR DBA tests were extensive and a complete tabulation is impracticable. However, sufficient data to permit independent heat transfer coefficient calculations have been provided in Tables B-VI through -IX. These tables contain heat plug temperature data for Tests 3 and 5 over the first 220 seconds which encompasses the steam injection period. The data of these tables are from the FSCAN data system and are the original data after smoothing with the LSPF program (Appendix A-III). Thermocouples 53 through 58 and 24 through 27 are associated with the bulk atmosphere temperature measurement and distance from the liner surface is provided for each thermocouple. Thermocouples 44 and 45 are located at the liner surface; Thermocouples 61 through 66 and 85 through 90 provide liner interior measurements and the distance from the liner surface is included; Thermocouples 67 and 92 are on the backside of the liner; and Thermocouples 68 and 92 are the first thermocouples in the interior of the concrete 3/8-in. from the concrete surface. Certain thermocouples have been identified as faulty, and data either did not exist or have been eliminated. Pretest calibration data were utilized for the thermocouple data reduction except for the data from thermocouples located in the concrete for which standard Chromel-Alumel calibration data were used. Other thermocouples in the concrete and associated with the heat plugs were monitored with the slow-scan system, and the time-scale is unsuitable for including the data in these tables. Temperature response in the concrete beyond the first thermocouple location was small and properly identified with the long-time containment response behavior which is a subject to which this report is not particularly addressed.

TABLE B-VI

HEAT TRANSFER DATA USED FOR HEAT TRANSFER CALCULATIONS -- THERMOCOUPLES OF HEAT PLUG 1 DURING STEAM TEST 3

Time (sec)	2 in. TC 58	1-1/2 in. TC 57	1 in. TC 56	1/2 in. TC 55	1/4 in. TC 54	Bulk Average	Liner Surface TC 44	ΔT Bulk Surface	0.044 in. TC 61	0.077 in. TC 62	0.109 in. TC 63	0.149 in. TC 64	0.219 in. TC 66	0.249 in. TC 67	Concrete 3/16 in. TC 68
0						80									
5.5	83.2	82.8	Faulty TC	81.5	80.6	82	74.4	7.6	72.9	72.6	72.9	72.6	73	69.6	71.4
11	102.7	101.1	Faulty TC	99.3	97.4	100.1	78.6	21.5	73.5	73.3	73.5	73.5	73.6	70.2	70.9
16.5	120.2	118.1	Faulty TC	115.9	113.5	116.9	83.3	33.6	74.3	74.1	74.3	74.5	74.7	71.1	71
22	135.5	133.5	Faulty TC	130.9	128.2	132	88.6	43.4	75.8	75.5	75.7	76	76.3	72.6	71.4
27.5	148.7	146.9	Faulty TC	144	141.3	145.2	94.4	50.8	78.1	77.1	78	78.2	78.7	74.8	71.8
33	159.9	158.4	Faulty TC	155.4	152.7	156.6	100.7	55.9	81.3	80.8	81.2	81.3	82	77.8	72
38.5	169.1	168	Faulty TC	164.9	162.4	166.1	107.5	58.6	85.5	84.8	85.3	85.3	86	81.6	72
44	176.8	175.9	Faulty TC	172.8	170.4	173.9	114.6	59.3	90.5	89.8	90.2	90.1	90.8	86.1	71.8
49.5	183	182.2	Faulty TC	179.2	177.1	180.4	121.8	58.6	96.4	95.4	95.9	95.6	96.2	91.3	71.6
55	188	187.4	Faulty TC	184.5	182.6	185.6	129	56.6	102.8	101.8	102.2	101.8	102.2	97.1	71.3
60.5	192	191.6	Faulty TC	188.8	187.2	189.9	136.1	53.8	109.8	108.6	109	108.6	108.7	103.2	71.2
66	195.7	195	Faulty TC	192.4	191	193.5	143	50.5	117.1	115.8	116.2	115.6	115.5	109.8	71.2
71.5	198.7	198	Faulty TC	195.6	194.4	196.7	149.6	47.1	124.6	123.2	123.5	122.9	122.5	116.5	71.5
77	201.5	200.6	Faulty TC	198.6	197.5	199.5	155.9	43.6	132.2	130.7	131	130.4	129.6	123.4	72.2
82.5	204.1	203.1	Faulty TC	201.3	200.4	202.2	161.8	40.4	139.6	138.2	138.4	137.8	136.8	130.3	73.2
88	206.7	205.6	Faulty TC	204	203.3	204.9	167.3	37.6	147.1	145.6	145.6	145.1	143.9	137.1	74.6
93.5	209.3	208.2	Faulty TC	206.9	206.2	207.6	172.5	35.1	154.3	152.8	152.7	152.3	150.9	143.8	76.4
99	211.9	210.8	Faulty TC	209.8	209.2	210.4	177.3	33.1	161.2	159.7	159.6	159.2	157.8	150.3	78.5
104.5	214.6	213.6	Faulty TC	212.9	212.3	213.4	181.9	31.5	167.8	166.4	166.2	165.9	164.5	156.6	81
110	217.4	216.5	Faulty TC	216	215.4	216.3	186.3	30.0	174.1	17 .7	172.5	172.3	170.9	162.7	83.8
115.5	220.2	219.4	Faulty TC	219.2	218.5	219.3	190.6	28.7	180	178.8	178.4	178.4	177.1	168.5	86.6
121	222.9	222.2	Faulty TC	222.4	221.5	222.2	194.7	27.5	185.6	184.5	184.1	184.3	183	174.1	89.8
126.5	225.4	225	Faulty TC	225.5	224.3	225.0	198.8	26.2	190.9	189.9	189.4	189.8	188.7	179.3	93
132	227.8	227.5	Faulty TC	228.4	226.9	227.6	202.8	25.8	195.9	195	194.5	195	194.1	184.3	96.1

P T_SAT
12.5 200
14.1 210

TABLE B-VI (Contd.)

HEAT TRANSFER DATA USED FOR HEAT TRANSFER CALCULATIONS -- THERMOCOUPLES OF HEAT PLUG 1 DURING STEAM TEST 3

Time (sec)	2 in. TC 58	1-1/2 in. TC 57	1 in. TC 56	1/2 in. TC 55	1/4 in. TC 54	Bulk Average	Liner Surface TC 44	ΔT Bulk Surface	0.004 in. TC 61	0.077 in. TC 62	0.109 in. TC 63	0.149 in. TC 64	0.219 in. TC 66	0.249 in. TC 67	Concrete 3/16 in. TC 68
137.5	229.9	229.8	Faulty TC	231	229.1	230	206.8	23.2	200.5	199.8	199.2	199.8	199.2	189	99.1
143	231.8	231.7	Faulty TC	233.2	231	231.9	210.6	21.3	204.8	204.3	203.6	204.4	203.9	193.4	102
148.5	233.2	233.3	Faulty TC	235.1	232.4	233.5	214.3	19.2	208.8	208.5	207.7	208.6	208.3	197.4	104.8
154	234.3	234.5	Faulty TC	236.5	233.4	234.7	217.8	16.9	212.5	212.2	211.5	212.4	212.3	201.2	107.4
159.5	235	235.3	Faulty TC	237.5	234	235.4	221	14.4	215.8	215.6	214.8	215.9	215.8	204.5	109.8
165	235.3	235.7	Faulty TC	238	234.2	235.8	223.7	12.1	218.7	218.6	217.8	218.9	218.9	207.5	112.2
170.5	235.4	235.8	Faulty TC	238.2	234	235.8	225.9	9.9	221.1	221.2	220.3	221.4	221.5	210.1	114.4
176	235.2	235.7	Faulty TC	238.1	233.5	235.6	227.5	8.1	223.1	223.2	222.2	223.4	223.5	212.2	116.7
181.5	234.7	235.3	Faulty TC	237.7	232.9	235.2	228.4	6.8	224.5	224.7	223.7	224.8	224.9	213.9	118.9
187	234.2	234.9	Faulty TC	237.1	232.3	234.6	228.7	5.9	225.5	225.6	224.6	225.7	225.8	215.1	121.2
192.5	233.7	234.5	Faulty TC	236.5	231.7	234.1	228.3	5.8	225.9	226	225	226	226.1	215.9	123.6
198	233.1	234.1	Faulty TC	235.9	231.2	233.6	227.4	6.2	225.9	226	225	225.8	225.9	216.2	125.9
203.5	232.5	233.6	Faulty TC	235.3	230.7	233	226.4	6.6	225.6	225.7	224.6	225.4	225.4	216.3	128.2
209	232	233	Faulty TC	234.6	230.3	232.5	225.7	6.8	225.2	225.3	224.2	224.8	224.7	216.1	130.2
214.5	231.2	231.9	Faulty TC	233.8	229.6	231.6	226.1	5.5	225	225.1	224	224.5	224.3	216	131.6
220	230	230	Faulty TC	232.7	228.3	230.2	228.5	1.7	225.5	225.6	224.5	224.9	224.4	216.2	131.9

TABLE B-VII

HEAT TRANSFER DATA USED FOR HEAT TRANSFER CALCULATIONS -- THERMOCOUPLES OF HEAT PLUG 2 DURING STEAM TEST 3

Time (sec)	2 in. TC 53	1-1/2 in. TC 26	1 in. TC 27	1/4 in. TC 24	1/2 in. TC 25	Bulk Average	Liner Surface TC 45	ΔT Bulk Surface	0.035 in. TC 85	0.067 in. TC 86	0.141 in. TC 88	0.175 in. TC 89	0.211 in. TC 90	0.248 in. Back of Liner TC 91	Concrete 3/16 in. TC 92
0		Faulty TC				80						Faulty TC			
5.5	90.3	Faulty TC	92.4	91.5	90.1	91.1	80.6	10.5	80	78.3	77.1	Faulty TC	75	70.5	70.3
11.0	112	Faulty TC	115.1	113.5	111.4	113	89.7	23.3	79	79.8	78.5	Faulty TC	74.4	72.3	70.1
16.5	130.3	Faulty TC	133.3	131.6	129.1	131	97.8	33.2	81.5	82.6	81.2	Faulty TC	76.6	73.9	70.2
22.0	145.5	Faulty TC	148	146.4	143.9	146	105.2	40.8	85.6	86.9	85.1	Faulty TC	80.9	75.9	70.4
27.5	158.1	Faulty TC	159.8	158.5	156.1	158.1	112.2	45.9	91.3	92.4	90.3	Faulty TC	87	78.9	70.8
33.0	168.4	Faulty TC	169.4	168.4	166.1	168.1	119.1	49.0	98.4	99	96.6	Faulty TC	94.4	82.9	71.1
38.5	176.6	Faulty TC	177.2	176.5	174.3	176.2	125.9	50.3	106.6	106.4	103.8	Faulty TC	102.7	88	71.4
44.0	183.3	Faulty TC	183.6	183	181	182.7	132.8	49.9	115.7	114.5	111.8	Faulty TC	111.6	94.2	71.6
49.5	188.6	Faulty TC	189	188.5	186.6	188.2	139.7	48.5	125.4	123.1	120.2	Faulty TC	120.8	101.2	71.8
55.0	193	Faulty TC	193.6	193	191.2	192.7	146.7	46.0	135.4	131.8	129	Faulty TC	130	108.9	72
60.5	196.6	Faulty TC	197.5	196.9	195.2	196.6	153.6	43.0	145.3	140.7	137.8	Faulty TC	139	117	72.1
66.0	199.7	Faulty TC	201	200.3	198.6	199.9	160.6	39.3	155	149.5	146.6	Faulty TC	147.6	125.3	72.3
71.5	202.4	Faulty TC	204.2	203.4	201.7	202.9	167.4	35.5	164.2	158	155.1	Faulty TC	155.8	133.5	72.5
77.0	205	Faulty TC	207.2	206.3	204.6	205.8	174	31.8	172.8	166.2	163.6	Faulty TC	163.4	141.5	72.7
82.5	207.5	Faulty TC	210	209	207.4	208.5	180.5	28.0	180.7	173.9	171	Faulty TC	170.4	149	73
88.0	210	Faulty TC	212.6	211.7	210	211.1	186.6	24.5	187.8	181.2	178.2	Faulty TC	176.8	156.1	73.5
93.5	212.6	Faulty TC	215.2	214.3	212.7	213.7	192.5	21.2	194.1	187.9	184.8	Faulty TC	182.6	162.5	74
99.0	215.3	Faulty TC	217.6	216.9	215.3	216.3	198	18.3	199.6	194.1	190.0	Faulty TC	187.9	168.3	74.6
104.5	218	Faulty TC	220	219.5	217.9	218.8	203.1	15.7	204.4	199.8	196.4	Faulty TC	192.8	173.4	75.3
110.0	220.8	Faulty TC	222.3	222	220.5	221.4	207.3	14.1	208.6	204.9	201.4	Faulty TC	197.2	177.9	76.2
115.5	223.6	Faulty TC	224.5	224.4	223	225.6	212.1	13.5	212.1	209.5	205.9	Faulty TC	201.2	181.8	77.2
121.0	226.4	Faulty TC	226.5	226.8	225.4	226.3	215.9	10.4	215.2	213.6	209.9	Faulty TC	205	185.2	78.2
126.5	229	Faulty TC	228.4	229.1	227.6	228.5	219.4	9.1	217.9	217.3	213.6	Faulty TC	208.6	188.1	79.4
132.0	231.4	Faulty TC	230.3	231	229.6	230.6	222.3	8.3	220.4	220.5	216.8	Faulty TC	211.8	190.7	80.6

Max T_{SAT} = 202

TABLE B-VII (Contd.)

HEAT TRANSFER DATA USED FOR HEAT TRANSFER CALCULATIONS -- THERMOCOUPLES OF HEAT PLUG 2 DURING STEAM TEST 3

Time (sec)	2 in. TC 53	1-1/2 in. TC 26	1 in. TC 27	1/4 in. TC 24	1/2 in. TC 25	Bulk Average	Liner Surface TC 45	ΔT Bulk Surface	0.035 in. TC 85	0.067 in. TC 86	0.141 in. TC 88	0.175 in. TC 89	0.211 in. TC 90	0.248 in. Back of Liner TC 91	Concrete 3/16 in. TC 92
137.5	233.5	Faulty TC	231.7	232.7	231.4	232.2	224.9	7.4	222.5	223.4	219.8	Faulty TC	214.9	193.1	81.9
143.0	235.3	Faulty TC	233	234.2	232.8	233.8	227	6.8	224.5	225.8	222.4	Faulty TC	217.8	195.2	83.2
148.5	236.7	Faulty TC	234	235.4	234	235	228.7	6.3	226.3	227.9	224.8	Faulty TC	220.4	197.2	84.6
154.0	237.6	Faulty TC	234.8	236.2	234.8	235.8	230	5.8	228	229.6	226.8	Faulty TC	222.7	199	86.1
159.5	238.2	Faulty TC	235.2	236.6	235.2	236.3	230.8	5.5	229.4	230.9	228.4	Faulty TC	224.7	200.7	87.6
165.0	238.3	Faulty TC	235.3	236.7	235.2	236.4	231.3	5.1	230.4	231.9	229.7	Faulty TC	226.2	202.3	89.1
170.5	238	Faulty TC	235,1	236.4	234.9	236.1	231.4	4.7	231.2	232.4	230.5	Faulty TC	227.2	203.7	90.7
176	237.3	Faulty TC	234.5	235.8	234.3	235.5	231.1	4.4	231.5	232.5	230.9	Faulty TC	227.8	204.8	92.3
181.5	236.3	Faulty TC	233.7	234.9	233.4	234.6	230.5	4.1	231.3	232.2	230.8	Faulty TC	227.7	205.6	93.8
187	235.1	Faulty TC	232.6	233.9	232.4	233.5	229.6	3.9	230.6	231.5	230.3	Faulty TC	227.1	206.1	95.4
192.5	233.9	Faulty TC	231.4	232.7	231.4	232.4	228.6	3.8	229.4	230.6	229.3	Faulty TC	226	206.2	97
198	232.7	Faulty TC	230.3	231.5	230.4	231.2	227.5	3.7	228	229.5	228.1	Faulty TC	224.7	205.9	98.6
203.5	231.7	Faulty TC	229.3	230.6	229.5	230.3	226.5	3.8	226.6	228.4	226.8	Faulty TC	223.4	205.3	100
209	231	Faulty TC	228.9	230	229.1	229.8	226	3.8	225.6	227.6	225.8	Faulty TC	222.6	204.6	101.2
214.5	230.9	Faulty TC	229.2	230	229.1	229.8	226	3.8	225.9	227.5	225.7	Faulty TC	222.9	204.2	102.3
220	231.4	Faulty TC	230.9	230.9	230	230.8	227	3.8	228.4	228.7	227.1	Faulty TC	225.3	204.7	102.9

TABLE B-VIII

HEAT TRANSFER DATA USED FOR HEAT TRANSFER CALCULATIONS -- THERMOCOUPLES OF HEAT PLUG 1 DURING STEAM TEST 5

Time (sec)	2 in. TC 58	1-1/2 in. TC 57	1 in. TC 56	1/2 in. TC 55	1/4 in. TC 54	Bulk Average	Liner Surface TC 44	ΔT Bulk Surface	0.044 in. TC 61	0.077 in. TC 62	0.109 in. TC 63	0.149 in. TC 64	0.219 in. TC 66	0.249 in. TC 67	Concrete 3/16 in. TC 68
0			Faulty TC			84									
5.5	89.3	87.3	Faulty TC	85.7	84.5	86.9	81.3	5.4	78.8	77.6	78.6	78.7	78.7	Faulty TC	77
11	109.3	105.5	Faulty TC	102.3	100.9	104.5	85.4	19.1	79.9	79.6	80.0	80.1	80.6	Faulty TC	76.5
16.5	125.6	121.9	Faulty TC	117.9	116.3	120.7	89.6	31.1	81.1	80.8	81.3	81.3	82	Faulty TC	76.8
22	141.2	136.5	Faulty TC	132.1	130.5	135	93.9	41.1	82.7	82.3	82.8	82.7	83.4	Faulty TC	77.3
27.5	153.6	149.1	Faulty TC	144.6	143.2	147.6	98.4	49.2	84.8	84.3	84.8	84.5	85	Faulty TC	77.8
33	163.9	160.0	Faulty TC	155.6	154.2	158.5	103	55.5	87.4	86.9	87.4	87	87.2	Faulty TC	78.1
38.5	172.5	169.2	Faulty TC	164.9	164.7	167.6	107.8	59.8	90.7	90.1	90.6	90.3	90.1	Faulty TC	78.2
44	179.5	176.8	Faulty TC	172.8	171.7	175.2	112.9	62.3	94.5	94.1	94.6	94.2	93.7	Faulty TC	78
49.5	185.3	183.1	Faulty TC	179.4	178.3	181.5	118.2	63.3	199.1	98.6	99.2	99	98.2	Faulty TC	77.7
55	190.1	188.3	Faulty TC	184.9	183.9	186.5	123.9	62.6	104.2	103.8	104.5	104.4	103.4	Faulty TC	77.4
60.5	194.1	192.6	Faulty TC	189.5	188.5	191.1	119.9	61.2	109.8	109.6	110.4	110.4	99.2	Faulty TC	77.1
66	197.5	196.1	Faulty TC	192.4	192.4	194.9	136.1	58.8	116.0	115.9	116.7	116.9	115.7	Faulty TC	76.9
71.5	200.4	199.6	Faulty TC	196.7	195.8	198	142.6	55.4	122.6	122.6	123.5	123.8	122.7	Faulty TC	77
77	203.1	201.8	Faulty TC	209.7	208.9	200.9	149.3	50.8	129.5	130.6	130.5	131.5	130	Faulty TC	77.4
82.5	205.6	204.3	Faulty TC	202.5	207.7	203.5	156.1	47.4	136.9	136.8	137.8	138.5	137.6	Faulty TC	78.3
88	208.0	206.6	Faulty TC	205.1	204.4	206	163	43	143.9	144.1	145.1	145.9	145.3	Faulty TC	79.5
93.5	210.4	208.9	Faulty TC	207.8	207.1	208.5	169.8	38.7	151.2	151.5	152.4	153.3	152.9	Faulty TC	81.1
99	212.9	211.1	Faulty TC	212.4	209.8	211.0	176.6	34.4	168.5	158.8	159.6	160.3	160.5	Faulty TC	83.2
104.5	215.4	213.5	Faulty TC	213.1	212.5	213.6	183.1	30.5	165.6	165.9	166.7	167.6	167.8	Faulty TC	85.6
110	217.9	215.9	Faulty TC	215.8	215.3	216.2	189.4	26.8	172.5	172.8	173.5	174.4	174.8	Faulty TC	88.3
115.5	220.4	218.3	Faulty TC	218 5	218.0	218.8	195.3	23.5	179.1	179.4	180.0	180.8	181.4	Faulty TC	91.2
121	222.9	220.8	Faulty TC	221.2	220.7	221.4	200.7	20.4	185.4	185.7	186.1	186.9	187.6	Faulty TC	94.4
126.5	225.4	223.2	Faulty TC	223.8	223.3	223.9	205.7	18.2	191.3	191.5	191.8	192.5	193.3	Faulty TC	97.6
132	227.8	225.5	Faulty TC	226.3	225.7	226.3	210.1	16.2	196.7	197.0	197.1	197.7	198.5	Faulty TC	100.8

TABLE B-VIII (Contd.)

HEAT TRANSFER DATA USED FOR HEAT TRANSFER CALCULATIONS -- THERMOCOUPLES OF HEAT PLUG 1 DURING STEAM TEST 5

Time (sec)	2 in. TC 58	1-1/2 in. TC 57	1 in. TC 56	1/2 in. TC 55	1/4 in. TC 54	Bulk Average	Liner Surface TC 44	ΔT Bulk-Surface	0.044 in. TC 61	0.077 in. TC 62	0.109 in. TC 63	0.149 in. TC 64	0.219 in. TC 66	0.249 in. TC 67	Concrete 3/16 in. TC 68
137.5	229.9	227.2	Faulty TC	228.6	227.9	228.5	214	14.5	201.7	201.9	201.9	202.5	203.2	Faulty TC	104
143	231.9	228.7	Faulty TC	230.6	229.8	230.5	217.4	13.1	206.2	206.4	206.3	206.9	206.5	Faulty TC	107
148.5	233.5	230.4	Faulty TC	232.3	231.4	232.1	220.2	11.9	210.2	210.5	210.2	210.7	211.1	Faulty TC	110
154	234.8	232.9	Faulty TC	233.7	232.7	233.5	222.6	10.9	213.8	214.1	214.7	214.2	214.4	Faulty TC	112.6
159.9	235.8	234.0	Faulty TC	234.8	233.6	234.5	224.4	10.1	216.9	217.2	217.7	217.2	217.2	Faulty TC	115.1
165	236.3	234.9	Faulty TC	235.6	234.2	235.3	226	9.3	219.6	219.7	219.4	219.9	219.7	Faulty TC	117.5
170.5	236.5	235.4	Faulty TC	236.0	234.5	235.6	227.1	8.5	221.9	222.2	221.6	222.1	221.8	Faulty TC	119.7
176	236.2	235.5	Faulty TC	236.2	234.5	235.6	228.1	7.5	223.8	224.2	223.5	224	224.1	Faulty TC	121.8
181.5	235.6	235.5	Faulty TC	236.1	234.3	235.4	228.9	6.5	225.8	225.7	225	225.5	225.1	Faulty TC	123.9
187	234.8	235.1	Faulty TC	235.9	234	234.9	229.5	5.4	226.6	227.0	226.2	226.6	226.3	Faulty TC	126
192.5	233.8	234.6	Faulty TC	235.5	233.5	234.3	230.1	4.2	227.5	227.9	227	227.4	227.2	Faulty TC	128.1
198	232.7	234.0	Faulty TC	235.0	233.0	233.7	230.4	3.3	228.1	228.5	227.4	227.9	227.8	Faulty TC	130
203.5	231.7	233.2	Faulty TC	234.4	232.5	231.9	230.5	1.4	228.3	228.7	227.5	228	228	Faulty TC	132.4
209	231.1	232.4	Faulty TC	233.7	231.7	232.2	230.1	2.1	228.1	228.5	227.5	227.7	227.7	Faulty TC	134.3
214.5	231.9	231.5	Faulty TC	232.7	230.6	231.5	229	2.5	227.3	227.8	226.3	229.1	226.8	Faulty TC	135.8
220	231.5	230.5	Faulty TC	231.3	229.0	231.2	226.7	4.5	225.9	226.5	224.9	226.2	224.5	Faulty TC	136.6

TABLE B-IX

HEAT TRANSFER DATA USED FOR HEAT TRANSFER CALCULATIONS -- THERMOCOUPLES OF HEAT PLUG 2 DURING STEAM TEST 5

Time (sec)	2 in. TC 53	1-1/2 in. TC 26	1 in. TC 27	1/2 in. TC 25	1/4 in. TC 24	Bulk Average	Liner Surface TC 45	ΔT Bulk Surface	0.035 in. TC 85	0.069 in. TC 86	0.141 in. TC 88	0.175 in. TC 89	0.211 in. TC 90	0.248 in. Back of Liner TC 91	Concrete 3/16 in. TC 92
0						84									
5.5	85.5	Faulty TC	99	95.2	97.0	96.7	88.7	8.2	83.2	83.6	77.6	Faulty TC	76.8	75.7	73.7
11.0	117.7	Faulty TC	122.1	116.8	119.2	119	97.3	21.8	85.4	85.8	78.6	Faulty TC	78	76.8	73.2
16.5	138	Faulty TC	139.5	133.7	136.6	137	104.4	32.7	88.5	88.8	81.1	Faulty TC	80.6	78.5	73
22.0	150.7	Faulty TC	152.7	146.9	150.3	150.3	110.8	39.7	92.7	93	85	Faulty TC	84.5	81	73.2
27.5	159.3	Faulty TC	162.9	157.3	161.3	160.3	116.9	43.6	98	98.2	90.2	Faulty TC	89.8	84.4	73.5
33.0	171.8	Faulty TC	171.1	166	170.1	170.5	123.1	47.6	104.3	104.6	96.7	Faulty TC	96.2	89	73.8
38.5	177.5	Faulty TC	177.7	173.1	177.3	176.4	129.5	47.1	111.6	111.8	104	Faulty TC	103.6	94.4	74.1
44.0	181.4	Faulty TC	183.3	179.1	183.4	181.8	136.3	45.7	119.6	119.8	112.1	Faulty TC	111.6	100.7	74.4
49.5	186.6	Faulty TC	188.2	184.3	188.6	186.9	148.4	43.7	128.1	128.3	120.6	Faulty TC	120.2	107.7	74.6
55	188.7	Faulty TC	192.6	188.9	193.1	190.8	150.7	40.3	136.9	137.1	129.5	Faulty TC	129	115.2	74.9
60.5	195.6	Faulty TC	196.7	193.2	197.2	195.7	158.1	37.8	145.8	146	138.4	Faulty TC	137.9	122.9	75.2
66	201.1	Faulty TC	201.5	197.1	201.0	200	165.4	34.7	154.6	154.8	147.1	Faulty TC	146.6	130.7	75.6
71.5	205.2	Faulty TC	204	200.8	204.4	203.6	172.6	31.2	163	163.3	155.6	Faulty TC	155	138.4	76.2
77.0	208.8	Faulty TC	207.3	204.2	207.6	207	179.4	27.8	171.1	171.4	163.7	Faulty TC	163	145.9	76.8
82.5	210.9	Faulty TC	210.4	207.5	210.7	209.9	185.9	24.2	178.6	179	171.3	Faulty TC	170.5	153	77.6
88	215.1	Faulty TC	213.3	210.5	213.6	213.1	191.8	21.5	185.5	185.9	178.3	Faulty TC	177.4	159.7	78.6
93.5	217.9	Faulty TC	216.1	213.5	216.3	215.9	197.3	18.8	191.8	192.2	184.7	Faulty TC	183.7	165.8	79.7
99	218.1	Faulty TC	218.6	216.2	219.1	217.9	202.2	15.9	197.4	197.9	190.6	Faulty TC	189.4	171.4	81
104.5	221.5	Faulty TC	221	218.8	221.4	220.7	206.7	14.2	202.4	203	195.8	Faulty TC	194.5	176.4	82.5
110.0	223.1	Faulty TC	223.3	221.2	223.8	222.8	210.6	12.4	206.8	207.6	200.4	Faulty TC	199	180.9	84.1
115.5	226.7	Faulty TC	225.5	223.5	226.1	225.5	214.1	11.6	210.7	211.4	204.6	Faulty TC	203.1	184.8	85.8
121	229	Faulty TC	227.6	225.7	228.2	227.6	217.2	10.6	214.1	215	208.3	Faulty TC	206.7	188.3	87.7
126.5	230	Faulty TC	229.6	227.8	230.3	229.4	220	9.6	19.1	218	211.5	Faulty TC	210	191.4	89.6
132	236.3	Faulty TC	231.7	229.5	232.2	232.3	222.5	10.1	219.7	220.8	214.4	Faulty TC	212.8	194.2	91.5

TABLE B-IX (Contd.)

HEAT TRANSFER DATA USED FOR HEAT TRANSFER CALCULATIONS -- THERMOCOUPLES OF HEAT PLUG 2 DURING STEAM TEST 5

Time (sec)	2 in. TC 53	1-1/2 in. TC 36	1 in. TC 27	1/2 in. TC 25	1/4 in. TC 24	Bulk Average	Liner Surface TC 45	ΔT Bulk Surface	0.035 in. TC 85	0.069 in. TC 86	0.141 in. TC 88	0.175 in. TC 89	0.211 in. TC 90	0.248 in. Back of Liner TC 91	Concrete 3/16 in. TC 92
137.5	233.4	Faulty TC	233.7	231.2	233.1	233.1	224.7	8.6	222.1	223.3	217	Faulty TC	215.5	196.7	93.5
143	235.2	Faulty TC	235.6	232.8	235.6	234.7	226.7	8.3	224.3	225.6	219.3	Faulty TC	217.8	198.9	95.5
148.5	237.0	Faulty TC	237.4	234.1	236.8	236.3	228.6	7.9	226.2	227.6	221.3	Faulty TC	220	200.9	97.4
154	237.0	Faulty TC	239	235.2	238.2	237.5	230.2	7.3	227.9	229.4	223.1	Faulty TC	221.9	202.8	99.4
159.5	239.8	Faulty TC	240.4	236	238.6	238.8	231.6	7.4	229.4	230.9	224.7	Faulty TC	223.6	204.5	101.3
165	241.9	Faulty TC	241.5	236.6	239.5	240	232.8	7.3	230.7	232.2	225.9	Faulty TC	225.1	206	103.2
170.5	242.1	Faulty TC	242.1	236.8	239.8	241.2	233.6	6.8	231.6	233.4	226.9	Faulty TC	226.2	207.4	105
173.46							Steam charge valve closed.								
176	240.1	Faulty TC	242.2	236.7	239.7	239.7	234	5.9	232.2	233.8	222.6	Faulty TC	227	208.5	106.8
181.5	239.6	Faulty TC	241.7	236.1	239.1	239.1	234	5.3	232.5	234	227.9	Faulty TC	227.5	209.3	108.6
187	236.7	Faulty TC	240.6	235.2	238.2	237.3	233.5	4.3	232.3	233.8	227.9	Faulty TC	227.5	209.8	110.4
192.5	236.5	Faulty TC	239.1	234.1	236.9	236.7	232.6	4.3	231.7	233.2	227.5	Faulty TC	227.1	210	112.2
198	235.7	Faulty TC	236.9	232.7	235.4	235.2	231.5	3.9	230.9	232.3	226.8	Faulty TC	226.2	209.9	113.9
203.5	236.0	Faulty TC	234.7	231.3	234.9	234	230.3	3.9	229.9	231.2	225.9	Faulty TC	225.1	209.5	115.4
209	234.7	Faulty TC	232.8	230.1	232.8	232.6	229.5	3.3	229	230.3	225	Faulty TC	223.8	209	116.8
214.5	235.4	Faulty TC	231.8	220.7	232.3	231.8	229.5	2.5	228.7	229.9	224.3	Faulty TC	222.7	208.6	117.8
220	230	Faulty TC	232.7	230.4	230.4	231.5	231.2	0.5	229.6	230.8	224.2	Faulty TC	222.2	208.6	118.3

APPENDIX C -- TAEH INVERSE HEAT CONDUCTION CODE

APPENDIX C -- TAEH INVERSE HEAT CONDUCTION CODE

Reference to the TAEH inverse heat conduction code has been extensive in this report, and, because the code is unpublished, a code description, listing, and sample problem are provided.

For the sample problem, the mesh point layout corresponds to Heat Plug 1 and temperatures are for Test 5, Heat Plug 1 (Appendix B-II) data. One internal temperature corresponding to an average of the five temperatures from internal liner thermocouples was assigned to Mesh Point 5.

C-I. IDENTIFICATION

Title: TAEH

Programming Language: FORTRAN IV for the IBM 360/75

C-II. PURPOSE

TAEH is an IBM-360 program written for the purpose of calculating unknown surface conditions from known internal temperature histories in a one-dimensional multi-region heat conducting body. The geometry may be plane, cylindrical, or spherical. The program can calculate surface conditions at one surface only; the second surface is assumed to be insulated (that is, surface flux equals zero). Input consists of parametric, control, and temperature data entered on cards. For CVTR, temperature data were also entered by other means, such as a FSCAN output file. The program calculates and prints surface temperature, flux, and the effective heat transfer coefficient.

C-III. DESCRIPTION

The problem treated by TAEH is known as the inverse problem of transient heat conduction - the calculation of surface conditions from internal temperatures - as opposed to the customary direct problem of calculating internal temperatures from surface conditions. Of the various methods suggested in the literature for treating this problem, that of Beck [C-1] was most suitable from the standpoint of combining accuracy with ease of computer implementation. It is basically a refinement of the method first used by Stolz [C-2] and consists of the numerical inversion of a suitable direct problem. A brief description follows; the complete mathematical derivation is given in Reference C-1.

If one surface of a one-dimensional heat conducting body is subjected to a time-varying heat flux, the internal temperature distribution at any time may be calculated by applying Duhamel's theorem [C-3].

$$T(x,t) = T_i(x) + \int_{\lambda=0}^{t} \phi(\lambda) \frac{\partial F(x, t-\lambda)}{\partial t} \partial\lambda \qquad \text{(C-1)}$$

where

$T(x,t)$ = the time-dependent temperature distribution

$T_i(x)$ = the initial temperature distribution

$\phi(t)$ = the surface heat flux

$F(x,t)$ = the temperature response at x due to step-rise in surface flux at time 0.

Using a modified trapezoidal rule and letting $\Delta t = \Delta\lambda$ Equation C-1 may be approximated by

$$T_M = \sum_{n=0}^{M-1} \phi_n \, \Delta F_{M-n} + \phi_M \, \Delta F_0 \qquad (\phi_0 \equiv 0) \qquad \text{(C-2)}$$

where

$$T_M = T(x, M\,\Delta t)$$

$$\phi_n = \phi\,[(n - 1/2)\,\Delta t]$$

$$\Delta F_{M-n} = F[x, (M - n + 1)\,\Delta t] - F[x, (M - n)\,\Delta t].$$

The most straight-forward procedure would be to solve this equation for ϕ_M, thus obtaining a recursive expression for the surface flux. However, for the inverse problem the calculation typically is unstable for small time-steps, and this instability limits the accuracy of the solution. One method of improving the stability is to use temperatures at times greater than $M\,\Delta t$ in calculating ϕ_M. Thus, the following temperatures are used:

$$T_{M+J} = \sum_{n=0}^{M-1} \phi_n \, \Delta F_{M-n+j} + \phi_M \, \Delta F_j + \ldots + \phi_{M+j} \, \Delta F_0 \quad \text{(C-3)}$$

where

$j = 0, 1, 2, \ldots, r$ in order to determine ϕ_M. An expansion of ϕ_{M+i} of the form

$$\phi_{M+i} = \sum_{k=0}^{\eta} A_k \, i^k, \quad A_0 = \phi_M \quad \text{(C-4)}$$

is assumed; and the function

$$E_r = \sum_{j=0}^{r} (T_{M+j} - T_{e,\,M+j})^2 \quad \text{(C-5)}$$

where

$T_{e,\,M+j}$ = the experimentally measured temperature distribution at $(M + j)\,\Delta t$

is minimized with respect to the A_k. TAEH uses $\eta = 0$ and $r = 1$. The resulting recursive expression for ϕ_M obtained thus is

$$\phi_M = \frac{C_{00}\, T_{e,\,M} + C_{01}\, T_{e,\,M+1} - \sum_{n=0}^{M+1} \phi_n \, \phi_{M-n}}{C_{00}^2 + C_{01}^2} \quad \text{(C-6)}$$

where

$$C_{00} = \Delta F_0$$

$$C_{01} = \Delta F_0 + \Delta F_1$$

$$\phi_{M-n} = C_{00}\, \Delta F_{M-n} + C_{01}\, \Delta F_{M-n+1}.$$

For points in the body $x_1, x_2, \ldots, x_p$ Equation (C-1) becomes

$$T(x_\ell, t) = T_i(x_\ell) + \int_{\lambda=0}^{t} \phi(\lambda) \frac{\partial F(x_\ell,\, t-\lambda)}{\partial t} \, \partial\lambda \quad \text{(C-7)}$$

where

$\ell = 1, 2, \ldots, p.$

By multiplying each equation by a weighting coefficient W_ℓ and adding the equations together the following is obtained.

$$\bar{T}(t) = T_i + \int_{\lambda=0}^{t} \phi(\lambda) \frac{\partial \bar{F}(t-\lambda)}{\partial t} \partial\lambda \qquad \text{(C-8)}$$

where

$$\bar{T}(t) = \sum_{\ell=1}^{P} W_\ell T(x_\ell, t)$$

$$\bar{T}_i = \sum_{i=1}^{P} W_\ell T_i(x_\ell)$$

$$\bar{F}(t-\lambda) = \sum_{\ell=1}^{P} W_\ell F(x_\ell, t-\lambda).$$

This equation is identical in form to Equation (C-1) and may be solved for ϕ_M in the same manner to obtain an expression identical to Equation (C-6) but with T_e and F replaced by T_e and F, where

$$\bar{T}_e = \sum_{\ell=1}^{P} W_\ell T_e (x_\ell).$$

Once the surface flux has been calculated, the surface temperature may be found by direct application of Equation (C-2); and the effective heat transfer coefficient is given by

$$h(t) = \frac{\phi(t)}{T_b(t) - T(x_s, t)} \qquad \text{(C-9)}$$

where

h(t) = effective heat transfer coefficient

$T_b(t)$ = bulk temperature of the medium adjacent to the surface of the conductor

x_s = surface of the conductor.

The temperature response function, F, is calculated by a direct solution where the surface conditions are unit flux at the surface being investigated and zero flux at the other surface. A complete derivation and discussion of the method used may be found in Reference C-4. It consists of the solution of a finite-difference approximation for the heat conduction equation

$$g(x) \frac{\partial T(x,t)}{\partial t} = k(x) \frac{\partial^2 T(x,t)}{\partial x^2} \qquad \text{(C-10)}$$

where

g(x) = volumetric heat capacity

k(x) = thermal conductivity.

Boundary conditions allowed by the method are of the general form

$$A \cdot T + B \cdot \frac{\partial T}{\partial x}\Big|_{x = 0} = D \cdot C(t). \qquad \text{(C-11)}$$

The following diagram illustrates the positioning of mesh points at which the temperature will be calculated.

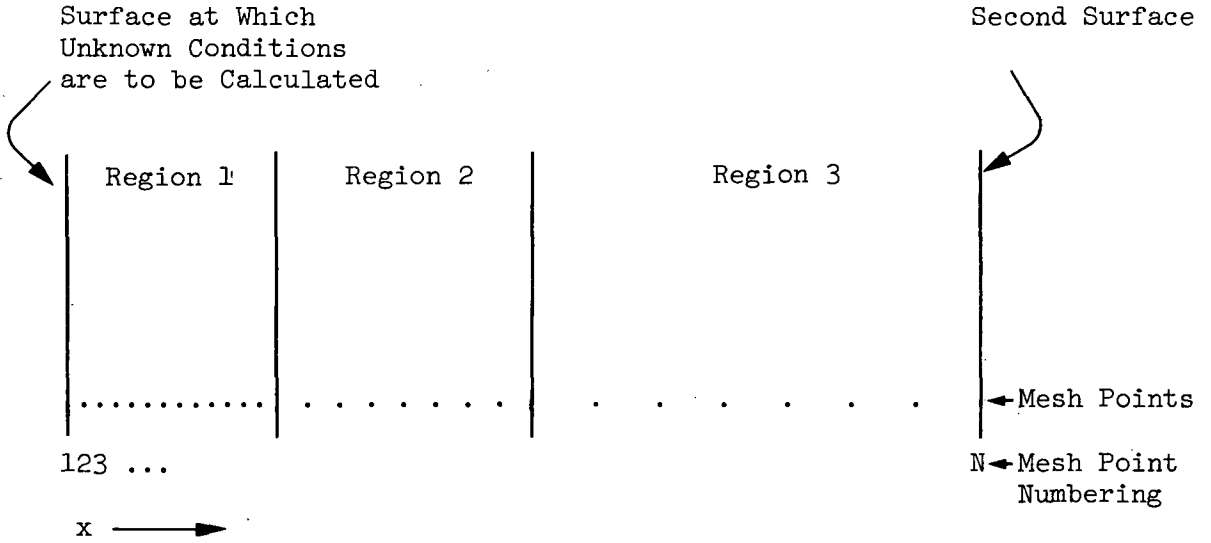

Mesh points are placed at external surfaces and internal interfaces between materials, and at equal intervals between surfaces or interfaces. A region contains one material and has constant mesh point spacing.

The use of small time-steps is desirable to increase the accuracy of the response function solution. However, as indicated, the inverse calculation becomes unstable if time-steps are made too small. To overcome this difficulty, the program allows the response function time-step to be a sub-multiple of the time-step used for the inverse calculation. That is, the response function may be calculated several times for each single time advancement of the inverse calculation.

The program allows a maximum of 101 mesh points, 10 regions, 10 different materials, 10 experimentally measured internal temperatures, and 1000 time-steps. The known temperatures (bulk temperature of the medium adjacent to Mesh Point 1 and measured internal temperatures) may be read in either from cards or from an FSCAN tape or sequential disk file. (Actually, thermocouple millivolt data is read from the FSCAN file and converted to temperature.) The program will begin processing with any desired data point on the FSCAN file and will then process every k^{th} data point until problem termination.

Three geometries may be treated - slab, cylindrical, and spherical. For the cylindrical and spherical cases, the surface at which the unknown conditions are to be calculated must be the inner surface of the body.

Card 1

NSETS = the number of data sets to be processed by this run (integer, Columns 1 through 5).

Each data set then consists of the following cards:

Card 1

Title card - all 80 columns may be used.

Card 2

TSTART = initial time (real, Columns 1 through 12).

TSTØP = final time (real, Columns 13 through 24).

DELT = time increment (real, Columns 25 through 36).

NLØØPS = the number of response function calculations per time-step (integer, Columns 37 through 41).

NPF = output print frequency (integer, Columns 42 through 46).

Card 3

NMPT = number of mesh points (integer, Columns 1 through 5).

NREG = number of regions (integer, Columns 6 through 10).

NMTRL = number of different materials (integer, Columns 11 through 15).

NKT = number of mesh points at which the temperature is known (integer, Columns 16 through 20).

ICØDE = 1 for temperature data on cards, 2 for temperature data on an FSCAN file (integer, Column 25).

USTART = initial temperature (real, Columns 26 through 37).

Card 4

IGEØM = 1 for slab geometry, 2 for cylindrical geometry, 3 for spherical geometry (integer, Column 5).

RADIUS = inner radius of cylinder of sphere - blank for slab (real, Columns 6 through 17).

FSTEP = flux used to compute response function (real, Columns 18 through 29).

Known Temperature Cards

One card for each mesh point at which the temperature is known.

MPK (I) = mesh point number (integer, Columns 1 through 5).

W (I) = the weighting coefficient (real, Columns 6 through 17).

Thermal Property Cards

One for each different material beginning with Material Number 1, then Material Number 2.

TC (I) = thermal conductivity (real, Columns 1 through 12).

VHC (I) = volumetric heat capacity (real, Columns 13 through 24).

Region Definition Cards

One for each region, from left to right.

MTRL (I) = material number (integer, Columns 1 through 5).

NINT (I) = number of intervals between mesh points (integer, Columns 6 through 10).

XR (I) = right boundary coordinate (real, Columns 11 through 22).

The following indented input option is pertinent only to the CVTR problem. If

ICØDE = 2, the following additional cards are required:

Data Selection Card

T1 = the time of the first data point to be processed (real, Columns 1 through 12).

KRUN = k, the processing frequency (integer, Columns 13 through 17).

Data Channel Card

Each entry is an integer occupying five columns.

LUBC = bulk temperature data track and channel identifier.

LUEXC (1) = first known temperature data track and channel identifier.

LUEXC (NKT)

Bulk Temperature Thermocouple Calibration Card

AOB = a_0 in calibration curve for bulk temperature thermocouple (real, Columns 1 through 12).

A1B = a_1 (real, Columns 11 through 24).

A2B = a_2 (real, Columns 25 through 36).

(Calibration curves of the form $mV = a_0 + a_1T + a_2T^2$ are assumed.)

Internal Temperature Thermocouple Calibration Cards

One card for each internal temperature thermocouple, same format as preceding card. Must be in order. Stored in AO(I), A1 (I), and A2 (I).

The known temperature data are read in next. The first values read in should be for time TSTART + DELT, and the final values for TSTØP + DELT. If these data are on cards, the format is as follows:

Known Temperature Cards

UB = bulk temperature (real, Columns 1 through 12).

UEX (1) = first experimental internal temperature (real, Columns 13 through 24).

.
.
.

Continue on this and subsequent cards as needed, 12 columns per entry, until reaching UEX (NKT).

```
C           PROGRAM TAEH
C           INVERSE TRANSIENT HEAT CONDUCTION PROGRAM FOR THE IBM 360:
C             CALCULATES UNKNOWN BOUNDARY CONDITIONS FROM KNOWN INTERNAL
C             TEMPERATURE HISTORIES IN A ONE-DIMENSIONAL, MULTI-REGION,
C             HEAT-CONDUCTING SOLID.  PLANE, CYLINDRICAL, OR SPHERICAL
C             GEOMETRIES MAY BE TREATED.
C
      COMMON /HTBLK/ X(101),U(101),TC(10),VHC(10),AO,BO,CC,DO,AN,BN,CN,
     &    DN,DT,MTRL(10),MBP(10),NMPT,IGEOM,AO OLD,CO OLD,DO OLD
      COMMON /INBLK/ UB,UEX(10),NKT,IFLAG
      COMMON /PAGBLK/ LPAGE,NAME
      DIMENSION DELTA U(10)
      DIMENSION URO(1002),URW(1002),UEXW(1002),FLUX(1002),XR(10),W(10),
     &    MPK(10),NINT(10),NAME(20)
      INTEGER*4 BCD(3,3)/36HPLANE       CYLINDRICAL SPHERICAL    /
      LPAGE=0
      LINES = 50
      AN = 0.
      CN = 0.
      DN = 0.
C
      READ (5,1000) NSETS
 1000 FORMAT (I5)
      DO 99 ISET=1,NSETS
      LPAGE=LPAGE+1
      READ (5,1001) NAME,TSTART,TSTOP,DELT,NLOOPS,NPF,NMPT,NREG,NMTRL,
     &    NKT,ICODE,USTART,IGEOM,RADIUS, F STEP
 1001 FORMAT (20A4/3E12.5,2I5/5I5,E12.5/I5,2E12.5)
      READ (5,1002) (MPK(I),W(I),I=1,NKT)
 1002 FORMAT (I5,E12.5)
      READ (5,1003) (TC(I),VHC(I),I=1,NMTRL)
 1003 FORMAT (2E12.5)
      READ (5,1004) (MTRL(I),NINT(I),XR(I),I=1,NREG)
 1004 FORMAT (2I5,E12.5)
      IF(F STEP .EQ. 0.) F STEP = 1
      NTS = (TSTOP-TSTART)/DELT+0.1
      NTS1 = NTS+1
      NTS2 = NTS+2
      DT = DELT/FLOAT(NLOOPS)
      M = MTRL(1)
      BO = TC(M)
      M = MTRL(NREG)
      BN = TC(M)
      IFLAG = 0
      MBP(1) = 1+NINT(1)
      IF (NREG.EQ.1) GO TO 25
      DO 1 K=2,NREG
    1 MBP(K) = MBP(K-1)+NINT(K)
   25 K = 1
      J = 1
      XL = RADIUS
      X(1) = RADIUS
    2 DX = (XR(K)-XL)/NINT(K)
    3 J = J+1
      X(J) = X(J-1)+DX
      IF (J.EQ.NMPT) GO TO 4
```

```
      IF (J.NE.MBP(K)) GO TO 3
      XL = XR(K)
      K = K+1
      GO TO 2
   4  WRITE (6,1005) LPAGE,NAME,ISET,TSTART,NTS,TSTOP,NLOOPS,DELT,NPF,
     &    (BCD(I,IGEOM),I=1,3)
1005  FORMAT ('1TAEH:  INVERSE TRANSIENT HEAT CONDUCTION PROGRAM',60X,
     &    'PAGE NO.',I4/1X,20A4//' DATA SET NO.',I3,10X,90('*')//
     &    ' INITIAL TIME    =',1PE12.5,10X,'NO. OF TIME STEPS =',I5/
     &    ' FINAL TIME      =',E12.5,10X,
     &    'NO. OF RESPONSE CALCULATIONS PER TIME STEP =',I3/
     &    ' TIME INCREMENT =',E12.5,10X,'PRINT FREQUENCY    =',I3//
     &    ' GEOMETRY:  ',3A4)
      IF (IGEOM.EQ.1) GO TO 5
      WRITE (6,1006) RADIUS
1006  FORMAT ('+',38X,'INSIDE RADIUS =',1PE12.5)
   5  WRITE (6,1007) NMPT,NMTRL,NREG,NKT,USTART,ICODE,F STEP,
     &    (MPK(I),W(I),I=1,NKT)
1007  FORMAT ('ONO. OF MESH POINTS =',I4,14X,'NO. OF MATERIALS =',I3/
     &    ' NO. OF REGIONS      =',I4,14X,
     &    'NO. OF POINTS AT WHICH MEASURED TEMP.S ARE KNOWN =',I3/
     &    ' INITIAL TEMP. =',1PE12.5,11X,'INPUT BY SUBR. INPUT',I1/
     &  '  FLUX STEP = ',E12.5//
     &    ' MEASURED TEMP. MESH POINTS AND WEIGHTS'/6(I5,E15.5)/
     &    4(I5,E15.5))
      WRITE (6,1008) (I,TC(I),VHC(I),I=1,NMTRL)
1008  FORMAT ('0MATERIAL PROPERTIES'//5X,'MATERIAL NO.',5X,
     &    'THERMAL CONDUCTIVITY',5X,'VOL. HEAT CAPACITY'/(9X,I2,15X,
     &    1PE12.5,11X,E12.5))
      WRITE (6,1009) (I,MTRL(I),NINT(I),XR(I),MBP(I),I=1,NREG)
1009  FORMAT ('0CONDUCTING BODY COMPOSITION'//5X,'REGION',5X,
     &    'MATERIAL NO.',5X,'NO. OF INTERVALS',5X,
     &    'RIGHT BOUNDARY COORD.',5X,'RIGHT BOUNDARY MESH POINT'/
     &    (7X,I2,11X,I2,17X,I3,15X,1PE12.5,22X,I3))
      WRITE (6,1010) (X(I),I=1,NMPT)
1010  FORMAT ('0MESH POINT COORD.S'/(1X,1P10E13.5))
      T = TSTART
      FLUX(1) = 0.
      URO(1) = USTART
      DO 6 J=1,NMPT
   6  U(J) = USTART
      SUM = 0.
      DO 7 K=1,NKT
   7  SUM = SUM+W(K)
      URW(1) = SUM*USTART
      UEXW(1) = SUM*USTART
      HTC = 0.
      UO = USTART
      UB = USTART
      AO = 0.
      CO = 1.
      DO = F STEP
      AO OLD = 0.
      CO OLD = 1.
      DO OLD = F STEP
      DO 13 I=2,NTS2
```

```
      DO 8 K=1,NLOOPS
    8 CALL HTCCN
      URW(I) = 0.
      UEXW(I) = 0.
      GO TO (9,10),ICODE
    9 CALL INPUT1
      GO TO 11
   10 CALL INPUT2
   11 DO 12 K=1,NKT
      J = MPK(K)
      URW(I) = URW(I)+W(K)*U(J)
   12 UEXW(I) = UEXW(I)+W(K)*UEX(K)
   13 URO(I) = U(1)
      LPAGE = LPAGE+1
      WRITE (6,1011) LPAGE,NAME,ISET,(MPK(I),I=1,NKT)
 1011 FORMAT ('0END OF INPUT DATA',8X,90('*')/
     &    '1TAEH:  INVERSE TRANSIENT HEAT CONDUCTION PROGRAM',60X,
     &    'PAGE NO.',I4/1X,20A4//' OUTPUT FOR DATA SET NO.',I3//5X,
     &  'TIME',7X'SURFACE TEMP.',2X'SURFACE FLUX',2X'HEAT TRANSFER',
     &  5X'MEASURED MINUS CALCULATED TEMPERATURES AT GIVEN MESH POINTS'
     &  /,46X'COEFFICIENTS',1X10(5X12)/)
      IPF = 0
      DO 100 J=1,NMPT
  100 U(J) = U START
      DT = DELT
      AO OLD = 0.
      CO OLD = U START
      DO OLD = 0.
      WRITE (6,1012) T,UO,FLUX(1),HTC
 1012 FORMAT(1PE13.5,3(3XE12.5),2XOP1GF7.1)
      LINES = 50.
   26 COO = URW(2)-URW(1)
      CO1 = URW(3)-URW(1)
      M = 2
   14 T = T+DELT
      N = 1
      SUM = 0.
   15 SUM = SUM+FLUX(N)*(COO*(URW(M-N+2)-URW(M-N+1))+
     &    CO1*(URW(M-N+3)-URW(M-N+2)))
      IF (N.EQ.M-1) GO TO 16
      N = N+1
      GO TO 15
   16 FLUX(M) = (COO*(UEXW(M)-UEXW(1))+CC1*(UEXW(M+1)-UEXW(1))-SUM)/
     &    (CCO**2+CO1**2)
      FLUXA =F STEP*(FLUX(M)+FLUX(M-1))/2.
      L = 1
      SUM = 0.
   17 SUM = SUM+FLUX(L)*(URO(M-L+2)-URO(M-L+1))
      IF (L.EQ.M) GO TO 18
      L = L+1
      GO TO 17
   18 UOOLD = UO
      UO = SUM+USTART
      UBOLD = UB
      IF(M .EQ. 2) GO TO 120
      HTC = FLUXA/(UBOLD-UOOLD)
```

```
      CO = UB
      AO = HTC
      DO = HTC
      CALL HTCCN
      DO 11C K=1,NKT
      J = MPK(K)
  110 DELTA U(K) = UEX(K) -U(J)
  12C GO TO (19,2C),ICODE
   19 CALL ENTRY1
      GO TO 21
   20 CALL ENTRY2
   21 IF (M.EC.2) GO TO 23
      IPF = IPF+1
      IF (IPF.NE.NPF) GC TO 22
      IPF = C
      WRITE (6,1012) TOLD,UOOLD,FLUXA,HTC,(DELTA U(K),K=1,NKT)
      LINES = LINES-1
      IF (LINES.GT.0) GO TO 22
      LPAGE = LPAGE+1
      LINES = 52
      WRITE (6,1013) LPAGE,NAME
 1013 FORMAT ('1TAEH:  INVERSE TRANSIENT HEAT CONDUCTION PROGRAM',60X,
     &    'PAGE NO.',I4/1X,20A4//5X,'TIME',9X,'SURFACE TEMP.',5X,
     &    'SURFACE FLUX',5X,'HEAT TRANSFER COEF.'/)
   22 IF (M.GE.NTS1) GO TC 24
   23 M = M+1
      TOLD = T
      GO TO 14
   24 FLUXA =(FLUX(M)+(FLUX(M)-FLUX(M-1))/2.)*F STEP
      HTC = FLUXA/(UB-UO)
      IPF = IPF+1
      IF (IPF.NE.NPF) GO TO 99
      WRITE (6,1012) T,UO,FLUXA,HTC
   99 WRITE (6,1014)
 1014 FORMAT ('OEND OF CUTPUT:  FINAL TIME REACHED')
      STCP
C          STATEMENT NUMBERS USEC:  1 - 26, 1000 - 1014.
      END
```

```
      SUBROUTINE HTCON
C          SOLVES ONE-DIMENSIONAL TRANSIENT OR STEADY STATE HEAT
C            CONDUCTION EQUATION.
C
      COMMON /HTBLK/ X(101),U(101),TC(10),VHC(10),AO,BO,CO,DO,AN,BN,CN,
     &    DN,DT,MTRL(10),MBP(10),NMPT,IGEOM,AO OLD,CO OLD,CO OLD
      DIMENSION A(101),B(101),C(101),D(101),E(101),F(101),UOLD(101)
      EQUIVALENCE (U(1),UOLD(1)),(C(1),E(1)),(A(1),F(1))
      DATA CNOLD/0./,S/1./
C
      M = MTRL(1)
      TCR = TC(M)
      VHCR = VHC(M)
      HRN = X(2)-X(1)
      GO TO (1,2,3),IGEOM
    1 HB = 1.
      HRS = 1./HRN
      HRV = HRN/2.
      GO TO 4
    2 HB = 6.283185*X(1)
      HRS = 6.283185*(X(1)+HRN/2.)/HRN
      HRV = 3.141593*(X(1)+HRN/4.)*HRN
      GO TO 4
    3 HB = 12.56637*X(1)**2
      HRS = 12.56637*(X(1)+HRN/2.)**2/HRN
      HRV = 4.188790*((X(1)+HRN/2.)**3-X(1)**3)
    4 C(1) = -TCR*HRS*DT/2.
      B(1) = VHCR*HRV + AO*HB*DT/2. - C(1)
      D(1) =  -C(1)*UOLD(2) + (VHCR*HRV+C(1)-(AO OLD*HB*DT/2.))*UOLD(1)
     1  + DT*HB*(DC*CO + DC OLD*CO OLD)/2.
      AO OLD = AO
      CO OLD = CO
      DO OLD = DO
      E(1) = C(1)/B(1)
      F(1) = D(1)/B(1)
      N = NMPT-1
      IF (NMPT.LT.3) GO TO 12
      KREG = 1
      TCL = TCR
      VHCL = VHCR
      HLN = HRN
      DO 11 I=2,N
      IF (I.NE.MBP(KREG)) GO TO 5
      KREG = KREG+1
      M = MTRL(KREG)
      TCR = TC(M)
      VHCR = VHC(M)
      HRN = X(I+1)-X(I)
    5 IF (KREG.EQ.1) GO TO 6
      IF (I.NE.MBP(KREG-1)+1) GO TO 6
      TCL = TCR
      VHCL = VHCR
      HLN = HRN
    6 HLS = HRS
```

```
      GO TO (7,8,9),IGEOM
    7 HRS = 1./HRN
      HLV = HRV
      HRV = HRN/2.
      GO TO 10
    8 HB = 6.283185*X(I)
      HRS = 6.283185*(X(I)+HRN/2.)/HRN
      HLV = 3.141593*(X(I)-HLN/4.)*HLN
      HRV = 3.141593*(X(I)+HRN/4.)*HRN
      GO TO 10
    9 HB = 12.56637*X(I)**2
      HRS = 12.56637*(X(I)+HRN/2.)**2/HRN
      HLV = 4.188790*(X(I)**3-(X(I)-HLN/2.)**3)
      HRV = 4.188790*((X(I)+HRN/2.)**3-X(I)**3)
   10 A(I) = -TCL*HLS*DT/2.
      C(I) = -TCR*HRS*DT/2.
      STORE = VHCL*HLV+VHCR*HRV
      B(I) = S*STORE-A(I)-C(I)
      D(I) = S*(-A(I)*UOLD(I-1)+(STORE+A(I)+C(I))*UOLD(I)-C(I)*
     &    UOLD(I+1))
      STORE = B(I)-A(I)*E(I-1)
      E(I) = C(I)/STORE
   11 F(I) = (D(I)-A(I)*F(I-1))/STORE
   12 TCL = TCR
      VHCL = VHCR
      HLN = HRN
      HLS = HRS
      GO TO (13,14,15),IGEOM
   13 HLV = HRV
      GO TO 16
   14 HB = 6.283185*X(NMPT)
      HLV = 3.141593*(X(NMPT)-HLN/4.)*HLN
      GO TO 16
   15 HB = 12.56637*X(NMPT)**2
      HLV = 4.188790*(X(NMPT)**3-(X(NMPT)-HLN/2.)**3)
   16 A(NMPT) = -TCL*HLS*DT/2.
      STORE = TCL*AN*HB*DT/(2.*BN)
      B(NMPT) = S*VHCL*HLV+STORE-A(NMPT)
      D(NMPT) = S*(-A(NMPT)*UOLD(N)+(VHCL*HLV-STORE+A(NMPT))*
     &    UOLD(NMPT))+TCL*HB*DN*DT*(CN+S*CNOLD)/(2.*BN)
      U(NMPT) = (D(NMPT)-A(NMPT)*F(N))/(B(NMPT)-A(NMPT)*E(N))
      DO 17 I=1,N
      II = NMPT-I
   17 U(II) = -E(II)*U(II+1)+F(II)
      RETURN
C         STATEMENT NUMBERS USED:  1 - 17.
      END
```

```
      SUBROUTINE INPUT
C          READS IN MEASURED INTERNAL AND BULK TEMP. DATA.
C
      COMMON /INBLK/ UB,UEX(10),NKT,IFLAG
      COMMON /PAGBLK/ LPAGE,NAME
      DIMENSION LUEXC(10),ICHAN(100),DATA(100)
      DIMENSION A0(10),A1(10),A2(10),NAME(20)
C   *    *    *    *    *    *    *    *    *    *    *    *    *    *
      ENTRY INPUT1
      IF (IFLAG.EQ.1) GO TO 1
      REWIND 8
      IFLAG = 1
    1 READ (5,1000) UB,(UEX(I),I=1,NKT)
 1000 FORMAT (6E12.5)
      WRITE(8) UB,(UEX(I),I=1,NKT)
      RETURN
C   *    *    *    *    *    *    *    *    *    *    *    *    *    *
      ENTRY ENTRY1
      ENTRY ENTRY2
      IF (IFLAG.EQ.2) GO TO 2
      REWIND 8
      IFLAG = 2
    2 READ(8) UB,(UEX(I),I=1,NKT)
      RETURN
C   *    *    *    *    *    *    *    *    *    *    *    *    *    *
      ENTRY INPUT2
      IF (IFLAG.EQ.3) GO TO 3
      IFLAG = 3
      READ (5,1003) T1,KFREQ,LUBC,(LUEXC(I),I=1,NKT)
 1003 FORMAT (E12.5,I5/11I5)
      READ (5,1012) A0B,A1B,A2B,(A0(I),A1(I),A2(I),I=1,NKT)
 1012 FORMAT (3E12.5)
      LPAGE = LPAGE+1
      WRITE (6,1006) LPAGE,NAME,T1,KFREQ,LUBC,(LUEXC(I),I=1,NKT)
 1006 FORMAT ('1TAEH:  INVERSE TRANSIENT HEAT CONDUCTION PROGRAM',60X,
     &    'PAGE NO.',I4/1X,20A4//' FIRST TIME POINT ON FSCAN FILE USED',
     &    ' = ',1PE12.5/' PROCESSING FREQUENCY = ',I3//
     &    ' BULK TEMPERATURE CHANNEL = ',I5/' KNOWN TEMPERATURE CHANNE',
     &    'LS = ',11I5)
      WRITE (6,1013) A0B,A1B,A2B,(A0(I),A1(I),A2(I),I=1,NKT)
 1013 FORMAT ('0THERMOCCUPLE CALIBRATION COEFFICIENTS IN MV = A0 + A1',
     &    '*T + A2*T**2'//7X,'A0',13X,'A1',13X,'A2'/(1P3E15.5))
      REWIND 8
      REWIND 9
      READ (9,1004) ID,NCHAN
 1004 FORMAT (A4,I4)
      WRITE (6,1007) ID
 1007 FORMAT ('0FSCAN FILE ID:  ',A4/)
      K = 0
      M = (NCHAN+4)/5
      MP1 = M+1
    7 READ (9,1002,END=9) TIME
 1002 FORMAT (E12.5)
      IF (TIME.GE.T1-0.001 .AND. TIME.LE.T1+0.001) GO TO 10
```

```
      DO 8 I=1,M
    8 READ (9,1008)
 1008 FORMAT (1X)
      GO TO 7
    9 WRITE (6,1009) T1
 1009 FORMAT ('ORECORD FOR TIME',1PE13.5,' CANNOT BE LOCATED')
      STOP
   10 READ (9,1010) (ICHAN(I),DATA(I),I=1,NCHAN)
 1010 FORMAT (5(I4,E10.3))
      GO TO 13
    3 K = K+1
      IF (K.EQ.KFREQ) GO TO 12
      DO 11 I=1,MP1
   11 READ (9,1008)
      GO TO 3
   12 K = 0
      READ (9,1005) (ICHAN(I),DATA(I),I=1,NCHAN)
 1005 FORMAT (/(5(I4,E10.3)))
   13 DO 5 L=1,NKT
      DO 4 I=1,NCHAN
      IF (ICHAN(I).NE.LUEXC(L)) GO TO 4
      UEX(L) = (-A1(L)+SQRT(A1(L)**2-4.*A2(L)*(A0(L)-DATA(I))))/
     &    (2.*A2(L))
      GO TO 5
    4 CONTINUE
      WRITE (6,1011) LUEXC(L)
 1011 FORMAT ('ODATA CHANNEL',I5,' CANNOT BE LOCATED')
      STOP
    5 CONTINUE
      DO 6 I=1,NCHAN
      IF (ICHAN(I).NE.LUBC) GO TO 6
      UB = (-A1B+SQRT(A1B**2-4.*A2B*(A0B-DATA(I))))/(2.*A2B)
      GO TO 14
    6 CONTINUE
      WRITE (6,1011) LUBC
      STOP
   14 WRITE(8) UB,(UEX(I),I=1,NKT)
      RETURN
C   *   *   *   *   *   *   *   *   *   *   *   *   *   *   *
C        STATEMENT NUMBERS USED:  1 - 14.
      END
```

C-VI. SAMPLE PROBLEM OUTPUT

```
TAEH:  INVERSE TRANSIENT HEAT CONDUCTION PROGRAM                                                    PAGE NO.    1
TAEH, CVTR TEST 5, ONE INTERNAL TEMP AT MESH PT 5, 7/1/70

DATA SET NO.  1          ********************************************************************************************

INITIAL TIME    = 0.0                    NO. OF TIME STEPS =   40
FINAL TIME      = 6.11111E-02            NO. OF RESPONSE CALCULATIONS PER TIME STEP =  1
TIME INCREMENT = 1.52778E-03             PRINT FREQUENCY    =  1

GEOMETRY:  CYLINDRICAL                   INSIDE RADIUS = 2.89790E 01

NO. OF MESH POINTS =  50                 NO. OF MATERIALS =  3
NO. OF REGIONS     =   3                 NO. OF POINTS AT WHICH MEASURED TEMP.S ARE KNOWN =  1
INITIAL TEMP. = 7.80000E 01              INPUT BY SUBR. INPUT1
 FLUX STEP =  1.00000E 04

MEASURED TEMP. MESH POINTS AND WEIGHTS
   5    1.00000E 00

MATERIAL PROPERTIES

    MATERIAL NO.      THERMAL CONDUCTIVITY      VOL. HEAT CAPACITY
         1                 2.50000E 01              5.50000E C1
         2                 1.51000E-02              1.85000E-C2
         3                 8.00000E-01              3.02000E 01

CONDUCTING BODY COMPOSITION

    REGION      MATERIAL NO.      NO. OF INTERVALS      RIGHT BOUNDARY COORD.      RIGHT BOUNDARY MESH POINT
      1             1                   23                 2.90000E 01                    24
      2             2                    2                 2.90052E 01                    26
      3             3                   24                 3.10052E 01                    50

MESH POINT COORD.S
  2.89790E 01  2.89799E 01  2.89808E 01  2.89817E 01  2.89826E 01  2.89835E 01  2.89844E 01  2.89853E 01  2.89862E 01  2.89871E 01
  2.89880E 01  2.89889E 01  2.89898E 01  2.89907E 01  2.89916E 01  2.89925E 01  2.89934E 01  2.89943E 01  2.89952E 01  2.89961E 01
  2.89970E C1  2.89979E 01  2.89988E 01  2.89997E 01  2.90023E 01  2.90049E 01  2.90882E 01  2.91715E 01  2.92549E C1  2.93382E 01
  2.94215E 01  2.95049E 01  2.95882E 01  2.96715E C1  2.97548E 01  2.98382E 01  2.99215E 01  3.00048E 01  3.00882E C1  3.01715E 01
  3.02548E 01  3.03381E 01  3.04215E 01  3.05048E 01  3.05881E 01  3.06714E 01  3.07548E 01  3.08381E 01  3.09214E 01  3.10048E 01

END OF INPUT DATA        ********************************************************************************************
```

OUTPUT FOR DATA SET NO. 1

TIME	SURFACE TEMP.	SURFACE FLUX	HEAT TRANSFER COEFFICIENTS	MEASURED MINUS CALCULATED TEMPERATURES AT GIVEN MESH POINTS 5
0.0	7.80000E 01	0.0	0.0	
1.52778E-03	7.91569E 01	7.37775E 02	9.78077E 01	-0.1
3.05555E-03	8.01394E 01	9.02028E 02	3.70281E 01	0.2
4.58333E-03	8.16009E 01	1.07592E 03	2.75178E 01	0.1
6.11110E-03	8.31586E 01	1.34945E 03	2.60303E 01	-0.2
7.63888E-03	8.53488E 01	1.69623E 03	2.72482E 01	-0.2
9.16665E-03	8.78980E 01	2.12282E 03	3.00674E 01	-0.4
1.06944E-02	9.12446E 01	2.63586E 03	3.45209E 01	-0.5
1.22222E-02	9.52213E 01	3.16055E 03	3.95174E 01	-0.6
1.37500E-02	9.99079E 01	3.61408E 03	4.42945E 01	-0.4
1.52778E-02	1.05044E 02	4.07461E 03	5.00221E 01	-0.5
1.68055E-02	1.10971E 02	4.52316E 03	5.64484E 01	-0.5
1.83333E-02	1.17235E 02	4.89531E 03	6.30314E 01	-0.3
1.98611E-02	1.24084E 02	5.19877E 03	7.03335E 01	-0.3
2.13889E-02	1.31090E 02	5.39861E 03	7.73332E 01	-0.1
2.29166E-02	1.38357E 02	5.53023E 03	8.48932E 01	-0.0
2.44444E-02	1.45660E 02	5.61278E 03	9.30197E 01	-0.1
2.59722E-02	1.53048E 02	5.60423E 03	1.01064E 02	0.1
2.75000E-02	1.60225E 02	5.53941E 03	1.09098E 02	0.1
2.90277E-02	1.67378E 02	5.40427E 03	1.16919E 02	0.1
3.05555E-02	1.74081E 02	5.19480E 03	1.23335E 02	0.2
3.20833E-02	1.80595E 02	4.97306E 03	1.30166E 02	0.1
3.36111E-02	1.86657E 02	4.72044E 03	1.35867E 02	0.1
3.51388E-02	1.92402E 02	4.41727E 03	1.40239E 02	0.2
3.66666E-02	1.97581E 02	4.08400E 03	1.42204E 02	0.2
3.81944E-02	2.02369E 02	3.76431E 03	1.44056E 02	0.1
3.97222E-02	2.06672E 02	3.46502E 03	1.45416E 02	0.0
4.12499E-02	2.10615E 02	3.17388E 03	1.47724E 02	0.0
4.27777E-02	2.14110E 02	2.85796E 03	1.47393E 02	-0.1
4.43055E-02	2.17137E 02	2.51482E 03	1.44839E 02	0.0
4.58333E-02	2.19685E 02	2.24098E 03	1.43516E 02	-0.1
4.73610E-02	2.22023E 02	1.97439E 03	1.45427E 02	-0.2
4.88888E-02	2.23784E 02	1.67112E 03	1.41433E 02	-0.0
5.04166E-02	2.25298E 02	1.41925E 03	1.40497E 02	-0.3
5.19444E-02	2.26421E 02	1.18664E 03	1.39947E 02	-0.3
5.34721E-02	2.27282E 02	9.38119E 02	1.33676E 02	-0.3
5.49999E-02	2.27735E 02	6.82039E 02	1.14339E 02	-0.3
5.65277E-02	2.27901E 02	4.08726E 02	1.02195E 02	-0.3
5.80555E-02	2.27613E 02	3.78652E 01	8.25479E 00	-0.3
5.95832E-02	2.26697E 02	-1.77028E 02	-3.68605E 01	-0.4
6.11110E-02	2.26080E 02	-1.47964E 02	-2.88986E 01	

END OF OUTPUT: FINAL TIME REACHED

C-VII. REFERENCES

C-1. J. V. Beck, "Calculation of Surface Heat Flux From an Internal Temperature History", ASME Paper No. 62-HT-46 (January 1963).

C-2. G. Stolz Jr., "Numerical Solution to an Inverse Problem of Heat Conduction for Simple Shapes", Journal of Heat Transfer, Transactions of ASME, Volume 82, Series C, 1962, pp 20-26.

C-3. K. S. Carslaw and J. C. Jaeyer, Conduction of Heat in Solids, (Second Edition), Oxford University Press, London, England, 1959, pp 30-31.

C-4. R. J. Wagner, HEAT 1 -- A One Dimensional Time Dependent or Steady-State Heat Conduction Code for the IBM-650, IDO-16807 (April 1963).